

DETERMINATION OF WELDING PARAMETER DEPENDENT  
HOT CRACKING SUSCEPTIBILITY OF 5086-H32 ALUMINIUM ALLOY  
WITH THE USE OF MVT METHOD

A THESIS SUBMITTED TO  
THE GRADUATE SCHOOL OF NATURAL AND APPLIED SCIENCES  
OF  
MIDDLE EAST TECHNICAL UNIVERSITY

BY

CANER BATIGÜN

IN PARTIAL FULFILLMENT OF THE REQUIREMENTS  
FOR  
THE DEGREE OF DOCTOR OF PHILOSOPHY  
IN  
METALLURGICAL AND MATERIALS ENGINEERING

JANUARY 2005

Approval of the Graduate School of Natural and Applied Sciences

---

Prof. Dr. Canan Özgen  
Director

I certify that this thesis satisfies all the requirements as a thesis for the degree of Doctor of Philosophy.

---

Prof. Dr. Tayfur Öztürk  
Head of Department

This is to certify that we have read this thesis and that in our opinion it is fully adequate, in scope and quality, as a thesis for the degree of Doctor of Philosophy.

---

Prof. Dr. Bilgehan Ögel  
Co-Supervisor

---

Prof. Dr. Alpay Ankara  
Supervisor

**Examining Committee Members**

Prof. Dr. Rıza Gürbüz	(METU,METE)	_____
Prof. Dr. Alpay Ankara	(METU,METE)	_____
Prof. Dr. Bilgehan Ögel	(METU,METE)	_____
Assoc. Prof. Dr. Hakan Gür	(METU,METE)	_____
Assist. Prof. Dr. Kazım Tur	(ÇANKAYA UNI.)	_____



**I hereby declare that all information in this document has been obtained and presented in accordance with academic rules and ethical conduct. I also declare that, as required by these rules and conduct, I have fully cited and referenced all material and results that are not original to this work.**

Name, Last name : **Caner Batigün**

Signature :

## **ABSTRACT**

### **DETERMINATION OF WELDING PARAMETER DEPENDENT HOT CRACKING SUSCEPTIBILITY OF 5086-H32 ALUMINIUM ALLOY WITH THE USE OF MVT METHOD**

Batıgün, Caner

Ph.D., Department of Metallurgical and Materials Engineering

Supervisor : Prof. Dr. Alpay Ankara

Co-Supervisor : Prof. Dr. Bilgehan Ögel

January 2005, 238 pages

Hot cracking is a serious problem that encounters during welding of aluminium-magnesium alloys. In the present study, solidification and liquation type of hot cracks in weld metal and the heat-affected zones of 5086-H32 aluminium alloy were investigated by using Modified Vareststraint Test (MVT) with TIG-AC and TIG-DC welding. With determining the size, type and number of cracks, a relation was established between welding line energy and strain on the hot crack formation. This information was used to determine the hot crack safe parameter ranges. The hot cracking tendency as a function of applied parameters were discussed in the frame of temperature fields around the moving heat source. Moreover, the characteristic hot crack locations on the 5086-H32 MVT specimens were generalized.

The results of the study indicated that the increase in line energy and strain increased the hot cracking tendency of the specified aluminium alloy. In the low line energy range, the main hot cracking mechanism is the solidification cracking which could be overcome by the use of a suitable

filler material. At high line energy range, due to the increased amount of interdendritic liquid, the amount of solidification cracking decreases by healing mechanism. However, because of the enlarged-temperature-field around the weld zone, fraction of HAZ cracking increases. The comparison between the hot cracking tendencies in low and high line energies indicates that the low line energy ranges with low augmented strains resulted in hot crack safer parameters.

Keywords: Welding, Modified Varestraint Test, Hot Cracking, 5086 Aluminium Alloy.

## ÖZ

### 5086-H32 ALÜMİNYUM ALAŞIMINDA KAYNAKLAMA PARAMETRELERİNE BAĞLI SICAK ÇATLAMA HASSASİYETİNİN MVT METODU İLE BELİRLENMESİ

Batıgün, Caner

Doktora, Metalurji ve Malzeme Mühendisliği Bölümü

Tez Yöneticisi : Prof. Dr. Alpay Ankara

Ortak Tez Yöneticisi : Prof. Dr. Bilgehan Ögel

Ocak 2005, 238 sayfa

Sıcak çatlama, alüminyum-magnezyum alaşımlarının kaynağı esnasında karşılaşılan ciddi bir problemdir. Bu çalışmada, 5086-H32 alüminyum alaşımının kaynak metali ve ısıdan etkilenmiş bölgesindeki katılma ve erime çatlakları, Modified Vrestraint Testi (MVT) yardımıyla araştırılmıştır. Test esnasında TIG-AC ve TIG-DC kaynak yöntemleri kullanılmıştır. Çatlak boyutu, tipi ve sayılarının tespitini takiben, sıcak çatlaklar ile hat enerjisi ve gerinim arasındaki ilişki ortaya konulmuş ve sıcak çatlak oluşumuna karşı güvenli parametre aralıkları belirlenmiştir. Ek olarak, uygulanan parametre setleri arasında meydana gelen sıcak çatlama eğilimi farkları, hareketli ısı kaynağı çevresindeki sıcaklık dağılımları çerçevesinde tartışılmıştır. Ayrıca, 5086-H32'deki karakteristik çatlak konumları genelleştirilmiştir.

Çalışma, hat enerjisi ve gerinimdeki artışın belirtilen alüminyum alaşımının sıcak çatlama eğilimini artırdığı sonucunu göstermiştir. Düşük hat enerjisi aralığında, esas sıcak çatlak mekanizması katılma çatlamasıdır. Bu çatlama, uygun bir dolgu malzemesi ilave edilerek önlenebilir. Yüksek hat enerjisi aralığında, dallantılar arasındaki sıvı miktarının artması sebebiyle

katılma atlaklarının oranı dşmektedir. Fakat, kaynak evresindeki sıcaklık alanının genişlemesi sebebiyle ısıdan etkilenmiş bölge atlaklarının oranı artmaktadır. Dşük ve yüksek hat enerjilerinde görülen sıcak atlama eğilimlerinin karşılaştırması, düşük ısı girdisi ve düşük gerinim değerlerinin sıcak atlamaya karşı daha emniyetli olduğunu işaret etmektedir.

Anahtar Kelimeler: Kaynak, Modified VarestRAINT Test, Sıcak atlama, 5086 Alüminyum Alaşımı.

## **ACKNOWLEDGMENTS**

The author would like to express his deepest gratitude to his supervisor, Prof. Dr. Alpay Ankara and co-supervisor Prof. Dr. Bilgehan Ögel for their guidance, advice, and supports in the completion of this study.

The author would like to thank Assistant Prof. Dr. Kazım TUR for his suggestions and comments.

The author is also grateful to the members of the METU Welding Technology and Nondestructive Testing Center, Mr. Zafer Filiz, Mr. Mehmet Tansal, Mr. Süha Tirkeş, Mr. İlker Kaşıkçı, Miss Özlem E. Güngör, Mr. Emin Mustaoğlu, Mr. Bedirhan Özener, Mr. Halil Öztürkler and Mr. Hüseyin Özdemir for their technical assistance.

Special thanks to Mr. Cengiz Tan for his valuable helps in scanning electron microscopy and Mr. Fatih Güner for his technical assistance.

A special note of thanks to the FNSS-Savunma Sanayi A.Ş. for her helps in providing the 5086 aluminium alloy sheets. And thanks to AS-Kaynak for the He gas.

Finally, author wishes his thanks to his family members for their patience and support.

## TABLE OF CONTENTS

PLAGIARISM .....	iii
ABSTRACT .....	iv
ÖZ .....	vi
ACKNOWLEDGMENTS.....	viii
TABLE OF CONTENTS .....	ix
LIST OF ABBREVIATIONS.....	xiii
CHAPTER	
1. INTRODUCTION .....	1
2. THEORETICAL BACKGROUND .....	4
2.1 Basic Microstructural Concepts of Welding .....	4
2.1.1 Solidification Concepts in the Weld Metal .....	4
2.1.2 The Weld Metal Neighbouring Zones .....	8
2.2 Hot Cracking in Weld Joints.....	9
2.2.1 Solidification Cracks .....	11
2.2.1.1 Theories about the Solidification Cracking in the Weld Metals.....	14
2.2.2 Liquation Cracks.....	23
2.2.1.1 Theories about the Liquation Cracking around the Weld Metals.....	26
2.3 Place of Varestraint and Modified Varestraint Tests among the Other Test Methods for the Assessment of the Hot Cracking Sensitivity .....	30
2.4 The Varestraint Test .....	32
2.5 The Modified Varestraint Test (MVT).....	32
2.6 Temperature Distribution around the Weld Pool.....	36
2.7 Tungsten Inert Gas Welding of Aluminium Alloys.....	39
2.8 Hot Cracking of Susceptibly of 5000 Series Alloys During Welding .....	42

3. MATERIALS, EXPERIMENTAL SETUP AND	
EXPERIMENTAL METHODS .....	46
3.1 Introduction .....	46
3.2 Properties of the Material Used .....	47
3.3 Experimental Setup .....	51
3.3.1 Modified Vastrestraint Test Equipment .....	51
3.3.2 Welding Equipment .....	55
3.3.3 Quench Test Setup .....	57
3.4 Experimental Methods and Procedure .....	58
3.4.1 Modified Vastrestraint Tests .....	58
3.4.1.1 MVT Specimen Preparation .....	59
3.4.1.2 Test Conditions .....	60
3.4.1.3 Reproducibility Tests .....	65
3.4.2 Heat Conduction Tests .....	65
3.4.3 Quench Tests .....	66
3.4.4 Weld Seam Width, Penetration Depth and Partially	
Melted Zone Width Measurements .....	67
3.4.5 Crack Length Measurements .....	70
3.4.6 Metallographic Investigation .....	70
3.4.7 Scanning Electron Microscope Investigation .....	72
3.4.8 Thermal analysis .....	73
4. RESULTS .....	74
4.1 General Weld Seam Features in the MVT Specimens of	
5086 Alloy .....	75
4.2 Results of the Weld Seam Profile Measurements .....	76
4.3 Results of the Crack Length Measurements .....	82
4.3.1 Results of the Crack Length Measurements on TIG-	
AC Welded MVT Specimens .....	83
4.3.1.1 Hot Cracking Tendency of TIG-AC Welded	
Specimens in Low Line Energy Range .....	89
4.3.1.2 Hot Cracking Tendency of TIG-AC Welded	
Specimens in Medium Line Energy Range .....	91



4.3.1.3 Hot Cracking Tendency of TIG-AC Welded Specimens in High Line Energy Range .....	92
4.3.2 Results of the Crack Length Measurements on TIG- DC Welded MVT Specimens .....	95
4.3.2.1 Hot Cracking Tendency of TIG-DC Welded Specimens in Low Line Energy Range .....	101
4.3.2.2 Hot Cracking Tendency of TIG-DC Welded Specimens in Medium Line Energy Range .....	102
4.3.2.3 Hot Cracking Tendency of TIG-DC Welded Specimens in High Line Energy Range .....	103
4.3.3 Results of the Supplementary Tests .....	106
4.4 Results of the Reproducibility Tests .....	108
4.5 General Features of the Hot Cracks in 5086 Aluminium Alloy MVT Specimens .....	109
4.6 Results of the BTR Measurements .....	113
4.7 Results of the Secondary Interdendritic Spacing Measurements .....	116
4.8 Results of the Thermal Analysis .....	120
4.9 Results of the Quench Tests .....	122
4.10 Results of the SEM Investigations .....	127
4.11 Results of the Optical Microscope Investigations .....	134
5. DISCUSSION .....	142
5.1 Weld Seam Characteristics in the 5086 Alloy MVT Specimens .....	142
5.2 Hot Cracking Behaviour in the TIG-AC and TIG-DC Welded MVT Specimens .....	145
5.2.1 Hot Cracking Behaviour in the TIG-DC Welded 5086 Alloy MVT Specimens .....	146
5.2.2 Hot Cracking Behaviour in the TIG-AC Welded 5086 Alloy MVT Specimens .....	149
5.3 Precipitates Observed During Cooling in 5086 Alloy .....	151
6. CONCLUSIONS .....	154

REFERENCES.....	156
APPENDICES	
A. STANDARD MODIFIED VARESTRAINT TEST PROCEDURE ..	162
B. CRACK MEASUREMENT RESULTS.....	164
CURRICULUM VITAE.....	237

## LIST OF ABBREVIATIONS

$\alpha$ :	Solid solution
$\lambda$ :	Heat conductivity
$\eta$ :	Efficiency in weld heat input
$\theta$ :	Dihedral angle
$\Delta T$ :	Solidification temperature range
$A$ :	Amperes
$AC$ :	Alternating current
$Al$ :	Aluminium
$BAM$ :	Bundesanstalt für Materialforschung und -prüfung
$C_0$ :	Solute content of an alloy
$C_E$ :	Eutectic composition
$C_x$ :	Compression zone
$cm$ :	Centimeters
$Cr$ :	Chromium
$DC$ :	Direct current
$DCEP$ :	Direct current, electrode charged with positive polarity
$DCEN$ :	Direct current, electrode charged with negative polarity
$DSC$ :	Differential scanning calorimetry
$E$ :	Line energy
$Fe$ :	Iron
$f_s$ :	Fraction of solid
$f_L$ :	Fraction of liquid
$G$ :	Temperature gradient
$G_L$ :	Temperature gradient in liquid
$gr$ :	Grams
$HAZ$ :	Heat affected zone
$HCl$ :	Hydrochloric acid
$HCS$ :	Hot cracking sensitivity

$HNO_3$ :	Nitric acid
$I$ :	Welding current in the welding circuit
$I_w$ :	Welding current in the welding circuit
$IIW$ :	International Institute of Welding
$k$ :	Partition coefficient
$kJ$ :	Kilo Joules
$L$ :	Liquid
$MAG$ :	Metal active gas welding process
$Mg$ :	Magnesium
$MIG$ :	Metal inert gas welding process
$min$ :	Minutes
$ml$ :	Milliliters
$m_L$ :	Slope of the liquidus line in a phase diagram
$MMA$ :	Manual metal arc welding process
$Mn$ :	Manganese
$MVT$ :	Modified Vrestraint Test
$PMZ$ :	Partially melted zone
$R$ :	Bending former radius
$R$ :	Growth rate
$R_S$ :	Growth rate in solid-liquid interface
$S$ :	Amount of augmented strain
$S$ :	Solid
$SEM$ :	Scanning Electron Microscope
$sec$ :	Seconds
$SLV$ :	Schweißtechnische Lehr und Versuchsanstalt
$Si$ :	Silicon
$T$ :	Temperature
$T_E$ :	Eutectic temperature
$T_F$ :	Fusion temperature
$T_L$ :	Liquidus temperature
$T_M$ :	Melting temperature
$T_S$ :	Solidus temperature

$T_x$ :	Tension zone
$T_V$ :	Solvus temperature
$t$ :	Specimen thickness
$t_r$ :	Stress relaxation period in the mushy zone
$t_v$ :	Period of time for the mushy zone formation
$TIG$ :	Tungsten inert gas welding process
$U$ :	Potential difference across the arc
$V$ :	Volts
$v_w$ :	Relative welding speed
$X_L$ :	Displacement in liquid from the solid-liquid interface

## **CHAPTER I**

### **INTRODUCTION**

Aluminium alloys are taking the role of steels in engineering structures in an increasing trend because of their good mechanical properties in combination with lower density and higher corrosion resistance. Since welding is widely used in joining processes of constructional components, overcoming the welding related problems is important in structural components of aluminium alloys. Among these problems, hot cracking during welding has been the major, persistent problem. Because of high crack sensitivity of the aluminium alloys, depending on the loading conditions, hot cracks may become initiation sites of any sudden or delayed failure of a component. Consequently, studies on the welding parameters, which can lead to the hot cracking problems, necessitate a study on the hot cracking mechanisms and their prevention, for constructional safety in industrial applications.

Research studies on the welding related hot cracking problem of various aluminium alloys were started in fifties. However, the development of recent hot cracking tests was started from the seventies and improved gradually with the increasing use of aluminium in the manufacturing industry [1]. The common point of the hot cracking tests is the use of a cracking media, which has an external or internal loading nature to produce cracks on the specimen surface during welding. Although the stressing conditions have similar aim, there are considerable differences between the hot cracking test methods in metallurgical and mechanical point of view. The Modified Varestraint Test (MVT) is one of the recent hot cracking test methods, and therefore selected for the present study. MVT was mainly developed to overcome the expensive specimen preparation and the time consuming long crack analysis periods. The process has also

been used successfully on the high alloy steels and nickel and copper based alloys. Although there are reports about hot cracking tests in some aluminium alloys with different hot cracking methods, there is no adequate report about the Modified Varestraint Test of the aluminium alloys in which the metallurgical factors are being considered. Moreover, existing literature has no information about the applicable heat input range for the consistency in hot cracking testing of the aluminium alloys.

Present study was initiated with the Modified Varestraint Tests that were performed in cooperation with the Federal Material Test Institute BAM-Berlin [2, 3]. As a result of that initial study, it was reported that the hot cracking tendency is closely related with the grain size of the parent material. In addition, the hot cracking tendency of different group of aluminium alloys can be classified from low tendency to high tendency as 1xxx, 3xxx, 5xxx and 7xxx series alloys. Here, 7xxx series Al alloys presented high hot cracking tendency even at the small amounts of augmented strain values. The conclusions about the 1xxx, 3xxx, 5xxx series aluminium alloys were verified with the study of Caymaz [4] who made Modified Verestraint Tests on non-heat treatable aluminium alloys on three different welding conditions.

In the light of the previous studies, 5086 type aluminium alloy that has a moderate hot cracking tendency among other series of aluminium alloys was selected to study the hot cracking behaviour in Modified Varestraint Test along the complete weldability line energy range. It is aimed to identify the hot cracking mechanisms of this aluminium alloy in MVT and to establish the hot crack safe welding conditions for the industrial applications. Besides the experimentally preferred TIG-DC welding under He-Ar mixture shielding, for a better industrial adaptation industrially preferred TIG-AC welding under Ar shielding was also applied as an heat input means in the tests. For that purpose, 165 sets of welding and bending experiments, and 30 sets of welding experiments without bending

were executed. After the standard crack analysis, metallurgical aspects were discussed with the use of heating and quenching experiments. The study was supported with optical metallography and scanning electron microscope investigations.

The results of the study showed that the hot-cracking tendency of 5086 alloys increases with the increase in line energy of welding. Modified Varestraint Test with low line energies give more consistent temperature distribution and better fit with the theory. The increase in line energy changed the mechanism of hot cracking. At low line energies, the main hot-cracking mechanism is the solidification cracking. As the line energy increases, liquation cracking gains more importance. On the other hand, the increase in augmented strain increases the hot-cracking tendency too.



## **CHAPTER II**

### **THEORETICAL BACKGROUND**

#### **2.1 Basic Microstructural Concepts of Welding**

In a weld zone there are mainly three different regions that can be distinguished microstructurally: Weld metal, heat affected zone and the unaffected base metal. The weld metal is the zone, where the base metal and filler material were heated over the melting temperature, form a molten weld pool and solidified thereafter. In case of an autogeneous welding, a weld pool is formed by melting only the base metal. A solidification structure is observed in the weld metal zone. On the other hand, the heat affected zone (HAZ) is the weld metal neighbouring base metal zone where mainly two distinguishable characteristic changes can be seen. In the first part of the HAZ, the heat of welding causes partial melting of the base metal. In the second part, microstructural changes occur in the base metal. The partial melting zone (PMZ) normally occurs in the alloys having a wide solidification range. This portion of the HAZ is located immediately outside the weld metal. Possible phase transformations, the resultant microstructure and the properties of the weld and HAZ were strongly affected by the heat flow during welding. Basic concepts about these two zones will be presented in the next two subsections.

##### **2.1.1 Solidification Concepts in the Weld Metal**

Weld metal microstructure is affected externally by the heat input to the weld zone and the heat flow towards the base metal during the welding process. Both of these determine the weld pool size and shape, which may have an effect on the weld metal composition as well. Like all solidification processes, weld metal solidification includes nucleation, grain formation and grain growth steps. There are several nucleation mechanisms during

weld metal solidification. Among these heterogeneous nucleation has a great probability in the weld pool solidification since the grains have a chance of epitaxial growth from the partially melted grains in the HAZ. Further weld metal microstructure and chemical inhomogeneities can be explained with the help of basic solidification concepts that depend on alloy composition, such as solute redistribution, and constitutional super cooling (Figure 2.1). Alloy composition, together with heat input and heat flow rates totally have an effect on the solidification mode of the weld metal. [5]

In general, different solidification modes presented in Figure 2.1 can be seen in the most of the alloys. All these modes are related with the constitutional super cooling which depends on two factors: The temperature gradient in liquid ( $G$ ) and growth rate of the weld metal grains ( $R$ ). Figure 2.2 summarizes the effect of temperature gradient  $G$  and the growth rate  $R$  on the solidification microstructure of alloys. Here, the ratio of  $G/R$  determines the solidification mode and the product of  $G$  and  $R$  gives the size of the solidification microstructure. [6]

In addition, weld metal microstructure is affected by the welding speed related weld pool shape. The shape of the pool is kept constant by having a balance between the rate of melting and the rate of solidification. The weld pool elongates or decreases in diameter depending on this balance. The resultant possible weld microstructures can be seen in Figure 2.3. Since the maximum temperature gradient and the direction of maximum heat removal is on the normal direction of the solid-liquid interface, solidification occurs in that direction.

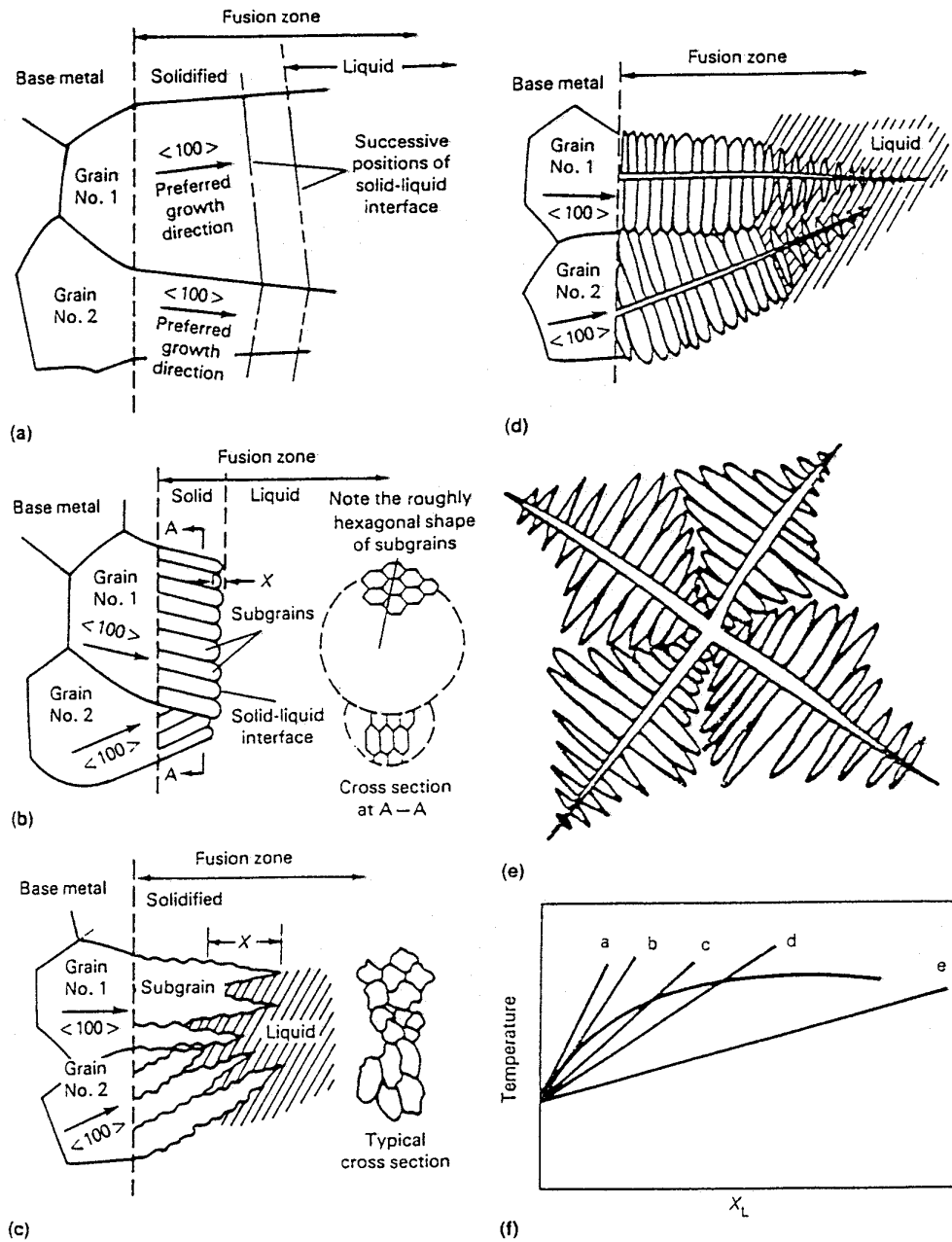


**Figure 2.1:** Microstructure of solid-liquid interface for different modes of solidification and the temperature gradients that generate each of the different modes. (a) Planar growth. (b) Cellular growth. (c) Cellular dendritic growth. (d) Columnar dendritic growth. (e) Equiaxed dendrite. (f) Five temperature gradients versus constitutional super cooling.  $X_L$  is the displacement in liquid from the solid-liquid interface. [5]

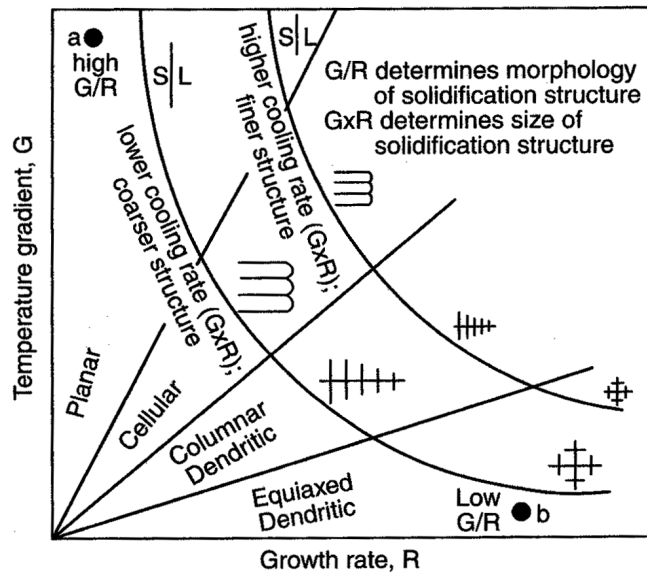


**Figure 2.2:** Effect of temperature gradient  $G$  and growth rate  $R$  on the morphology and size of solidification microstructure. [6]

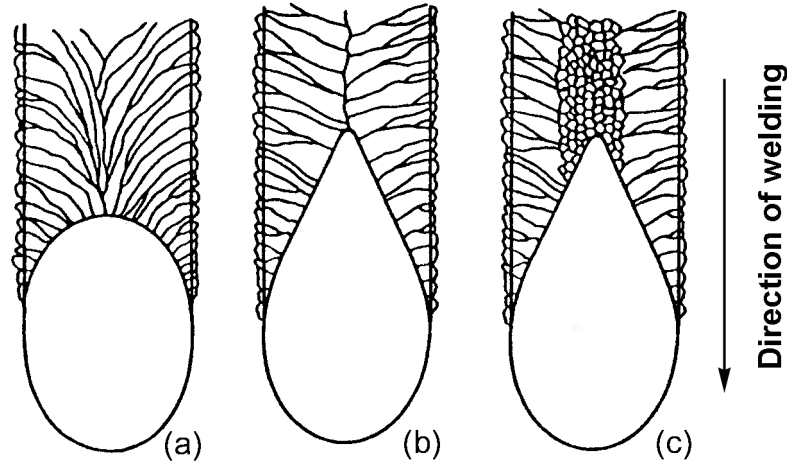


**Figure 2.3:** Effect of heat input and welding speed variations on weld grain structure. (a) Low heat input and low welding speed: Elliptical weld pool. (b) High heat input and high welding speed but not sufficient yet to cause heterogeneous nucleation: Tear-drop-shaped weld pool. (c) High heat input and high welding speed with heterogeneous nucleation. [5]

The temperature gradient and the growth rate are not constant along the solid-liquid interface as shown in Figure 2.4. In general, higher temperature gradient and lower growth rates obtained during weld solidification result in planar solidification at the sides of the weld pool. However, the extend of the non-planar solidification increases towards the center of the weld pool due to the decrease in temperature gradient and increase in growth rate [5] (Figure 2.2).

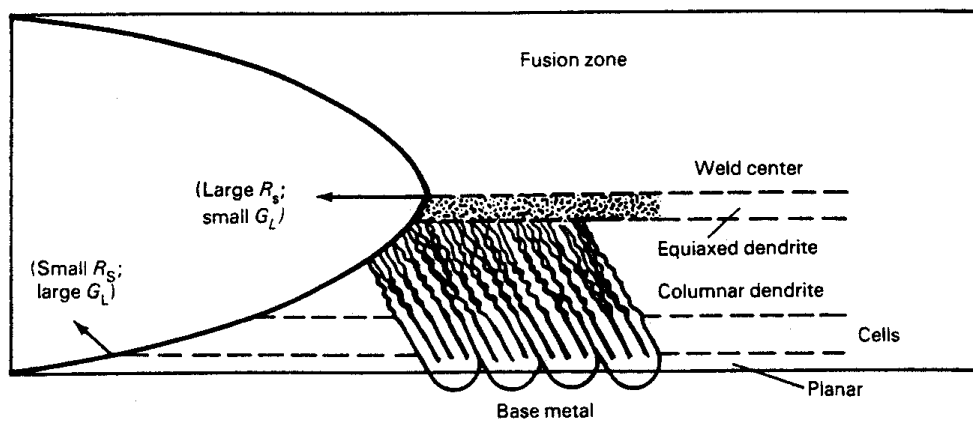


**Figure 2.4:** Variation of microstructures in response to variation of the solidification rate around the weld pool [5]

### 2.1.2 The Weld Metal Neighbouring Zones

The zone immediately outside the weld area is called as the partially melted zone (PMZ). This is seen in alloys with a wide solidification interval, such as aluminium alloys. Besides partial melting, grain growth and precipitation can also be seen in this area. Next to this zone towards the base material the highest temperature reached decreases gradually from the solidus temperature of the alloy to the environmental temperature if an infinitely large plate is assumed. As a result, extend of the associated microstructural changes decreases also in parallel to the temperature

distribution towards the base material. In aluminium alloys, especially the partially melted zone has a great importance for the liquation cracking.

Besides the subject of PMZ, aluminium alloys have other problems in the heat affected zone according to the strengthening mechanism that is associated with the composition of the alloy. Solution hardening, work hardening and precipitation hardening are several ways that can strengthen aluminium-based metals. Welding heat can reduce the effectiveness of the mentioned last two methods in the heat affected zone (HAZ). Solution hardened materials are usually less affected from the heat of welding unless they have been work hardened. Work hardened materials, on the other hand, usually show recrystallization and grain growth in HAZ, which will reduce the strength of that area considerably. The strength gained from work hardening will be lost in this manner. The initial strength in the heat affected zone can not be recovered again unless a deformation process applied at this location. Like work hardened materials, in precipitation hardened aluminium alloys the material loose its strength and ductility in HAZ. But this reduction in strength and ductility can be recovered with a suitable post weld aging procedure. [7]

## **2.2 Hot Cracking in Weld Joints**

Hot cracking is a phenomenon of crack formation in the weld metal and in the Heat Affected Zone (HAZ) (especially in the PMZ) depending both on the mechanical and metallurgical factors during welding.

Mechanical factors are mainly related with the contraction stresses and the degree of restraint. These factors depend on thermal strains, material size and thickness, weld joint design and size and shape of the weld pool. The non-uniform temperature distribution of welding around the weld zone generates stresses due to the different thermal gradients. Localized tensile

stresses support the crack formation. In the frame of mechanical factors only, normally there is a direct relationship between the hot cracking susceptibility and the present level of the stress and strains.

On the other hand, metallurgical factors are mainly related with the presence of a liquid phase at the grain boundaries during a specific temperature interval of freezing or melting. These factors can be listed as, solidification temperature range, amount and distribution of liquid at the last stages of solidification, primary solidification mode, surface tension of the grain boundary liquid and solidifying grain structure. Metallurgical factors are directly or indirectly depend on weld metal composition. However, metallurgical factors are not effective without the presence of the mechanical factors.

Hot cracks may be formed both in the heating and in the cooling period of the weld zone. In accordance with this fact, hot cracking in aluminium alloys may be classified into two main categories based on the mechanism responsible for cracking and the crack location: Liquation cracks and solidification cracks. The solidification cracking takes place within the weld fusion zone. If a solidifying structure, which is at the final stage of solidification, encounters tensile stresses such as from the solidification shrinkage strains, a tearing may form in the structure. Here, mainly a low melting point liquid phase is formed on the grain boundaries that have a brittle nature. After exceeding a critical amount of shrinkage stress and deformation rate, this phase may tear off and form the "solidification crack". On the other hand, liquation cracks occur adjacent to the fusion zone, i.e. starting from the partially melted zone. Because of their nature, solidification and liquation cracks are also designated as segregation cracks. They are mainly associated with the existence of low melting point phases along the grain boundaries. Therefore, hot cracks are typically always extending in an intergranular or intercellular manner.

Weld joint cracking is a serious problem, which may lead to the complete failure of the whole structure or system during the service life. Moreover, the cracks may act as the initiation sites for corrosion in appropriate corrosive environments. In practical applications, existence of hot cracking is difficult to detect even by non-destructive testing. This is true especially for the liquation cracks, which mainly occur as micro cracks that often do not even reach the surface of the material. A reliable method to prove the presence of hot cracks is the macro or micro metallography. Generally, the approval of welding procedure specifications requires micro and macro examinations for the hot crack susceptible materials. On the other hand, there is variety of solidification crack susceptibility tests to detect the HCS degree of a material.

### **2.2.1 Solidification Cracks**

These types of cracks are formed in weld metal, especially on the weld centerline or along the columnar grain boundaries, during the last stages of weld metal solidification (Figure 2.5). The causes of solidification cracking are explained with the segregation at the columnar grain boundaries and in front of the advancing solid-liquid interface in combination with the stresses acting on them. That means, as stated in Section 2.2, solidification cracking susceptibility of a weld metal depends on metallurgical and mechanical factors.

Segregants are low melting point phases or eutectics generally producing highly wetting films along the grain boundaries. The film formation stage, which is the final stage of solidification refers to a fraction of solid " $f_s$ " close to 1 at which a coherent interlocking solid network along the grain boundaries form. The size of the zone that contains a liquid film network on the grain boundaries is determined by the solidification temperature range, which increases with the impurities or the intentionally added alloying



elements. As a final effect, there is a direct relationship between the size of the film formation zone and the solidification cracking susceptibility of an alloy. [8]

Consequently, solidification cracks are formed, when the strains arising from solidification shrinkage and thermal contraction exceed the ductility of the almost solidified weld metal. If there is sufficient amount of remaining liquid present, the formed cracks can possibly be healed by liquid flow. Otherwise, the cracks will remain opened on the grain boundaries. Solidification cracks usually reach to the surface of the weld metal. They are mostly a few millimetres in length.

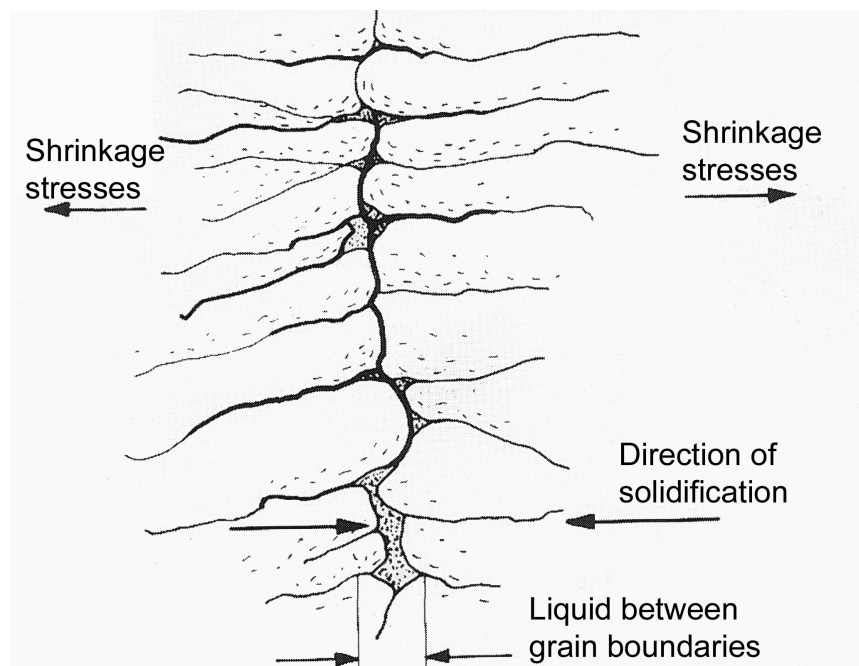


**Figure 2.5:** Solidification crack formation model in weld metal. (According to Pellini) [9]

Segregation is unavoidable in weld metal solidification of alloyed materials. However, the amount and as a result, the effect of segregation during the solidification can be controlled. For example, coarse columnar dendritic microstructures have a higher susceptibility to hot cracking than a fine equiaxed dendritic structure with high amount of interdendritic liquid. The reason for that is the higher segregation formation tendency in the coarser solidification structures. The size of the solidification microstructure depends on the solidification type, which is associated with the growth rate and the temperature gradient. High-speed welding processes produce finer cell spacing with lower segregation. On the other hand, lower welding speeds produce coarse microstructures. Besides the size of the structure, ductility of the solidifying weld metal is also important. A less ductile solidifying weld metal will most likely crack during solidification.

Impurities or alloying elements that have the affinity to cause solidification cracking have several characteristics: They have a low partition coefficient " $k$ " which is the ratio of the mole fractions of solute in solid and liquid that coexist with one another at a given temperature. They form compounds with the base metal. These compounds generally have a low melting point or form eutectics with the base metal. Finally, they have a low "wetting angle" with the grain boundaries of the final material. As a rule, the higher the surface tension of the grain boundary liquid, the larger is its dihedral angle. The susceptibility decreases with increasing dihedral angle of the grain boundary liquid (Figure 2.6). [8]

The joint geometry is effective on the solidification cracking susceptibility due to the stresses left in the structure. The residual stresses in the weld are being left because of the thermal cycle of the welding process. The level of these stresses depends on the restraint degree caused by the weld joint. For example, thicker and stronger parts cause high residual stresses, therefore more tendencies to hot cracking.

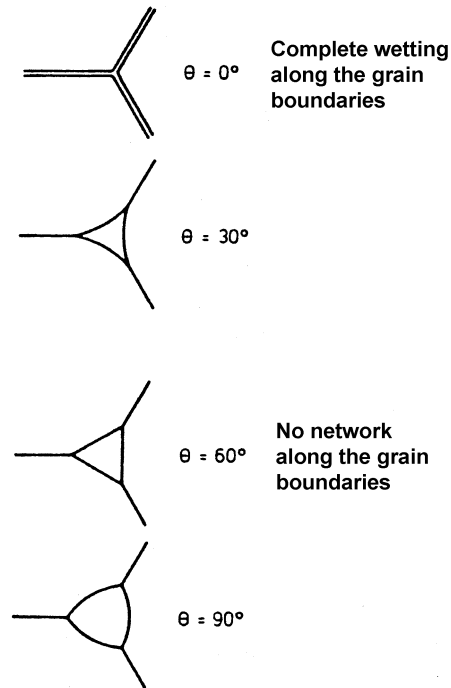


**Figure 2.6:** Wetting angles of the liquid phases. [9]

### 2.2.1.1 Theories about the Solidification Cracking in the Weld Metals

There are three theories to explain the solidification cracking in the alloys: “Shrinkage brittleness”, “strain” and “super solidus cracking” theories [10]. Based on these theories, several hot cracking models were developed.

First, the shrinkage-brittleness theory suggests that hot cracks develop during the mushy stage, if a critical level of strain is exceeded, causing the coherent network of dendrite cracking to relieve the strain. In this theory the range where the cracks can be formed is defined as the “brittleness temperature range” (BTR). According to Prochorov [11], all materials, which solidify over a temperature interval, have a brittleness temperature range. This range has an upper and a lower temperature limit. The upper boundary of BTR is called “the coherent temperature” where the

interdendritic liquid flow is restricted. The lower boundary of BTR is the temperature at which the strength of the grain boundaries is sufficient to absorb the stresses acting on them (Figure 2.7).

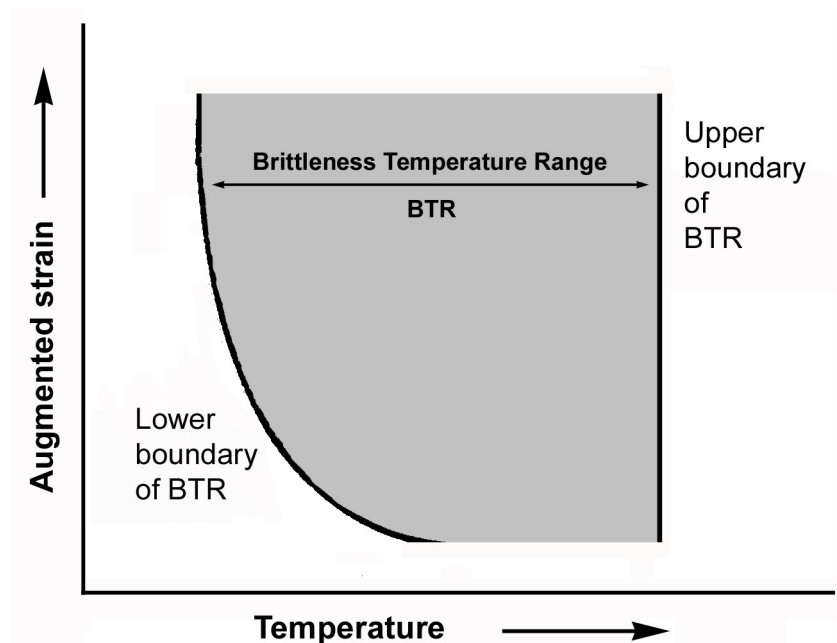


**Figure 2.7:** Schematic representation of the temperature and strain dependence of the brittleness temperature range (BTR) [12]

The shrinkage brittleness theory was developed mainly from studies of cracking behaviour in aluminium alloy castings and welds. The theory can be explained with the help of Figure 2.8 [11]. In this figure following stages can be distinguished:

- Stage 1: Nucleation of first dendrites (Area “acd”). There are only a few dendrites in the liquid and they move without any restriction. In this stage, hot crack formation is not possible.

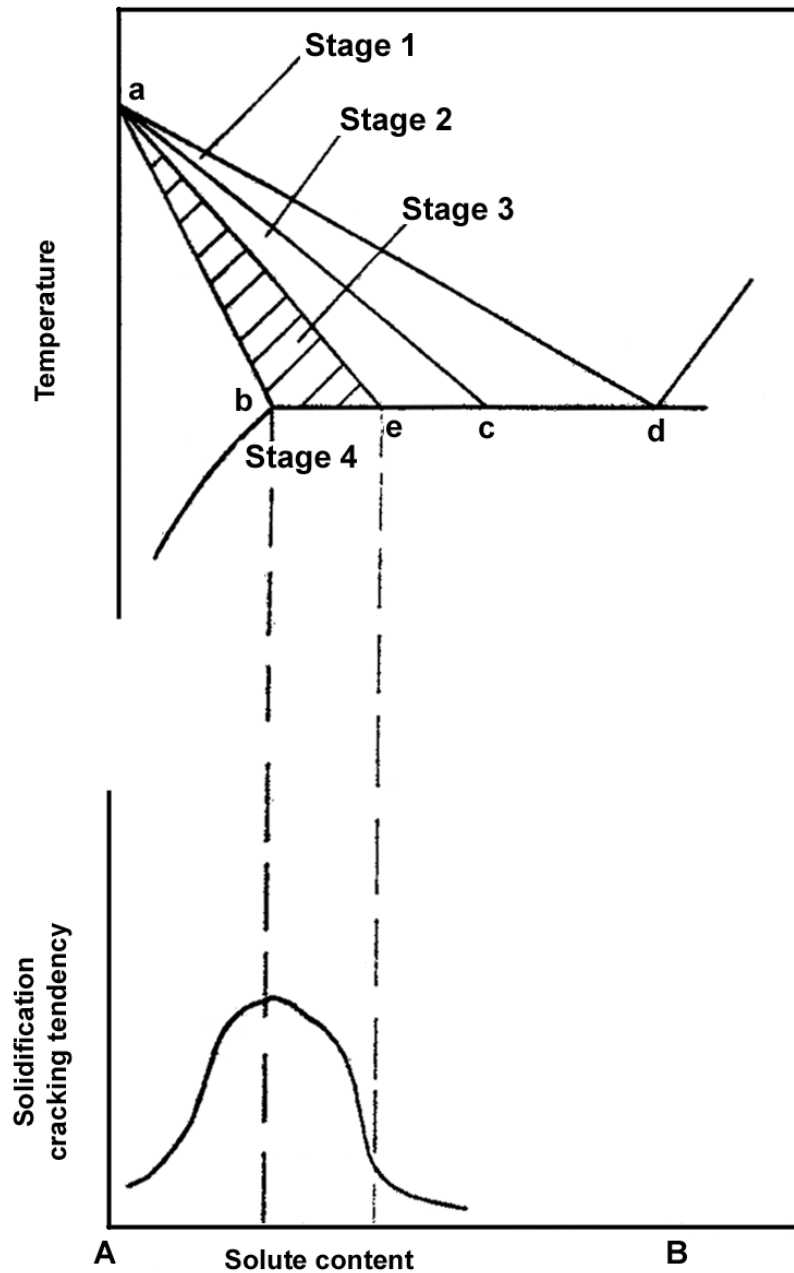


**Figure 2.8:** Concepts of shrinkage brittleness theory as modified by Borland. [11] Key: a-c, coherent temperature; a-e critical temperature; a-c-b, brittle temperature range; Stage 1, dendrites freely dispersed in liquid, no cracking; Stage 2, solid-solid bonding, “liquid healing” possible if cracks form; Stage 3, critical solidification range, no “healing” of cracks possible if fracture strain exceeded; Stage 4, solidification, no cracks.

- Stage 2: Dendritic growth (Area “ace”). Dendrites are in partial contact, but, the liquid has the ability to flow between the dendrites freely. In this stage, possibility of crack healing through liquid flow is high.
- Stage 3: Grain boundary formation (Area “abe”). An almost complete solid network along the grain boundaries is formed. The remaining liquid is enclosed between the dendrites and the liquid flow is limited. In this stage, if the fracture strain of grain boundaries is exceeded, no healing of cracks through liquid flow is possible.
- Stage 4: Solid structure. In this stage, all the structure is already solidified. Therefore, hot cracking is not possible.

It was stated that, the hot cracks start to form in stage 2, where the dendrites start to built a network. As the solidification continues, shrinkage stresses are concentrated on the dendrite network. When the tensile strength of the dendrites is exceeded, cracks can be formed. Since the amount of the interdendritic liquid is sufficient and its flow is not limited, crack healing through liquid fill up is possible. In the third stage, which is the critical solidification range, the amount of interdendritic liquid is quite low and due to the flow limitations, formed cracks will not be healed. Because of this fact, the third stage is the main stage for the hot crack formation and therefore alloy compositions between b and e (Figure 2.8) are sensitive to hot cracking. Eutectic alloys does not form hot cracks because of the discussion stated above. Starting from the upper limit of the last stage, all the structure has completed the solidification. Therefore, below the lower limit of third stage formation of hot cracks is not possible.

Nakata and Matsuda performed a comprehensive study on the BTR measurements on aluminium alloys. According to their studies, BTR was obtained by trans-varestraint tests together with a thermal analysis to measure the cooling rate. [13]

The strain theory of hot tearing on the other hand, suggests that cracking does not occur in the mushy stage of solidification since the shrinkage stresses are uniformly distributed. Cracking only takes place when the film stage is reached and localized strains by thermal gradients are too high. According to the strain theory of Pellini [14-15], the HCS of an alloy is dependent upon the interval between the liquidus and the solidus temperature. The alloying elements and the impurities can change the length of this interval (Figure 2.9). Theory of Pellini also applies to the HAZ cracking which will be presented in Section 2.2.2.1.

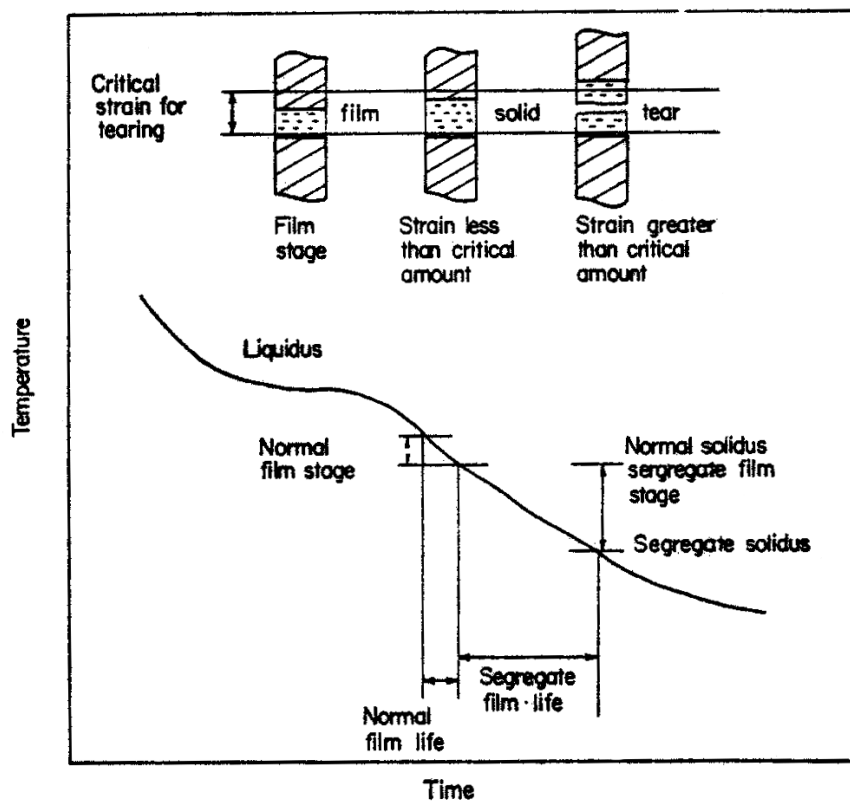


**Figure 2.9:** Low melting-point segregates located at grain boundaries promote hot cracking by increasing the time that the weld metal remains in liquid film stage (According to Pellini's theory). [15] Diagram showing the critical strain is needed for tearing of liquid film according to Pellini's strain theory [11]

At a parallel study to strain theory, Chihoski [16-17] has attempted to describe the nature of the stresses around a moving heat source. In his study, it was concluded that there are tension (T), compression (C) and zero (0) zones around a weld pool. Due to the thermal expansion from the preheat in front of the welding torch, a compression cell ( $C_1$ ) forms ahead of the weld pool. In reaction to this compressive stress, a tension zone ( $T_1$ ) appears next to the compressive zone ( $C_1$ ). Just behind of the weld pool, a tension over mushy zone ( $T_M$ ) is formed due to the shrinkage arising from the solidification. As a result of thermal expansion, a compressive zone ( $C_2$ ) and another tension zone ( $T_2$ ) are followed the weld pool as shown in Figure 2.10.

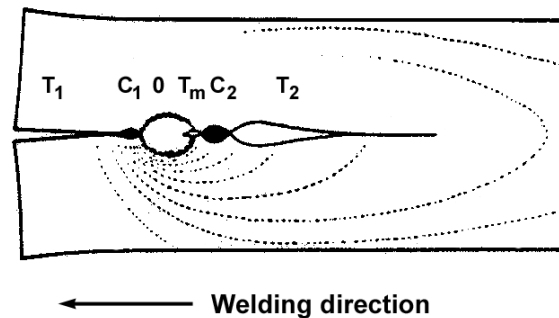


**Figure 2.10:** Nature of the transverse stresses around a weld pool according to the study of Chihoski [16].

In the study of Chihoski [16-17], it was also suggested that the lower welding speeds cause the ( $C_1$ ) to increase in size which causes the combination of the tension in the mushy zone ( $T_M$ ) and the ( $T_2$ ). As a result, all transverse stresses behind the weld pool will be tensile.

A more recent parallel study about the stress distribution around the solidifying weld pool was performed by Zacharia [10] who studied the influence of dynamic stresses, induced by thermal and mechanical loading, on weld metal hot cracking. He stated that hot cracking in a full-penetration



weld subjected to external restraint initiates at a location separated from the molten pool. The compressive stress immediately behind the pool prevents the formation of hot cracks at the edge of the weld pool (Figure 2.11). At a discrete distance behind the weld pool, the transverse stress changes from compressive to tensile. In this zone, if liquid is present, it is likely that hot cracks will form.

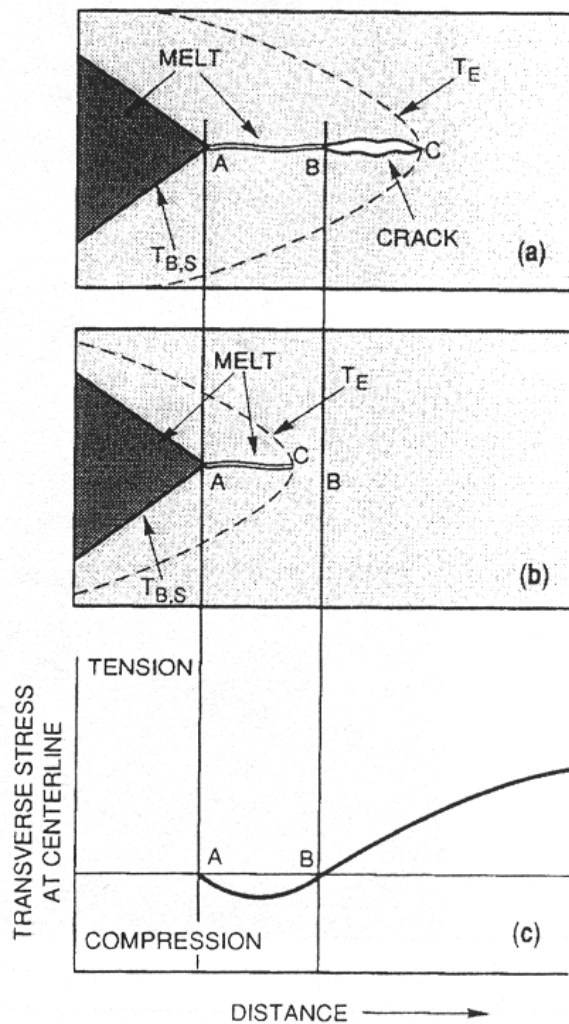


**Figure 2.11:** Schematic representation of the relationship of dynamic stresses observed in hot cracking behaviour study of Zacharia. [10]

These studies state that the presence of a compressive stress behind the weld pool would prevent separation of the weld at the trailing edge. In addition, changes in the thermal distribution (welding speed, heat input, etc.) and external restraint can also shift the transition location from compression to tensile stresses, influencing the hot cracking behavior. Factors such as mechanical restraint, thermal distribution, and plastic deformation can alter the local stress distribution near the weld pool.

The results of the study of Zacharia indicated especially the aspects about weld centerline cracking. He proved with the study that weld metal hot cracking is because of the presence of small quantities of liquid residing at solidification boundaries and at the same time, being subjected to tensile strains. Therefore, there is a dynamic relationship between the metallurgical and mechanical factors, which can be influenced by the welding conditions and mechanical restraint.

Johnson [18] also tried to characterize the transient strain fields around a moving welding arc. He studied principal and shear strains around gas tungsten arc (TIG) welds using a projected-grating Moiré fringe strain analysis technique. He concluded that the strain patterns correlate well with the temperature distribution around the moving weld pool. Due to the much steeper temperature gradients there, the compressive stresses will be much more intense in front of the arc than behind it. This asymmetry of compressive stresses means that when plastic flow occurs, there will be a net shifting of metal rearward, in order to reduce the unbalanced front-to-rear stress pattern. The effect of temperature distribution on the rearward deformation can be seen in Figure 2.12.

Johnson [18] suggests that the straining around the arc consists mainly of shear strain. The normal strains are much smaller. The planes of maximum shear strain are oriented almost exactly parallel and perpendicular to the weld bead.

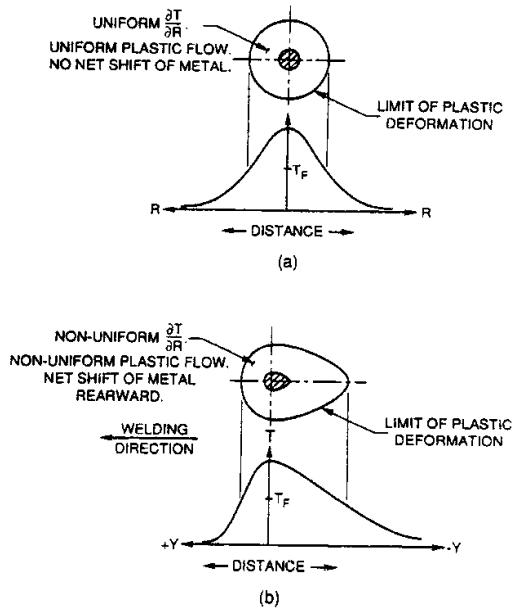


**Figure 2.12:** Comparison of thermal effects for a stationary (a) and a moving (b) heat source. [18]

The third hot cracking theory “super solidus cracking (generalized theory)” was suggested by Borland. It includes the relevant ideas from both the shrinkage brittleness and strain theories. According to the generalized theory, the presence of a wide freezing range was not a sufficient condition for the cracking to occur, in addition, high stresses should be built up between grains. That means, cracking can occur in regions where high stresses can be built up between grains or where by reasons of lack of constraints at free surfaces a parting of the liquid phase can occur as a result of the development of highly localized strains. Depending on this argument, there are three different possible situations:

- (1) Necking of liquid films, which are open to free surfaces;
- (2) Rupture of highly stressed thin liquid films;
- (3) Breaking of solid-solid bridges.

The third case was considered to be appearing most likely in industrial welding conditions. The generalized theory lies very close in concept to the strain theory but it does not disregard the possibility of cracking occurring in the mushy stage. The concept of generalized theory is that in most practical situations cracking takes place after a small amount of solid-solid bridging has occurred. [18]

In another study, Clyne and Davies [19] have introduced a HCS criterion, which is equal to  $t_v/t_r$ , where  $t_v$  is the period of time between the begin and end of the mushy zone and  $t_r$  is a normalization time during which stresses in the mushy zone can be relaxed. Here,  $t_v$  has chosen as the time difference separating the instants at which a volume of solid of 0.9 and 0.99 is reached.

Rappaz *et al* proposed a new criterion for the appearance of solidification cracking in metallic alloys [19]. In this theory, a hot-cracking sensitivity (HCS) index is defined with the help of a critical deformation rate beyond which nucleation of a first void occur. This critical value is an increasing function of the thermal gradient and a decreasing function of the viscosity of the interdendritic liquid. The shrinkage is directly associated with the tensile deformation of the dendritic skeleton. But, the HCS criterion of Rappaz *et al* is based only upon the appearance of a first void during the solidification of the material and not on crack propagation.

### **2.2.2 Liquation Cracks**

Liquation cracking is associated with the melting of the grain boundaries near the fusion line (Figure 2.13). The neighbouring area of the weld pool either in the base material (PMZ) or in adjacent weld bead is heated until its solidus temperature. The phases or segregations on the grain boundaries, whose melting points are lower than that of the parent material, are transferred into liquid form. This liquid may form a network

around the grain boundaries and makes them weaker against the tensile stresses, such as shrinkage or external stresses.

Liquation cracking occurs in the partially melted zone (PMZ), which is a region immediately outside the weld metal. Like solidification cracking, the nature of the cracking is intergranular too. In some cases, liquation cracking along the fusion boundaries is also possible.

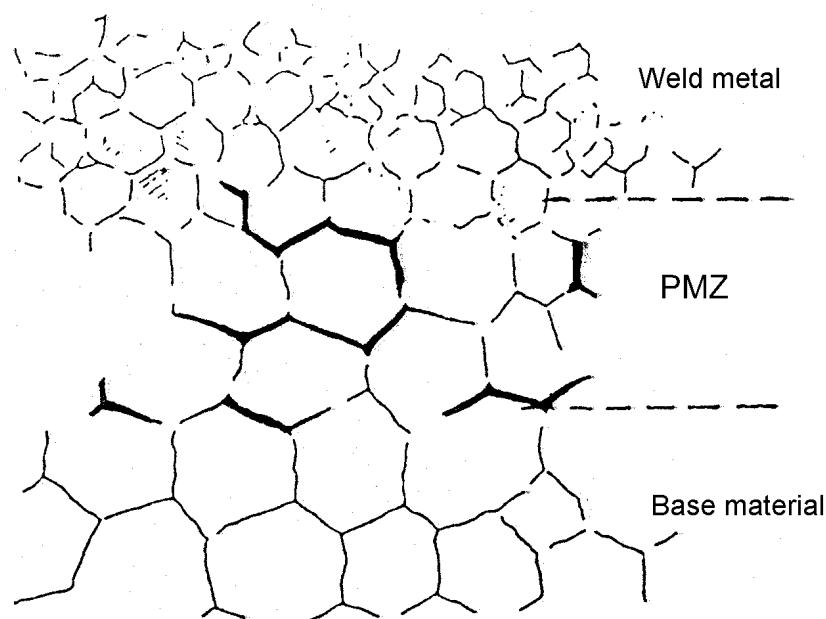


**Figure 2.13:** Liquation crack formation model. [8]

The origin of the segregation in liquation cracking is quite different from that of solidification cracking. Melting of grain boundaries at the fusion line occurs at temperatures between the solidus and liquidus boundaries. Since melting nucleates preferentially at high-energy crystal defects, such as surfaces and boundaries, there is a gradual increase in grain boundary melting in terms of width and length in the PMZ as one approaches to

melted zone. Impurities of low solubility in the matrix or from melted back inclusions near the fusion line tend to diffuse to the melted boundaries.

On cooling, these segregants form films of low melting point grain boundary compounds or even low melting point eutectics. In this respect, the criteria that govern liquation cracking are thus similar to those discussed in the solidification cracking.

Liquation cracking is dependent on the amount and type of impurities in the base metal, the volume fraction and density of inclusions and degree of restraint. The residual stresses are dependent on the strength and thickness of the plates being welded.

Because of the high cooling rate, equilibrium solidification does not take place during welding. In this non-equilibrium solidification, the fraction of liquid  $f_L$  at any given temperature  $T$  can be expressed as in the following equation [6]:

$$f_L = \left( \frac{(-m_L)C_0}{T_m - T} \right)^{\frac{1}{1-k}} \quad \{1\}$$

Where  $m_L$  ( $< 0$ ) is the slope of the liquidus line in the phase diagram,  $C_0$  solute content of the alloy,  $T_m$  the melting point of pure aluminium (933.4 °K),  $k$  is the equilibrium partition coefficient. In the equation, it can easily be seen that at any temperature  $T$ , the lower alloy concentrations  $C_0$  brings smaller liquid fraction  $f_L$  that means a stronger solid/liquid interface.

### 2.2.2.1 Theories about the Liquation Cracking around the Weld Metals

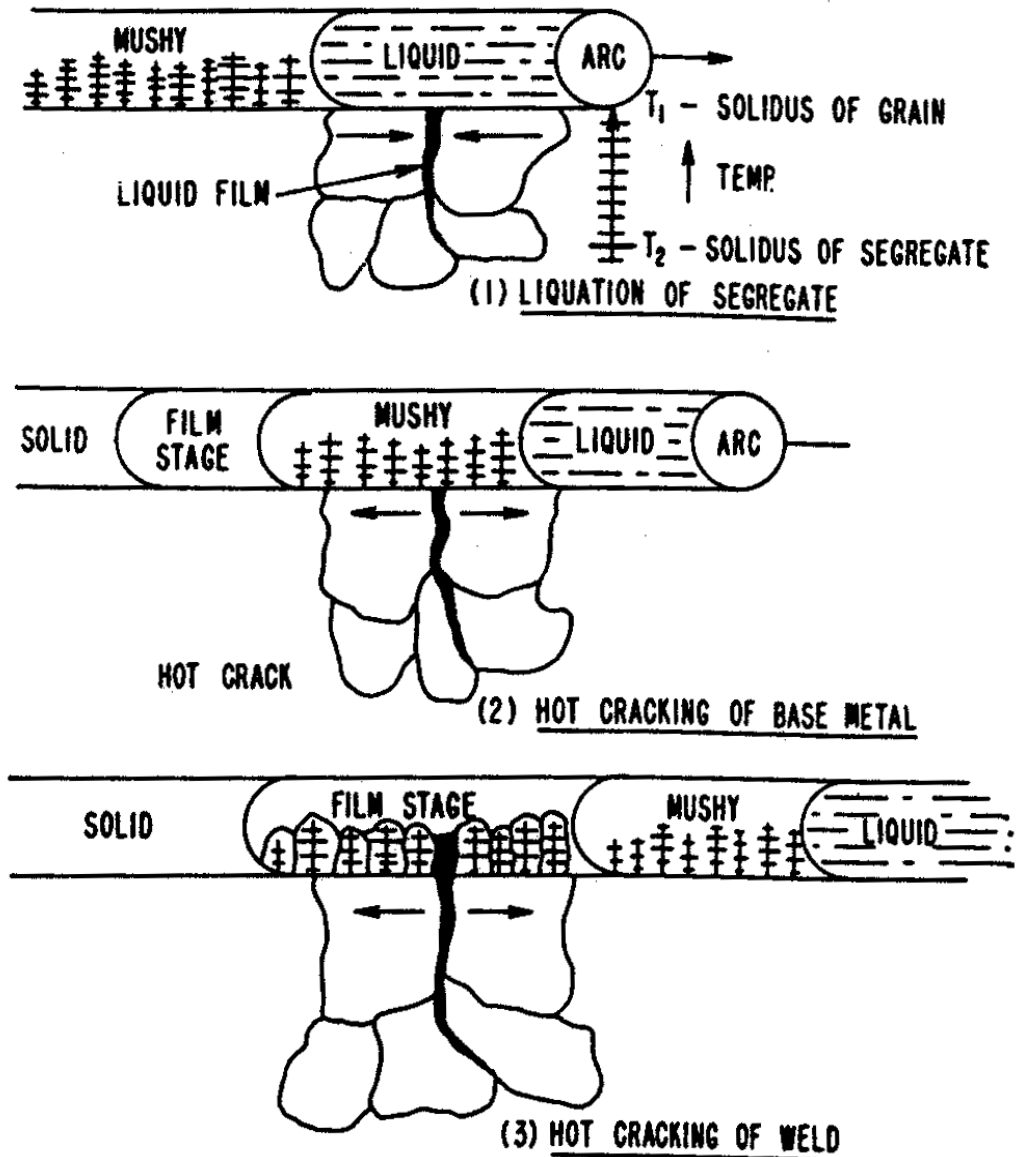
The first theory that can explain the liquation cracking is the strain theory as given in Figure 2.14. Here, the process of combined hot cracking of HAZ and weld can be seen. As the weld pool, which is following the arc passes the segregate region, grain boundaries transferred into liquid state; the thermal gradients perpendicular to the weld determine the lateral distance from the weld which develops melting.

Figure 2.14-(1) illustrates that grain boundary melting occurs up to a distance where the temperature corresponds to the solidus temperature of the segregate film. At this time, HAZ is under compressive stresses due to the thermal expansion of the hot metal near the fusion line. Upon cooling the contraction of the HAZ results in a separation of the film region, which produces the HAZ crack. At the moment of the formation of the HAZ crack, weld metal is in the mushy state and hot tearing is not possible. As cooling continues, the weld metal reaches film stage and a strain concentration is developed at the HAZ crack position. As a result, the natural shrinkage strain developed by cooling of the weld is concentrated at the HAZ crack point with consequent development of a hot crack in the weld, which is essentially a continuation of the HAZ hot crack.

Huang et al. have published some recent papers on liquation and solidification of the PMZ of aluminium welds after a series of studies. [20-25]. The results of these studies can be summarized as five liquation mechanisms, which can be seen in Figure 2.15.

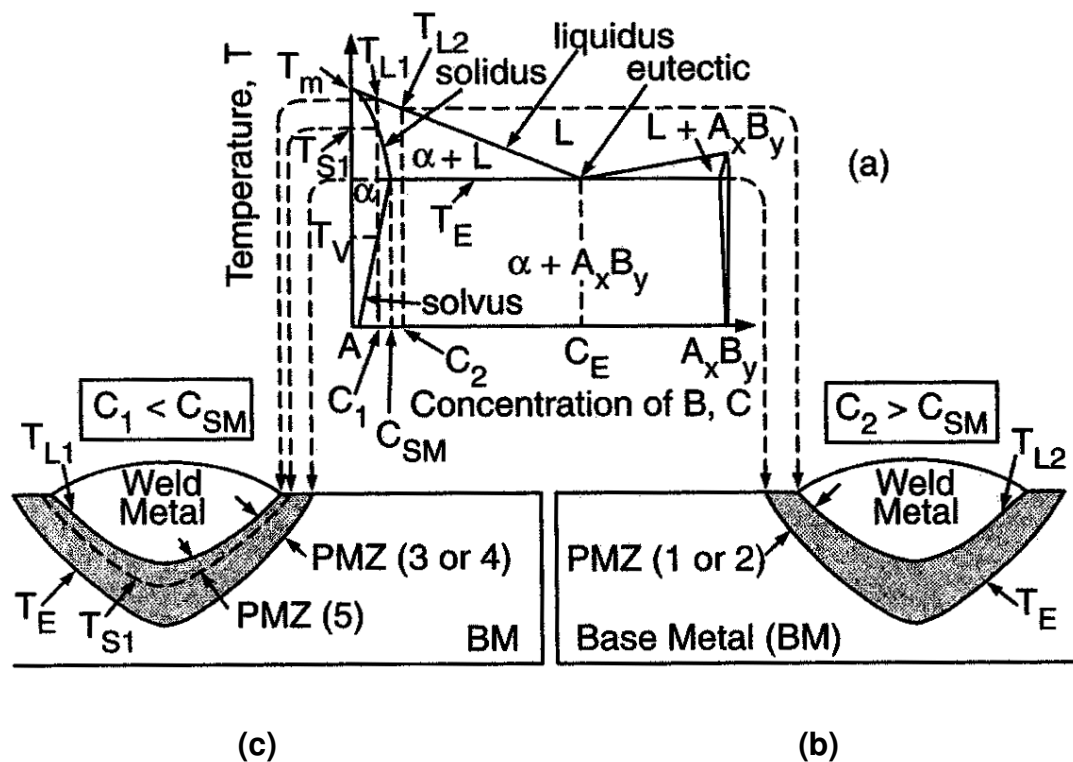
Mechanisms 1 and 2 are related with the alloy compositions greater than the solid solubility limit (Figure 2.15b). These alloys start to form liquid around the  $A_xB_y$  precipitates starting from the eutectic temperature with the reaction  $A_xB_y + \alpha \rightarrow L$  and the amount of the liquid increases with the

temperature increase. The alloy with eutectic composition melts totally from solid eutectic to liquid eutectic at eutectic temperature.



**Figure 2.14:** Liquation crack formation mechanism according to Pellini [15, 26]





**Mechanism 3:**  
Residual  $A_xB_y$  reacting with matrix:  
 if  $A_xB_y$  still present at  $T_E$   
 $A_xB_y + \alpha \rightarrow L$  at  $T_E$

**Mechanism 4:**  
Melting of residual eutectic:  
 if eutectic still present at  $T_E$   
 eutectic (S)  $\rightarrow$  eutectic (L) at  $T_E$

**Mechanism 5:**  
Melting of matrix:  
 if no  $A_xB_y$  or eutectic present at  $T_E$   
 $\alpha \rightarrow L$  at  $T_{S1}$

**Mechanism 1:**  
 $A_xB_y$  reacting with matrix:  
 regardless of heating rate  
 $A_xB_y$  always present at  $T_E$   
 $A_xB_y + \alpha \rightarrow L$  at  $T_E$

**Mechanism 2:**  
Melting of eutectic:  
 regardless of heating rate  
 eutectic always present at  $T_E$   
 eutectic (S)  $\rightarrow$  eutectic (L) at  $T_E$

**Figure 2.15:** Five mechanisms for liquation in PMZ of aluminium alloys (According to Huang et al.): (a) phase diagram; (b) two mechanisms for an alloy beyond the solid solubility limit ( $C_{SM}$ ); (c) three mechanisms for an alloy within the solid solubility limit.  $A_xB_y$  is a precipitate type of a compound of A and B atoms in the  $\alpha$  matrix. One molecule of this compound is composed of x atoms of A and y atoms of B [6, 23].

Mechanisms 3, 4 and 5 are related with the alloy compositions lower than the solid solubility limit (Figure 2.15a). In mechanisms 1 and 2 the heating rate was not important. But mechanism 3 assumes a rapid heating rate as in the case of the welding. Since the solid-state diffusion is slow, during such a rapid heating the  $A_xB_y$  precipitates does not have enough time to dissolve completely in  $\alpha$  matrix at the solvus temperature  $T_v$ . In other words,  $A_xB_y$  precipitates remain in the  $\alpha$  matrix above  $T_v$ . Heating to the eutectic temperature causes a reaction between the residual  $A_xB_y$  precipitates and the surrounding  $\alpha$  matrix resulting in the formation of liquid eutectic at the interface. More heating above the eutectic temperature gives more time for the dissolution of  $A_xB_y$  precipitates and further formation of the liquid phase. As a result, liquid formation is possible in the alloys having a composition below the solid solubility limit below the equilibrium solidus temperature.

Mechanism 4 is related with the liquation of the residual eutectic in the as cast structures. In such structures, the metal along the grain boundaries and in between the dendrite arms is at the eutectic composition. If this alloy is heated slowly, the eutectic phase can dissolve in the matrix and melting occurs first just above the solidus temperature. But upon rapid heating the condition explained in mechanism 3 occur and the first liquation is expected at the eutectic temperature at the named zones.

The mechanism 5 is explained with the melting of the matrix in the interval from solidus to the liquidus lines. Here it is assumed that there is a slow heating which causes the dissolution of the any possible  $A_xB_y$  precipitates.  
[6, 23]

### **2.3 Place of Varestraint and Modified Varestraint Tests among the Other Test Methods for the Assessment of the Hot Cracking Sensitivity**

There are numerous test methods developed in order to assess the HCS of the base and filler materials and their combinations. In all these methods hot cracking conditions are simulated using special equipment and specimens. But basically, hot cracking test methods can be classified into two categories: “self-loading test methods” and “external loading test methods”.

In the self loading test methods, the conditions leading to the hot cracking are simulated by the natural shrinkage stresses on the weld area and the related distortion and contraction on the base material. Specimen shape and size is specially designed to ensure the concentration of the mentioned stresses on the hot crack sensitive zone of the weld area. Self-loading tests have the advantage of ease in the test conduction and use of no special test equipment. However, the tolerance in test specimen preparation is a major parameter. As a result, the specimen preparation cost is generally high. Normally, the self-loading hot cracking tests are concentrated on the weld metal. Base metal and HAZ are generally not tested. The test results are in the form of “cracked” or “not cracked”. Due to the lower reproducibility in respect to quantitative analysis, the use of these methods has limited applicability for research purposes. Matsuda et al suggested that even the change of the welding process changes the susceptibility results considerably [27].

“T- and Lap-fillet weld test” [27], and “cylinder test” according to DIN 50129, “Houldcroft test” [27], “segmented circular patch test” according to VdTÜV Merkblatt 1153, “hook test” according to DIN 1912, “GMA weld crater crack test” [27] and “Fisco test” [28] can be given as several examples for the self-loading test methods [29].

On the other hand, in the external loading test methods, the conditions leading the hot cracking are simulated by the externally induced stress and strains on the weld area and the adjacent HAZ and base material of a relatively simple shaped specimen by the use of a special test equipment. External loading tests have the advantage of reproducibility of the test conditions, well defined loading conditions and parameter variation within a wide range.

In general, the external loading test methods are based on the “Brittleness Temperature Range” (BTR) theory of Prochorov [11] which is closely related with the temperature range in which hot cracking can occur, at critical amount of strain and the critical deformation rate. Therefore, these test methods use the total crack length, critical amount of augmented strain and the critical strain rate in the hot cracking susceptibility determination.

“Varestraint Test” [30], “Modified Varestraint Test (MVT)”, “Hot Deformation Rate Test (HDR)” [31], “Programmed Deformation Rate Test (PVR)”, “Cross Bead Test” [32], “The Fissure Bend Test” [33] and “Gleeble Test” are some examples of the external loading hot cracking tests.

The comparative study of Düchting [34] concluded that the standard hot cracking tests give more reproducible and comparable results about the hot cracking susceptibility during welding. As a result of other studies, ideal hot cracking evaluation test method was reported to have the following features [30, 35]:

- Ability to show a direct correlation with the structural components,
- Reproducibility of quantitative test results with freedom from variation due to the human element,
- Sensitivity to small changes in a test variable; Defined loading conditions,
- Ability to show the effects of several welding variables; Independent parameter adjustment within a wide range,

- Economical specimen preparation and test running
- Applicability to all welding processes

## **2.4 The Varestraint Test**

The Varestraint (VARIABLE RESTRAINT) test was developed by Savage and Lundin [30] in order to provide a reproducible way for simulating the shrinkage strains on an inexpensive laboratory specimen. The used augmented-strain technique permits the investigation of the influence of metallurgical, mechanical and welding process variables on hot cracking.

The total crack length produced in the weld deposit by a given combination of welding parameters and strain has been reported to be the best quantitative index of the cracking sensitivity of the weld metal. Similarly, the total crack length for heat affected zone cracks provides a quantitative index of base metal cracking sensitivity for a given set of welding parameters. Comparison of total crack length values also provides a useful method for comparing the effect of changes in welding procedure with the given base material.

## **2.5 The Modified Varestraint Test (MVT)**

The Modified Varestraint Test is a further development of the Varestraint and Transvarestraint test methods [1]. It is mainly a special bending test during the welding operation (Figure 2.16). The aim of the Modified Varestraint Test is the determination of hot cracking tendency of metallic alloys according to the applied welding and straining conditions. In contrast to the conventional varestraint tests, MVT is an automatically controlled version enabling better reproducibility. Like in the previous equipment, the bending unit applies a strain field on the surface of test piece around and inside the instantaneous weld pool location, where solid, semi-solid and

liquid phases are present at the same time. This nature of the specimen surface enables the assessment of solidification and liquation cracks at the same time on the same specimen. Bending position, as well as the bending speed can be adjusted on the control unit of the equipment. Normally the specimen is bent when the center of the weld pool reaches the location where the specimen has in contact with the lower die. Because of their simpler shape, test specimens can be prepared much more easily as compared with the conventional varestraint test versions.

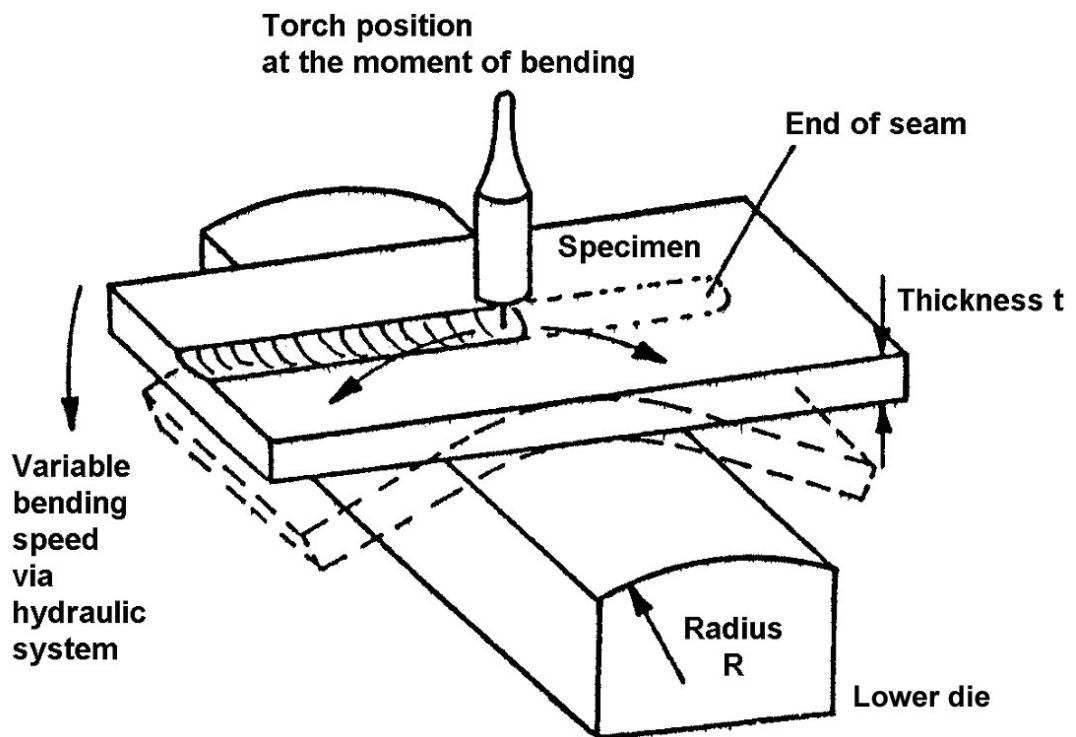


**Figure 2.16:** Principle of the Modified Varestraint Test [36-38]

With this test method, the HCS of base metals, welding fillers and weld joints can be distinguished. The sensitivity of the test method is enough to find out the HCS of the different charges of the similar materials and to establish the effects of the segregation in the materials. As a result, hot

crack free parameters together with the filler/auxiliary material and base material combinations can be stated. Hot cracks can be analysed in quantitative and qualitative ways. [1].

For the welding purpose, different fusion welding processes like manual metal arc welding (MMA), metal inert gas and metal active gas welding (MIG/MAG) and tungsten inert gas welding (TIG) can be used. However, conventionally in the standard testing procedure, mechanized and autogeneous TIG welding process is the unique process to be applied for the better reproducibility and the control of the welding parameters. Moreover, TIG welding process has advantages in oxide removal during welding of aluminium alloys. Maximum standard line energy used in the test is 25 kJ/cm. Furthermore; the standard line energy values for the iron based materials can be stated as 7.5 kJ/cm ( $I_w = 183$  A;  $v_w = 18$  cm/min) and 14.5 kJ/cm ( $I_w = 204$  A;  $v_w = 11$  cm/min) for normal and less crack susceptible materials respectively. [35]

Standard deformations that are applied to the specimen surface are usually 0.5, 1.0, 2.0 and 4.0 %. Conventionally, the tests are started with die radius giving 2.0 % deformation. Usually, only one test per deformation is considered as sufficient, since the scatter in test results is smaller than 10 %. On materials having high scatter in results, additional specimens are tested. For a general idea concerning the hot cracking sensitivity (HCS) of the material tested, it is adequate to conduct the test with only one specimen with 2.0 % deformation. The amount of augmented strain corresponding to a given die radius is calculated according to the equation {2}. [9]

$$S = \frac{100 \times t}{2 \times R} \quad \{2\}$$

Where;

S: Bending strain (%)

t: Thickness of the specimen (mm)

R: Radius of the lower die (mm)

The standard specimen of the MVT method is a bar having dimension of 100 x 40 x 10 mm. However, the specimen thickness can be changed in a range between 2.5 and 20 mm. It is also possible to reduce the length of the specimen to 80 mm. The test is applied normally on the rolling surface of the material. The rolling direction is conventionally along the longitudinal axis.

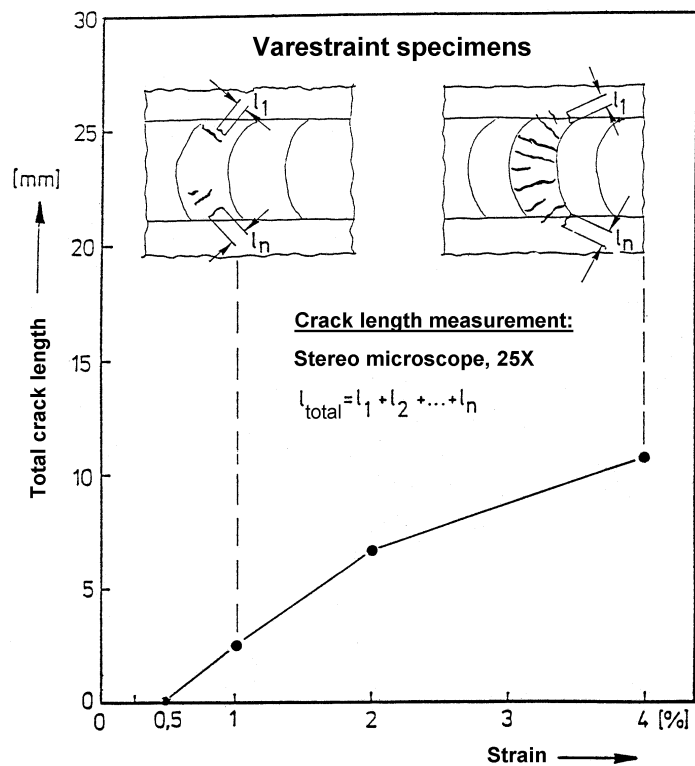


**Figure 2.17:** Typical MVT result representation method [37, 39]

The deformation speed can be regulated between 0.05 mm/sec and 4.00 mm/sec. The maximum deformation speed can only be obtained with



relatively soft materials. For the comparison tests under standard conditions, a deformation speed of 2 mm/sec is set. This guarantees the hot cracks are formed when the material under testing is sensitive to hot cracking.

The specimen is etched with a suitable solution before the evaluation. The formed hot cracks are measured using a stereomicroscope under 25X magnification. The calculated total crack length is and plotted against the augmented strain as shown in Figure 2.17.

## 2.6 Temperature Distribution around the Weld Pool

The temperature distribution around the weld pool is an important factor in the determination of the partially melted zone and the brittleness temperature range in the heat affected zone. The temperature distribution surrounding the weld pool can be expressed by the Rosenthal's equation. The equation defining the temperature distribution (T) around a weld pool for the welding of thick plates with a moving heat source is given as follows [6]:

$$T - T_0 = \frac{q_0}{2\pi\lambda} \left( \frac{1}{R} \right) \exp \left[ -\frac{v}{2a} (R + x) \right] \quad \{3\}$$

Where:

T: temperature

T<sub>0</sub>: initial temperature of the base material

q<sub>0</sub>: heat transferred from heat source to base material

λ: thermal conductivity of the base material

R: radial distance from the centre of the arc  $(x^2 + y^2 + z^2)^{1/2}$

- v: weld travel speed
- a: thermal diffusivity of the base metal
- x: distance from the arc centre in the welding direction

In the above equation, the thermal diffusivity of pure aluminium can be taken as  $8.5 \times 10^{-5}$  (m<sup>2</sup>/s) and thermal conductivity of pure aluminium is 229.0 (J/msK).

Roshental's equation was derived by using several assumptions including steady state heat flow, point heat source, neglecting the heat of fusion, constant thermal properties, no heat losses from the work piece surface and no convection in the weld pool.

The equation defines that, all isotherms on the transverse cross section of the weld including fusion line and the outer boundaries of the heat affected zone are semicircular in shape. With the help of the equation the steady state temperature at any point with respect to the moving heat source in the three dimensional work piece can be calculated. For example, the point  $x = 1$  cm,  $y = 4$  cm and  $z = 0$  cm is illustrated in Figure 2.18. [6]

The calculated surface isotherms for aluminium can be seen in Figure 2.19. The decrease in thermal diffusivity and conductivity, and increase in weld travel speed or the thickness cause an elongation of isotherms towards the negative  $x$  values. In this way the weld pool shape is also affected as described in Section 2.1.1. [8]

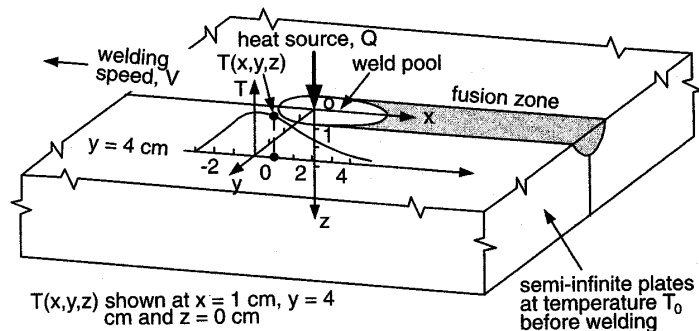


**Figure 2.18:** Three-dimensional heat-flow during welding of semi-infinite workpiece. [6]

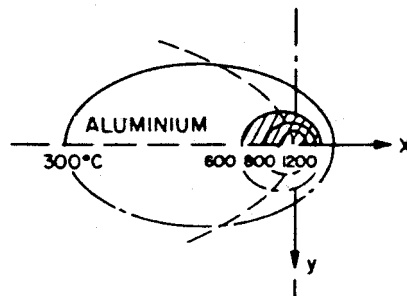


**Figure 2.19:** Isotherm shapes for aluminium calculated from Rosenthal equation. [8]

Rosenthal equation assumed a point heat source, but, in the TIG welding the heat source, which is arc, is affected first by the electrode tip shape and the current used. Figures 2.20 and 2.21 illustrate these effects respectively. The flat tip shown in Figure 2.20 is used generally in DC welding of aluminium. [6]

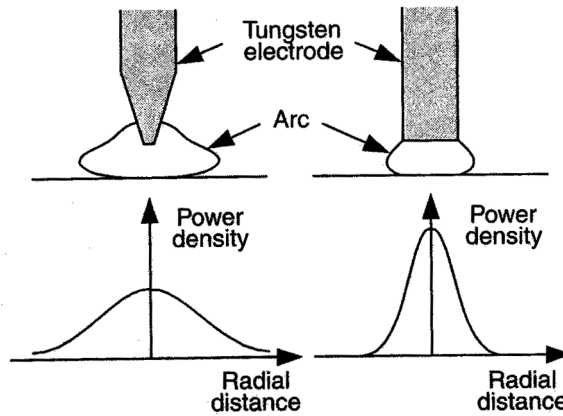


**Figure 2.20:** Effect of electrode tip angle on power density and as a result temperature distribution in the TIG arc. [6]

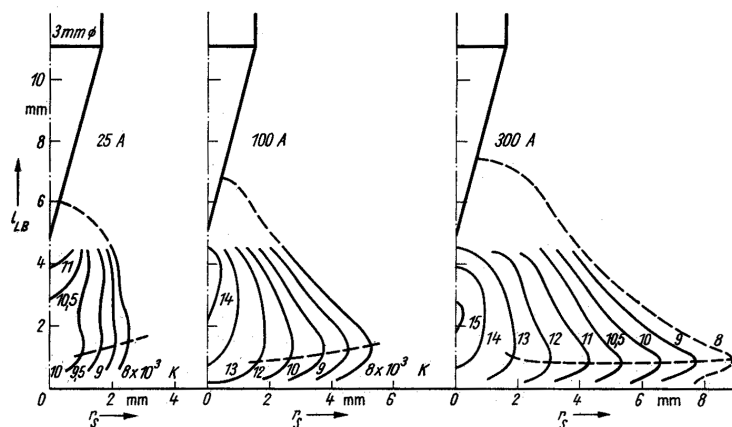


**Figure 2.21:** Temperature field at tip of a TIG arc at different welding currents. [40]

## 2.7 Tungsten Inert Gas Welding of Aluminium Alloys

In Modified Vrestraint Test, “Tungsten Inert Gas Welding” process was applied to produce a melting run on the specimens. Tungsten Inert Gas (TIG) welding is an arc welding process, which is widely used for welding of nonferrous metals, especially for aluminium. In this process, heat of welding is supplied by an AC or DCEN arc, burning between the base

metal and a nonconsumable electrode of tungsten (or tungsten alloy) (Figure 2.22). The characteristic penetration profiles of these current variations can be seen in Figure 2.23. In addition to current type, electrode tip shape also has an effect on the penetration profile (Figure 2.23). The electrode is shielded by an inert gas atmosphere that flows through the nozzle of the TIG torch. The shielding gas, which prevents any reaction between the weld metal and the surrounding air, is usually argon, helium, or a mixture of the two. The gas also protects heated base metal adjacent to the weld. The weld metal may be composed of base metal alone or a mixture of base and filler metal. [7, 41]

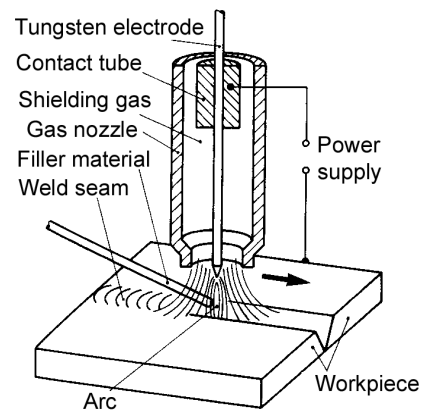


**Figure 2.22:** Schematic representation of TIG welding. [41]

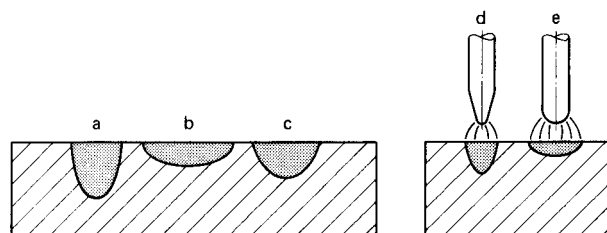


**Figure 2.23:** Current type and electrode tip shape dependent characteristic penetration profiles in TIG welding. [41] (a) DCEN; (b) DCEP; (c) AC; (d) Point tip electrode; (e) Flat tip electrode.

During welding, aluminium surface is covered with an impermeable natural oxide layer ( $\text{Al}_2\text{O}_3$ ). The formation of this oxide layer is inevitable even in very low oxygen concentrations. For that reason, arc instability is the main risk that can arise during welding of aluminium. [42]

The alternating current TIG process provides an efficient balance between cleaning action to remove the surface oxide during the positive electrode half cycle and a penetrating arc when the electrode is operated at negative polarity. In this method, the used shielding gas is usually only argon.

Another TIG welding variation that can be used for aluminium alloys is the DC-TIG welding with negatively charged electrode. This process utilizes generally helium or helium rich shielding gases. This variation enables welding with lower heat input as compared with TIG-AC welding. [7, 43] The deep penetration profile of helium can be explained with its better heat conductivity in arc plasma as compared with argon Figure 2.24. [40].

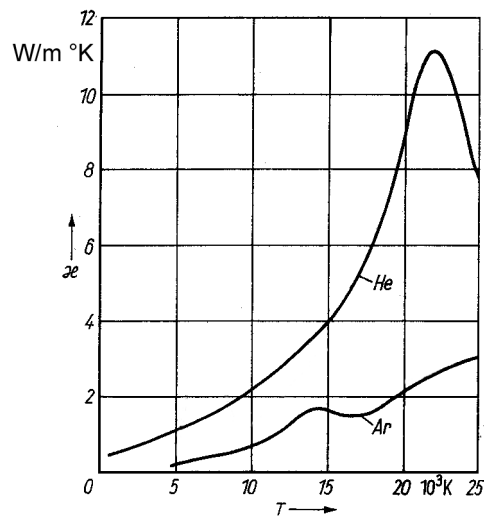


**Figure 2.24:** Heat conductivity of gases in arc plasma. [40]

## 2.8 Hot Cracking of Susceptibly of 5000 Series Alloys During Welding

The properties and performance of welded aluminium joints are influenced by many factors, including the metallurgical and welding parameters. Among these, composition and grain size have a great importance.

The cracking susceptibility of several types of aluminium alloys in TIG welding was shown in several comparative studies. [12-13, 44-45] Nakata and Matsuda have obtained the minimum augmented strain to cause cracking and brittleness temperature range (BTR) as a criteria representing the ductility characteristics of the solidifying weld metal [13]. They found that the BTR of 5000 series alloys increased with increasing Mg content of the alloy.

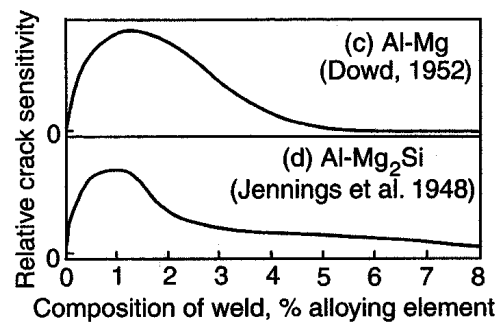


**Figure 2.25:** Effect of composition on crack sensitivity of aluminium-magnesium alloys and Al-Mg<sub>2</sub>Si system. [6]

The similar conclusion was found in other references as well. Figure 2.25 shows the effect of composition on the solidification cracking sensitivity of Al-Mg alloys and Al-Mg<sub>2</sub>Si system. In pure aluminium, there are no low-melting-point eutectics present at the grain boundaries. For that reason, pure aluminium is not susceptible to solidification cracking. However, in the aluminium alloys that contain high amount of alloying elements, the amount

of low melting point interdendritic eutectic is high enough to heal the early stage cracks. On the other hand, at the alloy compositions between pure aluminium and high-alloyed aluminium, the amount of interdendritic liquid can only be enough to form a thin continuous grain boundary film, but not so abundant as in the case of the high alloyed aluminium based materials. Due to the lack of the extra liquid for healing the cracks, aluminium alloys with a composition between pure aluminium and high-alloyed aluminium based material are rather susceptible to the solidification type of cracking. Moreover, with the similar logic, a fine equiaxed structure with high amount of liquid between the grains can deform easily than a coarse dendritic structure with low amount of intergranular liquid. For that reason, coarse columnar grains are often more susceptible to hot cracking than fine equiaxed grains. [6]

Most aluminium alloys are susceptible to liquation cracking due to their wide PMZ (wide solidification temperature range and high thermal conductivity), large solidification shrinkage (solid density is significantly greater than liquid density) and large thermal contraction (large thermal expansion coefficient). The solidification shrinkage of aluminium is as high as 6.6% and the thermal expansion coefficient of aluminium is roughly twice that of iron base alloys.

In the study of Nakata and Matsuda [45], for example, the BTR and the minimum strain to cause cracking of 5083 alloy was found as 140 °C and 0.05 % respectively. This is a relatively wider BTR. In general, a smaller minimum strain to cause cracking and wider BTR indicates a higher susceptibility for solidification cracking. The relationship between the BTR and the solidification temperature range for most alloys are expressed as [6]:

$$\text{BTR} = 2.1 \cdot \Delta T \quad \{4\}$$



Where  $\Delta T$  stands for the solidification temperature range. BTR is directly related with the chemical composition of the alloy. Therefore, it is a material property especially for the aluminium alloys.

Since in this study mainly hot cracking susceptibility behavior of aluminium-magnesium alloys is investigated, aluminium-magnesium phase diagram should be considered in order to obtain the solidification range (Figure 2.26) [46]. Here, a slight change is expected in the liquidus and solidus lines in different types of 5000 series alloys due to the effect of other alloying elements. In order to discuss the second-phase particles Al-Mg-Si ternary phase diagram should be used (Figure 2.27) [43].

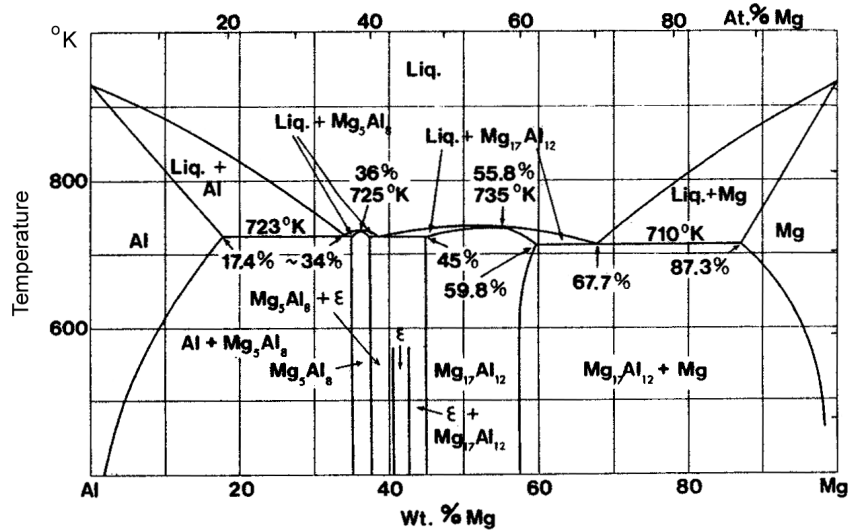


**Figure 2.26:** Aluminium-magnesium phase diagram. [46]

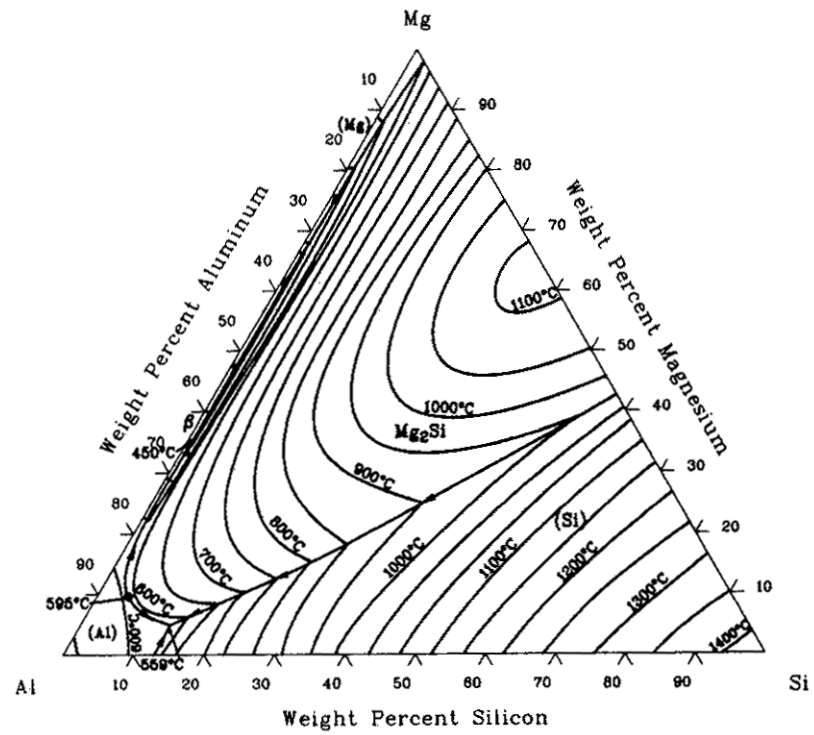


Figure 2.27: Aluminium-magnesium-silicon liquidus projection. [43]

## CHAPTER III

### MATERIALS, EXPERIMENTAL SETUP AND EXPERIMENTAL METHODS

#### 3.1 Introduction

In this study, the hot cracking tests are based on the Modified Varestraint Test “MVT”, which is a relatively fast method for evaluating the welding related hot cracking tendency of the metallic materials. The Modified Varestraint Test “MVT” is a test method developed mainly for hot cracking testing of high alloy steels and nickel based alloys. In the present study, hot cracking susceptibility of 5086-type aluminium-magnesium alloy was investigated. In addition, an adoption of the MVT conditions for this alloy was developed.

In the literature, there is inadequate information about Modified Varestraint Test of aluminium alloys in the following aspects:

- i) Hot cracking behaviour with the increasing augmented strain;
- ii) Ideal line energy range in order to evaluate the welding related hot cracking tendency.

Work has been started with preliminary studies on 1xxx, 3xxx, 5xxx and 7xxx series of aluminium alloys [2-4]. Based on the results of these preliminary studies, 5086 H32 (AlMg4) type of aluminium alloy, which has a moderate hot cracking tendency, was selected to investigate the hot cracking susceptibility (HCS) behaviour of the aluminium alloys in Modified Varestraint Test.

In order to study the ideal line energy range for the Modified Varestraint Test of this alloy, welding conditions were varied to give different line

energy values ranging from the beginning of the surface melting to the complete penetration bead. Line energy range was varied by changing the current type, welding current, welding speed and as well as using the two different types of shielding gases. In order to see the effect of straining conditions on hot cracking behaviour, several tests were performed using different die radiuses on each line energy value. Cracks formed during testing were measured under stereomicroscope and the cracks were classified into weld metal and heat affected zone cracking categories. Microstructural changes were analysed on the surface of the hot cracking specimens as well as on the specimens of the quench test experiments. Further microstructural investigations were performed using scanning electron microscopy, especially in distinguishing the different types of precipitates around and inside the hot cracks.

Study was extended by test series for the measurement of reproducibility in Modified Vrestraint Tests. In addition, the changes in the MVT specimen solidification and cooling rates with the changing die contact surfaces were investigated in separate test series. These tests were performed using the same line energy but changed strain forming die radiuses.

### **3.2 Properties of the Material Used**

Study was based on the hot cracking behaviour of the “5086 H32” aluminium alloy. This is an aluminium alloy, which has the magnesium as its major alloying element. The chemical composition of the alloy used is shown in Table 3.1. The given chemical analysis results were obtained by the spectral analysis of the outer plate surface.

**Table 3.1:** Chemical composition of the test material 5086 H32 Al-alloy.

<b>Element</b>	<b>Nominal composition range* (%)</b>	<b>Analysis results (%)</b>
<b>Mg</b>	3.5 to 4.5	4.06
<b>Si</b>	max. 0.40	0.10
<b>Mn</b>	0.2 to 0.7	0.52
<b>Fe</b>	max. 0.50	0.24
<b>Cr</b>	0.05 to 0.25	0.14
<b>Ti</b>	max. 0.15	0.01
<b>Cu</b>	max. 0.10	0.02
<b>Zn</b>	max. 0.25	0.01
<b>Sb</b>	max. 0.05	0.01
<b>Al</b>	rest	rest

\* Nominal composition range values were taken from Reference [5]

The temper designation “H32” indicates that the alloy was strengthened by strain hardening and the mechanical properties were stabilized by a "low temperature thermal treatment" or because of heat introduced during fabrication. Stabilization treatment was performed in order to prevent age softening at room temperature, and it usually increases ductility of this alloy. “2” in temper designation was assigned to indicate tempers having a

final degree of strain-hardening equivalent to that resulting from approximately 25 % reduction of area.

Possible phases present in wrought and cast structures of the 5086 alloy can be summarized as follows [43]:

Wrought:  $(\text{Fe,Mn,Cr})_3\text{SiAl}_{12}$ ,  $\text{Mg}_2\text{Si}$ ,  $\text{Mg}_2\text{Al}_3$ ,  $\text{Cr}_2\text{Mg}_3\text{Al}_{18}$

Cast:  $(\text{Fe,Mn,Cr})\text{Al}_6$ ,  $(\text{Fe,Mn,Cr})_3\text{SiAl}_{12}$ ,  $\text{Mg}_2\text{Al}_3$ ,  $(\text{Cr,Mn,Fe})\text{Al}_7$

After the autogeneous TIG welding of the wrought alloys, phases of the cast structure may appear in the weld metal. The types of the phases that appear in this cast structure depend on the rate of solidification. Therefore, the phases given for the cast structure above may not appear simultaneously depending on the weld metal solidification rate.

In wrought alloys, magnesium is largely present in solid solution, but it can appear as eutectic  $\text{Mg}_2\text{Al}_3$  in increasing amounts in as-cast structures as the magnesium content increases. In the same manner, magnesium forms increasing amounts of  $\text{Mg}_2\text{Si}$ , but the solubility of this phase is low so that a certain amount may remain out of solution and visible in wrought products. When the magnesium content exceeds about 3.5 %,  $\text{Mg}_2\text{Al}_3$  may precipitate in grain boundaries or within grains, resulting from low-temperature thermal operations. Chromium is a frequent additive and may appear as a fine dispersoid of  $\text{Cr}_2\text{Mg}_3\text{Al}_{18}$ . When manganese also is present, iron-rich phases become quite complex, and  $\text{MnAl}_6$ , probably containing some chromium, appears as dispersoid. Cold working of aluminium-magnesium alloys produces prominent deformation bands.

In general, 5086-type aluminium alloy possess good welding characteristics and good resistance to corrosion in marine atmospheres. Applications for 5086 alloy include welded structures, marine, automotive

and aircraft parts, cryogenics, TV towers, drilling rigs, transportation equipment, missile components and armour plate [43]. General physical properties of 5086 H32 were shown in Table 3.2.

**Table 3.2:** General physical properties of aluminium alloy 5086 H32. [43]

<u><i>Mechanical properties:</i></u>	
Tensile strength*:	275 – 325 MPa
Yield strength:	195 MPa
% Elongation*:	6 – 12 %
Shear strength:	185 MPa
Compressive yield strength:	195 MPa
Elastic modulus (tension):	71.0 GPa
Elastic modulus (shear):	26.4 GPa
Elastic modulus (comp):	72.4 GPa
<u><i>Mass characteristics:</i></u>	
Density at 20 °C:	2.66 gr/cm <sup>3</sup>
<u><i>Thermal properties:</i></u>	
Approximate melting range:	585 – 640 °C
Linear thermal exp. coefficient:	23.8 µm/m.K at 20-100 °C
Thermal conductivity:	127 W/m.K
Specific heat:	900 J/kg.K
<u><i>Electrical properties:</i></u>	
Electrical conductivity:	31 % IACS
<u><i>Fabrication characteristics:</i></u>	
Annealing temperature:	345 °C
Hot working temperature:	315 – 480 °C
* Tensile strength and percent elongation are approximately equal in longitudinal and transverse directions.	

### 3.3 Experimental Setup

#### 3.3.1 Modified Vareststraint Test Equipment

The hot cracking tests were carried out using the MVT equipment that was manufactured by Herion-Stuttgart. The standard test results of the equipment were controlled with an another MVT equipment in Germany. Comparison study was done on 60 steel MVT specimens in order to ensure the reproducibility among the equipments. The comparison study was conducted by German Federal Institute of Material Research and Testing (Bundesanstalt für Materialforschung und –prüfung) (BAM) Berlin and the reproducibility and the consistency of the equipment was approved [47].

The equipment consisted of three main parts as shown in schematic representation in Figure 3.1. First part is the electronic control unit (Figure 3.2) the second one is the welding and bending unit (Figure 3.3). The third part is a welding power source which is connected to the control and bending units.

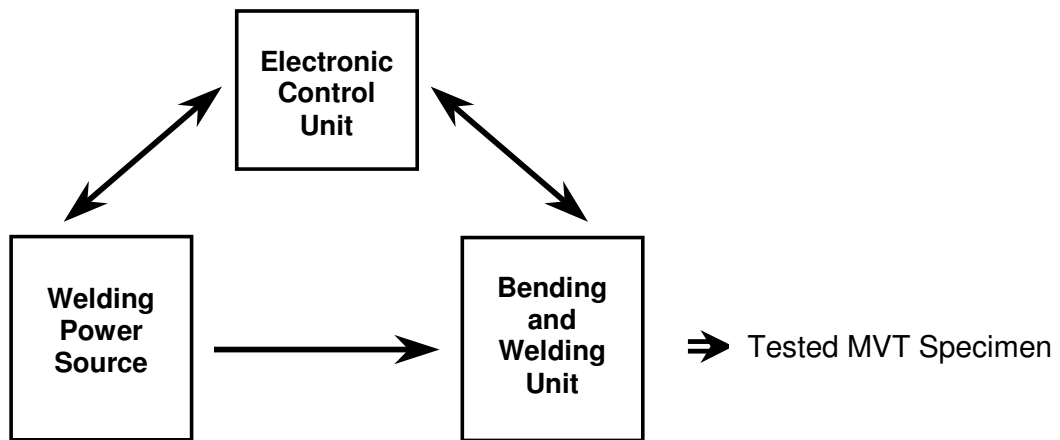


**Figure 3.1:** Schematic representation of the parts in the MVT equipment.





**Figure 3.2:** Electronic control unit of the MVT equipment.

Electronic control unit is connected to both welding power source and the bending unit. Besides the adjustment of torch and bending speeds, electronic control unit of the equipment enabled the adjustment of the following conditions as well: Test starting position, torch adjustment position, shielding gas on position, arc ignition position, bending position, arc stop and shielding gas off positions. These positions were given in terms of the displacement of the welding torch from the park position. Torch and bending mechanism displacements were shown digitally on this unit. Welding torch and the bending mechanism could be activated manually by a remote control device for initial adjustment purposes.

There are three possible test types, which can be adjusted on mechanical part shown in Figure 3.3: Standard test, welding without bending, bending without welding. In the standard test, the test specimen was bent during welding operation at the specified torch position given on the control unit. Conventionally, this position was adjusted on the vertical axis of the upper and lower dies.



**Figure 3.3:** Mechanical part of the MVT equipment.

To start the test, the test piece was placed on the machine and then the equipment was set for the torch positioning at the start point. Since the mechanical part of the machine was run on nitrogen gas, it was pumped to the gas chamber at 100 bars. For that purpose, the system was equipped with a hydraulic pump. During the test, the torch and bending system utilized the power of this accumulated nitrogen pressure in their motion in order to get rid of the noise effect from any vibration due to the instabilities of the hydraulic system. Bending and torch position could be seen digitally on the equipment and these data could be recorded with an X-Y recorder.

The bending mechanism (Figure 3.4) consisted of two upper and one lower dies. These dies could be changed according to the strain to be applied on the specimen. During the test, the specimen was placed between these dies (Figure 3.5) and a weld seam was formed on the surface of it. At the time when the welding torch reached the bending position (just at the middle of the specimen), the upper dies were moved towards the lower one

simultaneously with the specified bending speed. During and after bending, the welding process continued without any interruption. Each of the upper dies pressed a surface area of 10 x 50 mm on the specimen edge. As a result, the remaining 20 mm space between the two upper dies was used for the free specimen surface to be welded.

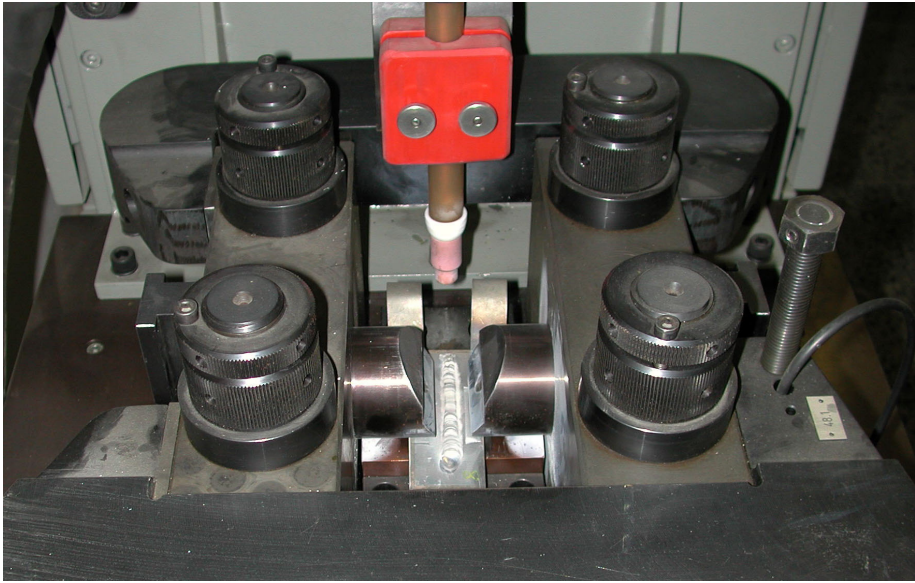


**Figure 3.4:** Overview of the bending mechanism and the welding torch. Welding torch is in the park position.

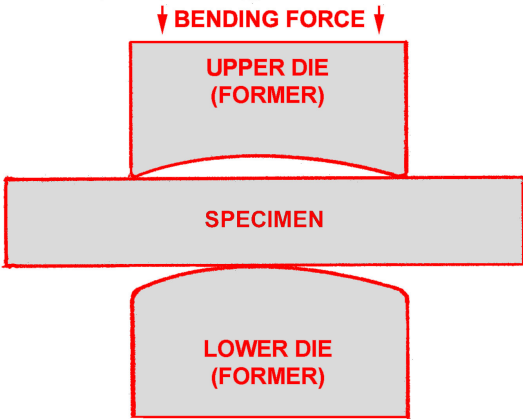


**Figure 3.5:** Schematic side view of the bending mechanism

### 3.3.2 Welding Equipment

The welding power was supplied by “Rehm Schweißtechnik – Invertig 250 GW” TIG welding machine that was connected to the MVT equipment as shown in Figure 3.6. The welding machine was an inverter type power source containing six pulsing thyristor sets and a smoothing inductive spool. It had a falling characteristic potential difference versus current curve. The machine was operated on 3 phases 380 V mains supply and 50 Hz alternating current. The highest possible welding current at the 100 % duty cycle was 220 A at 19 V (both alternating and direct current outputs were possible). The  $\cos \phi$  of the power supply was 0.98, which means a good efficiency in the welding current supply. Arc was ignited by a high frequency generator “Rehm-Zetronic-G1” without any contact between the tungsten electrode and the aluminium specimen providing the standard arc distance to be kept at the beginning of the welding process and preventing any tungsten inclusion formation at the beginning of the weld seam. The torch and the current conductors were cooled with water circulation. In order to minimize the resistance heating losses, the work piece power cable was directly connected on to the bending mechanism near the specimen.

The welding power supply and the MVT equipment was connected with a two directional communication cable ensuring the synchronization as shown in Figure 3.1. The welding current was set on the digital screen of the welding power source. During the welding operation, the display shows the actual welding current applied on the arc. The arc voltage was measured with “FLUKE 45 dual display digital multimeter”. This is an AC and DC voltage measurement unit with a  $1\mu\text{V}$  sensitivity. Due to the high frequency pulses at the ignition of the arc, the measurement unit was always connected to the circuit after a stable arc has been obtained. Especially, the voltage measurement at the point of bending was more important. The welding machine used had a system that shuts down the

welding current in the case of any short circuit between the electrode and the work piece, which may probably occur during bending. In such a case, the test was repeated again.



**Figure 3.6:** Welding power supply and the gas mixer.

In one of the test series, the TIG welding was performed under a Helium and Argon shielding gas mixture. This gas composition and the flow rate were adjusted using a gas mixer of “WITT-Gasetechnik Mini Mixer KM 60-3” as shown in Figure 3.6. The use of this mixer enabled the compositional reproducibility in the mixing of these two gases. Although the gas mixer has the ability to regulate the final flow rate of the shielding gas, the outlet flow rate of the shielding gas was also controlled with a flow meter placed on the gas nozzle of the torch (Figure 3.7). On the other hand, in the second test series, 100% Argon shielding was used. The flow rate of this Argon shielding gas was adjusted with the use of a standard flow meter placed at the end of the pressure reducer. In addition, the final out coming gas flow rate at the tip of the torch was controlled as above again. Inside diameter of the ceramic gas nozzle in front of the TIG welding torch was 9 mm in both of these test series.

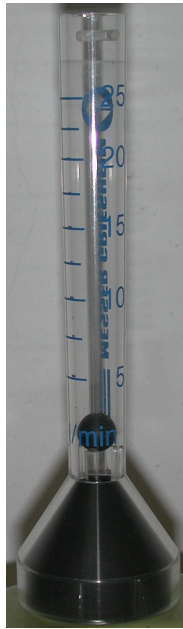


**Figure 3.7:** Flow meter used to control the shielding gas flow rate at the tip of the gas nozzle of the torch.

### 3.3.3 Quench Test Setup

Quench tests were performed to study the phases formed in the melting range of the alloy. These tests were performed with the use of a vertical tube furnace as shown in Figure 3.8. This was a resistance heated ceramic tube furnace with controlled inert atmosphere of 100 % Argon gas to protect the specimens against oxidation at high temperatures. The temperature of the furnace was controlled with two thermocouples at the point where the specimen was placed. After the required temperature was reached, approximately 15 minutes was allowed to achieve the temperature stability. Afterwards, the specimen was placed at the hearth of the furnace. The specimen was hanged in a basket inside the tube. After isothermal holding at the preset specified time, the basket together with the specimen was dropped in water bath at room temperature.





**Figure 3.8:** Vertical furnace used for the quench tests.

### **3.4 Experimental Methods and Procedure**

#### **3.4.1 Modified Vareststraint Tests**

For the standard testing, the prepared specimen was clamped between the upper and lower dies, which have the preselected required radius. Then, the electrode to specimen distance was adjusted. The test was conducted automatically. The automatic operation included, torch motion on the ignition point, shielding gas start and arc start, welding with constant speed, bending, arc stop and shielding gas stop. The complete modified vareststraint test procedure was given in Appendix A.

### 3.4.1.1 MVT Specimen Preparation

MVT specimens were cut from the 5086 H32 alloy plates by shearing. Afterwards the sides were machined to have the final dimensions of 100 x 40 x 10 mm with the tolerances given in Figure 3.9. The longitudinal dimension was selected as the rolling direction of the plate. The test surfaces were ground up to 500 grits just before the test to get rid of the oxides. Final grinding direction was parallel to the rolling direction. After degreasing with acetone and ethyl alcohol, specimen surfaces were dried with hot air. The test was performed immediately after this final cleaning stage.

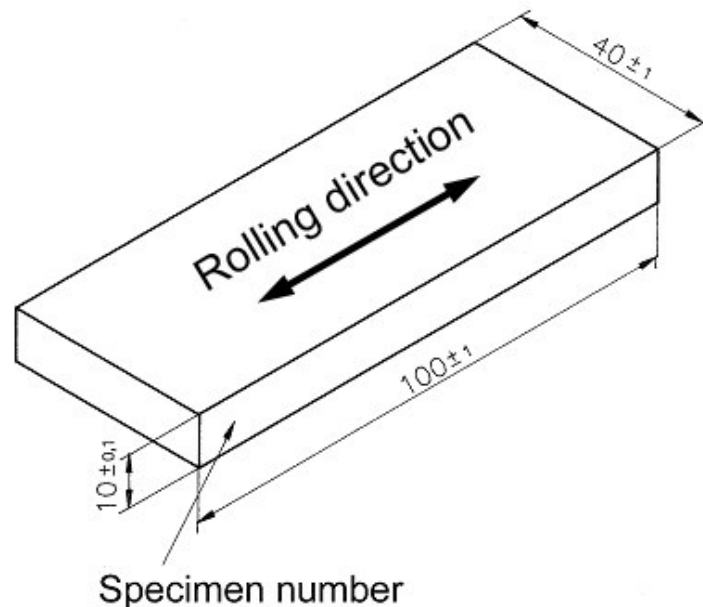


**Figure 3.9:** Standard modified varestraint test specimen



### 3.4.1.2 Test Conditions

There were two sets of standard test parameters used for the Modified Varestraint Test. The first set was used for the alternating current (AC) welding under the technologically pure Argon gas shielding (Table 3.3). The other set was for direct current (DC) welding under the shielding gas mixture of Helium and Argon (Table 3.4). Specimens were bent during welding operation. Bending radius and welding parameters were changed systematically. The following bending dies were used with the radius of 1000, 500, 250 and 125 mm creating 0.5, 1.0, 2.0 and 4.0 % strain on the surface of the 10 mm thick specimen respectively. The augmented strain values were selected according to the internal stresses produced in real constructions. The internal stresses due to partial melting produce a stress field around the weld zone of the construction parts. Experimental measurements of the longitudinal static internal stresses in aluminum magnesium alloys with about 6 % magnesium was found as high as 80 to 120 MPa [53]. The flow stress limit of the same alloy under the welding conditions was reported as 160 MPa. Using the obtained room temperature strength values of 5086 alloy, such level of internal stresses could produce about 2 % of strain in the weld zone. The calculated strain value at the proof stress level is around 3 % at room temperature. Under this condition, the maximum selected augmented strain value of 4 % would be above the proof stress level. However, considering the high temperatures reached during welding, it can be expected that 4 % strain can be easily obtained at lower stress levels. Therefore, it can be concluded that the selected range of augmented strains represents the reported possible strain values on the weld zone of the real construction parts of 5086 type aluminum alloy.

The welding parameters examined during the Modified Varestraint Test are shown in Tables 3.5 to 3.7. The effective line energy value, was calculated using the following equation [40]:

$$E = \eta \times \frac{U \times I}{v_w} \times 60 \quad \{5\}$$

Where:

$E$ : Line energy; in kJ/cm

$\eta$ : Efficiency in welding heat input

$U$ : Potential difference across the arc; in V

$I$ : Welding current in the welding circuit; in A

$v_w$ : Relative welding speed; in cm/min

The term “ $\eta \times U \times I$ ” is called as the effective heat input. The efficiency factor in front of the equation is mainly dependent on the applied welding process, current type, current level and the shielding gas composition. The main effect of shielding gas composition in heat input efficiency is due to its thermal conductivity (Figure 2.24). In the TIG-AC welding under argon shielding using the applied parameters an efficiency factor of  $\eta = 0.84$  was taken [40, 42, 48]. On the other hand, the efficiency factor of TIG-DC welding under % 75 He and % 25 Ar for the applied current level was found to be  $\eta = 0.50$  [40, 42, 48].

In both of the series, the welding parameters were selected to cover the whole weldability range for the given alloy and for the given material thickness. i.e. from the beginning of the surface melting until the complete penetration. Always a stable arc, which is characterized by the absence of a snapping or cracking sound, was maintained. In case of any instability, the corresponding test was repeated. The electrode tip was ground before each test to maintain the constant arc angle and therefore the constant power density in each test (Figure 2.20). The electrode tip form was semi-spherical in TIG-AC welding and flat in TIG-DC welding. After the test, the specimens were air cooled to room temperature naturally without any artificial cooling method. Before beginning the next test, enough time was

given to the TIG torch and the dies to cool down to room temperature. The detailed test procedure, the specimen preparation, equipment adjustment and the hot cracking testing in the Modified Varestraint Test is given in Appendix A.

**Table 3.3:** Test conditions for TIG – alternating current welding under pure Argon shielding.

<i>MVT conditions:</i>	
Type of test.....	Varestraint (V)
Bending point .....	Middle of the specimen
Bending speed .....	200 mm/min
<i>Welding conditions:</i>	
Welding process.....	TIG (autogenously)
Power source .....	Rehm INVERTIG 250 GV
Current type.....	AC (alternating current)
Electrode type [49].....	Pure tungsten electrode
Electrode diameter .....	2.4 mm
Electrode tip form .....	Semi sphere
Electrode-specimen distance .....	3 mm
Gas nozzle-specimen distance.....	5 mm
Shielding gas type .....	Argon 99.99%
Shielding gas flow rate .....	8 lt/min
Gas nozzle diameter.....	9 mm
Current rise time.....	1 sec
Current drop time .....	1 sec
Shielding gas flow time after arc....	8 sec
Balance .....	80 % Negative
Welding current .....	140 A (AC)
Welding speed .....	varied
Weld seam length .....	80 mm

**Table 3.4:** Test conditions for TIG – direct current welding under He and Ar gas mixture shielding.

<i>MVT conditions:</i>	
Type of test.....	Varestraint (V)
Bending point .....	Middle of the specimen
Bending speed .....	200 mm/min
<i>Welding conditions:</i>	
Welding process.....	TIG (autogenously)
Power source .....	Rehm INVERTIG 250 GV
Current type.....	DC (direct current)
Electrode type [49].....	Tungsten electrode with 2 % CeO <sub>2</sub>
Electrode diameter .....	2.4 mm
Electrode tip form .....	Flat (90°)
Electrode-specimen distance .....	3 mm
Gas nozzle-specimen distance.....	5 mm
Shielding gas type .....	% 70 He, % 25 Argon
Shielding gas flow rate .....	15 lt/min
Gas nozzle diameter.....	9 mm
Current rise time.....	1 sec
Current drop time .....	1 sec
Shielding gas flow time after arc....	8 sec
Welding current .....	180 A (DCEP)
Welding speed .....	varied
Weld seam length .....	80 mm

**Table 3.5:** Welding and straining conditions for specimens welded under the shielding gas of 75 % He + 25 % Ar.

Shielding gas: 75 % He + 25 % Ar				
Welding speed	Welding current	Potential difference	Effective line energy	Applied strains
mm/min	A	V	kJ/cm	%
120	180 ±	13.0	5.9	0.5;1.0;2.0;4.0
130	180 ±	13.0	5.4	0.5;1.0;2.0;4.0
140	180 ±	13.0	5.0	0.5;1.0;2.0;4.0
150	180 ±	13.0	4.7	0.5;1.0;2.0;4.0
160	180 ±	13.0	4.4	0.5;1.0;2.0;4.0
170	180 ±	13.0	4.1	0.5;1.0;2.0;4.0
180	180 ±	13.0	3.9	0.5;1.0;2.0;4.0
200	180 ±	13.0	3.5	0.5;1.0;2.0;4.0
220	180 ±	13.0	3.2	0.5;1.0;2.0;4.0
240	180 ±	13.0	2.9	0.5;1.0;2.0;4.0
260	180 ±	13.0	2.7	0.5;1.0;2.0;4.0
280	180 ±	13.0	2.5	0.5;1.0;2.0;4.0
300	180 ±	13.0	2.3	0.5;1.0;2.0;4.0
320	180 ±	13.0	2.2	0.5;1.0;2.0;4.0
340	180 ±	13.0	2.1	0.5;1.0;2.0;4.0
360	180 ±	13.0	2.0	0.5;1.0;2.0;4.0
380	180 ±	13.0	1.9	0.5;1.0;2.0;4.0
400	180 ±	13.0	1.8	0.5;1.0;2.0;4.0

**Table 3.6:** Welding and straining conditions for specimens welded under the shielding gas of 100 % Ar.

Shielding gas: 100 % Ar				
Welding speed	Welding current	Potential difference	Effective line energy	Applied strains
mm/min	A	V	kJ/cm	%
35	140 ~	4.5	9.1	0.5;1.0;2.0;4.0
40	140 ~	4.5	7.9	0.5;1.0;2.0;4.0
45	140 ~	4.5	7.1	0.5;1.0;2.0;4.0
50	140 ~	4.5	6.4	0.5;1.0;2.0;4.0
55	140 ~	4.5	5.8	0.5;1.0;2.0;4.0
60	140 ~	4.5	5.3	0.5;1.0;2.0;4.0
65	140 ~	4.5	4.9	0.5;1.0;2.0;4.0
70	140 ~	4.5	4.5	0.5;1.0;2.0;4.0
75	140 ~	4.5	4.2	0.5;1.0;2.0;4.0
80	140 ~	4.5	3.9	0.5;1.0;2.0;4.0

### 3.4.1.3 Reproducibility Tests

The reproducibility of the Modified Vareststraint Test with 5086 H32 aluminium alloy was studied by repeating the test on five specimens at each selected line energy and augmented strain values. These tests were performed using TIG-AC welding under the conditions given in Table 3.3 at 5.8 kJ/cm with 0.5% strain, 7.1 kJ/cm with 1.0 % strain, 4.2 kJ/cm with 2.0 % strain and 3.9 kJ/cm with 4.0 % strain. The given line energies are effective vales calculated from equation {5}.

### 3.4.2 Heat Conduction Tests

Heat conduction tests were run in order to show the effect of heat conduction differences at different die radiuses. The dies with larger radius contacted a larger surface area on the reverse side of the specimen specimen. On the other hand, the dies with smaller radiuses touched a smaller surface area on the specimen. The tests were run using one-millimeter thick stainless steel backing plate between the lower die and the specimen. The welding parameters used in heat conduction tests are summarized in Table 3.7.

**Table 3.7:** Welding and straining conditions for heat conduction tests.

Shielding gas: 75 % He + 25 % Ar				
Welding speed mm/min	Welding current A	Potential difference V	Effective line energy kJ/cm	Applied strains %
120	180 ±	13.0	5.9	0.5;1.0;2.0;4.0
150	180 ±	13.0	4.7	0.5;1.0;2.0;4.0
180	180 ±	13.0	3.9	0.5;1.0;2.0;4.0
300	180 ±	13.0	2.3	0.5;1.0;2.0;4.0

**Table 3.7 (continued)**

Shielding gas: 100 % Ar				
Welding speed mm/min	Welding current A	Potential difference V	Effective line energy kJ/cm	Applied strains %
40	140 ~	4.5	7.9	0.5;1.0;2.0;4.0
50	140 ~	4.5	6.3	0.5;1.0;2.0;4.0
65	140 ~	4.5	4.9	0.5;1.0;2.0;4.0
80	140 ~	4.5	3.9	0.5;1.0;2.0;4.0

**3.4.3 Quench Tests**

Quench tests were performed on 10 mm x 10 mm x 20 mm specimens. Below are the heat treatment conditions used (Table 3.8). The equipment and procedure were explained in Section 3.3.3.

**Table 3.8:** Quench test conditions.

Temperature °C	Holding time Seconds
560	30 – 60 – 300
570	30 – 60 – 300
580	30 – 60 – 300
590	30 – 60 – 300
600	30 – 60 – 300
610	30 – 60 – 300
620	30 – 60 – 300
630	30 – 60 – 300
640	30 – 60 – 300
650	30 – 60 – 300

### 3.4.4 Weld Seam Width, Penetration Depth and Partially Melted Zone Width Measurements

Initial tests were run to inspect the weld penetration profiles on the non-bent MVT specimens. Here, welding without bending option of the equipment was used. Applied welding parameters are listed in Table 3.9:

**Table 3.9:** Parameters applied for the weld dimension measurements.

Welding current A	Welding speed mm/min	Effective line energy kJ/cm	Shielding gas composition
140 A ~	30	10.6	100 % Ar
140 A ~	35	9.1	100 % Ar
140 A ~	40	7.9	100 % Ar
140 A ~	45	7.1	100 % Ar
140 A ~	50	6.4	100 % Ar
140 A ~	55	5.8	100 % Ar
140 A ~	60	5.3	100 % Ar
140 A ~	65	4.9	100 % Ar
140 A ~	70	4.5	100 % Ar
140 A ~	75	4.2	100 % Ar
140 A ~	80	3.9	100 % Ar
180 A ±	120	5.9	75 % He, 25 % Ar
180 A ±	125	5.6	75 % He, 25 % Ar
180 A ±	130	5.4	75 % He, 25 % Ar
180 A ±	135	5.2	75 % He, 25 % Ar
180 A ±	140	5.0	75 % He, 25 % Ar
180 A ±	145	4.8	75 % He, 25 % Ar
180 A ±	150	4.7	75 % He, 25 % Ar
180 A ±	155	4.5	75 % He, 25 % Ar
180 A ±	160	4.4	75 % He, 25 % Ar
180 A ±	165	4.3	75 % He, 25 % Ar
180 A ±	170	4.1	75 % He, 25 % Ar
180 A ±	175	4.0	75 % He, 25 % Ar
180 A ±	180	3.9	75 % He, 25 % Ar
180 A ±	190	3.7	75 % He, 25 % Ar
180 A ±	200	3.5	75 % He, 25 % Ar
180 A ±	210	3.3	75 % He, 25 % Ar
180 A ±	220	3.2	75 % He, 25 % Ar
180 A ±	230	3.1	75 % He, 25 % Ar



**Table 3.9 (continued)**

<b>Welding current</b> <b>A</b>	<b>Welding speed</b> <b>mm/min</b>	<b>Effective line energy</b> <b>kJ/cm</b>	<b>Shielding gas composition</b>
180 A ±	240	2.9	75 % He, 25 % Ar
180 A ±	250	2.8	75 % He, 25 % Ar
180 A ±	260	2.7	75 % He, 25 % Ar
180 A ±	280	2.5	75 % He, 25 % Ar
180 A ±	300	2.3	75 % He, 25 % Ar
180 A ±	320	2.2	75 % He, 25 % Ar
180 A ±	340	2.1	75 % He, 25 % Ar
180 A ±	360	2.0	75 % He, 25 % Ar
180 A ±	380	1.9	75 % He, 25 % Ar
180 A ±	400	1.8	75 % He, 25 % Ar

In order to mark the position of bending correctly, end of the specimen was taken as the reference point. From this point, 58 mm against the welding direction was marked as the cutting line as shown in Figure 3.10. Specimens cut from this point was epoxy mounted, and then surfaces were prepared with 220, 320, 500 and 800 grit grinding following with 6 µm and 1 µm polishing steps. Specimens have to be mounted in order to measure the near surface PMZ and the weld metal width. Fresh polished specimen surfaces were etched using Weck colour reagent for aluminium [50-51], which was composed of 4 gr of potassium permanganate, 1 gr of sodium hydroxide and slightly warmed 100 ml of distilled water. Dry etching method was used. Because the pot life of the solution was 3 to 4 hours, each time fresh-prepared reagent was used. In about 20 seconds of etching, the specimen surfaces turned to a yellow-green colour. During etching, the Weck colour reagent deposits a film layer on the surface of aluminium. Since it is a neutral solution, it did not attack the intermetallic phases. With this etching, weld metal and the heat-affected zone could be distinguished clearly.

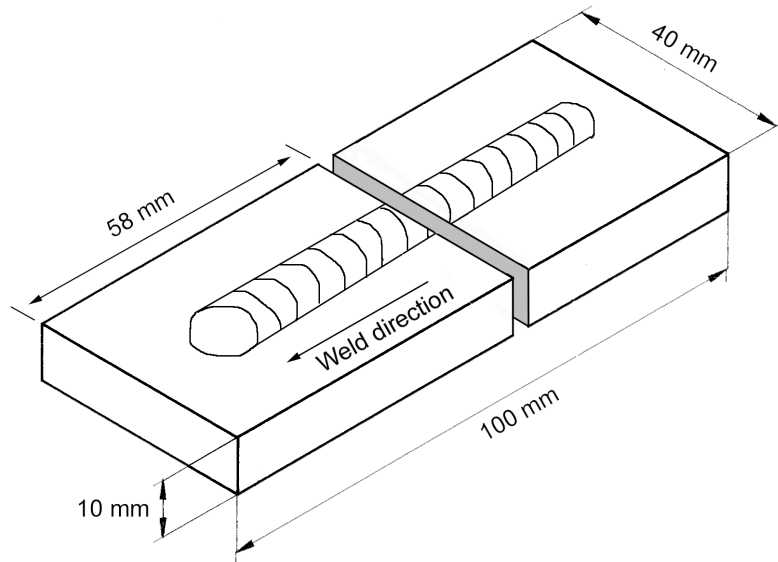


**Figure 3.10:** Cross-section location for the weld profile measurements.

Measurements were performed using a stereomicroscope. Weld metal width and the penetration depth were measured under 10X magnification. The PMZ width was measured under 25X magnification.

In order to compare the experimentally obtained weld dimensions with the theoretically calculated ones, plots were obtained by solving the Rosenthal's temperature distribution equation around moving heat source for the surface of the MVT specimen {3}. In order to get the necessary preheat temperature data, temperature measurements were run in accordance with the "guidance on the measurement of preheating temperature" [52]. In the plots, the liquidus temperature was used in order to interpret the instantaneous weld pool dimensions. The solidus temperature showed the end of the PMZ range. Again, in order to use in the BTR discussion the brittle temperature fields for the different strain levels which was reported by Arata et. al. [12] for alloy 5083 was plotted.

### 3.4.5 Crack Length Measurements

In as welded state, surface of the weld seam and the neighbouring area was covered with a thick oxide layer that had a negative influence on crack length measurement and the location identification. In order to investigate the cracks and the surface microstructure, a two-step etching process was used. In the first step, surface was dry etched approximately for 60 seconds with modified Adler reagent which is composed of 100 ml base Adler solution and 1 gr potassium metabisulphite [ $K_2S_2O_5$ ] with 70 ml distilled water [50-51]. Adler base reagent is a solution of 25 ml distilled water, 50 ml HCl, 15 gr ferric chloride [ $FeCl_3 \cdot 6H_2O$ ] and 3 gr ammonium chlorocuprate (II) [ $(NH_4)_2[CuCl_4] \cdot 2H_2O$ ] [36, 41]. Reagent was applied continuously with cotton wool until the entire oxide layer was removed. After rinsing, the specimen was placed inside a bath of lukewarm 50%  $HNO_3$  and 50% distilled water solution for about 3 minutes to remove the surface deposits formed in the first etching step. Following that, specimen was rinsed again and dried. Crack length measurement was performed with Nikon SMZ-2T stereomicroscope under 25X magnification. The scale on the microscope was calibrated with a calibrated objective micrometer.

### 3.4.6 Metallographic Investigation

Metallographic investigation was performed using Nikon OPTIPHOT Metallographic Microscope under 50X, 100X, 200X, 400X and 600X magnifications. Specimen surfaces were ground up to 1000 grit with Si-C papers and polished with 6 and 3  $\mu m$  grain sized diamond solutions. In order to have a scratch-free surface, final polishing stage was performed using colloidal silica with a grain size of approximately 0.04  $\mu m$ . Investigation was undergone with as polished and etched specimens. For this purpose, mainly Weck etching solution as given in Section 3.4.4 was used [50-51].

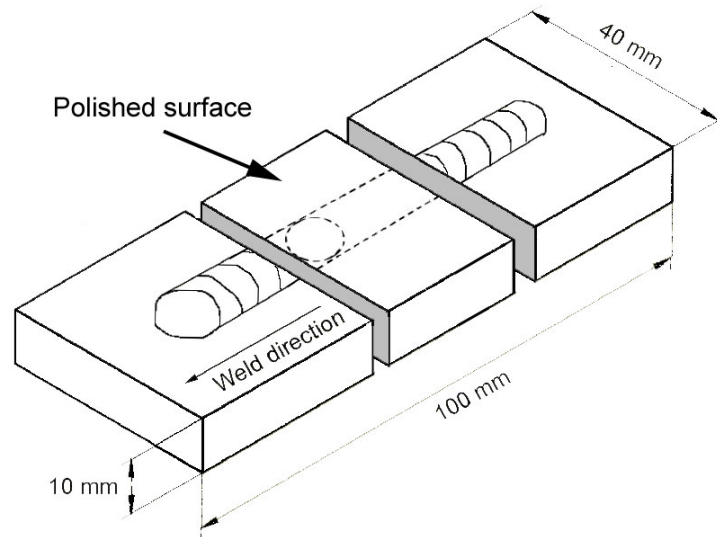


**Figure 3.11:** Surface to be inspected in metallographic investigation.

Metallographic investigation was used for the grain size comparison and inspection of the open and healed hot cracks. For this purpose, a part of the surface area of the MVT specimen shown in Figure 3.11 was prepared. This surface section is the part where the hot cracks are found, and included the bending zone where in general a crater was formed depending on the parameters used. This section included the solidification zone (just before the bending point) and the neighbouring heat affected zones. To reduce the number of test sections, specimens from four selected line energies and four augmented strains from each line energy level were inspected for each welding method. The line energies chosen for the specimen inspection were 3.9; 4.9; 6.4 and 7.9 kJ/cm in TIG-AC welding and 2.3; 3.9; 4.7 and 5.9 kJ/cm in TIG-DC welding. Grain size comparison was performed on secondary dendrite arm spacing measurements on each specimen mentioned above and the equivalent specimens prepared from the heat conduction test series. Measurements were made on the photographs taken under 400X magnification. Here, the

number of dendrite arms per unit cross-sectional area was counted. Final secondary dendrite arm spacing was calculated as the main distance between the centers of the dendrites. A calibrated objective micrometer was photographed under the same magnification with the microstructures to use the exact magnification on the photographs (Figure 3.12).

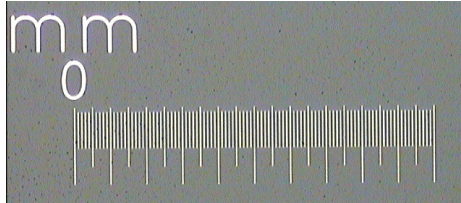


**Figure 3.12:** Objective micrometer photographed under 50X magnification.

### **3.4.7 Scanning Electron Microscope Investigation**

Scanning electron microscopy was used to identify the type of the precipitates and their changes at different temperature levels. For this purpose, quench test samples and selected weld zones were examined. Magnifications up to 6500X were used. The type of the precipitates were identified with the help of microanalysis. In these investigations, “JSM-6400 Electron Microscope (JEOL)” equipped with “NORAN System 6 X-Ray Microanalysis System” was used.

Quench test specimens were ground and polished same as in the metallographic investigation. These samples were deep etched with Keller’s reagent [51] before the examination. On the other hand, hot cracks were examined on the as welded specimens without any etching process. The specimens were broken through the crack line to have a better access to the crack surface.

### 3.4.8 Thermal Analysis

Thermal analysis of the 5086 alloy was performed using Differential Scanning Calorimetry (DSC) technique, which measures the amount of energy (heat) absorbed or released by a sample as it is heated, cooled, or held at a constant temperature. With this analysis, it was aimed to determine the solidus and liquidus temperatures of the used alloy and the presence of any solid-state interaction during the thermal period.

The analysis was made in two temperature ranges. In the temperature range of 350°C to liquidus temperature, “SETARAM SETSYS TG-DTA/DSC” thermal analyser was used. This equipment has sensitivity for quantitative and qualitative calorimetric studies between 350°C to 1650°C because of the used thermocouple. A 23.02 mg sample was heated in a 100 µl ceramic crucible ( $\text{Al}_2\text{O}_3$ ) in the inert atmosphere of Argon gas, above liquidus temperature at a rate of 20°C/min and cooled again at the same rate. Reactions on both heating and cooling periods were analysed.

The sensitive analysis between room temperature to 350°C was performed on “SETARAM DSC 131” thermal analyser, which is capable of thermal analysis in the temperature range of (-170 °C to 600 °C). In this analysis, a 29.75 mg sample was put into a pure aluminium crucible. Heating and cooling rates were again 20°C/min.

## CHAPTER IV

### RESULTS

The results of the study will be presented in the following order:

- 4.1 General weld seam features in the MVT specimens of 5086 alloy.
- 4.2 Results of the weld seam profile measurements.
- 4.3 Results of the crack length measurements.
  - 4.3.1 Results of the crack length measurements on TIG-AC welded MVT specimens.
  - 4.3.2 Results of the crack length measurements on TIG-DC welded MVT specimens.
  - 4.3.3 Results of the supplementary tests.
- 4.4 Results of the reproducibility tests.
- 4.5 General features of the hot cracks in 5086 aluminium alloy MVT specimens.
- 4.6 Results of the BTR measurements.
- 4.7 Results of the secondary interdendritic spacing measurements.
- 4.8 Results of the thermal analysis.
- 4.9 Results of the quench tests.
- 4.10 Results of the SEM investigations.
- 4.11 Results of the optical microscope investigations.

To present the results in a simpler way, applied line energies were divided into three categories as low, medium and high. In TIG-DC welding, line energies up to 3.0 kJ/cm were regarded as low. Line energies from 3.0 to 4.0 kJ/cm were taken as medium. Moreover, the line energies greater than 4.0 kJ/cm were regarded as high. On the other hand, in TIG-AC welding, low line energies were the values up to 5.0 kJ/cm. The line energies

between 5.0 to 6.0 kJ/cm were taken as medium, line energies greater than 6.0 kJ/cm was regarded as high.

The applied augmented strain values were classified as low (0.5 %), low-medium (1.0 %), medium (2.0 %) and high (4.0 %) in the both test series.

#### **4.1 General Weld Seam Features in the MVT Specimens of 5086 Alloy**

There is a characteristic weld metal surface appearance in the aluminium MVT specimens. During constant speed TIG welding operation, high thermal conductivity of the aluminium-based alloy has increased the time for the establishment of steady state temperature distribution and delayed the formation of a uniform weld seam width. Therefore, TIG welding without filler metal produced an expanding weld seam width from the start till about 10 mm weld length has been reached. After this point, the seam width remained constant. This is due to the cold base metal at the ignition point of the arc, thus the weld pool was considerably small at the start of welding (left side of the Figures 4.1 and 4.2). As the welding proceeded, weld pool enlarged due to the heat accumulation in the specimen. Finally, the seam width and the temperature distribution around the weld pool reached equilibrium prior the point of bending. In order to have a correct comparison, it was important to consider the dimensions of the weld metal and heat affected zone at the point of bending, where equilibrium conditions has been reached. The results of these measurements are given in Section 4.2.

The welding heat applied in Modified Vareststraint Test causes the surface of the weld seam and the adjacent base material to form a thick oxide layer. At this condition, some of the cracks were visible but very fine cracks were mostly hidden under the oxide layer (Figure 4.1). To make the weld



surface macrostructure, grain growth zone in the HAZ and hot cracks visible, the oxide layer was removed as explained in Section 3.4.5.

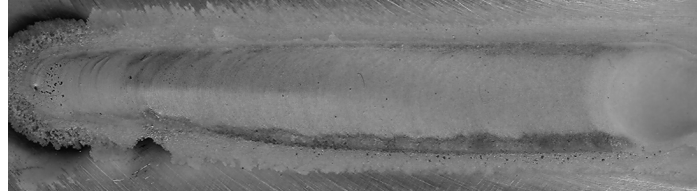


**Figure 4.1:** Surface view of an as welded 5086 MVT specimen. Welding direction is from left to right. Left is the arc ignition point; right is the point of bending. Not etched. Magnification: 2X.

At the point of bending a crater was formed in weld pool due to the gravitational forces. In general, hot cracks were located around and inside this weld metal crater (Figure 4.2). This crater was more apparent and deeper in the weld seams tested with smaller bending (die) radiuses (i.e. with higher strains).

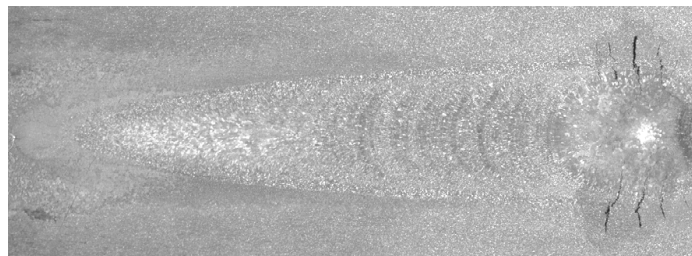
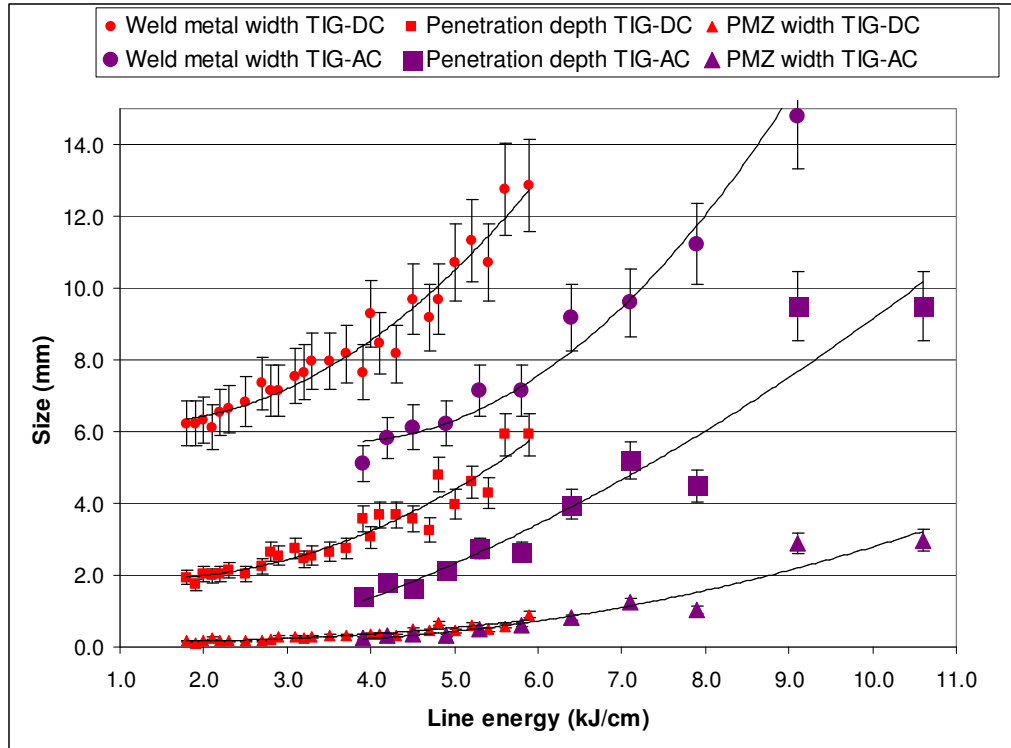


**Figure 4.2:** Typical appearance of the etched 5086 MVT specimen surface. Left: Arc start point; Right: Bending point. Etching procedure as given in Section 3.4.5. Magnification: 2.5X.

## 4.2 Results of the Weld Seam Profile Measurements

The temperature distribution around the bending zone was affected by the applied welding parameters. The distribution of the temperature fields was investigated by measuring the weld profile dimensions. The results of the

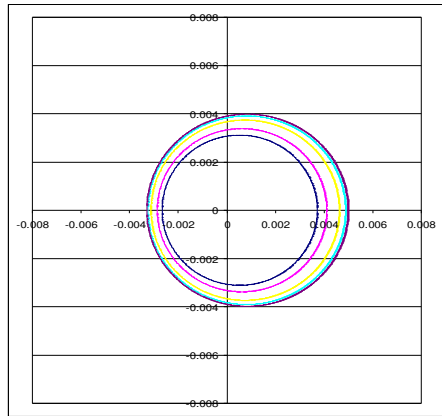
TIG-AC and TIG-DC welding test series, which were explained in Section 3.4.4 are given in graphical form in Figure 4.3.



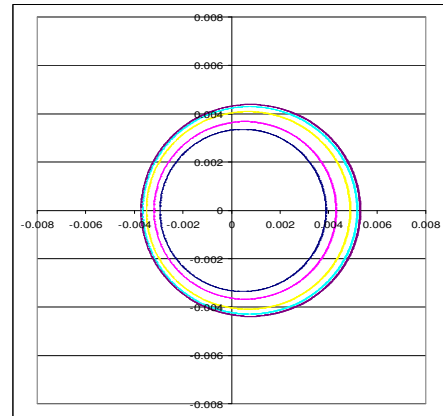
**Figure 4.3:** Change in “weld metal width”; “penetration depth” and “PMZ width” with changed “line energy” in TIG-DC and TIG AC welded MVT specimens. No bending was applied.

Figure 4.3 shows that the weld metal width, penetration depth and the PMZ width increased with increasing line energy.

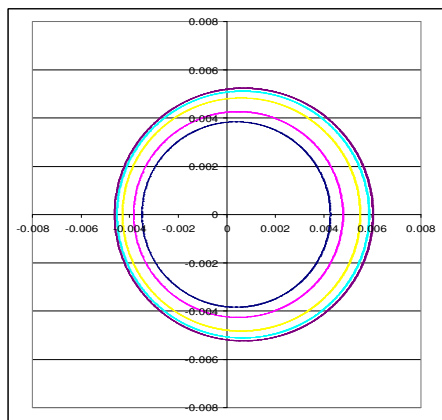
The effect of the welding parameters on the temperature distribution equation given by Rosenthal {3}, was used to obtain the surface temperature distribution diagrams for 5086 alloy. Results are plotted at selected welding parameters in Figures 4.4 and 4.5. In these diagrams, width of the 640 °C zone on the vertical axis indicates the weld metal width. In addition, the distance between the liquidus-solidus temperature zones, i.e. 640 °C to 585 °C zone along the vertical axis was the PMZ width.



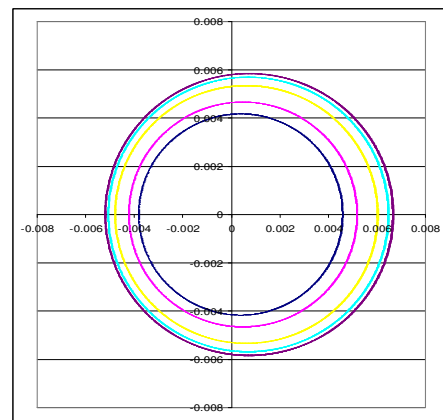
a)  $E = 1.8 \text{ kJ/cm}$



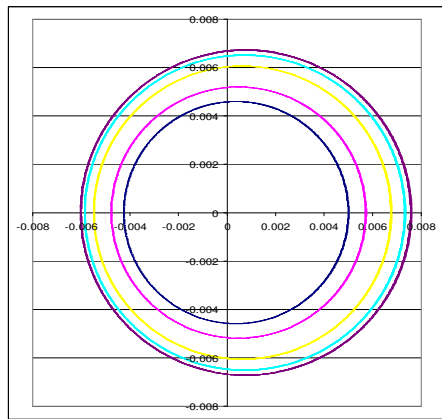
b)  $E = 2.3 \text{ kJ/cm}$



c)  $E = 3.9 \text{ kJ/cm}$



d)  $E = 4.7 \text{ kJ/cm}$



e)  $E = 5.9 \text{ kJ/cm}$

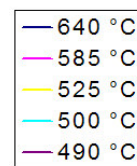
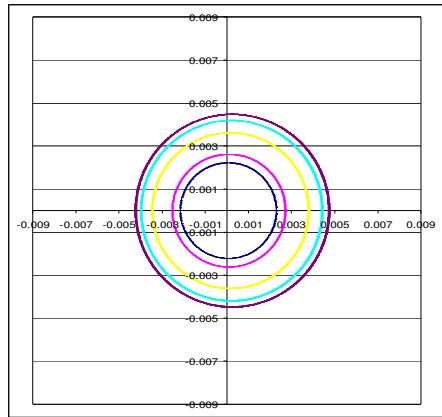
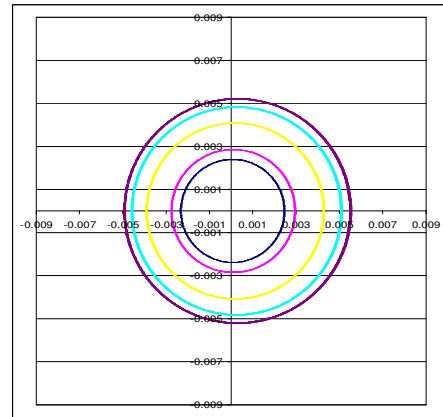


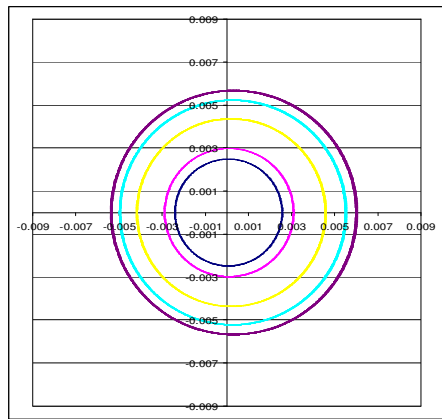
**Figure 4.4** Surface temperature distribution diagrams in TIG-DC welding of 5086 alloy at selected line energies, plotted by solving Rosenthal's equation. Welding direction: Towards left. Dimensions in meters.



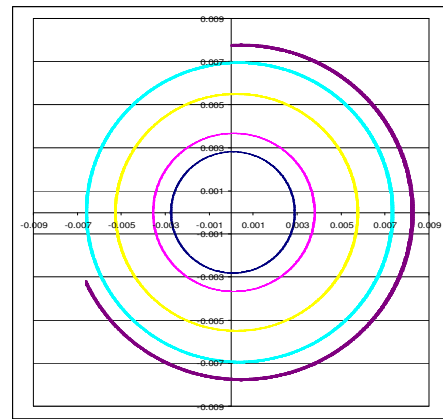
a)  $E = 3.9 \text{ kJ/cm}$



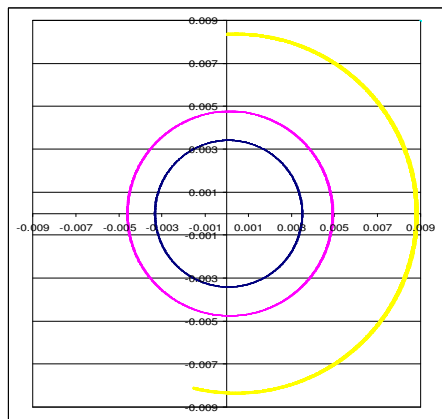
b)  $E = 4.5 \text{ kJ/cm}$



c)  $E = 4.9 \text{ kJ/cm}$



d)  $E = 6.4 \text{ kJ/cm}$



e)  $E = 7.9 \text{ kJ/cm}$

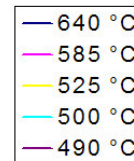


**Figure 4.5** Surface temperature distribution diagrams in TIG-AC welding of 5086 alloy at selected line energies, plotted by solving Rosenthal's equation. Welding direction: Towards left. Dimensions in meters.

Arata et. al. [12] and Nakata [45] have found the critical temperature for BTR in 5083 alloy. This alloy has nearly similar composition to 5086 and therefore for the comparison purposes the same temperatures were used to find the BTR in the 5086 alloy. In Figures 4.4 and 4.5, the 525, 500 and 490 °C temperature distribution lines show the BTR at 0.5, 1.0 and 2.0 % strain levels respectively. The BTR at 4.0 % strain level was reported to be similar with the 2.0 % strain level [12].

Theoretical weld-metal-width data gained from Figures 4.4 and 4.5 and the data obtained from the experimental weld-metal-width measurements are given in Figure 4.6.

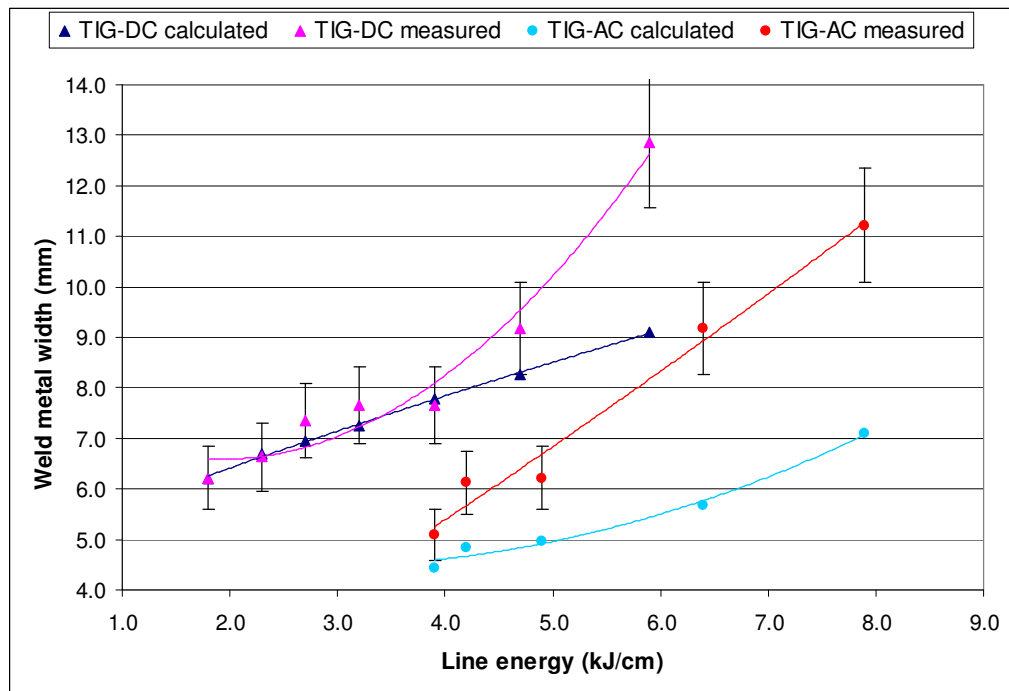


**Figure 4.6** Comparison in the calculated and measured weld metal width values with the change in line energy for TIG-DC and TIG-AC welded 5086 aluminium alloy.

Here, the theoretical and experimental results are closer to each other at the corresponding low line energies of each series. However, the

experimental results were generally higher than the theoretically calculated ones. The difference between the experimental and the theoretical results increased as the line energy increased. This was more emphasized in TIG-AC welded series. In TIG-DC welding, the theoretical and experimental results were close to each other at low line energy range.

The PMZ width results are compared in Figure 4.7. Here, the experimentally obtained results were generally lower than the theoretically calculated ones. As the line energy increased, the experimental results get closer to the theoretical ones. Moreover, the experimentally obtained PMZ widths exceeded the theoretical ones at high line energy level.

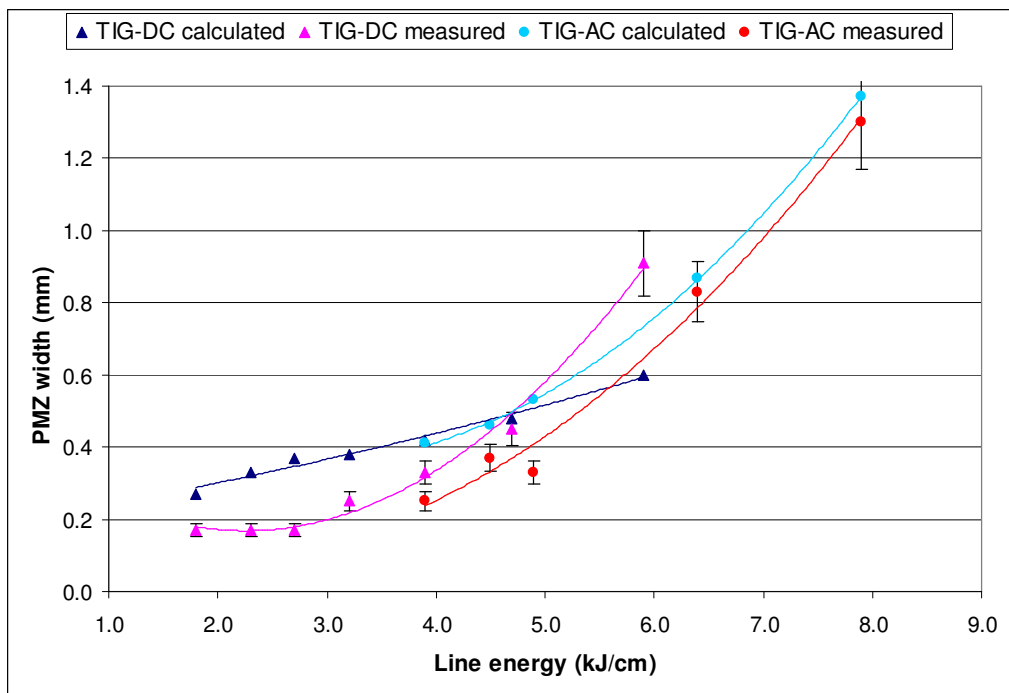


**Figure 4.7** Comparison in the calculated and measured PMZ width values with the change in line energy for TIG-DC and TIG-AC welded 5086 aluminium alloy.

### 4.3 Results of the Crack Length Measurements

To investigate the hot cracking behaviour, quantitative and qualitative crack analysis were performed using the surface crack measurements under 25X magnification. The results of the individual crack length measurements on the TIG-AC, TIG-DC and isolated data series are given in Appendix B.

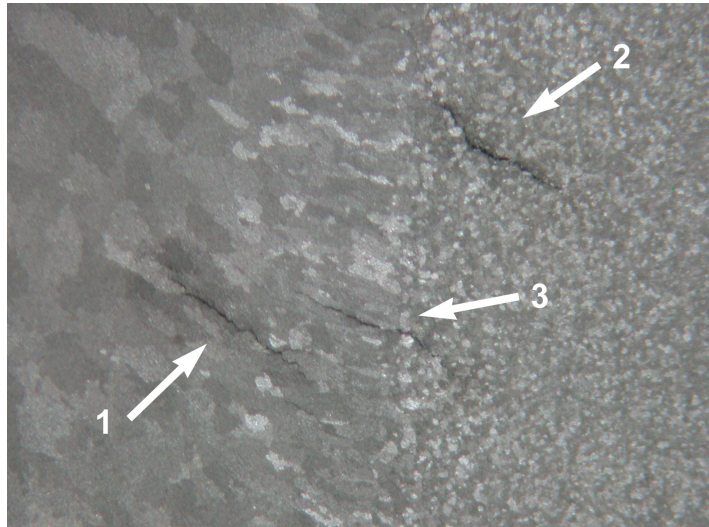


**Figure 4.8:** Hot crack types on 5086 MVT specimen surface. Macro etched with modified Adler reagent. Crack 1: Weld metal crack; Crack 2: HAZ crack; Crack 3: Transition crack. Magnification: 25X

In the qualitative analysis, hot cracks were classified as “weld-metal-cracks” which are the cracks seen only in the weld metal and the “HAZ-cracks” which are located in the weld metal neighbouring area (Figure 4.8). Moreover, some cracks crossed through the fusion line and run in both the weld metal and HAZ. The weld metal part of these cracks was added into the TOTAL-WELD-crack-length and the part on the HAZ was added into the TOTAL-HAZ-crack-length. However, in the calculation of total-NUMBER-of-cracks and the MAXIMUM-crack-length measurements, these transition cracks were considered as one crack.

The data obtained from the crack length measurements are shown in the “TOTAL-crack-length versus augmented strain” diagrams (Figures 4.9 and 4.19) and in the “TOTAL-crack-length versus line energy diagrams” (Figures 4.10 and 4.20). The change in total-NUMBER-of-cracks and MAXIMUM-crack-length with changing line energy and augmented strain were also analysed and is given in graphical forms (Figures 4.13, 4.16, 4.23 and 4.26).

#### **4.3.1 Results of the Crack Length Measurements on TIG-AC Welded MVT Specimens**

The crack length measurement data of Modified Varestraint Test with TIG-AC welding process is given in Appendix B, from Table B1 to Table B40. The data is illustrated as a function of applied augmented strain and line energy on the change of TOTAL-crack-length, change of number-of-cracks and change of MAXIMUM-crack-length. Due to the high number of applied line energies whole results could not be clearly illustrated in the TOTAL-crack-length versus augmented strain diagram. To interpret the general tendency, only some selected data were plotted (Figure 4.9). Whole data could be better illustrated in TOTAL-crack-length versus line energy diagram in Figure 4.10. Tests at 9.1 kJ/cm line energy resulted in very long and large number of cracks. For that reason this line energy was excluded from the normal weldability range. The error bars in all diagrams were put based on the reproducibility study given in Section 3.4.1.3.

All the cracks were classified as weld-metal-cracks and HAZ-cracks (Appendix B). The change in TOTAL-crack-length as a function of line energy under this type of classification is shown in Figures 4.11 and 4.12 respectively.



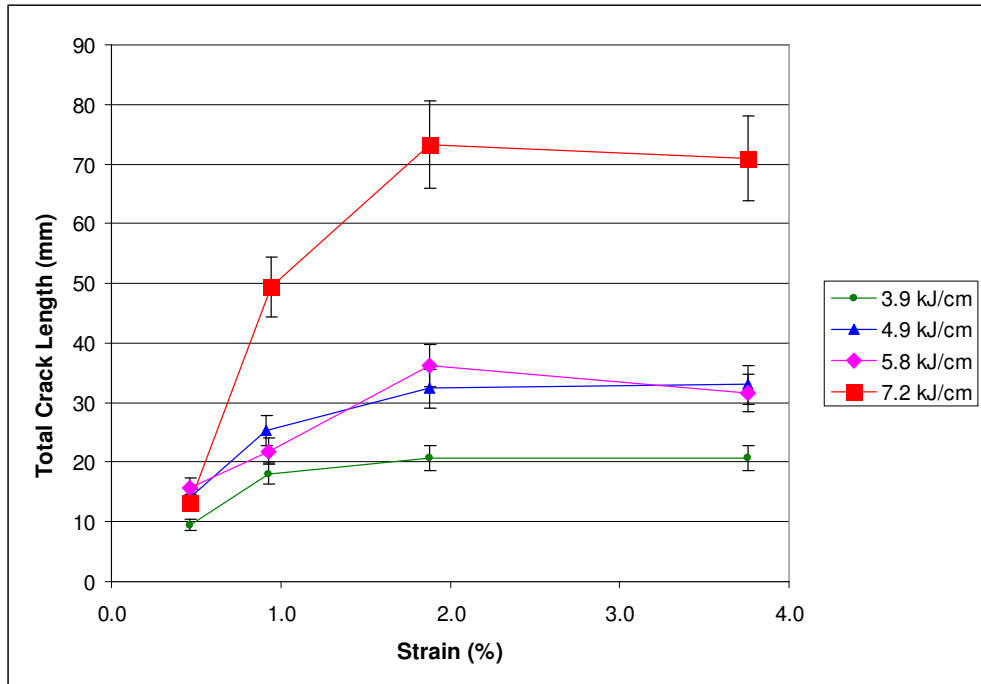


**Figure 4.9:** TOTAL-crack-length versus augmented strain diagram for selected line energy values in Modified Varestraint Test with TIG-AC welding.

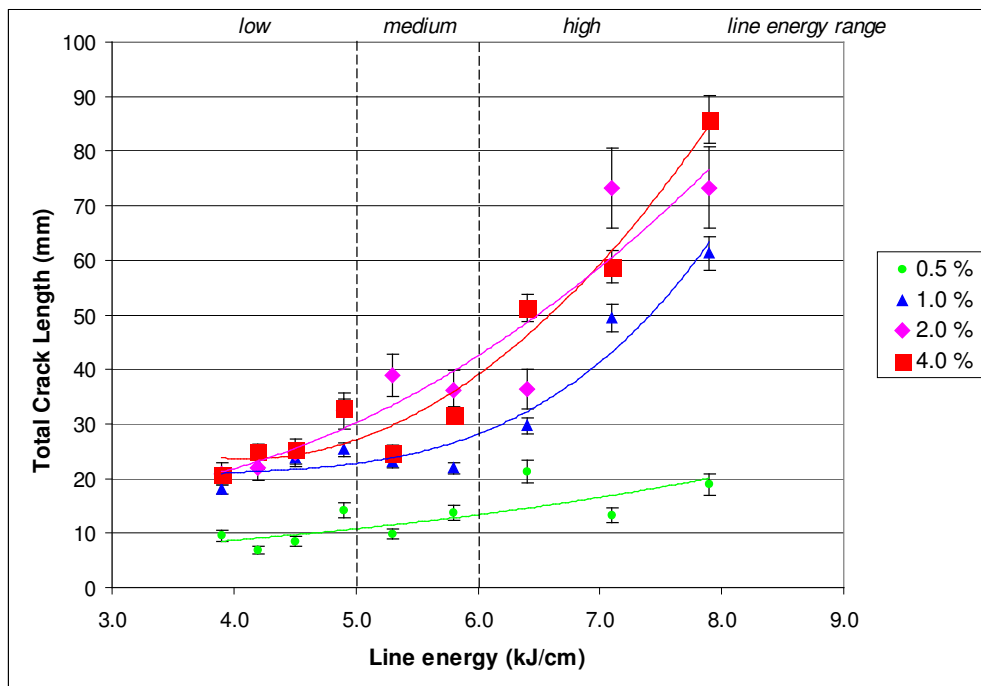


**Figure 4.10:** TOTAL-crack-length versus line energy diagram for different augmented strain values in Modified Varestraint Test with TIG-AC welding.

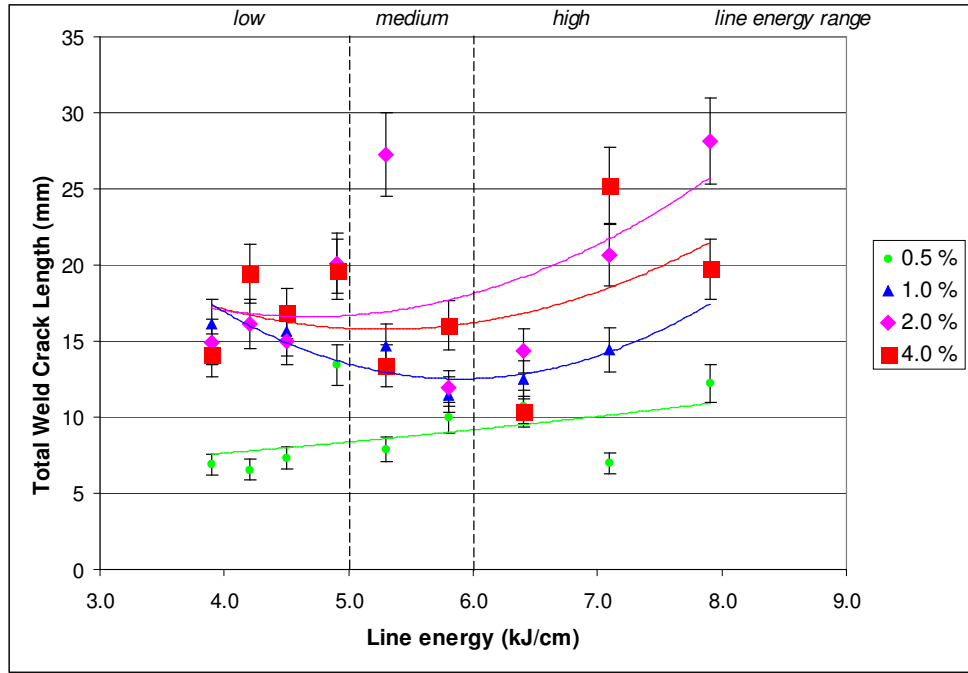


**Figure 4.11:** TOTAL-WELD-crack-length versus line energy diagram for different augmented strain values in Modified Varestraint Test with TIG-AC welding.

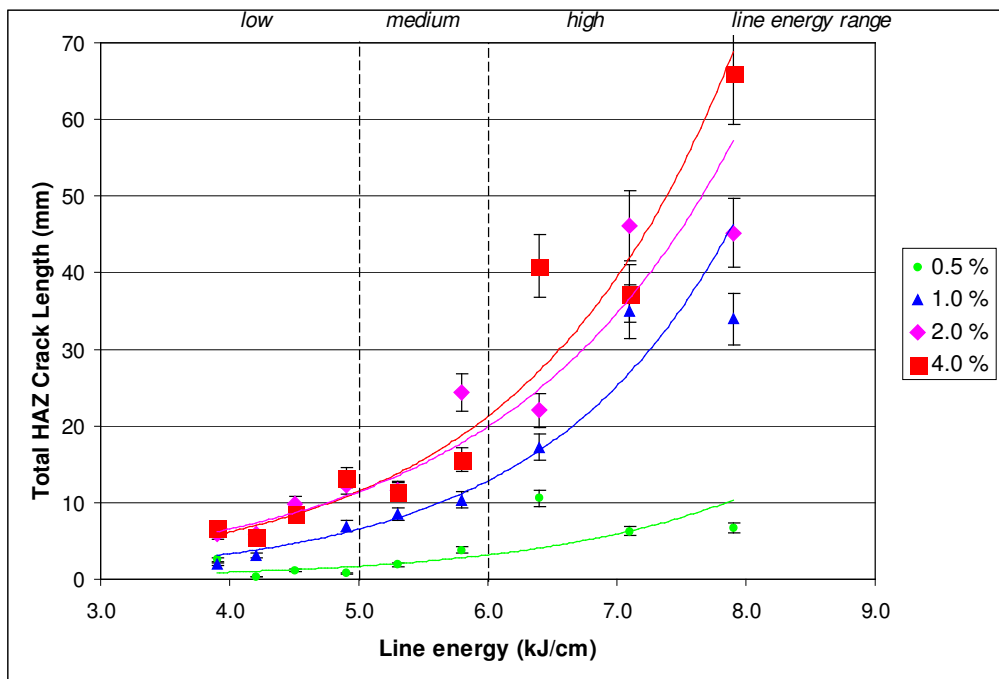


**Figure 4.12:** TOTAL-HAZ-crack-length versus line energy diagram for different augmented strain values in Modified Varestraint Test with TIG-AC welding.

For TIG-AC welding, Figures 4.13 to 4.15 shows the total-NUMBER-of-cracks and the crack distribution in weld metal and heat affected zone i.e. number of solidification and liquation cracks as a function of strain and line energy.

The MAXIMUM-crack-length data for TIG-AC welds are summarized in Figure 4.16 showing the dependence on the line energy at various strain levels. Line energy and strain dependence of MAXIMUM-crack-lengths in weld metal and HAZ are given in Figures 4.17 and 4.18 respectively.

The results of the cracking tendency in low, medium and high line energy ranges will be presented in the subsequent sections.

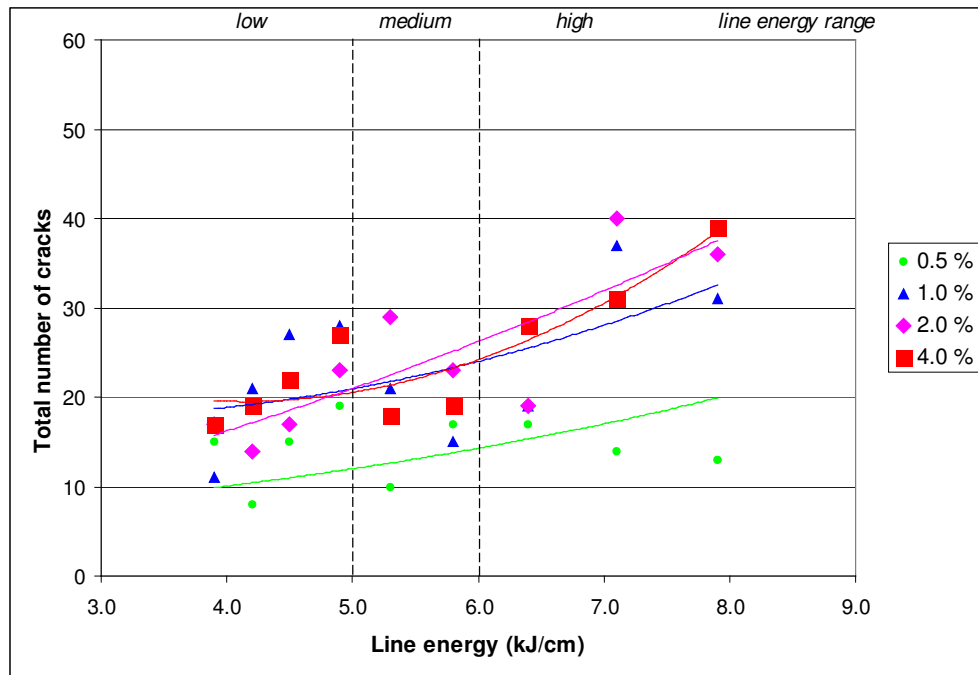


**Figure 4.13:** Total-NUMBER-of-cracks versus line energy diagram for different augmented strain values in Modified Varestraint Test with TIG-AC welding.

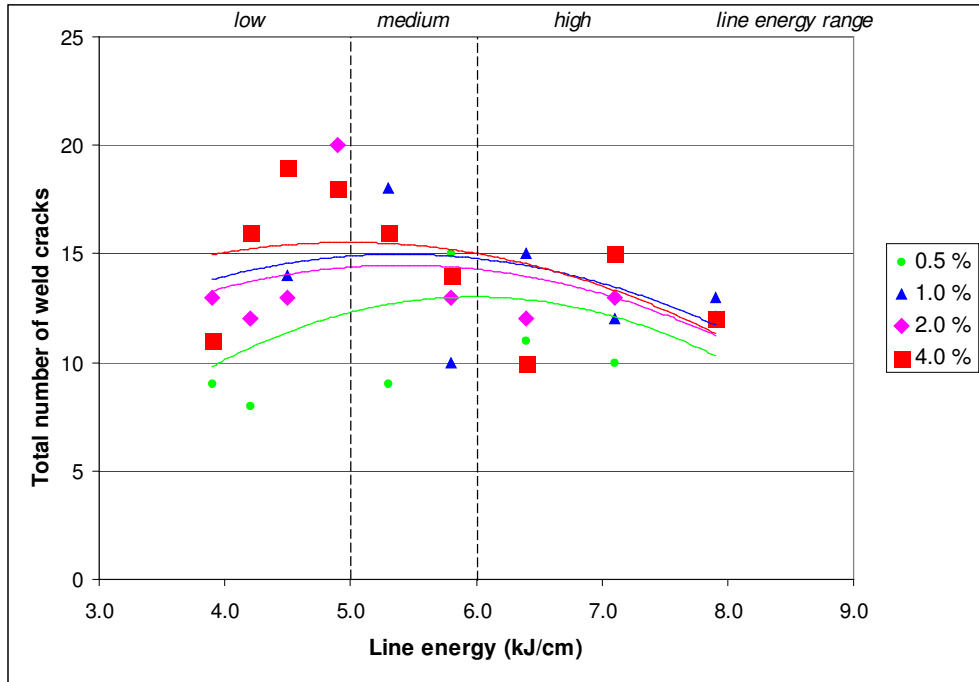


**Figure 4.14:** Total-**NUMBER**-of-**WELD**-cracks versus line energy diagram for different augmented strain values in Modified Varestraint Test with TIG-AC welding.

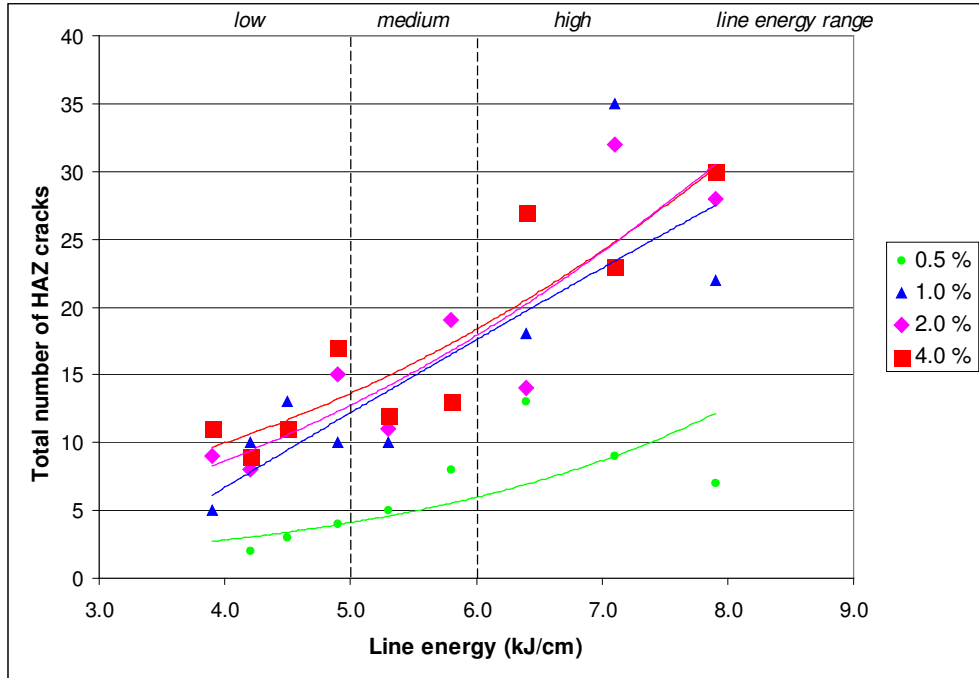


**Figure 4.15:** Total-**NUMBER**-of-**HAZ**-cracks versus line energy diagram for different augmented strain values in Modified Varestraint Test with TIG-AC welding.

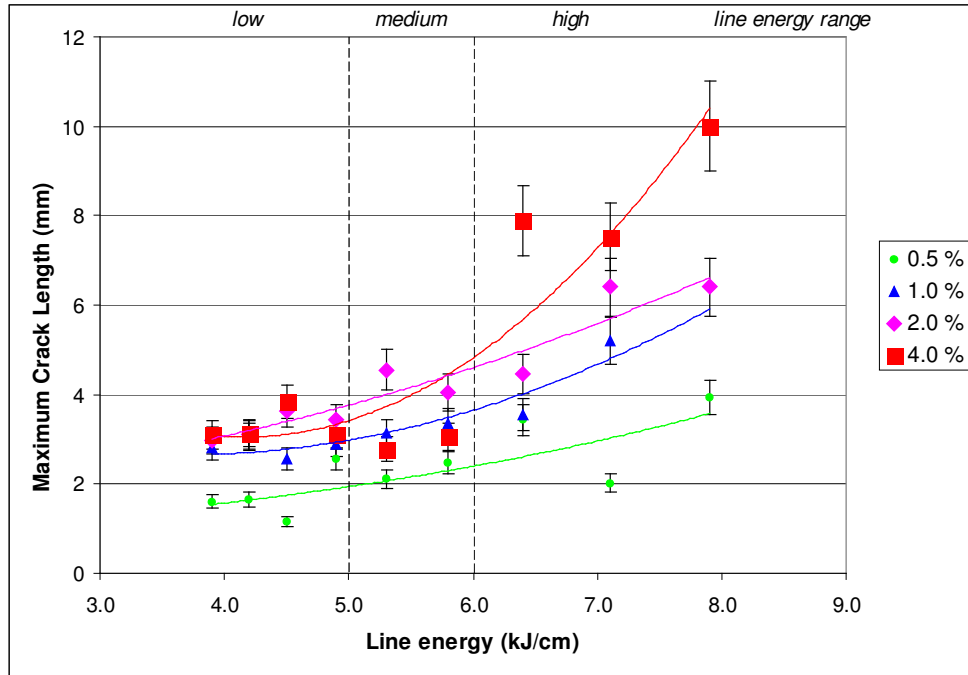


**Figure 4.16:** MAXIMUM-crack-length versus line energy diagram for different augmented strain values in Modified Varestraint Test with TIG-AC welding.

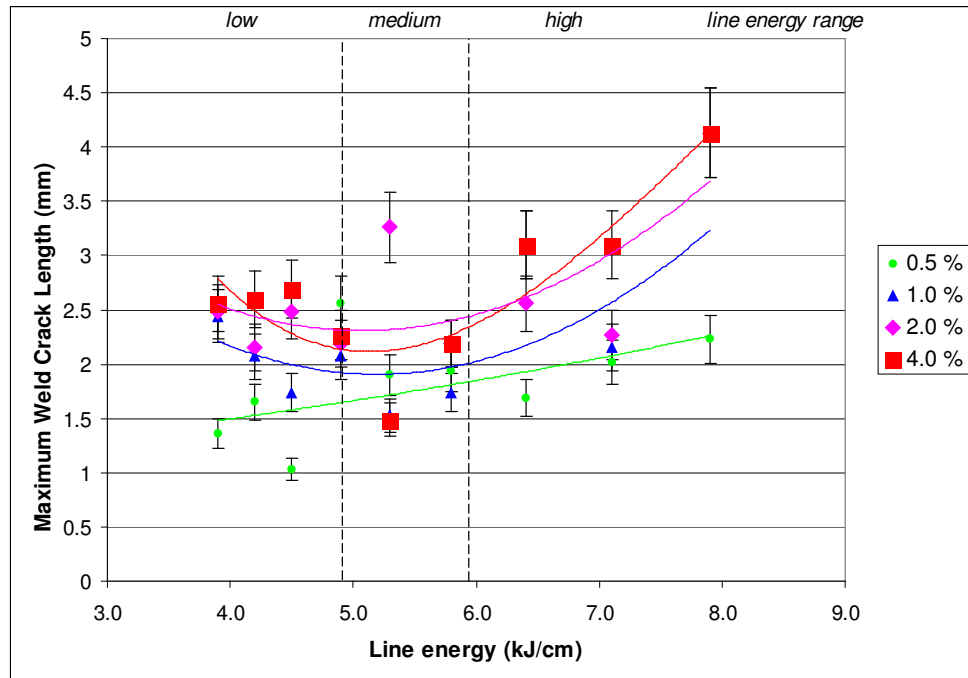


**Figure 4.17:** MAXIMUM-WELD-crack-length versus line energy diagram for different augmented strain values in Modified Varestraint Test with TIG-AC welding.

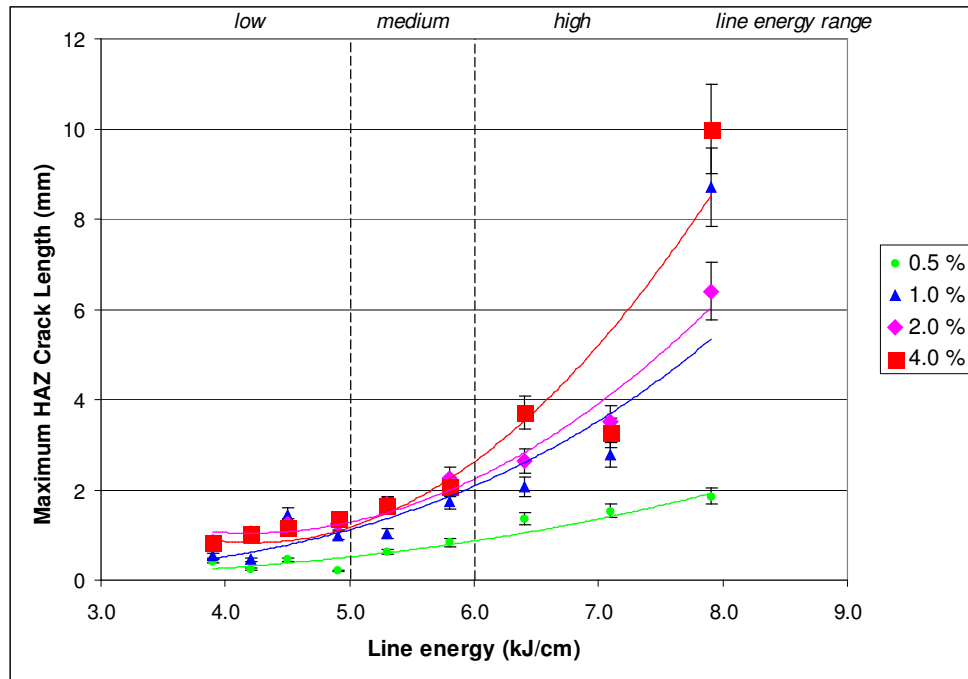


**Figure 4.18:** MAXIMUM-HAZ-crack-length versus line energy diagram for different augmented strain values in Modified Vareststraint Test with TIG-AC welding.

#### 4.3.1.1 Hot Cracking Tendency of TIG-AC Welded Specimens in Low Line Energy Range

##### *a) TOTAL-crack-length in low line energy range:*

As shown in Figure 4.9, the TOTAL-crack-length results indicated a fast increase between low and low-medium strains. Above 1 % strain level, the rate of increase in hot cracking tendency with increasing strain level has decreased. The TOTAL-crack-length values obtained at medium and high strain levels were close to each other (Figures 4.9 and 4.10). On the other hand, the increase in line energy caused an increase in TOTAL-crack-length.

The amount of TOTAL-WELD-crack-length values was clearly higher at medium and high strain levels than the values obtained at low strain level (Figure 4.11). The tendency curves in TOTAL-WELD-crack-length showed

a low increasing rate at low and medium strain levels, a fast decreasing rate at 1 % strain level and slow decreasing rate at high strain level.

The general trend in TOTAL-HAZ-crack-length increased with the increasing in line energy at low, medium and high strain levels (Figure 4.12). The rate of increase in TOTAL-HAZ-crack-length was low at low strain level. An increase in augmented strain resulted in an increase in the TOTAL-HAZ-crack-length. The tendencies of TOTAL-HAZ-crack-length values for medium and high strains were close to each other.

*b) Total-NUMBER-of-cracks in low line energy range:*

In general, the tendency in the total-NUMBER-of-cracks increased with increasing in line energy (Figure 4.13). The magnitudes obtained in tendency curves for low-medium and high strains were close to each other. At low strain, less number of cracks was observed. The total-NUMBER-of-cracks results had a large scatter band.

The total-NUMBER-of-WELD-crack formation tendencies increased with a decaying rate (Figure 4.14).

The total-NUMBER-of-HAZ-cracks showed almost linear increase with the increasing line energy at each strain level (Figure 4.15). The rate of increase in total-NUMBER-of-HAZ-cracks at low strain was lower than for higher strains.

*c) MAXIMUM-crack-length in low line energy range:*

Here, there was an increase in MAXIMUM-crack-length with the increase in line energy (Figure 4.16). The MAXIMUM-crack-length increased as the applied strain was increased. However, less crack length was found for high straining as compared to medium straining.

The tendencies observed in MAXIMUM-WELD-crack-length and MAXIMUM-HAZ-crack length (Figures 4.17 and 4.18) were similar with the ones presented in TOTAL-crack-length data respectively (Figure 4.11 and 4.12).

#### **4.3.1.2 Hot Cracking Tendency of TIG-AC Welded Specimens in Medium Line Energy Range**

##### *a) TOTAL-crack-length in medium line energy range:*

With increasing strain, the TOTAL-crack-length has increased in a nearly linear rate up to medium strain level. Above this point the results showed a decrease in TOTAL-crack-length at high strains (Figure 4.9). The increase in line energy caused a low increasing rate in TOTAL-crack-length for low and low-medium strain levels and a high increasing rate in TOTAL-crack-length for medium and high strains (Figure 4.10).

For low and medium strain levels, the TOTAL-WELD-crack-length values increased with the increase in line energy. For low-medium strain level, there was a decreasing tendency with decaying rate (Figure 4.11).

In general the TOTAL-HAZ-crack-length showed an increasing trend at low, medium and high strain levels (Figure 4.12). The rate of increase in TOTAL-HAZ-crack-length was a power law function. However, the values obtained at high strain were lower than the ones obtained at medium strain.

##### *b) Total-NUMBER-of-cracks in medium line energy range:*

For low, low-medium, medium and high strain levels the tendencies in total-NUMBER-of-cracks increased with an increase in line energy (Figure 4.13). For low-medium and high strains, the tendency curves of total-NUMBER-of-cracks were close to each other. The highest total-NUMBER-of-cracks were obtained for medium strain level.



The total-NUMBER-of-WELD-cracks at low strain level increased with an increase in line energy (Figure 4.14). But the increase was a transient one. On the other hand, for low-medium, medium and high strains the trend was decreasing one.

With increasing line energy, the total-NUMBER-of-HAZ-cracks showed almost a linear increase at each strain level (Figure 4.15). The rate of increase in total-NUMBER-of-HAZ-cracks at low strain was lower than the ones obtained in higher strains.

*c) MAXIMUM-crack-length in medium line energy range:*

In general, the MAXIMUM-crack-length has increased with increase in line energy (Figure 4.16). However, high straining resulted in shorter lengths as compared with medium straining.

The tendencies observed in MAXIMUM-WELD-crack-length and MAXIMUM-HAZ-crack length (Figures 4.17 and 4.18) were similar with the ones presented in TOTAL-crack-length data respectively (Figure 4.11 and 4.12).

#### **4.3.1.3 Hot Cracking Tendency of TIG-AC Welded Specimens in High Line Energy Range**

*a) TOTAL-crack-length in high line energy range:*

The rate of increase in the TOTAL-crack-length from low to medium strains was rapid (Figure 4.9). But, above medium strain level, the rate has decreased. The TOTAL-crack-lengths obtained at medium and high strain levels were close to each other (Figures 4.9 and 4.10).

For all strain levels, the TOTAL-WELD-crack-length has increased with an increase in line energy. At low-medium, medium and high strains, the rate of increase was a power law function (Figure 4.11).

The TOTAL-HAZ-crack-length increased with an increase in line energy (Figure 4.12). The rate of increase was a power function of augmented strain.

*b) Total-NUMBER-of-cracks in high line energy range:*

For low, low-medium, medium and high strain levels the total-NUMBER-of-cracks increased with increasing in line energy (Figure 4.13).

For all strain levels, the total-NUMBER-of-WELD-cracks have decreased with increasing in line energy (Figure 4.14).

With increasing line energy, TOTAL-NUMBER-of-HAZ-cracks showed almost a linear increase at each strain level (Figure 4.15).

*c) MAXIMUM-crack-length in high line energy range:*

In general, for all strain levels the MAXIMUM-crack-length increased with an increasing rate with an increase in line energy (Figure 4.16).

MAXIMUM-WELD-crack-length has also increased with increasing line energy (Figure 4.17). The tendencies obtained here was similar with that of observed in TOTAL-WELD-crack-length data. (Figure 4.11).

MAXIMUM-HAZ-crack length has also increased with the increasing in line energy. The corresponding rate of increase was low for the low strain levels (Figure 4.18).

The general cracking tendencies observed in TIG-AC welded MVT specimens were summarized in Table 4.1.

**Table 4.1:** Hot cracking tendencies observed in TIG-AC welded MVT specimens.

Strain level	Compared property	Line energy range		
		< 5 kJ/cm <b>Low</b> ⇒ increasing	5 to 6 kJ/cm <b>Medium</b> ⇒ increasing	> 6 kJ/cm <b>High</b> ⇒ increasing
Low	TOTAL crack length	↑    ↑    ↑	↑    ↑    ↑	↑    ↑    ↑
Low-medium		→    ↓↓    ↑↑	↑    ↓→    ↑↑	↑↑↑    ↑↑    ↑↑↑
Medium		↑    ↓    ↑↑	↑↑    ↑    ↑↑	↑↑↑    ↑↑    ↑↑↑
High		→    ↓    ↑↑	↑↑    →    ↑↑	↑↑↑    ↑↑    ↑↑↑
Low	Total NUMBER of cracks	↑    ↑    ↑	↑    ↑→    ↑	↑    ↓    ↑
Low-medium		↑    ↑    ↑↑	↑    ↓    ↑↑	↑    ↓    ↑↑
Medium		↑↑    ↑    ↑↑	↑↑    ↓    ↑↑	↑    ↓    ↑↑
High		→    ↑    ↑↑	↑    ↓    ↑↑	↑    ↓    ↑↑
Low	MAXIMUM crack length	↑    ↑    ↑	↑    ↑    ↑	↑    ↑    ↑
Low-medium		↑    ↓    ↑	↑    →↑    ↑↑	↑    ↑↑    ↑↑
Medium		↑    ↓    →↑	↑    →↑    ↑↑	↑    ↑↑    ↑↑
High		→↑    ↓    →↑	↑    →↑    ↑↑	↑↑    ↑↑    ↑↑↑

**Key:**

↑ : Increasing tendency

→ : Stable magnitude

↓ : Decreasing tendency

Frequency of arrows indicate the rate of change

Black arrows : GENERAL tendency

Blue arrows : Tendency in WELD metal cracks

Red arrows : Tendency in HAZ cracks

⇒ : Shows the increase in line energy in a given range

**Strain level:**

Low: 0.5 %

Low-medium: 1.0 %

Medium: 2.0 %

High: 4.0 %

### 4.3.2 Results of the Crack Length Measurements on TIG-DC Welded MVT Specimens

The crack measurement results of the TIG-DC welded MVT specimens are given in Appendix B from Tables B41 to Table B112. The results were presented in a similar way as in Section 4.3.1. To show the general tendency, selected data were plotted in the TOTAL-crack-length versus augmented strain diagram (Figure 4.19). The whole data of TOTAL-crack-lengths were plotted in TOTAL-crack-length versus line energy diagram (Figure 4.20).

Diagrams showing the contribution of solidification and liquation cracks on the TOTAL-crack-length as a function of line energy can be seen in Figures 4.21 and 4.22 respectively.

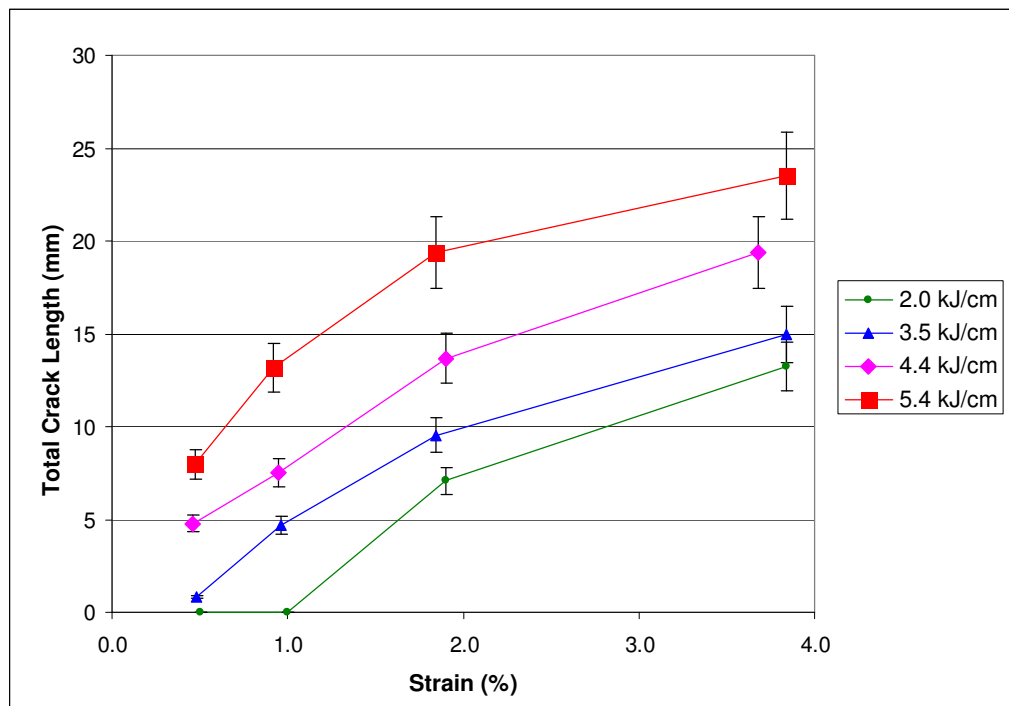


**Figure 4.19:** TOTAL-crack-length versus augmented strain diagram for selected line energy values in Modified Varestraint Test with TIG-DC welding.

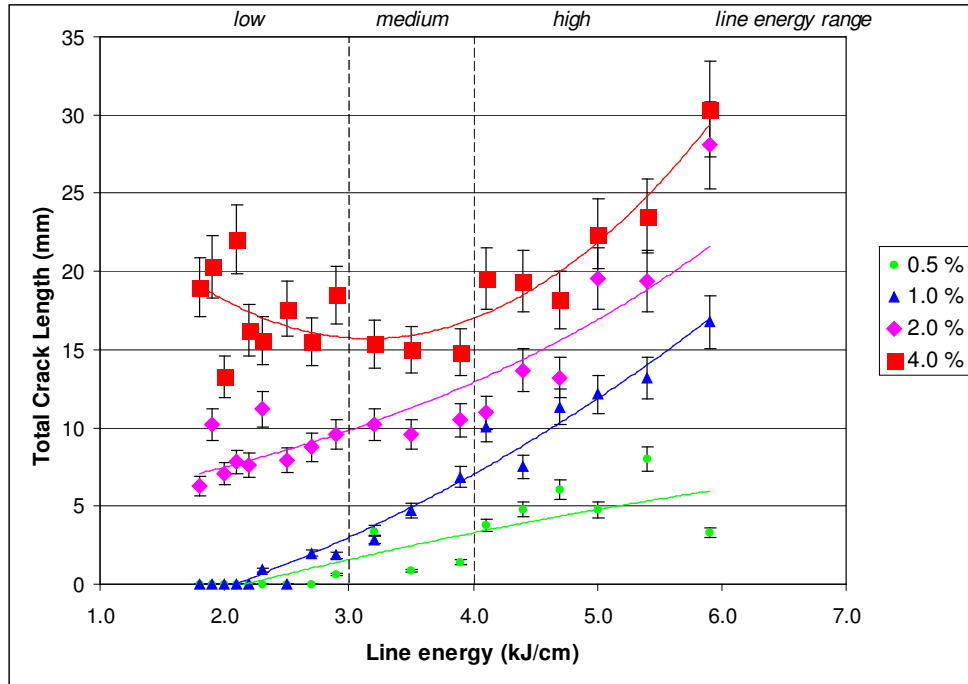


**Figure 4.20:** TOTAL-crack-length versus line energy diagram for different augmented strain values in Modified Varestraint Test with TIG-DC welding.

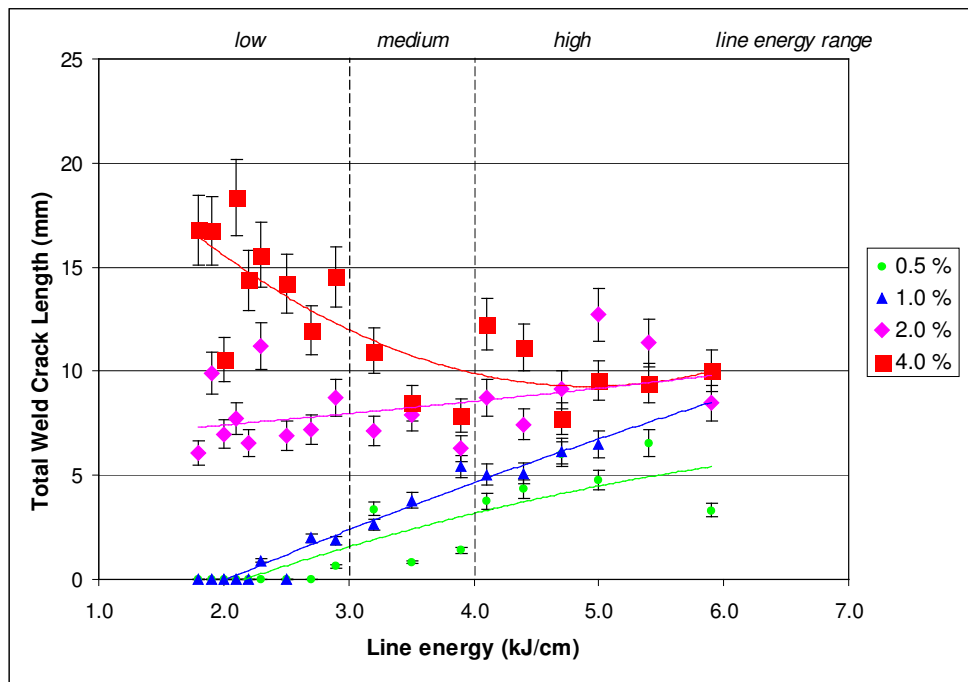


**Figure 4.21:** TOTAL-WELD-crack-length versus line energy diagram for different augmented strain values in Modified Varestraint Test with TIG-DC welding.

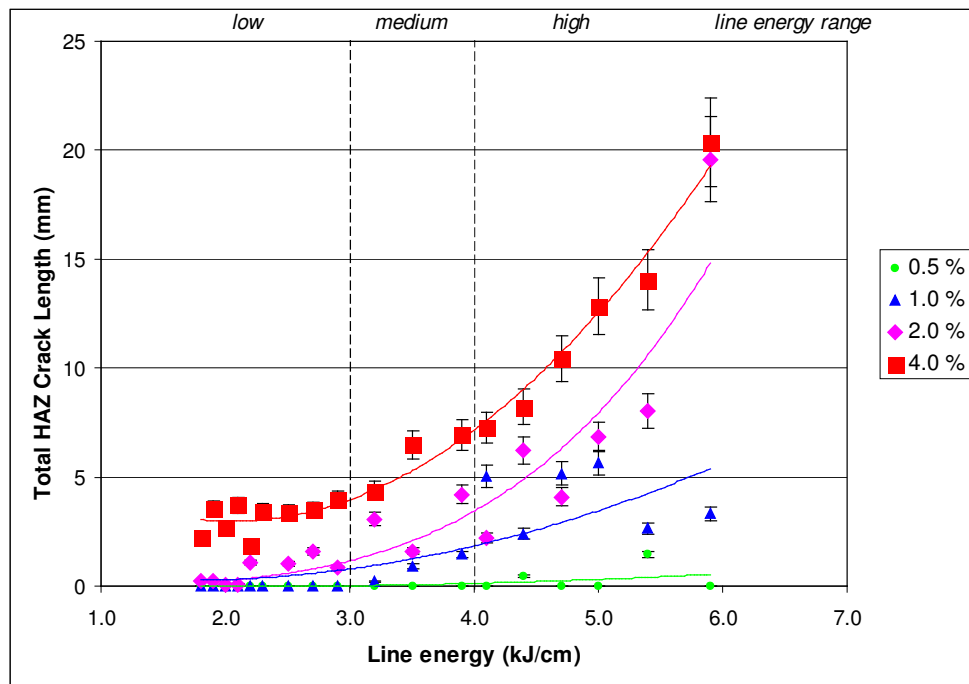


**Figure 4.22:** TOTAL-HAZ-crack-length versus line energy diagram for different augmented strain values in Modified Varestraint Test with TIG-DC welding.

The data obtained in TIG-DC welded MVT specimens are also classified by the total-NUMBER-of-cracks as a function of line energy (Figure 4.23). The change in NUMBER-of-WELD-cracks and NUMBER-of-HAZ-cracks as a function of line energy is shown in Figures 4.24 to 4.25.

The line energy dependence of the MAXIMUM-crack-length is given in graphical form in Figure 4.26. Line energy and strain dependence of MAXIMUM-WELD-metal and HAZ crack lengths are given in Figures 4.27 and 4.28 respectively.

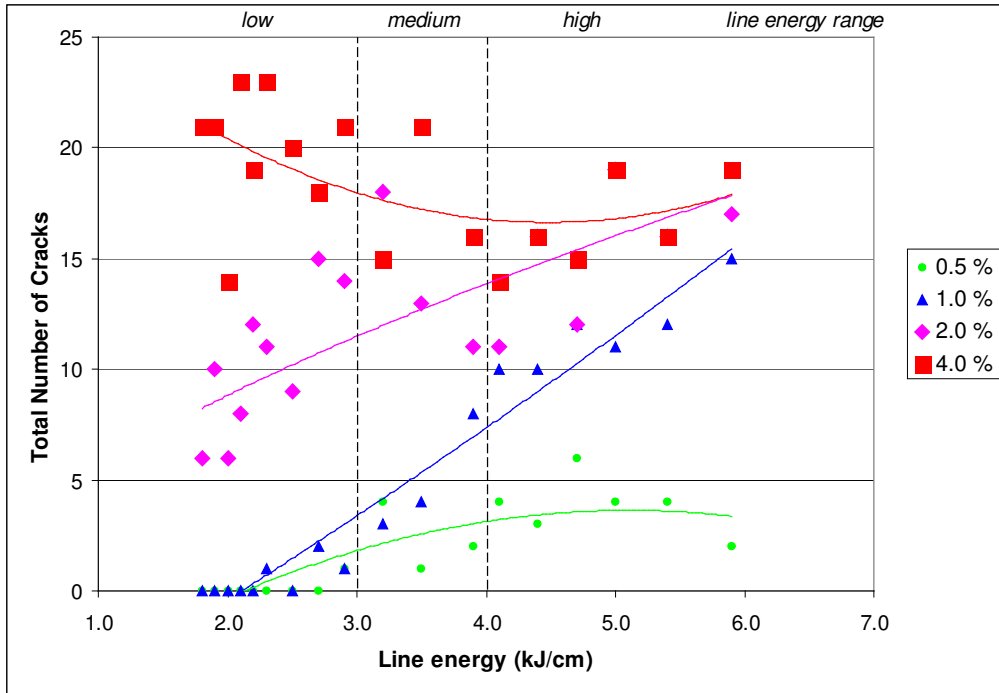


**Figure 4.23:** Total-NUMBER-of-cracks versus line energy diagram for different augmented strain values in Modified Varestraint Test with TIG-DC welding.

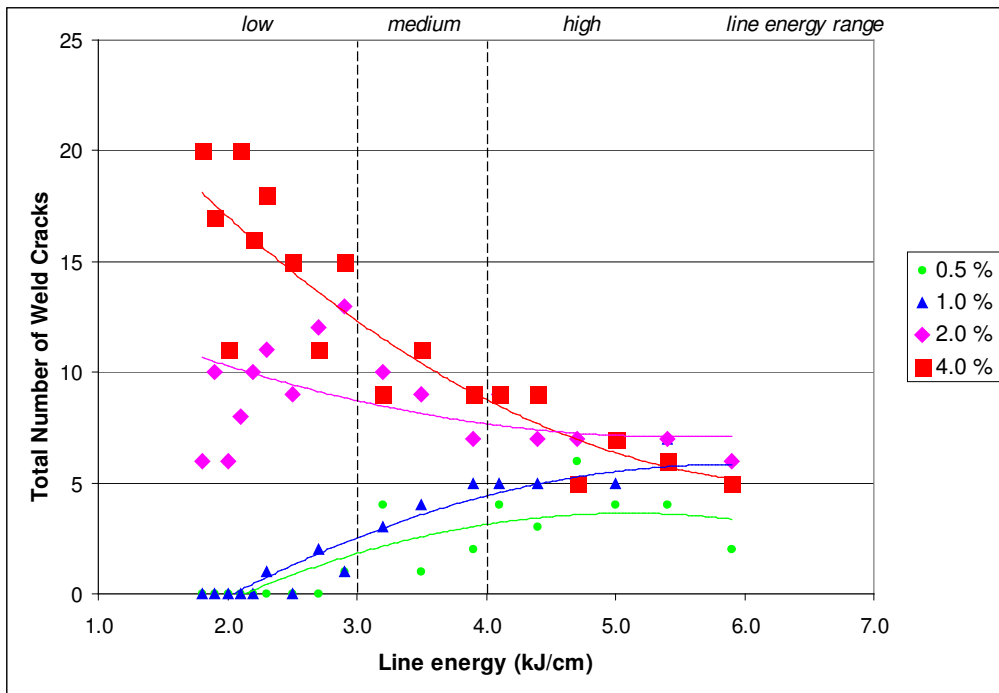


**Figure 4.24:** Total-NUMBER-WELD-cracks versus line energy diagram for different augmented strain values in Modified Varestraint Test with TIG-DC welding.

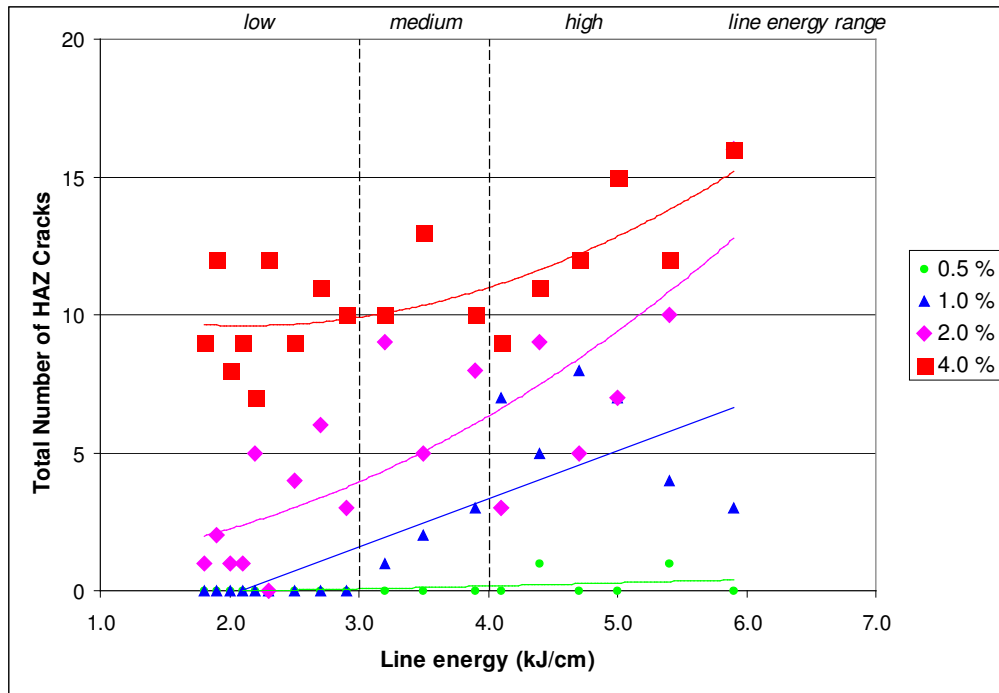


**Figure 4.25:** Total-NUMBER-of-HAZ-cracks versus line energy diagram for different augmented strain values in Modified Varestraint Test with TIG-DC welding.

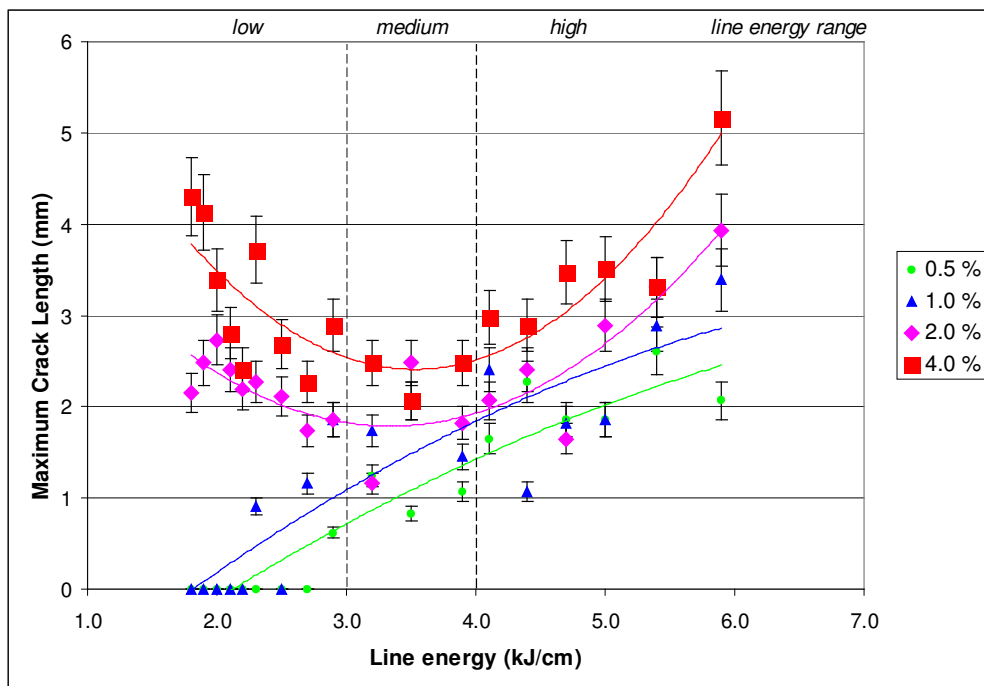


**Figure 4.26:** MAXIMUM-crack-length versus line energy diagram for different augmented strain values in Modified Varestraint Test with TIG-DC welding.



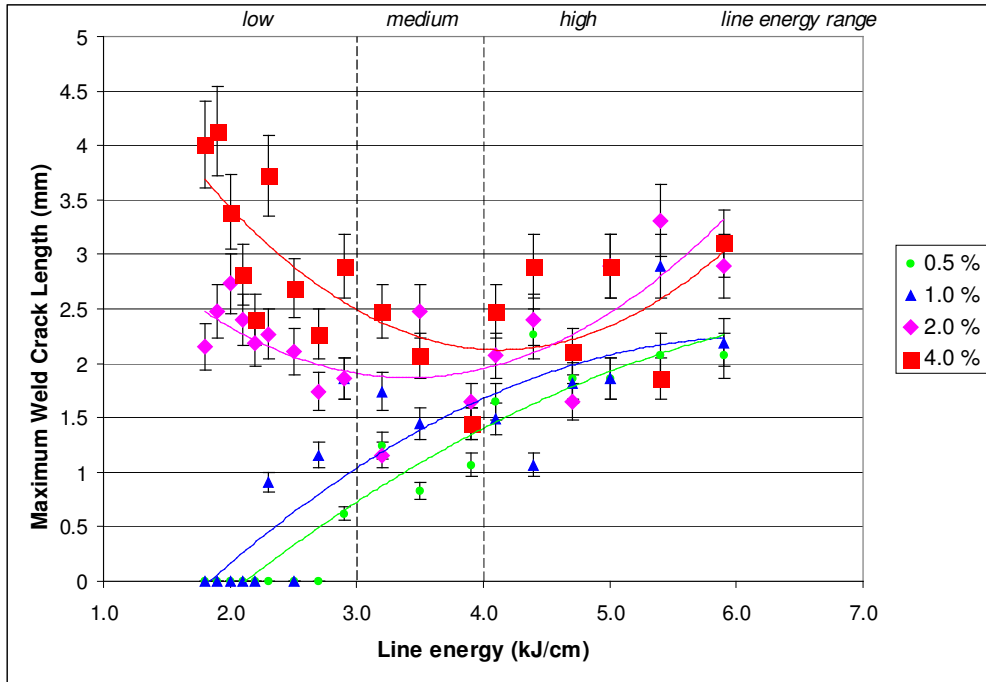


**Figure 4.27:** MAXIMUM-WELD-crack-length versus line energy diagram for different augmented strain values in Modified Varestraint Test with TIG-DC welding.

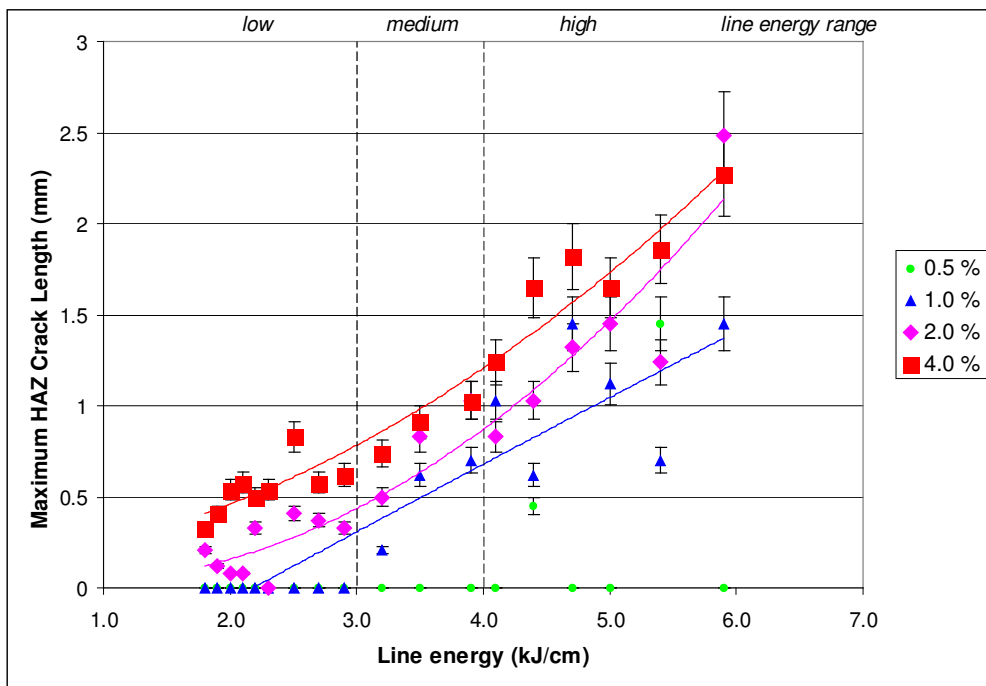


**Figure 4.28:** MAXIMUM-HAZ-crack-length versus line energy diagram for different augmented strain values in Modified Varestraint Test with TIG-DC welding.

#### 4.3.2.1 Hot Cracking Tendency of TIG-DC Welded Specimens in Low Line Energy Range

##### *a) TOTAL-crack-length in low line energy range:*

Hot cracking tendency at all line energy levels showed a transient decrease (Figure 4.19). In general, the magnitude of the TOTAL-crack length was proportional with the applied strain (Figure 4.20). However, no cracking was observed for low and low-medium strain levels and cracking started at about 2.2 kJ/cm. For high strain level, the tendency in TOTAL-crack-length decreased with the increasing in line energy.

The tendencies in TOTAL-WELD-crack-length as a function of line energy (Figure 4.21) were similar with that of obtained in TOTAL-crack-length (Figure 4.20).

The contribution of the TOTAL-HAZ-crack-length to the TOTAL-crack-length is low. At high and medium strains there was an increasing trend in TOTAL-HAZ-crack-length with a low rate (Figure 4.22). No HAZ cracking was seen for low strain. At low-medium strains the tendency curve showed an increase above 2.2 kJ/cm line energy.

##### *b) Total-NUMBER-of-cracks in low line energy range:*

At low, low-medium and medium strains the total-NUMBER-of-cracks increased with the increase in line energy (Figure 4.23). At low line energies no cracks formed at low and low-medium strains. At high strain, tendency in total-NUMBER-of-cracks decreased with the increase in line energy.

At low and low-medium strain levels, the total-NUMBER-of-WELD-cracks increased with the increase in line energy (Figure 4.24). At high strain, there was a fast decreasing trend with the increase in line energy.

At low strain level, no HAZ cracks formed (Figure 4.25). At low-medium strain level, HAZ cracks were observed above 2.2 kJ/cm line energy. At low-medium and medium strain levels the total-NUMBER-of-HAZ-cracks increased with a high rate. At high strain, the slope of the tendency curve was nearly zero.

*c) MAXIMUM-crack-length in low line energy range:*

An increase in line energy has resulted a decrease in MAXIMUM-crack-length at medium and high strains and increased at low and low-medium strains (Figure 4.26).

As shown in Figure 4.27, the tendency in MAXIMUM-WELD-crack-length was similar to the tendency in MAXIMUM-crack-length.

MAXIMUM-HAZ-crack-length linearly increased as a function of line energy (Figure 4.28). At the low line strain level, no cracks were observed.

#### **4.3.2.2 Hot Cracking Tendency of TIG-DC Welded Specimens in Medium Line Energy Range**

*a) TOTAL-crack-length in medium line energy range:*

The TOTAL-crack-length have increased with an increase in line energy and strain level(Figure 4.20).

At medium line energy, the TOTAL-WELD-crack-length has increased with low, low-medium and medium strain levels (Figure 4.21). At high strain, the TOTAL-WELD-crack-length decreased with increasing in line energy.

At low-medium, medium and high strain levels, TOTAL-HAZ-crack-lengths have increased with increase in line energy (Figure 4.22). At low strain level, no HAZ cracks were observed.

*b) Total-NUMBER-of-cracks in medium line energy range:*

At low, low-medium and medium strain levels total-NUMBER-of-cracks increased with the increase in line energy (Figure 4.23). At high strain level total-NUMBER-of-cracks decreased in a decaying trend with the increase in line energy.

At low and low-medium strain levels total-NUMBER-of-WELD-cracks increased with the increase in line energy (Figure 4.24). At medium and high strain levels there was a decreasing tendency with the increase in line energy.

At low strain level, no HAZ cracks formed (Figure 4.25). At low-medium, medium and high strain levels total-NUMBER-of-HAZ-cracks increased with the increasing line energy.

*c) MAXIMUM-crack-length in medium line energy range:*

At low and low-medium strains, MAXIMUM-crack-lengths increased with linear tendency. At medium and high strains the curve deviated from linearity (Figure 4.26). The tendency in MAXIMUM-WELD-crack-length was similar to the tendency in MAXIMUM-crack-length (Figure 4.27).

MAXIMUM-HAZ-crack-length linearly increased as a function of line energy (Figure 4.28). At the low line strain level, no cracks were observed.

#### **4.3.2.3 Hot Cracking Tendency of TIG-DC Welded Specimens in High Line Energy Range**

*a) TOTAL-crack-length in high line energy range:*

At all strain levels the TOTAL-crack-length increased with an increase in line energy (Figure 4.20). At low strain level, the rate of increase of TOTAL-crack-length was low.

At low, low-medium and medium strain levels the TOTAL-WELD-crack-lengths have increased with line energy (Figure 4.21). At high strain level the TOTAL-WELD-crack-length decreased with the increase in line energy.

At medium and high strain levels, the TOTAL-HAZ-crack-lengths increased with a high trend (Figure 4.22). Below medium strain level, rate of increase in TOTAL-HAZ-crack length decreased with decreasing in strain level.

*b) Total-NUMBER-of-cracks in high line energy range:*

At low-medium, medium and high strain levels, the tendency in total-NUMBER-of-cracks increased with the increase in line energy (Figure 4.23). At low strain level the trend has decayed.

At low, low-medium and medium strain levels the tendency curves of total-NUMBER-of-WELD-cracks showed nearly zero slope (Figure 4.24). At high strain level, total-NUMBER-of-WELD-cracks decreased with increase in line energy.

At all strain levels, the tendency in total-NUMBER-of-HAZ-cracks increased with increasing in line energy (Figure 4.25). At low strain level, increasing rate was low.

*c) MAXIMUM-crack-length in high line energy range:*

At all strain levels, MAXIMUM-crack-length increased with increase in line energy (Figure 4.26). The tendency in MAXIMUM-WELD-crack-length was similar with the tendency in MAXIMUM-crack-length (Figure 4.27). The tendency in MAXIMUM-HAZ-crack-length results increased linearly with increasing line energy (Figure 4.28). At the low strain level, almost no cracks were observed.

The general cracking tendencies observed in TIG-AC welded MVT specimens were summarized in Table 4.2.

**Table 4.2:** Hot cracking tendencies observed in TIG-DC welded MVT specimens.

Strain level	Compared property	Line energy range								
		< 3 kJ/cm <b>Low</b> ⇒ increasing			3 to 4 kJ/cm <b>Medium</b> ⇒ increasing			> 4 kJ/cm <b>High</b> ⇒ increasing		
Low	TOTAL crack length	o↑	o↑	o	↑	↑	o	↑	↑	↑
Low-medium		o↑↑	o↑	o↑	↑↑	↑	↑	↑↑	↑	↑
Medium		↑↑	↑	→↑	↑↑	↑	↑↑	↑↑	↑	↑↑↑
High		↓	↓↓	→↑	→↑	↓	↑↑	↑↑↑	↓→	↑↑↑
Low	Total NUMBER of cracks	o↑	o↑	o	↑	↑	→	→	→	→
Low-medium		o↑↑	o↑	o↑↑	↑↑	↑	↑↑	↑↑	↑→	↑↑
Medium		↑↑	↓	↑	↑	↓	↑↑	↑↑	→	↑↑
High		↓	↓↓	→↑	↓	↓↓	↑	→↑	↓↓	↑↑
Low	MAXIMUM crack length	o↑↑	o↑↑	o	↑↑	↑↑	o	↑↑	↑↑	→
Low-medium		o↑↑	o↑↑	↑↑	↑↑	↑↑	↑↑	↑↑	↑↑	↑↑
Medium		↓↓	↓↓	↑↑	↓→↑	↓→	↑↑	↑↑↑	↑↑↑	↑↑↑
High		↓↓	↓↓	↑↑	↓→↑	↓→	↑↑	↑↑↑	↑↑↑	↑↑↑

Key:

o : No cracking

↑ : Increasing tendency

→ : Stable magnitude

↓ : Decreasing tendency

Frequency of arrows indicate the rate of change

Black arrows : GENERAL tendency

Blue arrows : Tendency in WELD metal cracks

Red arrows : Tendency in HAZ cracks

⇒ : Shows the increase in line energy in a given range

Example:

o↑ : Cracking starts above a critical line energy

Strain level:

Low: 0.5 %

Low-medium: 1.0 %

Medium: 2.0 %

High: 4.0 %

### 4.3.3 Results of the Supplementary Tests

The supplementary tests were run to show the effect of changing die heat conductivity on the hot cracking behaviour of 5086 alloy. Crack measurement results for the whole supplementary test series are given in Appendix B from Table B113 to Table B144. For TIG-AC welded MVT specimens, the change in TOTAL-crack-length as a function of line energy is given in Figure 4.29. In addition, for TIG-DC welded MVT specimens, the change in TOTAL-crack-length as a function of line energy is given in Figure 4.30.

In Figure 4.29, which gives the behaviour in TIG-AC welding, it can be seen that the tendency in TOTAL-crack-length at 0.5 % strain decreased with increasing in line energy. On the other hand, above 0.5 % strain as the augmented strain value increased the tendency in TOTAL-crack-length increased. The obtained TOTAL-crack-length values were proportional with the applied strain on the whole line energy range.

The tendency in TOTAL-crack-length versus line energy obtained in TIG-DC welding showed similar behaviour with the results obtained in TIG-AC welding at low and high strain levels (Figure 4.30).

However, there was a decreasing trend in TOTAL-crack-length at medium strain. The resulting tendency curve was close to that of obtained at 1 % strain level. Moreover, the TOTAL-crack-length values obtained at medium strain at high line energies were between that of obtained at 0.5 and 1 % strain levels.

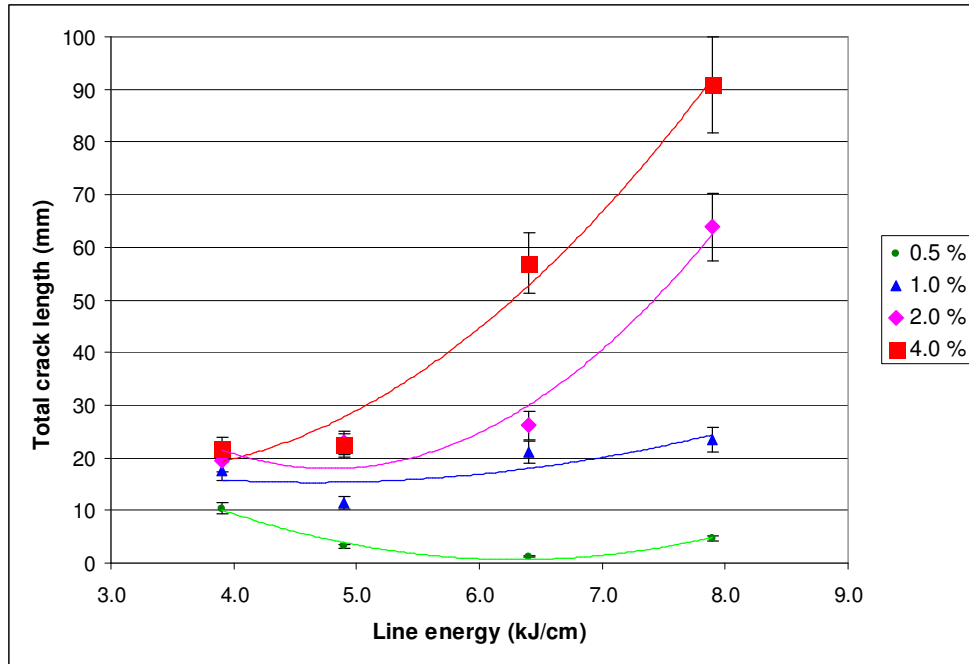


**Figure 4.29:** TOTAL-crack-length versus line energy at different augmented strain values in Modified Varestraint Test with TIG-AC welding. Results from the insulated specimens.

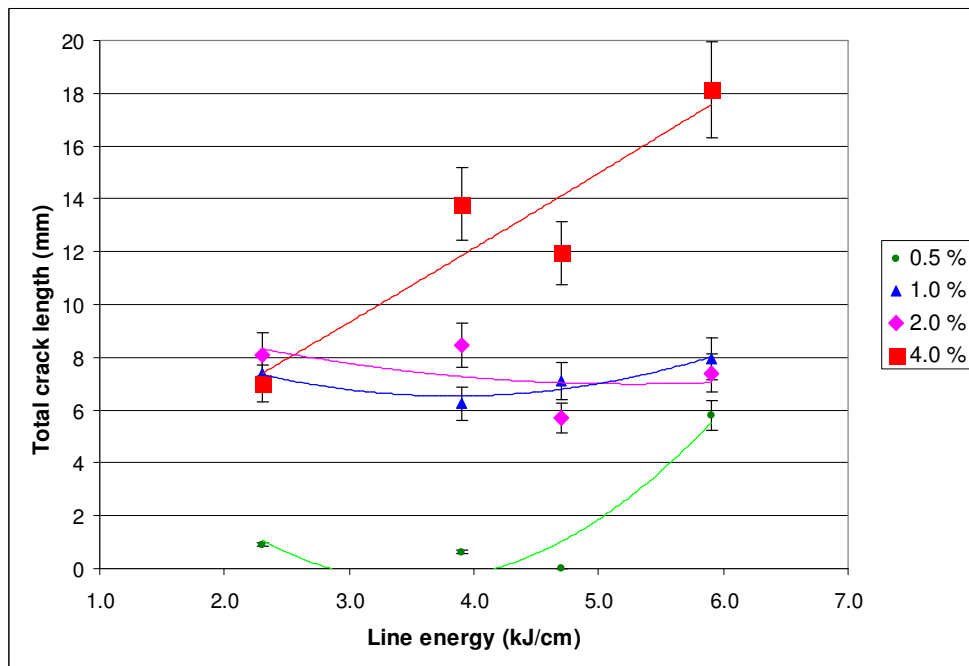


**Figure 4.30:** TOTAL-crack-length versus line energy at different augmented strain values in Modified Varestraint Test with TIG-DC welding. Results from the insulated specimens.



#### 4.4 Results of the Reproducibility Tests

Results of the reproducibility tests are given in Figure 4.31. The data was obtained for TIG-AC welding. Using the results, the maximum deviation from the arithmetic mean of the measured TOTAL-crack-lengths was taken as  $\pm 10\%$ . Actually, the deviation was  $\pm 9.4\%$  at 4.2 kJ/cm;  $\pm 8.6\%$  at 4.9 kJ/cm;  $\pm 8.2\%$  at 5.8 kJ/cm;  $\pm 9.0\%$  at 7.1 kJ/cm. Because of the lower line energies used in TIG-DC welding better reproducibility is expected in TIG-DC welding.

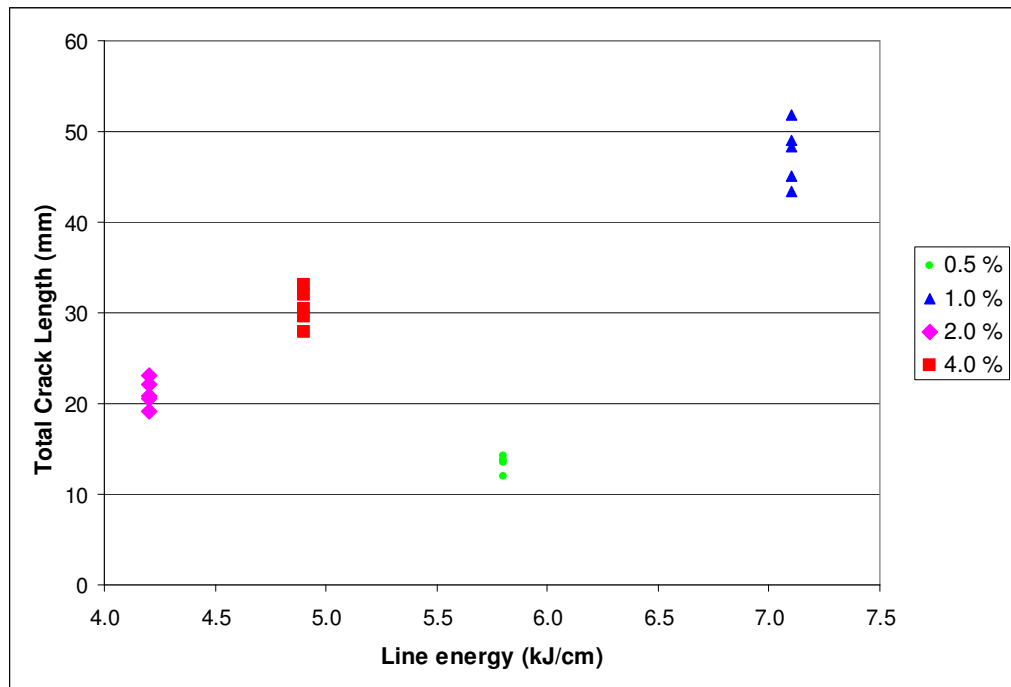


**Figure 4.31:** Results of the reproducibility tests, in the form of the TOTAL-crack-length versus line energy.

#### 4.5 General Features of the Hot Cracks in 5086 Aluminium Alloy MVT Specimens

The results of the metallographic investigations showed that, as expected the formed cracks were in intergranular nature. The cracks, which formed during bending, were located behind and at the sides of the weld pool boundaries. With a careful analysis, it was found that there were four characteristic locations around the weld pool where the cracks were preferentially formed. These locations are illustrated schematically in Figure 4.32. In further discussions depending on the locations of the cracks, the types of the cracks will be designated as “A”, “B”, “C” and “D” as shown in Figure 4.32.

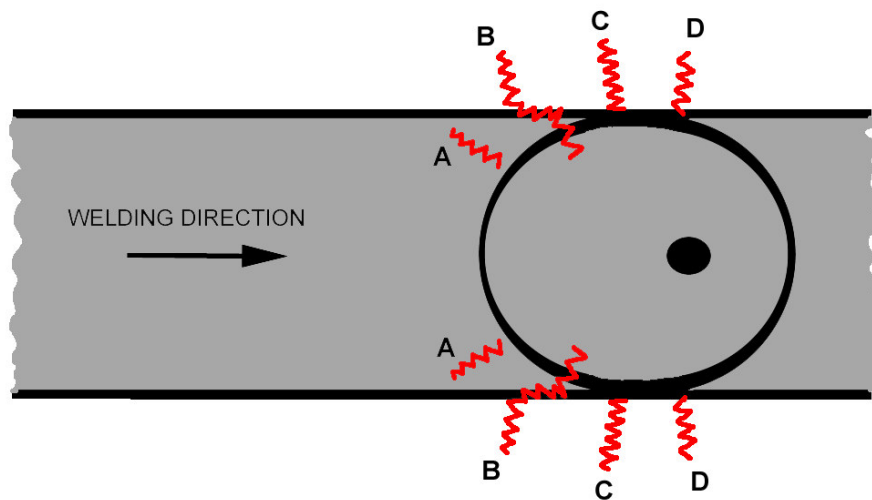


**Figure 4.32:** General locations of the hot cracks on the surface of the 5086 aluminum alloy MVT specimen

There could be more than one crack on each of these locations. Further, depending at the applied parameters, some of them would not form or back-filled (healed) with the interdendritic liquid. Some of the cracks were propagated towards the inside of the solidified pool.

The type “A” cracks represent the solidification cracks at the backside of the pool. These cracks are mostly found in the weld metal (Figure 4.33). The type “B” cracks were always transition cracks. They always started in the PMZ and propagated in both directions i.e. to the weld metal and base material (Figure 4.34). In most of the cases, the longest cracks were found in this zone. The type “C” cracks were found mostly outside the fusion line and are located on a vertical central axis of the elliptical weld pool (Figure 4.35). There was generally more than one crack in this zone. The type “D” cracks were found in the zone starting from vertical central axis towards the welding direction (Figure 4.36). They were generally located outside of the PMZ. Type “D” cracks could be easily healed with the liquid flow from the molten pool.

Since type “B” and “D” cracks are mostly healed, the type “A” and “C” cracks are of most importance in the determination of the hot cracking tendency.

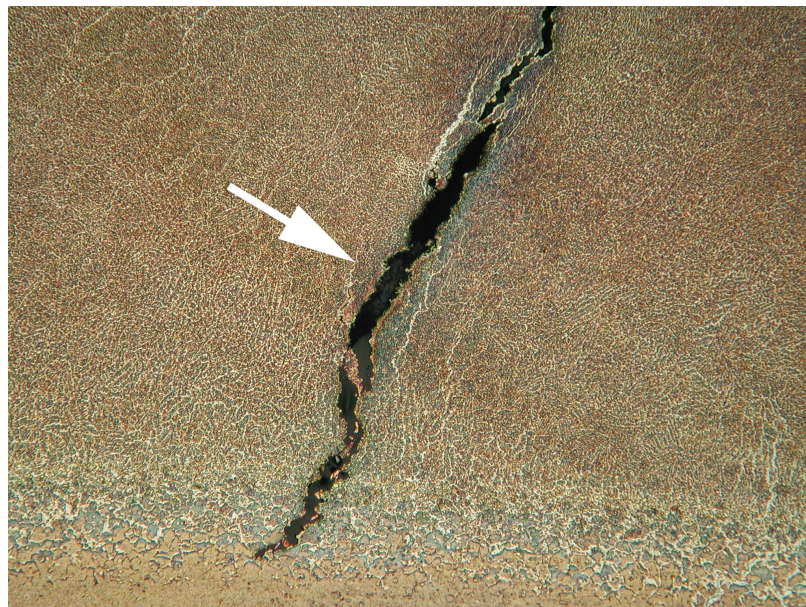


**Figure 4.33:** An example of type “A” crack. The crack is inside the weld metal zone and extended inside the PMZ. White river patterns are healed cracks. 50X; Weck etching.



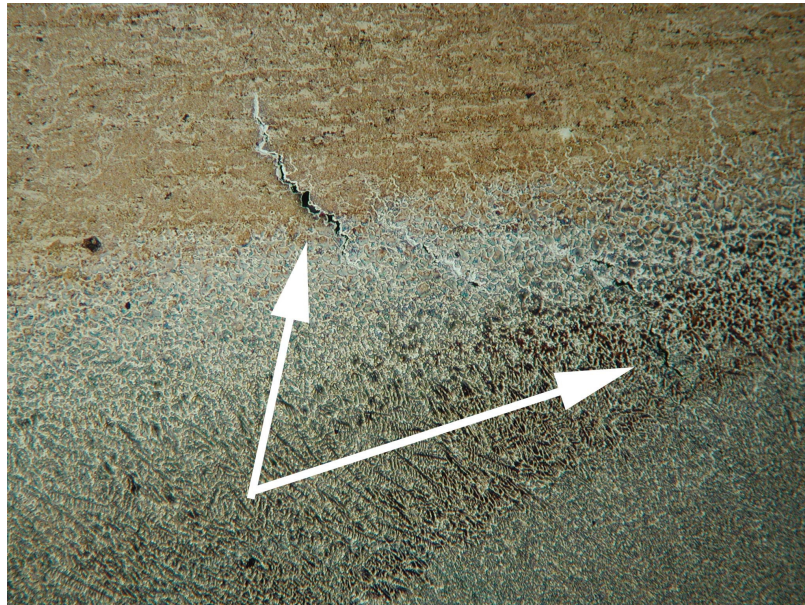


**Figure 4.34:** An example of type “B” crack. Extended both inside the base material and weld metal. The part in the PMZ was partially healed. 50X; Weck etching.

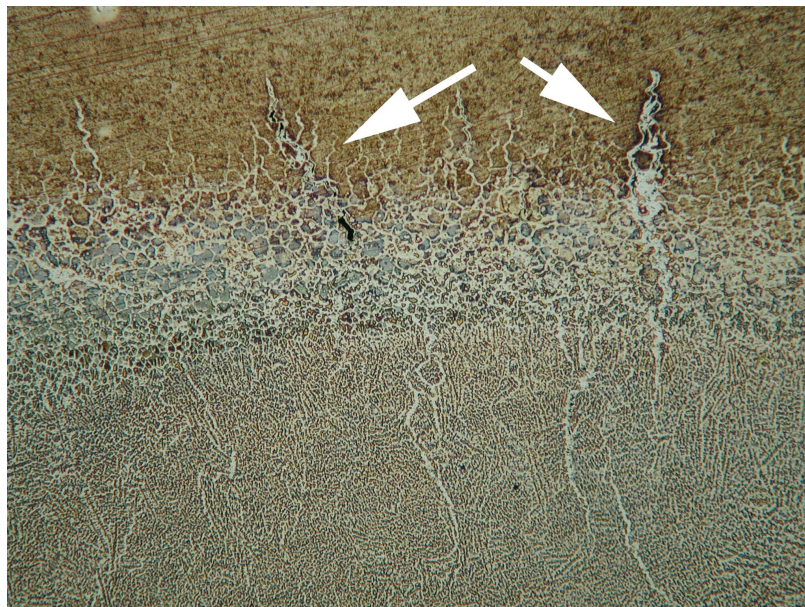


**Figure 4.35:** An example of type “C” cracks. Started from the PMZ and extended mainly towards the base material. There are also healed extensions in the weld metal. 50X; Weck etching.

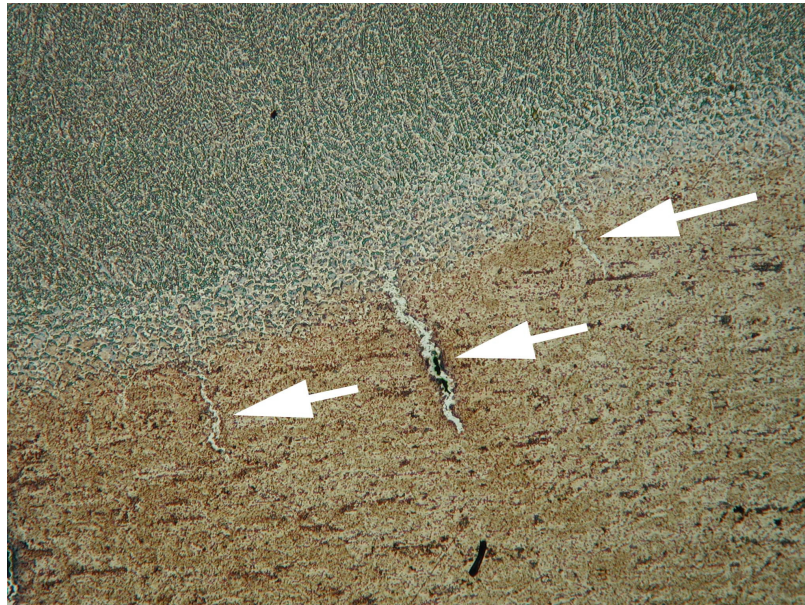


**Figure 4.36:** An example of type “D” cracks. Started from PMZ and extended mainly towards the base material. 50X; Weck etching.

Tables 4.3 and 4.4 summarize the affect of the line energy and strain on the crack type formation in TIG-DC and TIG-AC welded specimens respectively.

In general, in the TIG-DC welded specimens at low strain and medium line energies only type “A” cracks were observed (Table 4.3). With increasing strain type “B”, “C” and “D” cracks formed. However, at high line energies, type “A” cracks were not seen at all.

In TIG-AC welding with low line energy at medium and high strains type “A” cracks rarely formed. Same effect is observed for low strains at medium line energy (Table 4.4). At very high line energies, type “B” cracks were not seen at low strains.

**Table 4.3:**Types of the hot cracks observed in selected TIG-DC welded MVT specimens according to the applied strain and line energy.

Strain	Line energy			
	2.3 kJ/cm	3.9 kJ/cm	4.7 kJ/cm	5.9 kJ/cm
0.5 %	-	A	A	C
1.0 %	A	A,B	A,B,C,D	B,C,D
2.0 %	A,B,C	A,B,C,D	A,B,C,D	B,C,D
4.0 %	A,B,C,D	A,B,C,D	A,B,C,D	B,C,D

**Table 4.4:**Types of the hot cracks observed in selected TIG-AC welded MVT specimens according to the applied strain and line energy.

Strain	Line energy			
	3.9 kJ/cm	4.9 kJ/cm	6.4 kJ/cm	7.9 kJ/cm
0.5 %	C,D	A,B,C,D	B,C	C
1.0 %	A,B,C,D	A,B,C,D	B,C	C,D
2.0 %	A,B,C,D	B,C,D	B,C,D	B,C
4.0 %	A,B,C,D	B,C,D	B,C,D	B,C,D

#### 4.6 Results of the BTR Measurements

The length of cracks running from fusion line towards the base metal was depended on the ductility range of the 5086 alloy. This was explained with the brittleness temperature range “BTR” in the study of Arata et. al. [12]. Figures 4.37 and 4.38 gives the experimental maximum BTR sizes for changed strain and line energy obtained in TIG-DC and TIG-AC welded MVT specimens respectively. Here, the maximum BTR size was based on the maximum type “C” crack lengths found in the present study. Moreover, in Figures 4.37 and 4.38 the experimental results are compared with the BTR sizes for alloy 5083 given by the study of Arata et. al. [12].



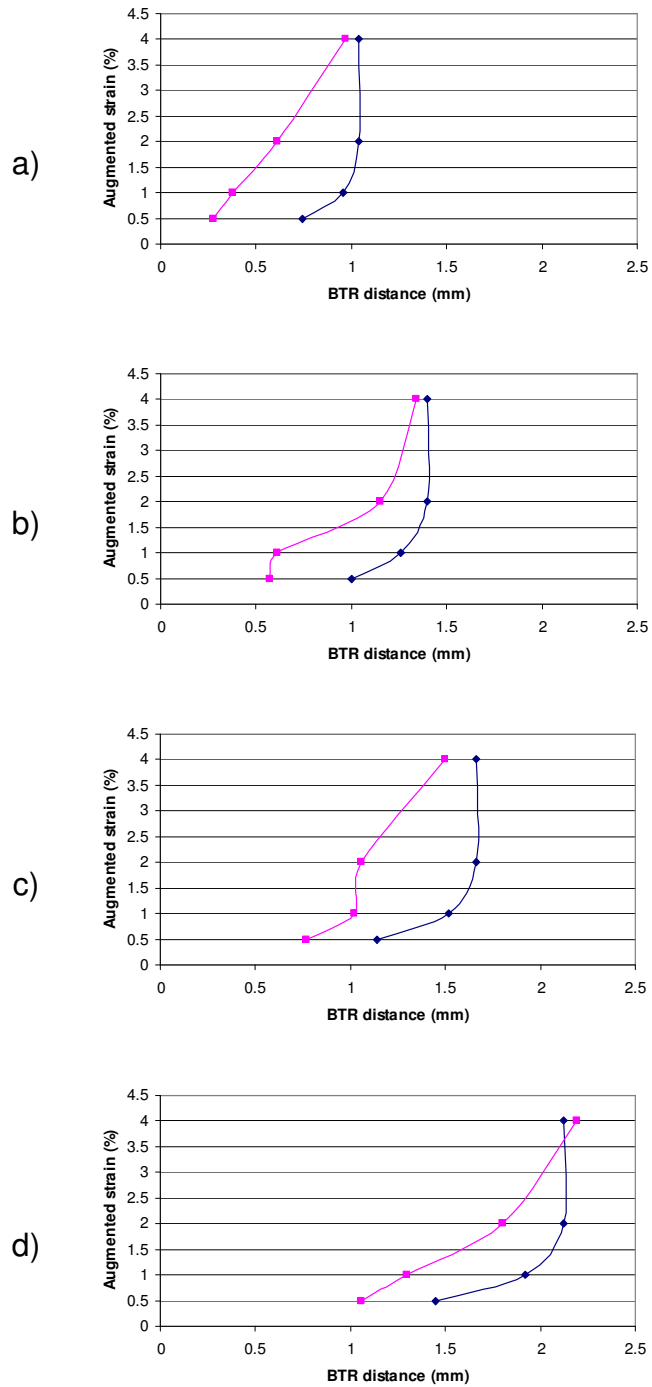


**Figure 4.37:** Augmented strain versus BTR distances in TIG-DC welded MVT specimens. a) 2.3 kJ/cm line energy; b) 3.9 kJ/cm line energy; c) 4.7 kJ/cm line energy; d) 5.9 kJ/cm line energy; Legend: Red line: experimental; blue line: theoretical results.

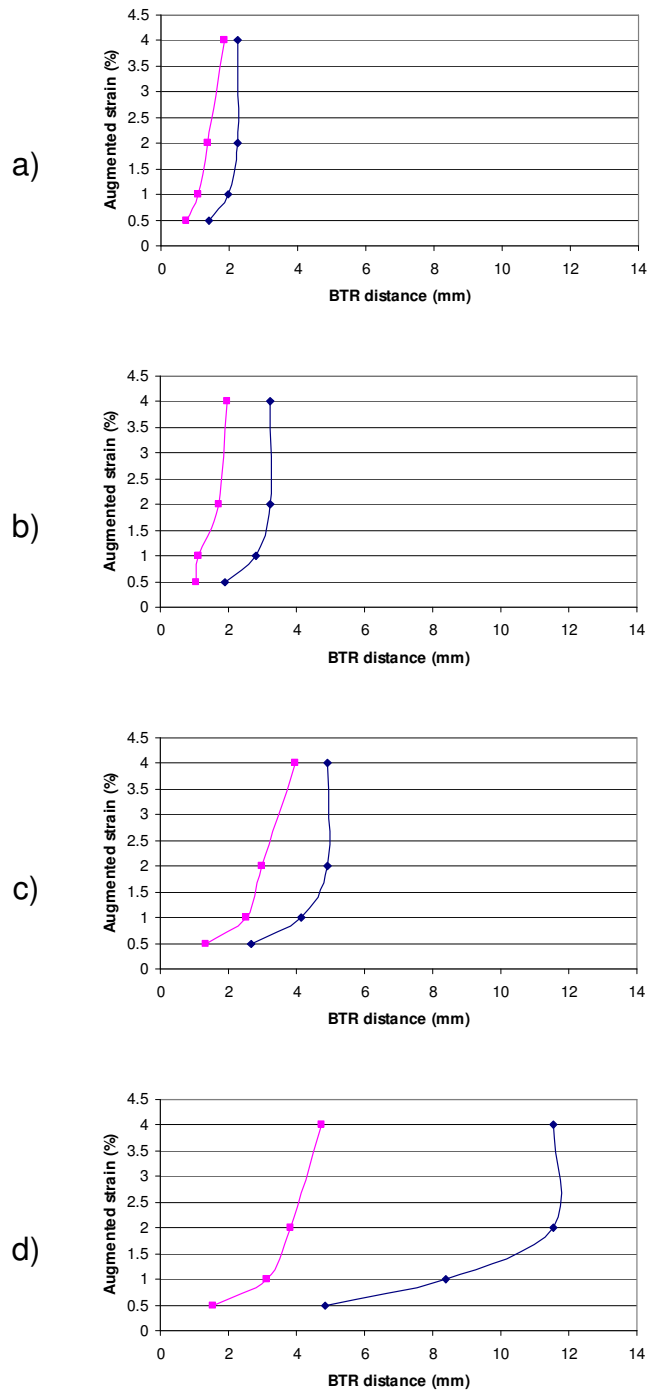


**Figure 4.38:** Augmented strain versus BTR distances in TIG-AC welded MVT specimens. a) 3.9 kJ/cm line energy; b) 4.9 kJ/cm line energy; c) 6.4 kJ/cm line energy; d) 7.9 kJ/cm line energy; Legend: Red line: experimental; blue line: theoretical results.



Because no type “C” cracks were observed at 2.3 and 3.9 kJ/cm line energies at 0.5 and 1.0 % strain levels for TIG-DC welded specimens, plotted experimental data was obtained by measuring the length of the partially melted grain boundaries in the PMZ (Figure 4.37).

BTR measurement results were generally lower than the theoretically calculated ones (Figures 4.37 and 4.38). However, the experimental and theoretical results showed similar trend. The results showed that the increase in strain and in line energy caused an increase in BTR size in both TIG-DC and TIG-DC welded specimens.

#### 4.7 Results of the Secondary Interdendritic Spacing Measurements

Secondary dendrite arm spacing measurements were performed on the photographs as explained in Section 3.4.6. Figure 4.40 shows examples of weld metal microstructures obtained from the center of the weld metal just behind the bending point. The exact location where microstructural specimens are taken is shown in Figure 4.39. In these series of photographs, the welding line energy was constant. Only the augmented strain values were changed.

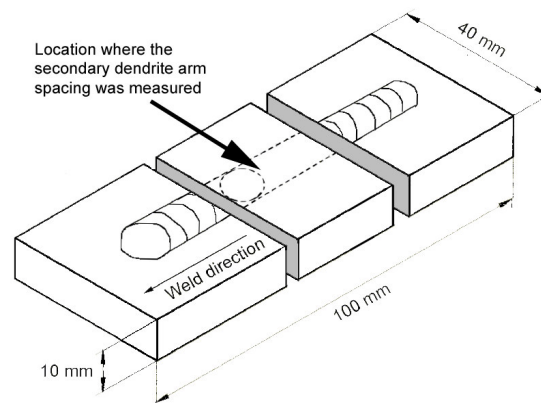
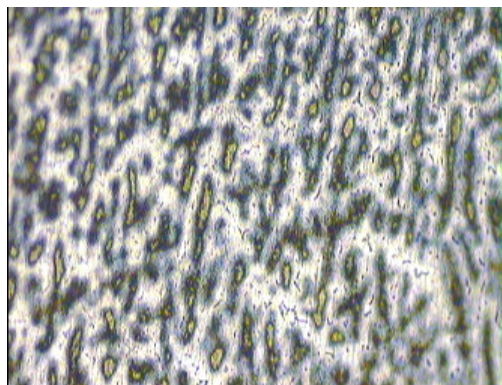
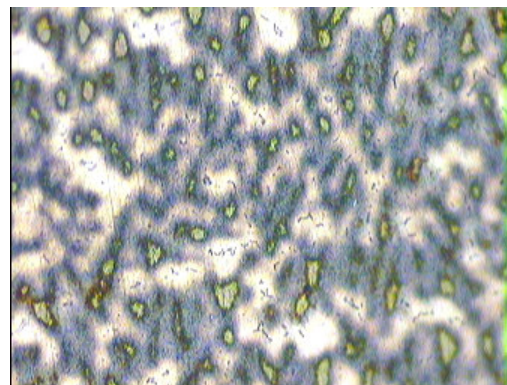


**Figure 4.39:** Location where the secondary dendrite arm spacing was measured

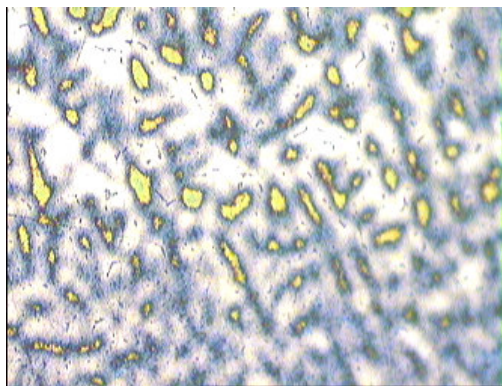
Results of the secondary dendrite arm spacing measurements are given in Figures 4.41 to 4.44 in graphical form. Generally, the secondary dendrite arm spacing increased with the increasing line energy. However, the effect of strain caused a change on secondary dendrite arm spacing. This change was low in the case of limited heat conduction (Figures 4.42 and 4.44).



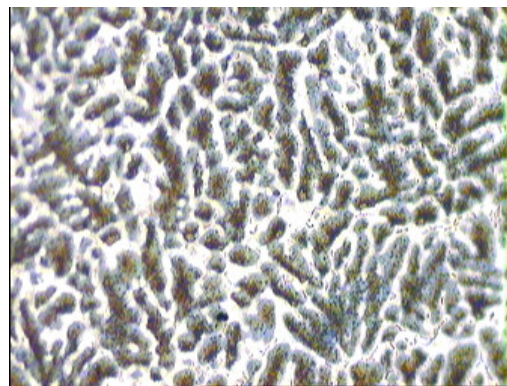
a) Strain: 0.5 %



b) Strain: 1.0 %

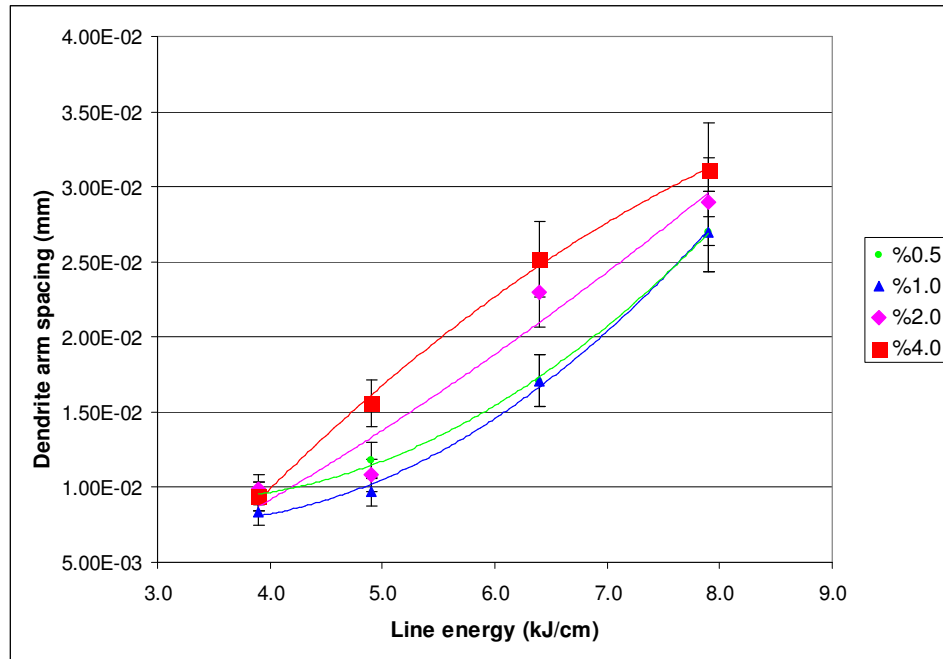


c) Strain: 2.0 %

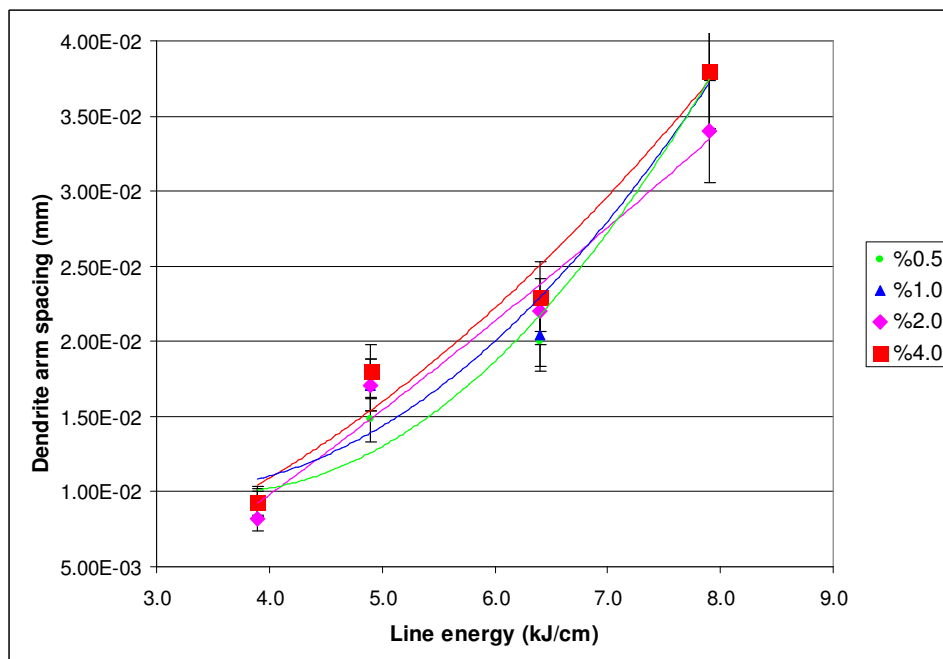


d) Strain: 4.0 %

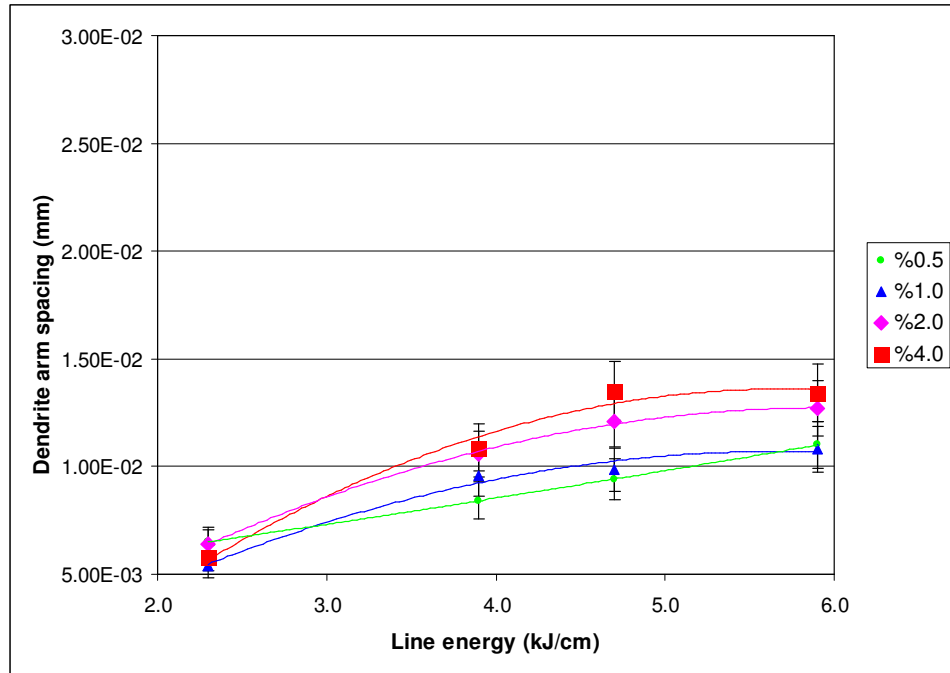
**Figure 4.40:** Central weld metal surface microstructure just before the pool formed due to bending in MVT test of 5086 alloy (see Figure 4.39). The yellow-brown areas show the core section of the secondary dendrite arms. The white zones are the sections filled with interdendritic liquid. Welding parameters: TIG-AC welding, 6.4 kJ/cm heat input, Augmented strain: a) 0.5 %; b) 1.0 %; c) 2.0 %; d) 4.0 %. Magnification on photographs: 225X. Etching solution: Weck.



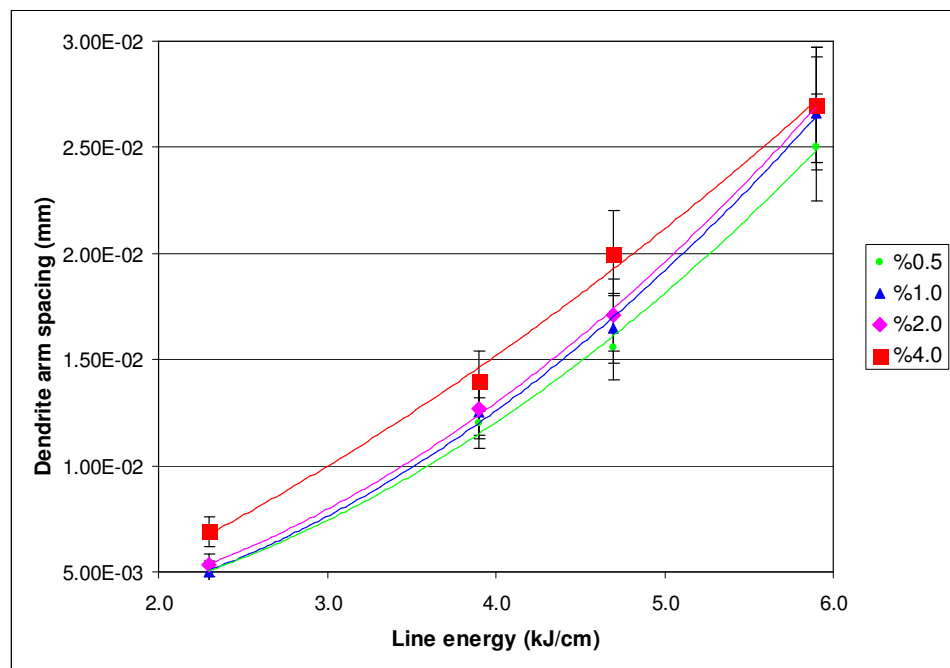
**Figure 4.41:** Secondary dendrite arm spacing versus line energy at different augmented strain values for the Modified Varestraint Test with TIG-AC welding.



**Figure 4.42:** Secondary dendrite arm spacing versus line energy at different augmented strain values for the Modified Varestraint Test with TIG-AC welding. Results from the changed heat conduction.



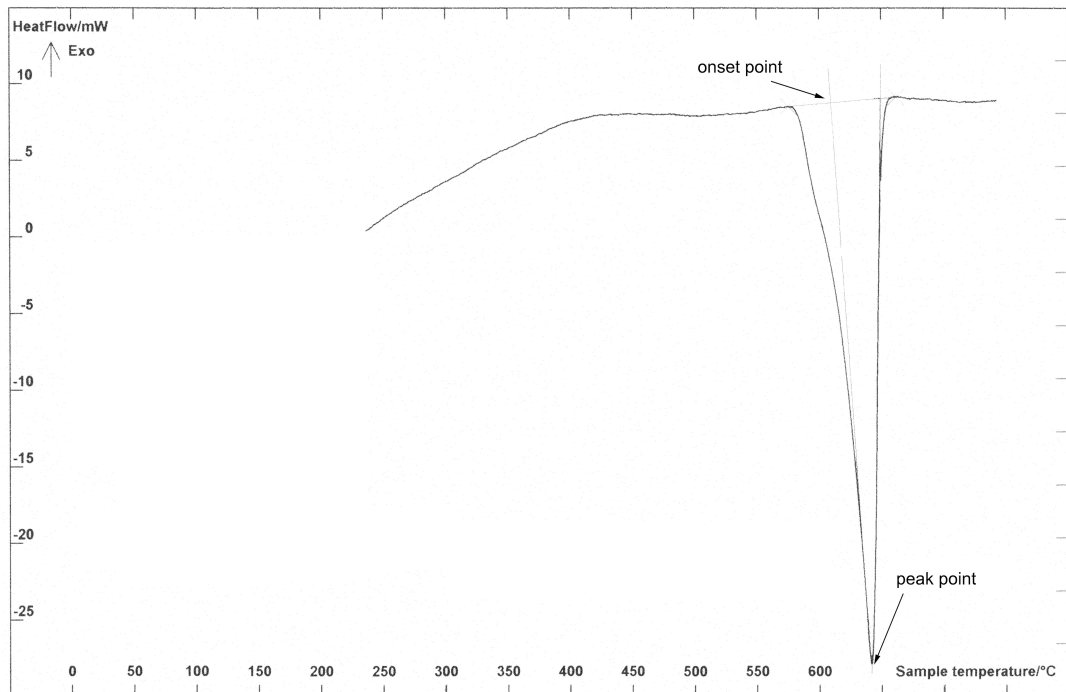
**Figure 4.43:** Secondary dendrite arm spacing versus line energy at different augmented strain values for Modified Varestraint Test with TIG-DC welding.



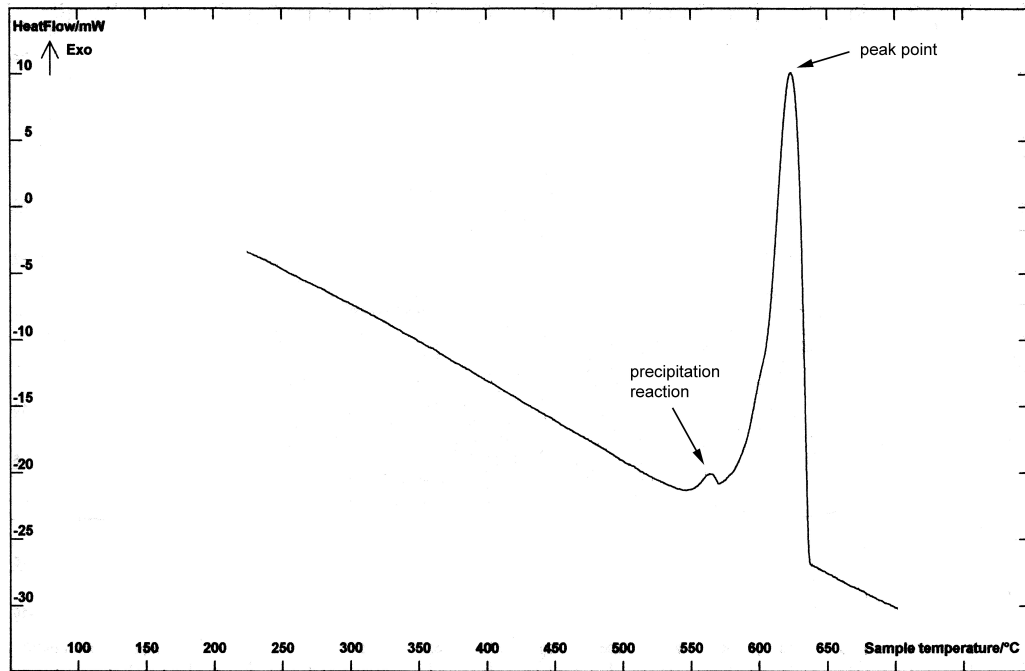
**Figure 4.44:** Secondary dendrite arm spacing versus line energy at different augmented strain values for Modified Varestraint Test with TIG-DC welding. Results from the changed heat conduction.

## 4.8 Results of the Thermal Analysis

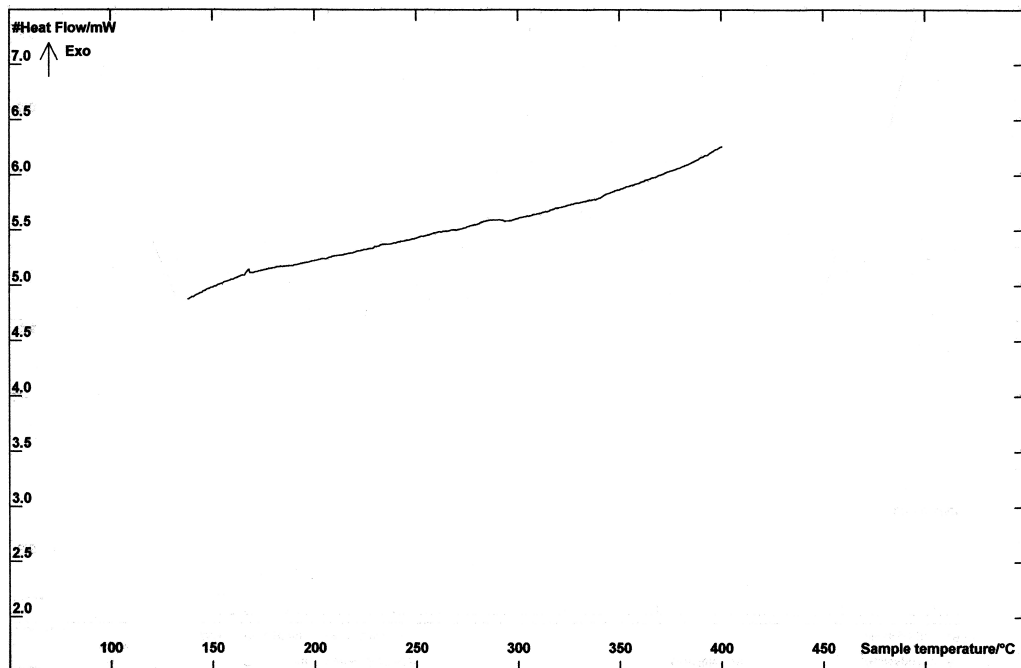
Figure 4.45 shows the heating stage of the 5086 alloy above its liquidus temperature. Here, the onset point at the beginning of the endothermic reaction was obtained as 609 °C. The peak, which can be regarded as liquidus temperature, was seen at 641 °C.



**Figure 4.45:** Heat flow versus sample temperature measured during the heating stage in the thermal analysis of the alloy 5086 in “SETARAM SETSYS TG-DTA/DSC” thermal analyzer.



**Figure 4.46:** Heat flow versus sample temperature measured during the cooling stage in the thermal analysis of the alloy 5086 in “SETARAM SETSYS TG-DTA/DSC” thermal analyzer.



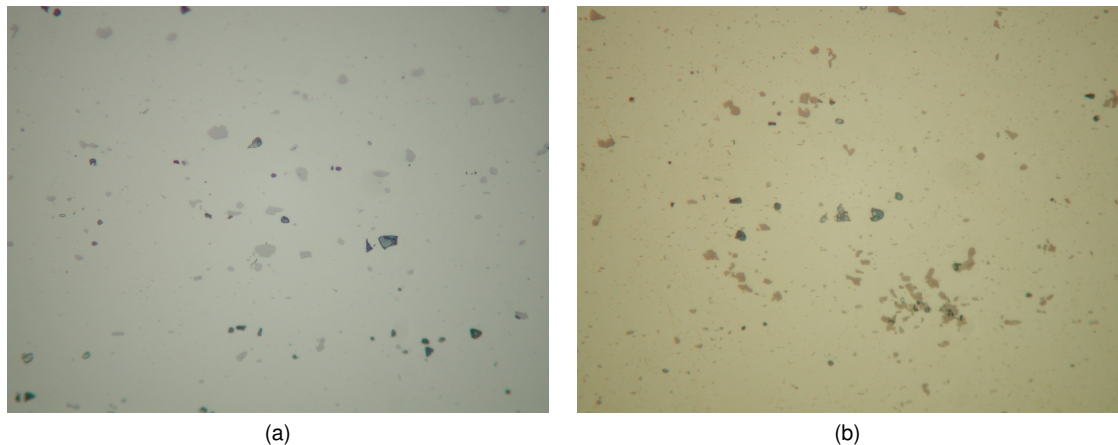
**Figure 4.47:** Heat flow versus sample temperature measured during the cooling stage in the thermal analysis of the alloy 5086 in “SETARAM DSC 131” thermal analyzer.

Figure 4.46 shows the cooling stage of the 5086 alloy below its liquidus temperature. Here, the onset on peak point of the exothermic reaction was obtained as 636°C. The onset of the lowest temperature of the exothermic reaction was 585°C. Just below the main exothermic reaction there was a small sized secondary exothermic reaction, which was obtained as onset 569°C and peak 563°C.

The DSC analysis that was performed between the room temperature to 350°C revealed no clear sign of a solid-state reaction. Only a very tiny exothermic point was seen at 170°C (Figure 4.47).

#### 4.9 Results of the Quench Tests

As explained in Section 3.4.3, microstructures obtained in specimens that were heated to different temperatures are given in the following figures. On each specimen one etched and one as polished structure was photographed.



**Figure 4.48:** Unheated microstructure of 5086 alloy. a) Unetched section: Light gray areas are iron rich precipitates. Dark areas are voids from broken precipitates. b) Specimen etched with Weck etching solution: No grain boundaries can be seen. Brown areas are iron rich precipitates. Magnification: 384X.



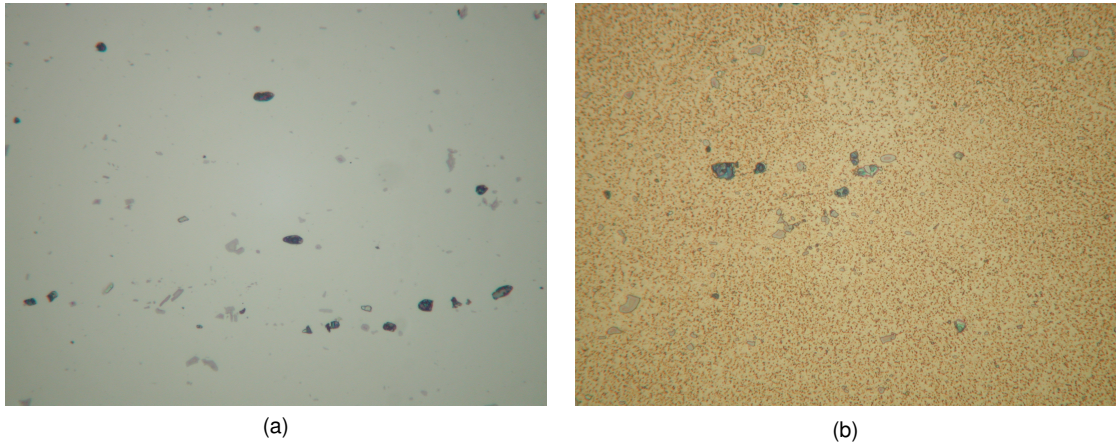


**Figure 4.49:** Microstructure of the 5086 alloy hold at 570°C for 300 s. a) Unetched specimen: No sign of melting. Light gray areas are iron rich precipitates. Dark areas are voids from broken precipitates. b) Specimen etched with Weck etching solution: No grain boundaries can be seen. Brown areas are iron rich precipitates. Magnification: 384X.

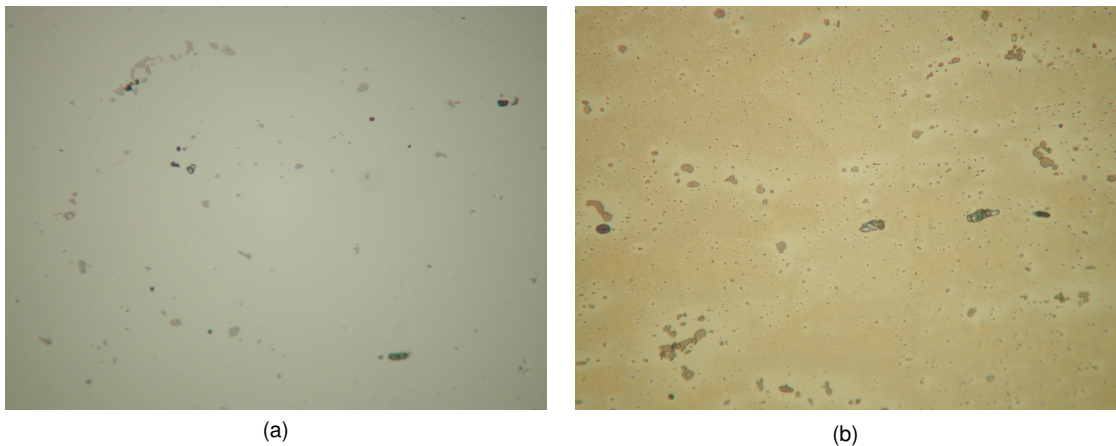


**Figure 4.50:** Microstructure of the 5086 alloy hold at 580°C for 300 s. a) Unetched specimen: No change in precipitates. Light gray areas are iron rich precipitates. Dark areas are voids from broken precipitates. b) Specimen etched with Weck etching solution: No clear sign of melting. Brown areas are iron rich precipitates. Magnification: 384X.



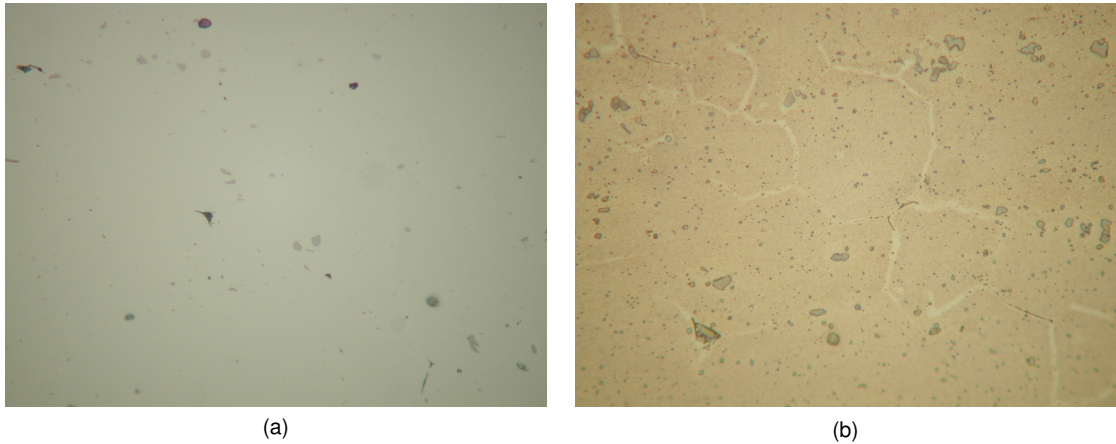


**Figure 4.51:** Microstructure of the 5086 alloy hold at 590°C for 300 s.  
 a) Unetched specimen: Precipitates start to form on grain boundary junctions. Light gray areas are iron rich precipitates.  
 b) Specimen etched with Weck etching solution: White network is the melted grain boundaries. Brown areas are iron rich precipitates. Magnification: 384X.

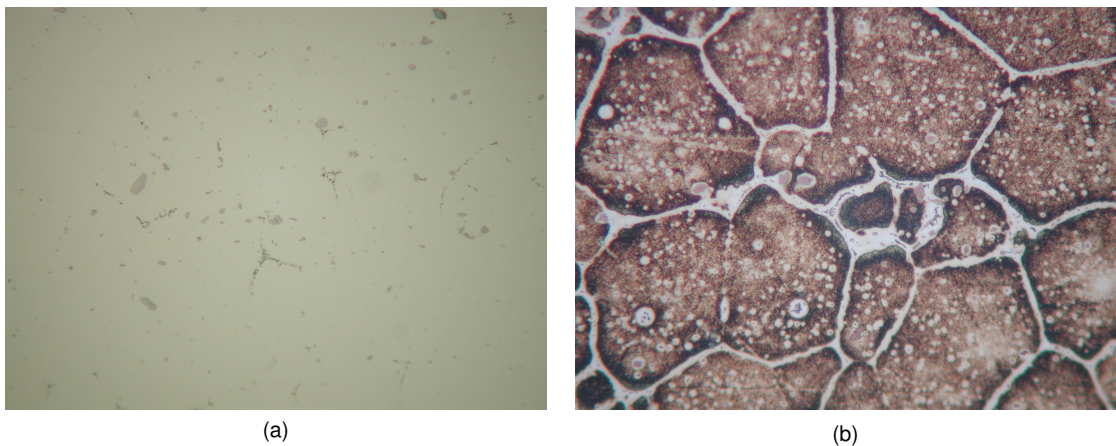


**Figure 4.52:** Microstructure of the 5086 alloy hold at 600°C for 300 s.  
 a) Unetched specimen: More precipitates formed at grain boundary junctions. Light gray areas are iron rich precipitates.  
 b) Specimen etched with Weck etching solution: More grain boundary melting. Magnification: 384X.

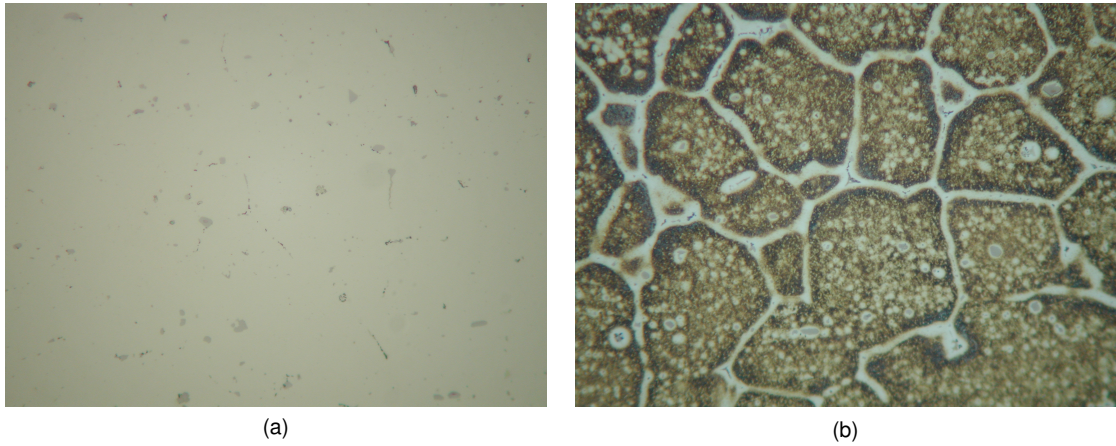


**Figure 4.53:** Microstructure of the 5086 alloy hold at 610°C for 300 s.  
a) Unetched specimen: More precipitates formed at grain boundary junctions. Light gray areas are iron rich precipitates.  
b) Specimen etched with Weck etching solution: More grain boundary melting. Magnification: 384X.

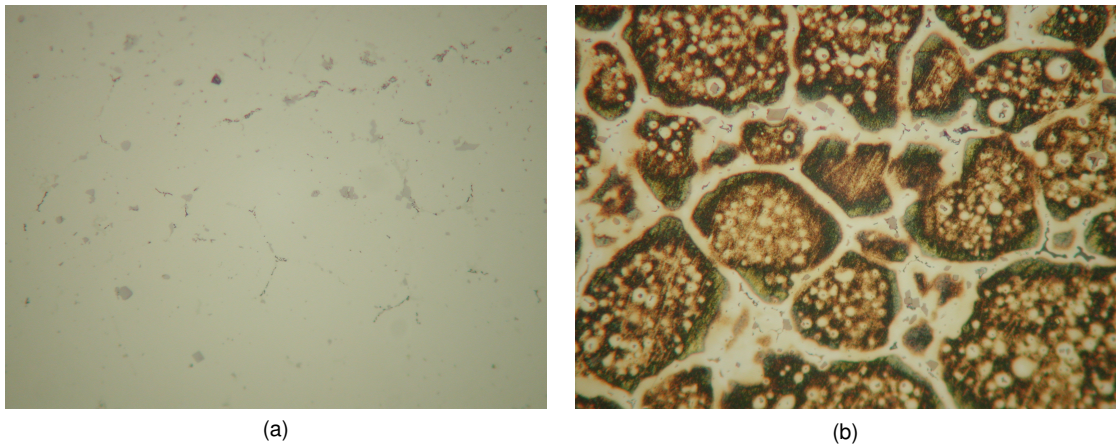


**Figure 4.54:** Microstructure of the 5086 alloy hold at 620°C for 300 s.  
a) Unetched specimen: More precipitates formed at grain boundary junctions. Light gray areas are iron rich precipitates.  
b) Specimen etched with Weck etching solution: More grain boundary melting. Magnification: 384X.



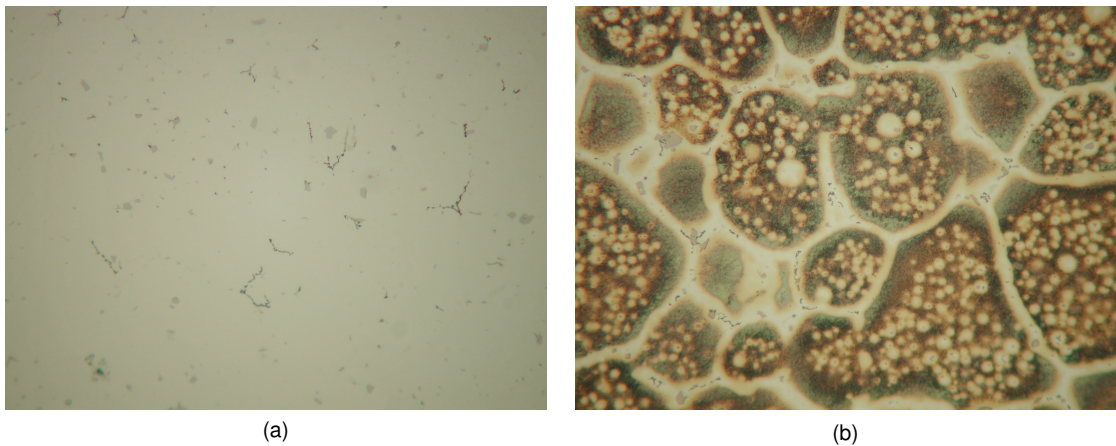


**Figure 4.55:** Microstructure of the 5086 alloy hold at 630°C for 300 s.  
 a) Unetched specimen: More precipitates formed at grain boundary junctions. Light gray areas are iron rich precipitates.  
 b) Specimen etched with Weck etching solution: More grain boundary melting. Magnification: 384X.

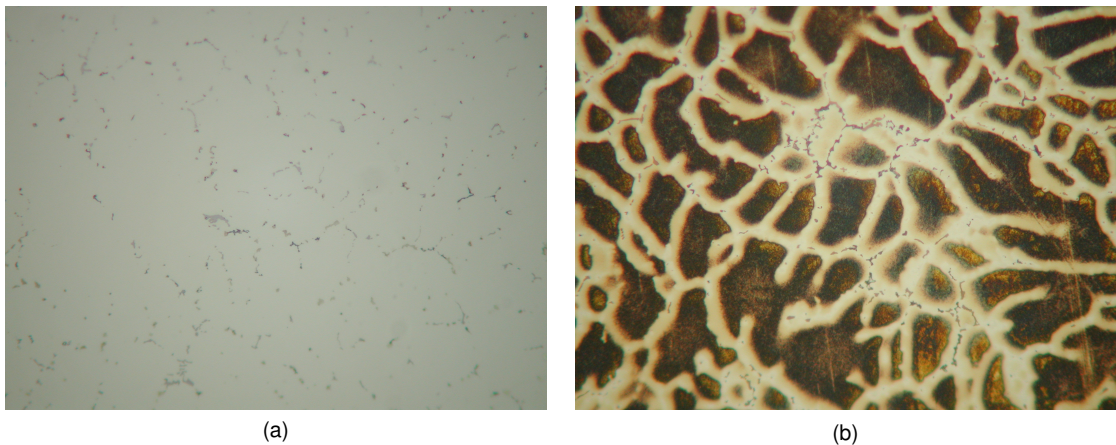


**Figure 4.56:** Microstructure of the 5086 alloy hold at 640°C for 300 s.  
 a) Unetched specimen: More precipitates formed at grain boundary junctions. Light gray areas are iron rich precipitates.  
 b) Specimen etched with Weck etching solution: Almost completely melted and solidified structure. Magnification: 384X.

#### 4.10 Results of the SEM Investigations

SEM investigations were performed in order to identify the type of the precipitates formed. In the SEM investigations of the quench test samples, only the iron-rich precipitates could be detected. The second-phase constituents precipitated along the grain boundaries could not be seen without etching. The reason could be the atomic weight of the elements that build up this type of precipitate which has an atomic weight close to aluminium. In order to identify them, a topographical layout was needed. This could be obtained by etching the surface. Etching solutions have reacted with the grain boundary second-phase constituents rapidly and dissolved them out. Finally, dilute Keller's reagent was used to analyse the grain boundary constituents.

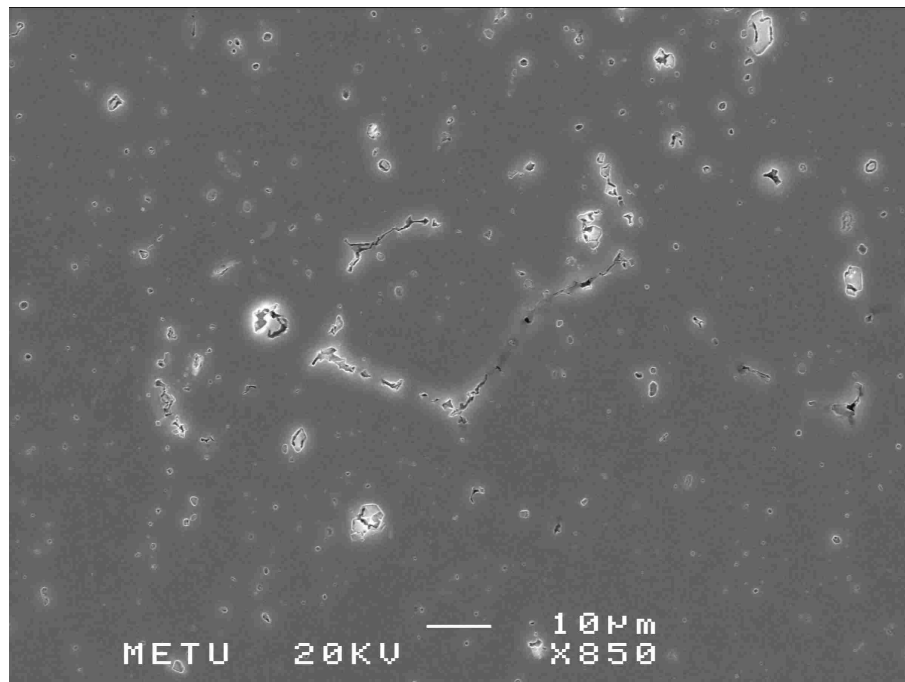
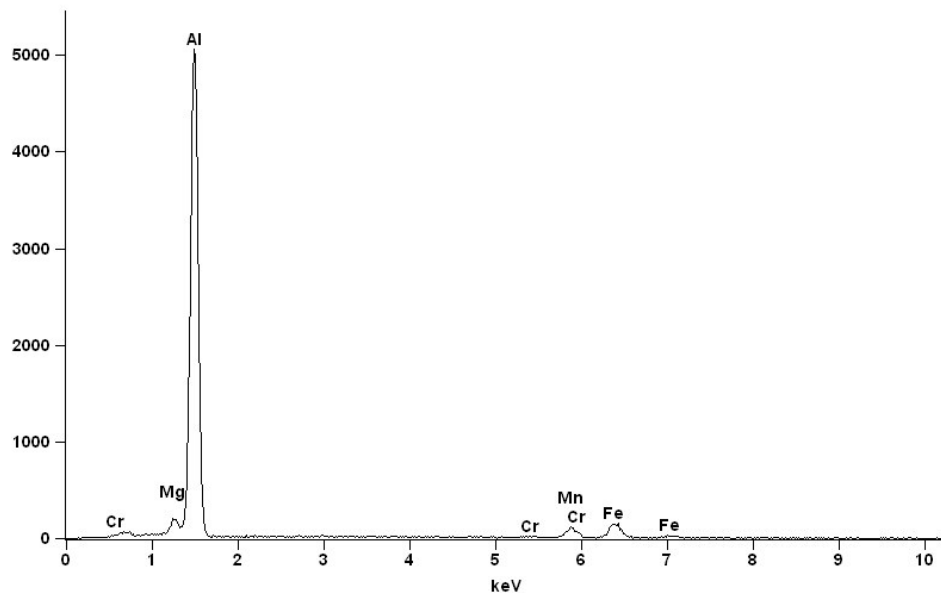


**Figure 4.57:** SEM picture taken from quench test specimen hold at  $T=600^{\circ}\text{C}$ ; Etched with Keller's solution. Light colored isolated precipitates are iron rich precipitates. The ones precipitated preferentially on the grain boundary junctions are magnesium rich precipitates.

Two different type of precipitates were observed. One of them was isolated inside the grains or on the grain boundaries, having irregular shapes with sharp edges. The other type of precipitate was found along the grain boundaries, preferentially precipitated at the junction points (Figure 5.57 and 4.59). The chemical compositions obtained from the X-ray microanalysis from these precipitates is given in Figures 4.58 and 4.60.



<i>Element</i>	<i>Weight Conc %</i>	<i>Atom Conc %</i>
<i>Mg</i>	1.58	1.91
<i>Al</i>	81.94	89.34
<i>Cr</i>	0.51	0.29
<i>Mn</i>	5.73	3.07
<i>Fe</i>	10.24	5.40

**Figure 4.58:** X-ray microanalysis taken from an isolated precipitate in the specimen shown in Figure 4.57.

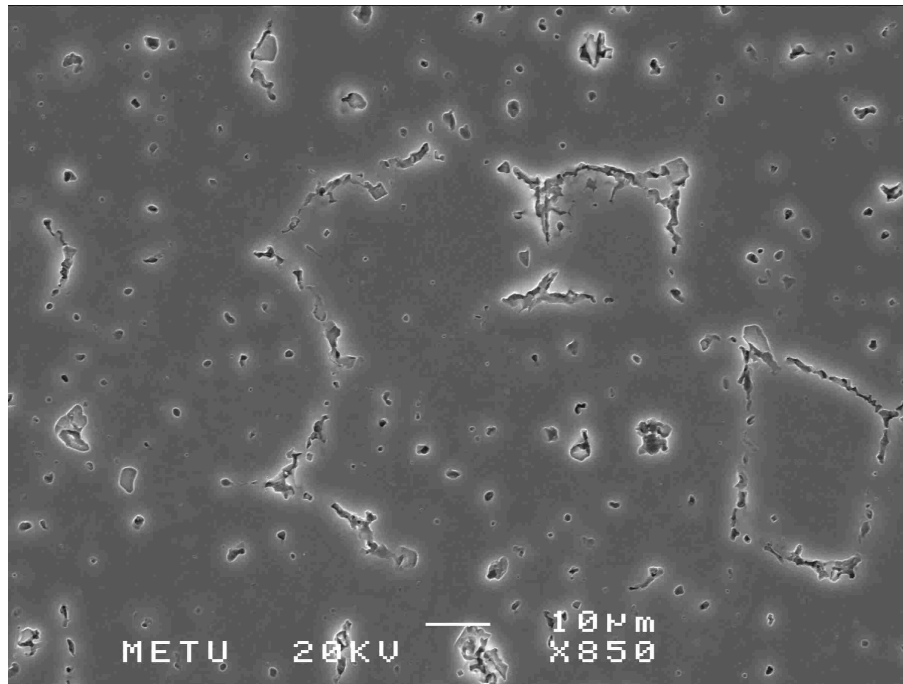
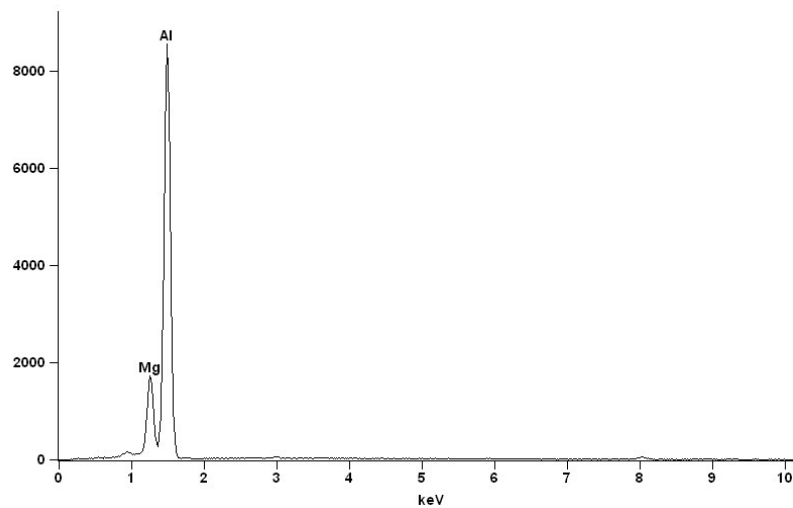


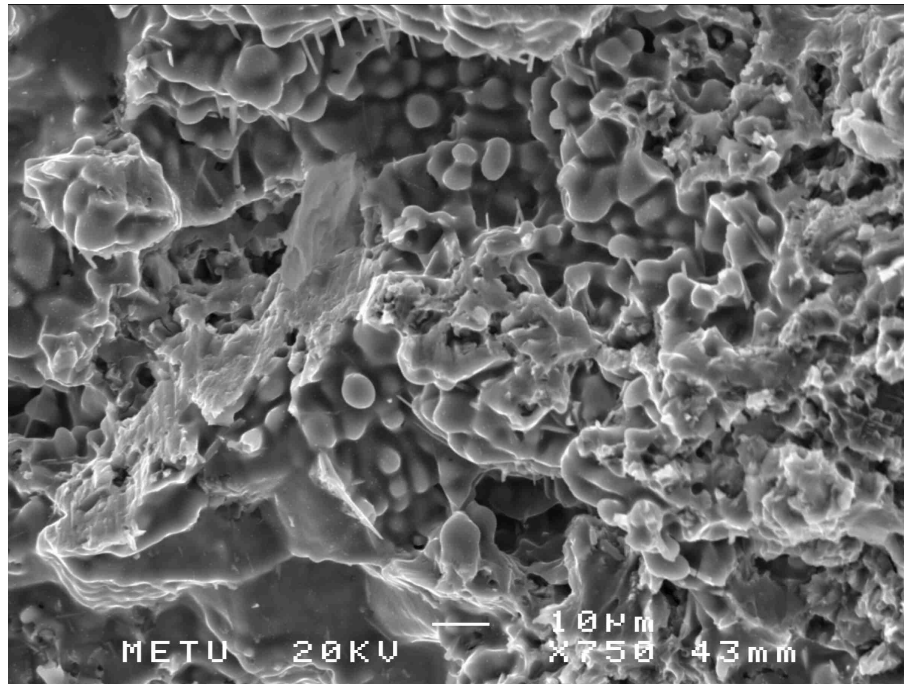
**Figure 4.59:** SEM picture taken from quench test specimen hold at T=620°C; Etched with Keller’s solution. Light colored isolated precipitates are iron rich precipitates. The ones precipitated preferentially on the grain boundary junctions are magnesium rich precipitates.



<i>Element</i>	<i>Weight Conc %</i>	<i>Atom Conc %</i>
<i>Mg</i>	12.49	13.68
<i>Al</i>	87.51	86.32

**Figure 4.60:** X-ray microanalysis results from networking precipitate in the specimen shown in Figure 4.59.

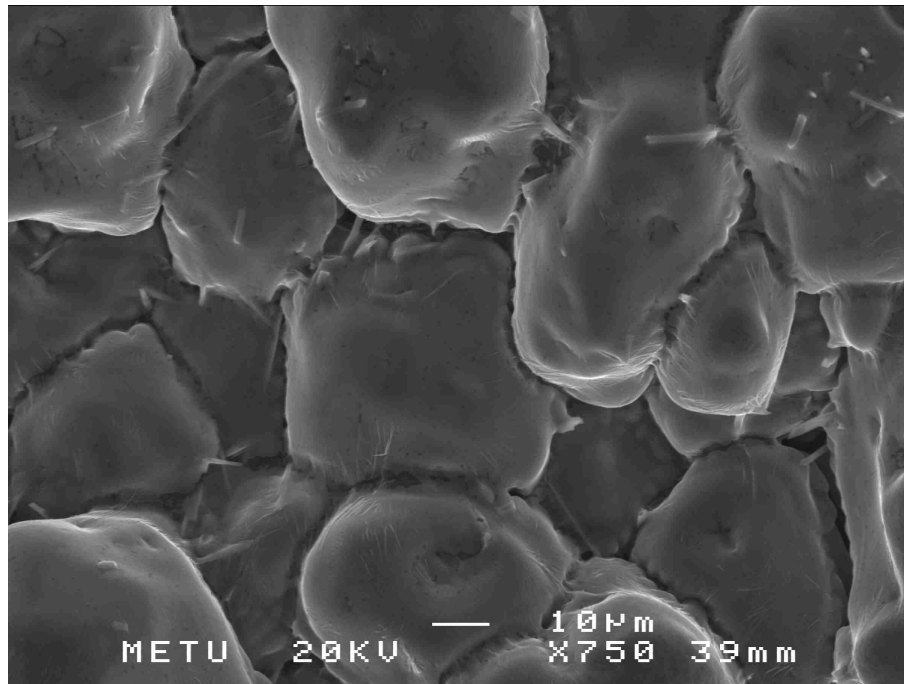
SEM investigations were also performed on the hot crack surfaces. In this frame, Figure 4.61 gives the SEM photograph of a type “A” crack surface.



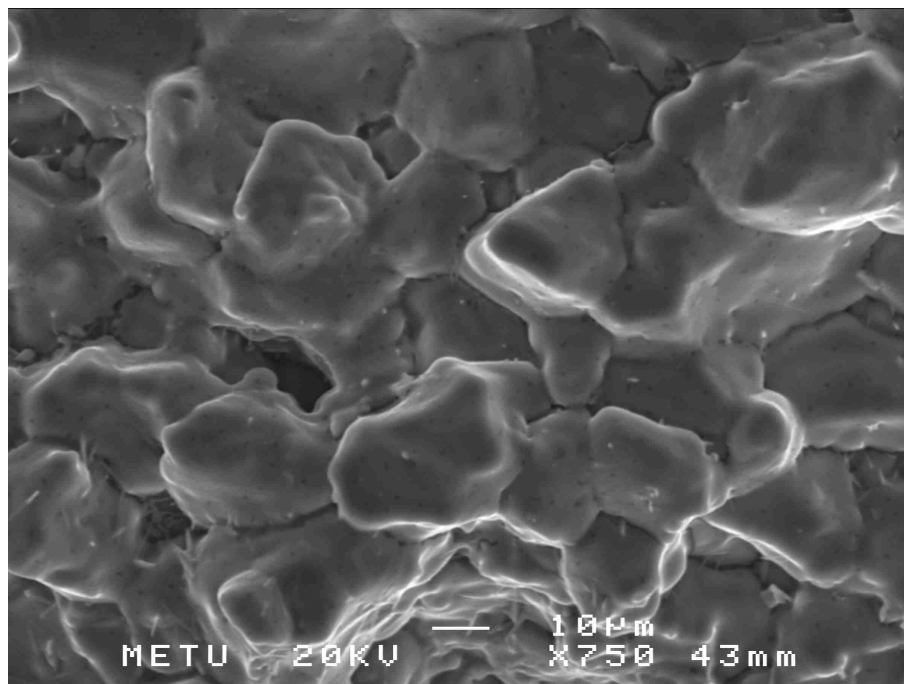
**Figure 4.61:** SEM photograph of type “A” crack from specimen welded with 4.2 kJ/cm line energy in TIG-AC welding; Surface strain was 4 %. Dendrite tips can be identified. Not etched.

Figure 4.62 shows the SEM photographs of a type “B” crack surface. The cracks were in intergranular nature and there are partial liquid bridges between the individual grains. The rod shaped dispersed phases are iron rich precipitates.

Figure 4.63 shows the SEM photographs of a type “C” crack surface. The photograph was taken from the partially melted zone. The networking precipitate had Al, Mg and Si chemical constituents (Figure 4.64). Along the same crack surface, the structure was dendritic on the weld metal section (Figures 4.65 and 4.66). The chemical composition of the precipitates dispersed in these figures are given in Figure 4.67.

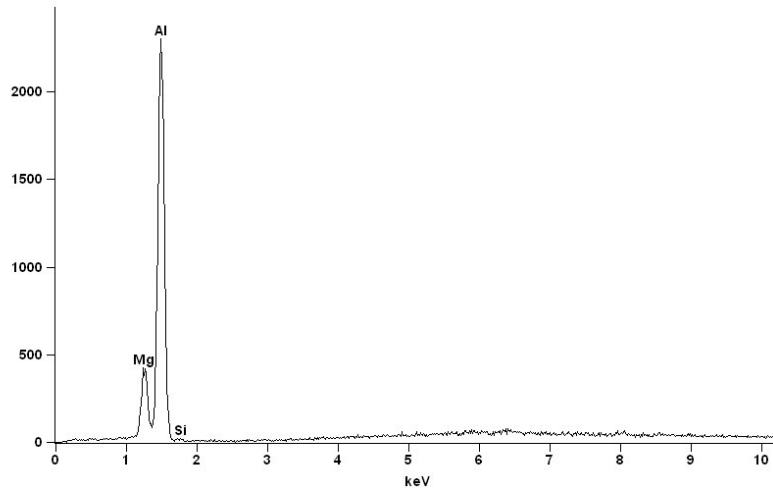


**Figure 4.62:** SEM photograph of type “B” crack surface from specimen welded with 4.2 kJ/cm line energy in TIG-AC welding; Surface strain was 4 %. Liquid bridging between the grains is a sign of grain boundary melting.



**Figure 4.63:** SEM photograph of type “C” crack surface (liquation side) from specimen welded with 7.1 kJ/cm line energy in TIG-AC welding. Surface strain was 4 %.





<i>Element</i>	<i>Weight Conc %</i>	<i>Atom Conc %</i>
<i>Mg</i>	11.19	12.28
<i>Al</i>	87.83	86.80
<i>Si</i>	0.97	0.92

**Figure 4.64:** X-ray microanalysis results from networking precipitate on the specimen shown in Figure 4.63.

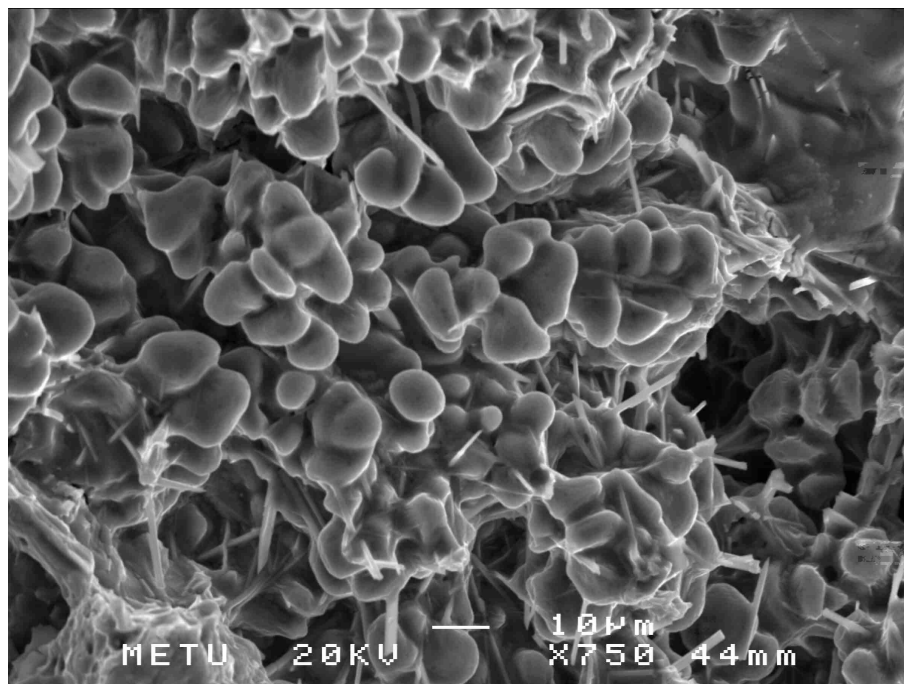


**Figure 4.65:** SEM photograph of type “C” crack surface (solidification side) from specimen welded with 7.1 kJ/cm line energy in TIG-AC welding. Surface strain was 4 %.

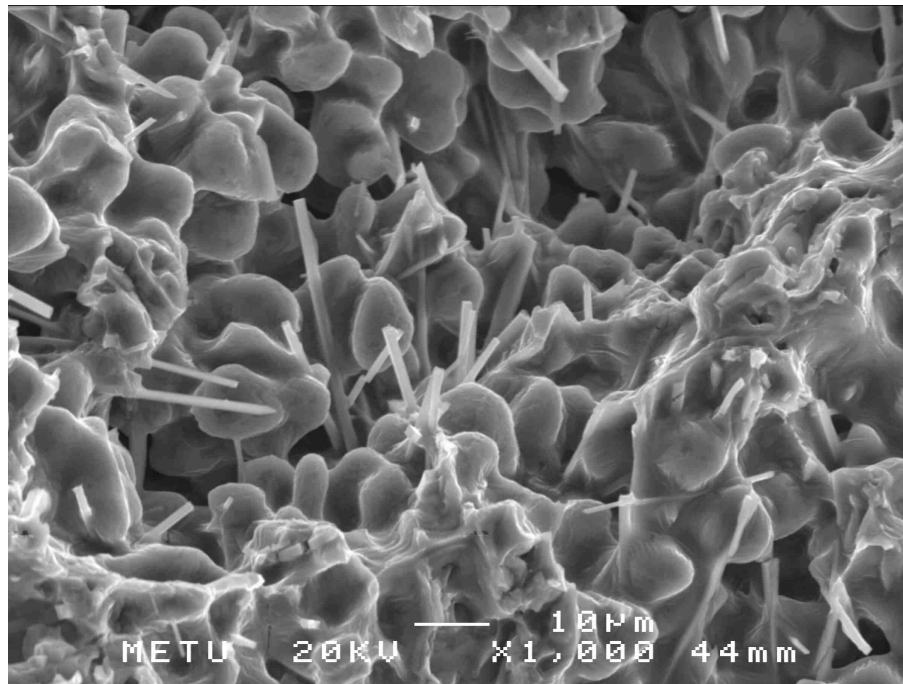
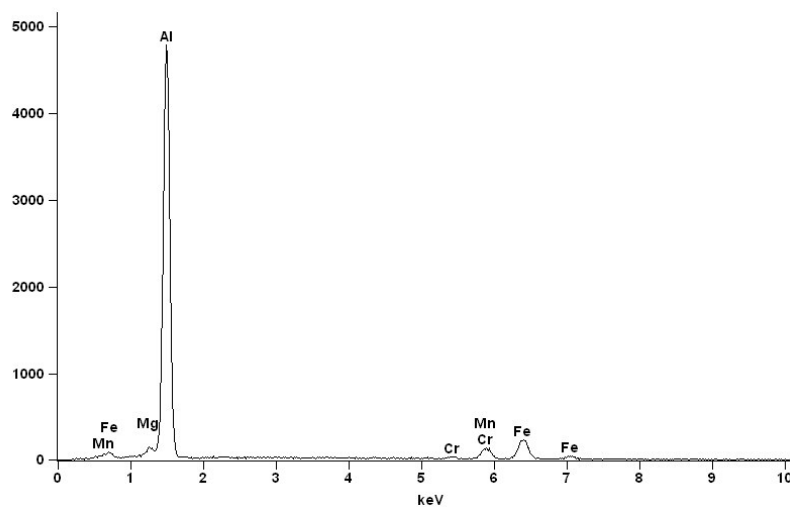


**Figure 4.66:** SEM photograph of type “C” crack surface (solidification side) from specimen welded with 7.1 kJ/cm line energy in TIG-AC welding. Surface strain was 4 %. Precipitates through the dendrites near the end of the crack.



<i>Element</i>	<i>Weight Conc %</i>	<i>Atom Conc %</i>
<i>Mg</i>	0.76	0.96
<i>Al</i>	76.62	86.60
<i>Cr</i>	0.78	0.46
<i>Mn</i>	7.01	3.89
<i>Fe</i>	14.83	8.10

**Figure 4.67:** X-ray microanalysis taken from an isolated precipitate in the specimen shown in Figure 4.65 and 4.66.

Figure 4.68 gives a SEM picture of a type “C” crack surface in base metal.

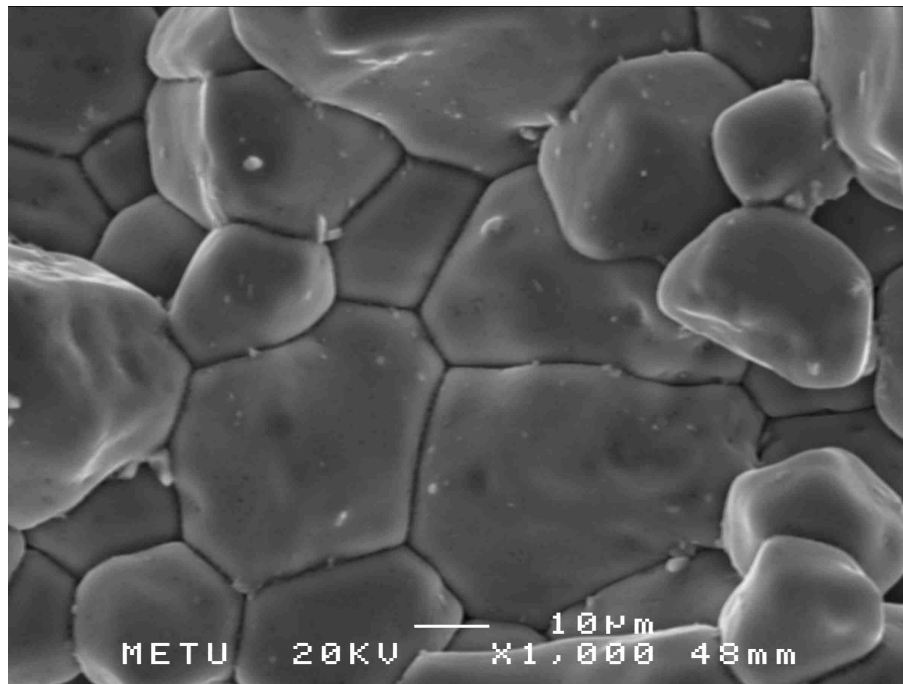


**Figure 4.68:** SEM photograph of type “C” crack surface (in base metal). Specimen welded with 9.1 kJ/cm line energy in TIG-AC welding. Surface strain was 4 %.

#### **4.11 Results of the Optical Microscope Investigations**

Metallographic examinations were performed on the surface of the specimens given in Section 3.4.6. Here, microstructure around and inside the weld pool at bending point was investigated. In the microstructure, grain size, liquated grain boundaries, hot crack locations, any healing effect inside a crack and precipitates were identified.

Following photographs that were taken under the optical microscope are given to support the discussion in the welding parameter dependence of the hot cracking tendency.

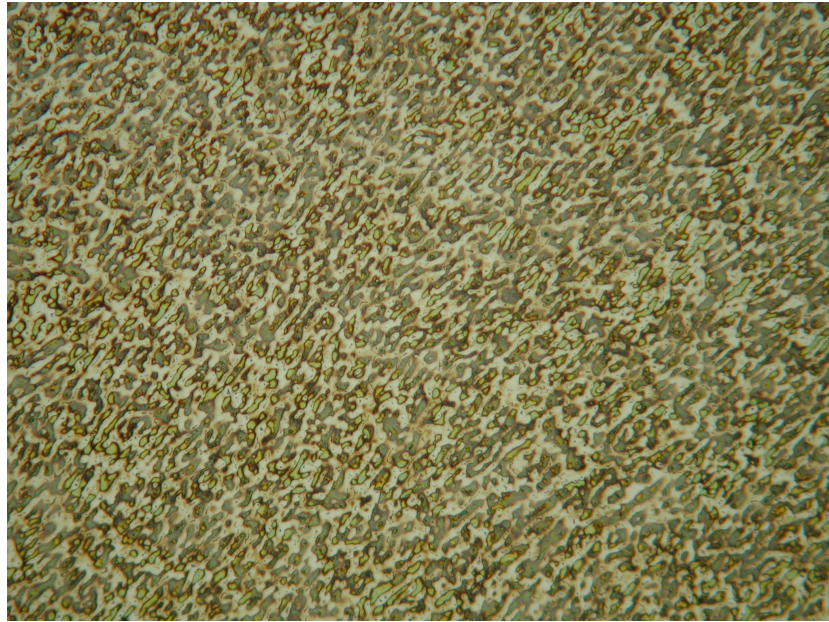


**Figure 4.69:** Weld metal surface microstructure. Before the bending point where the type “A” cracks preferentially form. Fine solidification structure. TIG-DC welded specimen. Line energy: 2.3 kJ/cm; Augmented strain: 0.5 %. Weck etching. 400X magnification.



**Figure 4.70:** Weld metal surface microstructure before the bending point. Type “A” crack inside fine solidification structure. TIG-DC welded specimen. Line energy: 2.3 kJ/cm; Augmented strain: 1.0 %. Weck etching. 200X magnification.



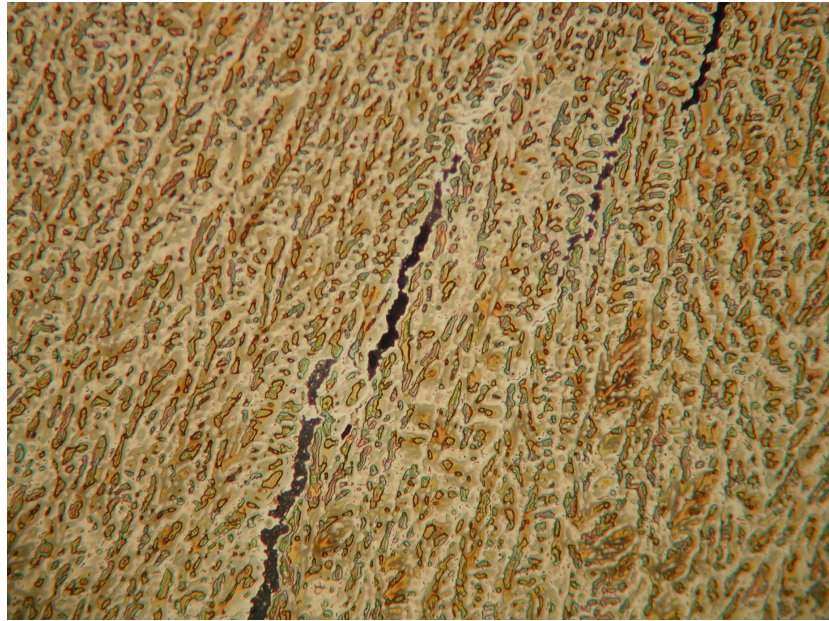


**Figure 4.71:** Weld metal surface microstructure before the bending point. Type “A” cracks between columnar dendritic microstructure. TIG-DC welded specimen. Line energy: 4.7 kJ/cm; Augmented strain: 0.5 %. Weck etching. 400X magnification.

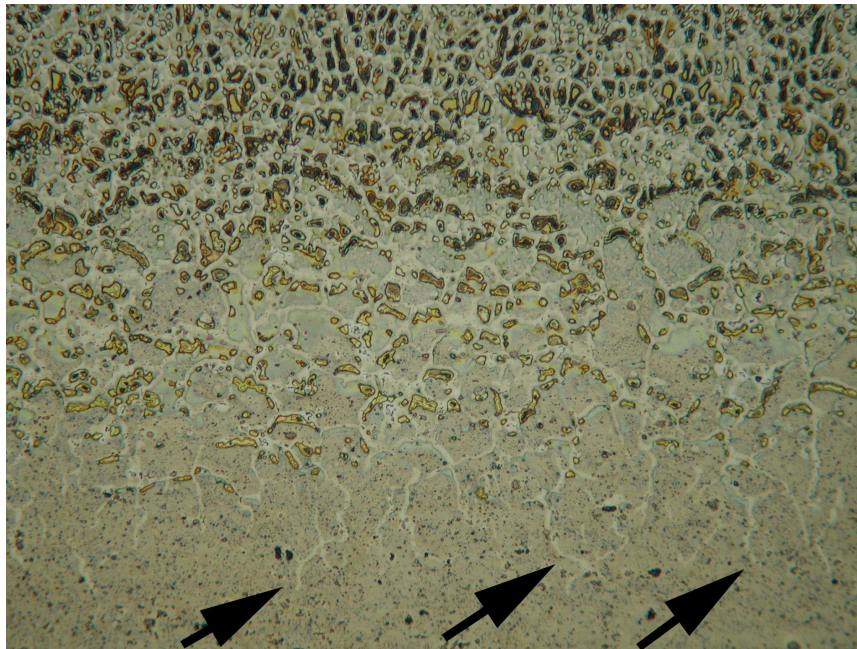


**Figure 4.72:** PMZ surface microstructure at the bending point. Healed type “C” cracks extended towards base metal. TIG-DC welded specimen. Line energy: 2.3 kJ/cm; Augmented strain: 1.0 %. Weck etching. 200X magnification.



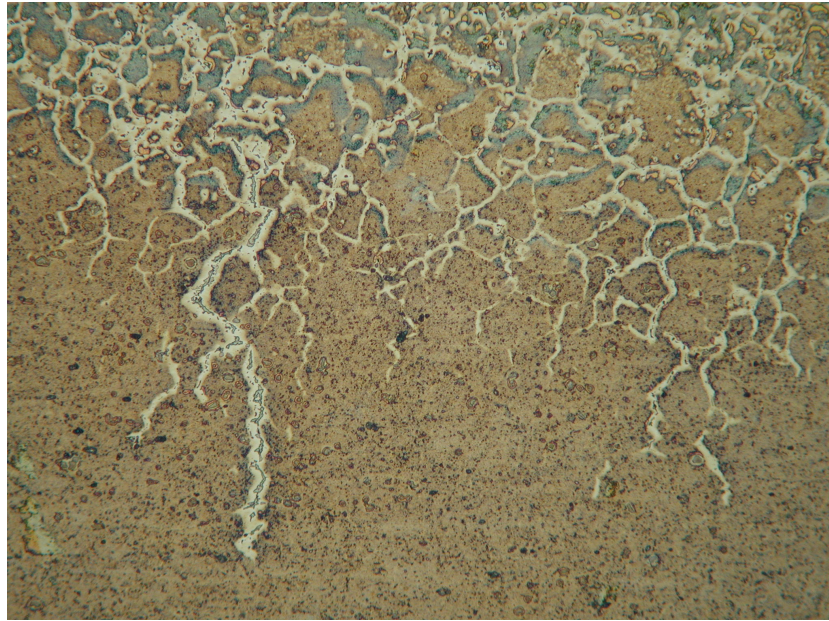


**Figure 4.73:** Healed (filled) type "C" crack. Crack-centerline precipitation at healed crack. TIG-DC welded specimen. Line energy: 2.3 kJ/cm; Augmented strain: 2.0 %. Weck etching. 200X magnification.

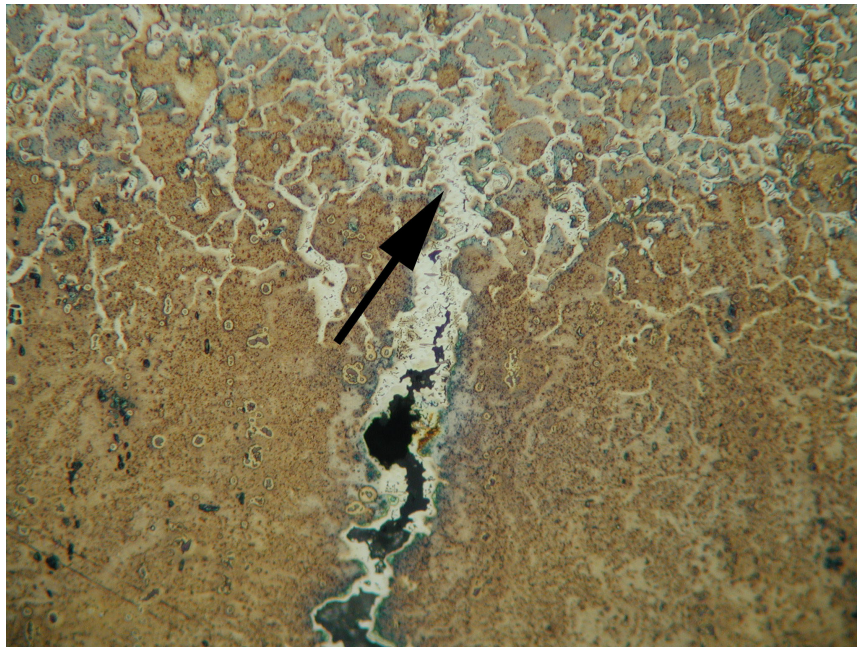


**Figure 4.74:** Partially healed type "C" crack extended towards base metal. Crack-centerline precipitation. TIG-DC welded specimen. Line energy: 2.3 kJ/cm; Augmented strain: 4.0 %. Weck etching. 200X magnification.



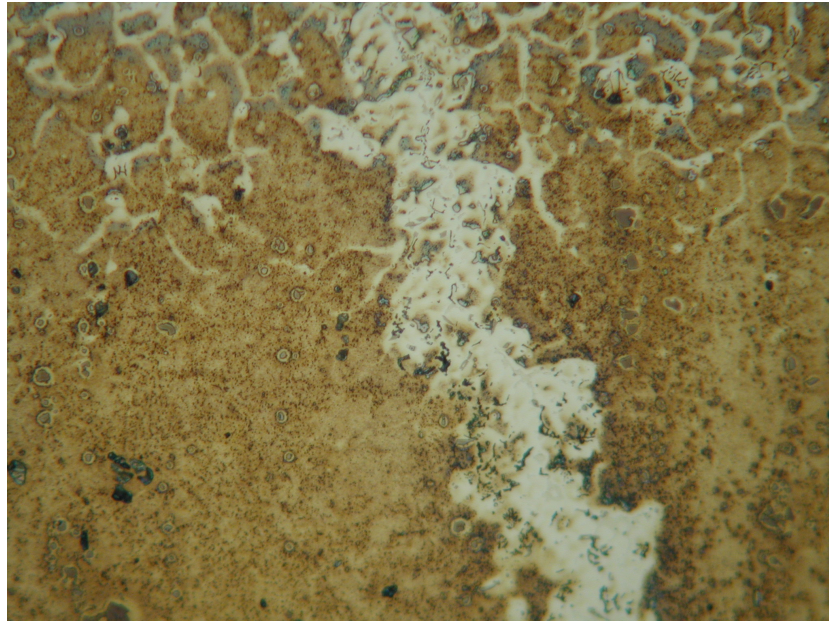


**Figure 4.75:** Completely healed type “D” crack mainly in base metal. Precipitates inside the healed crack can be seen. TIG-DC welded specimen. Line energy: 2.3 kJ/cm; Augmented strain: 4.0 %. Weck etching. 200X magnification.

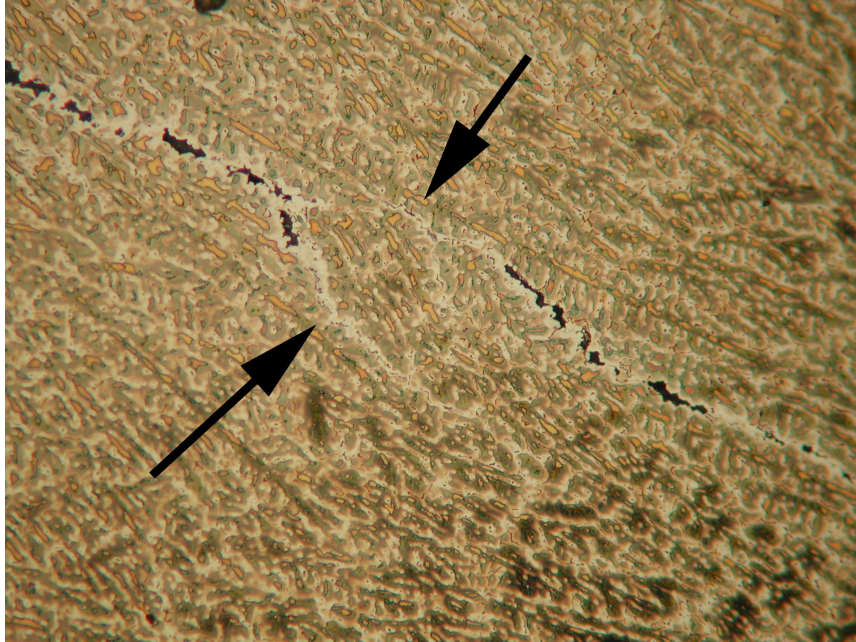


**Figure 4.76:** Partially healed type “A” cracks inside the columnar dendritic weld metal. TIG-DC welded specimen. Line energy: 4.7 kJ/cm; Augmented strain: 1.0 %. Weck etching. 200X magnification.



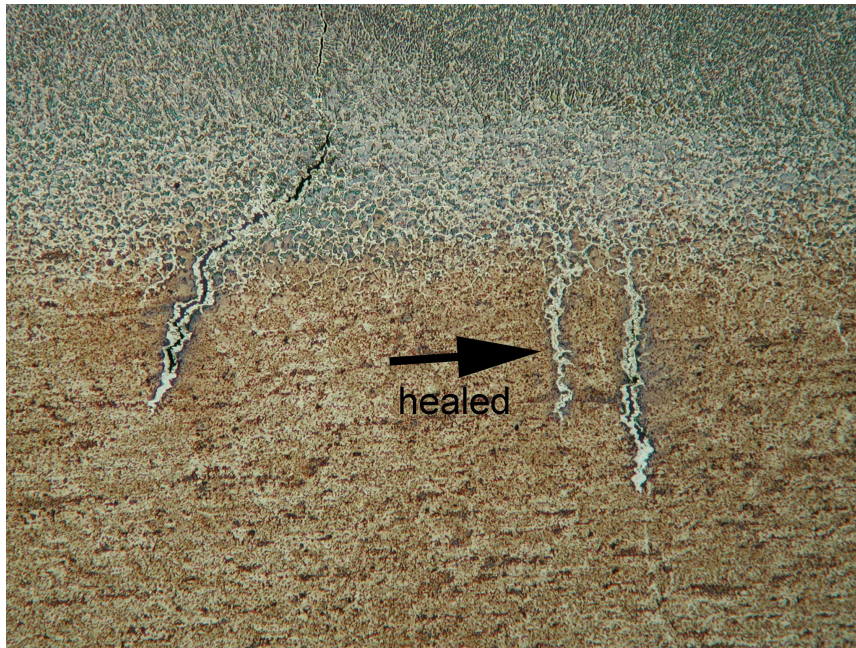


**Figure 4.77:** Type “B” and “C” cracks. Type “B” crack (crack on the left) was started in the PMZ and extended both towards base metal and weld metal. Type “C” cracks extended mainly towards base metal. TIG-DC welded specimen. Line energy: 3.9 kJ/cm; Augmented strain: 2.0 %. Weck etching. 50X magnification.

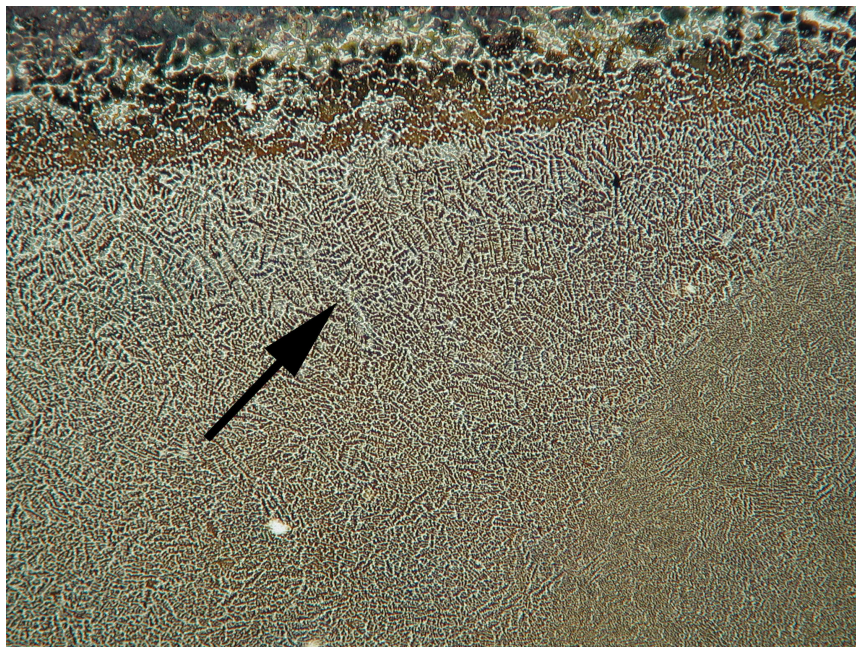


**Figure 4.78:** Healed type “A” crack in the weld metal. TIG-AC welded specimen. Line energy: 3.9 kJ/cm; Augmented strain 0.5 %. Weck etching. 50X magnification.



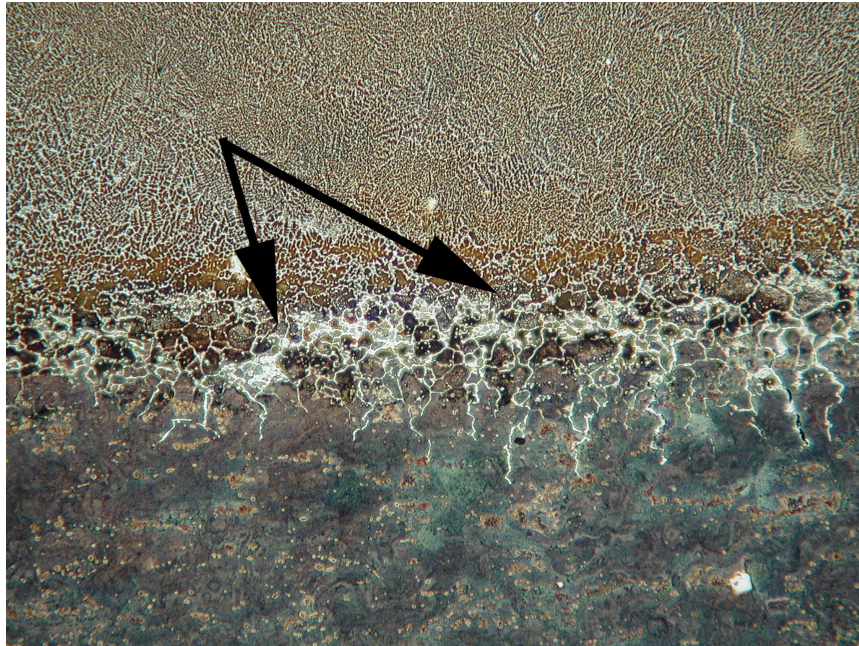


**Figure 4.79:** Healed type "B" crack in the PMZ. TIG-AC welded specimen. Line energy: 3.9 kJ/cm; Augmented strain: 0.5 %. Weck etching. 50X magnification.

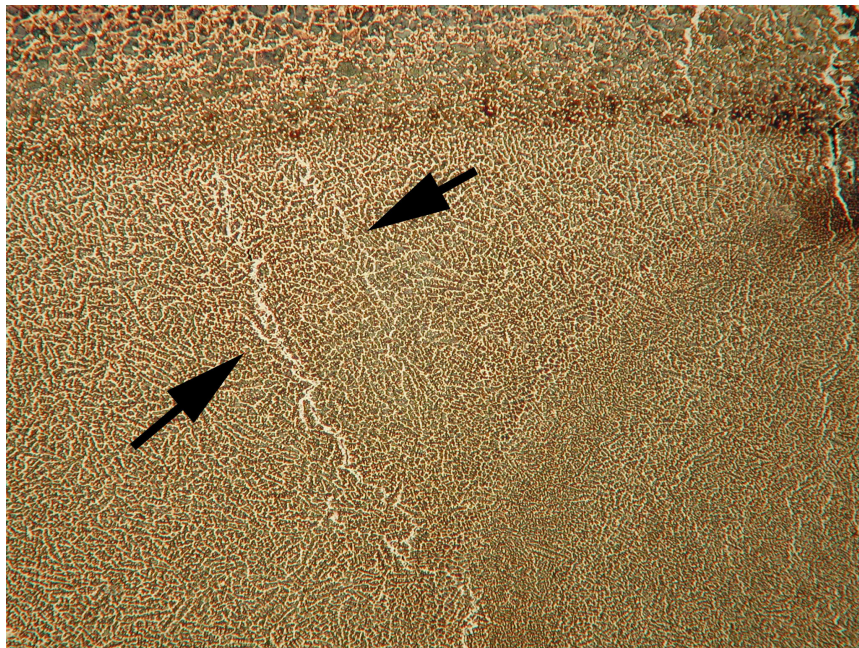


**Figure 4.80:** Healed type "A" cracks in the weld metal. TIG-AC welded specimen. Line energy: 3.9 kJ/cm; Augmented strain: 2.0 %. Weck etching. 50X magnification.



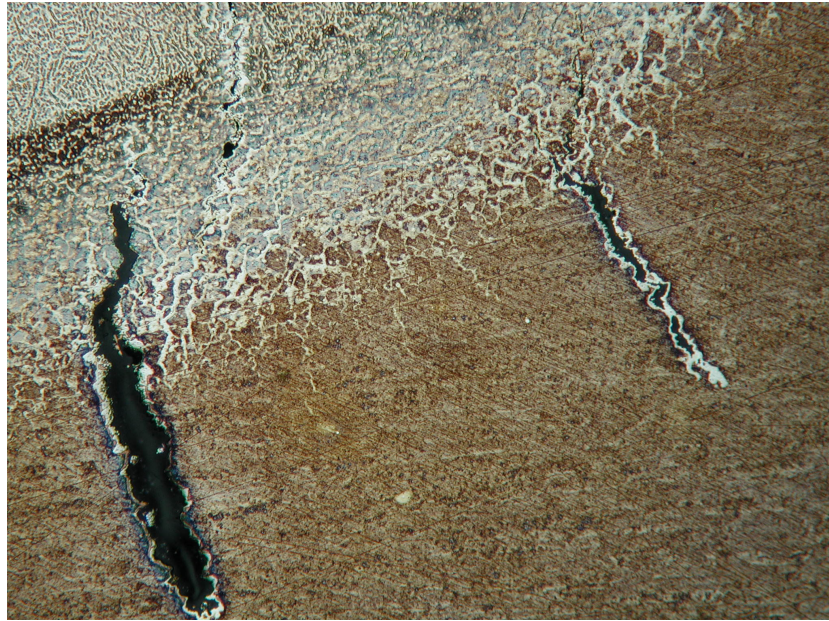


**Figure 4.81:** Type “D” cracks started from PMZ, extended towards base metal. TIG-AC welded specimen. Line energy: 4.9 kJ/cm; Augmented strain: 2.0 %. 50X magnification.

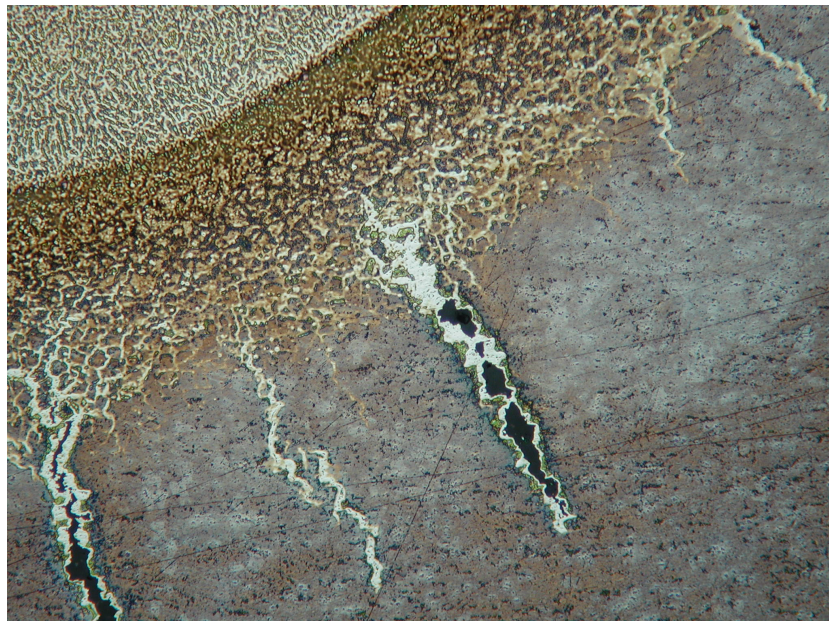


**Figure 4.82:** Type “D” cracks started from PMZ, extended towards base metal. Partial healing in left and right cracks near the PMZ. TIG-AC welded specimen. Line energy: 4.9 kJ/cm; Augmented strain: 4.0 %. 50X magnification.

## **CHAPTER V**

### **DISCUSSION**

The discussion intends to establish a relation between the hot cracking behaviour of 5086 alloy and the welding and straining parameters. In this frame, the discussion will be made in following sections:

- 5.1 Weld seam characteristics in the 5086 alloy MVT specimens.
- 5.2 Hot cracking behaviour in the TIG-AC and TIG-DC welded MVT specimens.
  - 5.2.1 Hot cracking behaviour in the TIG-DC welded 5086 alloy MVT specimens.
  - 5.2.2 Hot cracking behaviour in the TIG-AC welded 5086 alloy MVT specimens.
- 5.3 Precipitates observed during cooling in 5086 alloy.

#### **5.1 Weld Seam Characteristics in the 5086 Alloy MVT Specimens**

Two important factors in the welding related solidification and liquation cracking are the amount of energy absorbed by the material under consideration and the rate of cooling as a result of the conditions depending on the welding process and the environment. For that reason, before comparing the hot cracking behaviours observed in the applied welding conditions, the parameter dependent absorbed energy and the parameter dependent solidification rates will be discussed.

Welding parameter dependent absorbed energy data were compared in the weld geometry versus line energy diagram (Figure 4.3). In general, an increase in line energy resulted in an increase in weld-metal-width and

weld-metal-penetration-depth for each of the applied welding processes. In spite of the low level of applied line energy in TIG-DC welding, its better efficiency in energy input resulted in a larger weld metal volume. Actually, the larger volume of weld metal has a negative influence on the hot cracking safety. However, 3 to 4 times faster welding speeds permitted in the TIG-DC welding, resulted in finer microstructures, which are highly resistant for hot cracking in the weld metal. In TIG-AC welding on the other hand, a higher range of line energy with considerably low welding speeds was applied. That resulted in relatively coarser microstructures, which have a lower resistance to hot cracking. The presence of this difference in energy input was also stated by the theoretical weld metal width calculations (Figure 4.6). At low line energy ranges, although the difference between experimental and calculated weld metal widths was small, this difference became larger at higher line energies. This may be due to the temperature increase in the relatively small MVT specimen size.

On the other hand, welding with TIG-DC and TIG-AC resulted in equal PMZ size which is directly related with the liquation cracking tendency in the common range of line energies (Figure 4.3). Therefore, the experimental HAZ crack data were similar in TIG-AC and TIG-DC welded MVT specimens (Figures 4.12 and 4.22). The difference in experimental and theoretical PMZ width data indicate the time needed for the phase transformations to take place around the moving pool (Figure 4.7). Thus, faster welding speeds i.e. lower line energies would result in a narrower PMZ size than the expected one, which is advantageous in respect to the liquation cracking safety. The time needed for the phase transformation to take place was also proved by the results of the quench tests.

In MVT specimens, the line energy dependence of the cooling rate has a direct effect on the solidification structure size. The dependence is given in in Figures 4.41 to 4.44. The results indicate that, for both TIG-AC and TIG-DC welding the secondary dendrite arm spacing increased with the

increase in line energy. The dendrite arm spacing is directly related with the type and size of the solidification structure and therefore the temperature gradient to the growth rate ratio [6]. At a given line energy, the growth rate "R" is directly depended on the welding speed. In lower welding speeds i.e. with the higher line energies, the temperature gradient to growth rate ratio (G/R) is expected to be high. As a result, the solidification structure will show an increase in the dendrite arm spacing. The results of the experimental investigation are in agreement with the theory of the weld metal solidification.

Further, the dendrite arm spacing at a given line energy level changed with augmented strain (Figures 4.41 and 4.43). Different amount of straining was obtained by using several dies with different radius. With decreasing die radius, the secondary dendrite arm spacing of the solidification structure was increased. Because, smaller die radiuses caused lower temperature gradients due to the decreased contact surface area between die and specimen. In TIG-AC welded specimens, this effect was more pronounced because of the low welding speeds. Restriction in heat escape towards the die surface increased the temperature of the specimen intentionally. Therefore, secondary dendrite arm spacing has increased especially at medium and high line energy ranges (Figures 4.42 and 4.44). The effect of amount of strain on secondary-dendrite-arm-spacing was limited. The heat escape towards the die surface was mainly controlling the solidification structure size. This effect was less pronounced in TIG-DC welded specimens. The reason could be explained as the high welding speeds applied in TIG-DC welding method.

## 5.2 Hot Cracking Behaviour in the TIG-AC and TIG-DC Welded MVT Specimens

This part of the discussion intends to make a general comparison between the hot cracking behaviour of 5086 alloy obtained in the Modified Varestraint Test with TIG-AC and TIG-DC welding.

The complete hot cracking behaviour of 5086 alloy as a function of line energy and augmented strain obtained in the Modified Varestraint Test with TIG-AC and TIG-DC welding methods are summarized in Figures 4.10 and 4.20 respectively. In general, the total-crack-lengths obtained in MVT with TIG-AC welding is greater than the TIG-DC welding. In TIG-AC welded specimens the total crack lengths were longer because of the lower temperature gradients due to the slower cooling rates. Welding the Al alloy in question, with TIG-DC welding is more advantageous because it yields less number and sizes of cracks that forms.

The most important and practically meaningful result is the hot crack safe parameter range observed in TIG-DC welded MVT specimens. Unfortunately, there was no hot crack safe region found in the TIG-AC welding tests at any straining condition. However, by using a suitable filler material, solidification crack formation can be avoided and one can reach hot cracking safety in the low line energy range and low straining conditions in TIG-AC welding too. Experiments revealed only small amount of liquation cracks in the indicated parameters range (Figure 4.12). In case a suitable filler material would be used in TIG-DC welding, a wider hot crack safe zone could be obtained (Figure 4.22).

In TIG-AC and TIG-DC welding, the increase in the total-crack-length is not only due to the increase in the size of the individual cracks but also due to the increase in the number of cracks (Figures 4.13 to 4.15 for TIG-AC welding; Figures 4.23 to 4.25 for TIG-DC welding). The maximum crack

lengths data have a similar tendency with the total crack length results (Figures 4.16 to 4.18 for TIG-AC welding; Figures 4.26 to 4.28 for TIG-DC welding). Thus, by measuring only the maximum crack length, the hot cracking trend depending on the line energy and the strain can be assessed.

The following subsections of the discussion intend to correlate between the hot cracking behaviour of 5086 alloy and the applied welding and straining conditions for TIG-DC and TIG-AC welded MVT specimens separately.

### **5.2.1 Hot Cracking Behaviour in TIG-DC Welded 5086 Alloy MVT Specimens**

In TIG-DC welded 5086 alloy MVT specimens, the low and high line energies showed different hot cracking behaviour. In the low line energy range, low and low-medium strains resulted in no solidification and liquation cracking. Increased strain on this line energy range resulted in a sudden start in the weld metal and HAZ cracking. This result is in agreement with the shrinkage-brittleness theory, which states “hot cracks develop during the mushy stage, if a critical level of strain is exceeded”. The results have shown that the critical amount of strain for hot crack formation decreased as the line energy increased.

In order to understand the hot cracking behaviour in TIG-DC welding, the line energy dependence of weld pool size should be considered. At low line energy range, there was a fast moving small sized weld pool with high temperature gradient. On the other hand, at high line energy range, the weld pool size was big and the welding speed was relatively low, causing low temperature gradients. Therefore, at low line energy range, if the critical amount of strain is exceeded, the solidification cracks that form behind the fast moving pool (type “A” cracks) could not be back filled with

the remaining small amount of interdendritic liquid (Figure 4.70). As the line energy is increased, the amount of interdendritic liquid would increase and the TOTAL-WELD-crack-length would decrease (Figure 4.21). In the low line energy range, the contribution of the TOTAL-WELD-crack-length to the TOTAL-crack-length is dominating (Figure 4.20). For that reason, in the low line energy range the TOTAL-crack-length values have decreased with an increase in line energy in medium and high strain range.

On the other hand, at low and low-medium strain levels the TOTAL-crack-length was low because of the resistance to solidification and liquation cracking. This resistance has decreased with the increase in line energy. At medium line energies, the HAZ cracks contributed in a greater extend to the total crack length. Therefore the rate of increase in TOTAL-crack-length showed an increase with the increase of line energy.

At the low line energy levels, type “B” and “C” cracks started to form above medium strain level. Actually, these types of cracks were present at the lower strain levels too. However, their crack openings were small and were filled-back (healed) completely with the capillary effect (Figure 4.72) i.e. critical level of strain was not exceeded. At medium and high strain levels, the healing effect was more emphasized. With an increase in line energy, a crack-centerline precipitation started inside the healed cracks (Figure 4.73). These precipitates did not cause cracking. But, at some lower line energies, these precipitates teared off from the matrix at high strain level (Figure 4.74). This was because; at the high strain level, straining was completed in a longer time duration. In this time duration, the initially formed cracks were back-filled. However, during later stages of bending the healed cracks were teared off by the crack-centerline precipitates and could not be healed any more. As a result, partially healed cracks were observed at the locations of “B” and “C” (Figure 4.74). On the other hand, “D” type of cracks had more opportunity to be re-healed as they contacted the molten pool for longer times (Figure 4.75).



With an increase in line energy, the solidification microstructure tended to become coarser columnar dendritic. In addition, the amount of interdendritic liquid tended to increase. As a result, healing of type “A” cracks increased (Figure 4.76). In parallel, the increased temperature field around the moving pool, increased the amount of HAZ cracks. The total effect was that, at the medium line energy range and especially for medium and high strains, a transition behaviour in the total-weld-crack-length was observed.

At extremely high line energies, the solidification structure became equiaxed dendritic. Therefore, type “A” cracks were not seen. There are two possible reasons for this behaviour. First, because of the abundance in the interdendritic liquid, type “A” cracks could be healed off completely. Secondly, conditions resulting from the strain field and temperature distribution relationship could be effective. The strain field was mainly concentrated at the bending point of the sample. And, at high line energies the weld pool enlarged so that the location where the type “A” cracks preferentially would form could not be exposed to the specified high amount of strain. Since no sign of any healing effect was seen on weld metal microstructure, the second hypothesis seems to be more realistic. The weld metal cracks seen at the high line energy range in Figure 4.21 were only the weld metal extensions of the type “B” and “C” cracks.

At medium and high line energy ranges, the type “B”, “C” and “D” cracks propagated towards the base metal and even crossed the partially melted zone (Figure 4.77). Actually, the temperatures at the crack tip were below the solidus temperature of the alloy. This was also proved by the results of the quench test samples. This crack extension towards the base material can be explained with wrought state BTR of the alloy. The interdendritic liquid fills the crack by capillary action as seen in Figure 4.77. In Figure 4.37, it was seen that the experimentally found BTR sizes were small and had a parallel trend with the theoretically calculated BTR values. The

theoretical BTR values presented are based on the dendritic solidification in the weld metal [12, 45]. At higher augmented strain values the experimentally obtained BTR sizes get closer to the theoretical values indicating a lower resistance for hot cracking. At higher strains, the increase in specimen temperature due to smaller die contact surface results in larger BTR. Figure 4.68 shows the separated grain boundaries in base metal at a distance further from the fusion line. The teared surface is due to the cracking through grain boundary brittleness.

In summary, the 5086 alloy showed resistance for hot cracking at the low line energy and low strain range. The hot cracks seen in the low-line-energy range was mainly the weld-metal-cracks that formed at medium and high strains. These could be overcome with a suitable choice of filler material.

### **5.2.2 Hot Cracking Behaviour in TIG-AC Welded 5086 Alloy MVT Specimens**

The TIG-AC welding data can be classified in two groups of tendencies. One is the hot cracking tendency obtained at low strain level, the other group is the hot cracking tendency at higher strains. In the both groups, commonly there existed an increase in total crack length with the increase in line energy (Figure 4.10). On the other hand, the total-crack-length values obtained at medium and high strain levels were very close to each other. Normally, higher strains resulted in longer total crack lengths.

The TOTAL-HAZ-crack-lengths increased with increasing line energy (Figure 4.12). This type of cracks is directly related with the width of the temperature fields around weld pool. At low line energies majority of cracks were mainly formed in weld metal. (Figure 4.11). Finally, above medium

line energies the contribution of the HAZ and weld cracks in the total crack length was almost equivalent.

At low line energies, the solidification microstructure was columnar dendritic near the fusion line and equiaxed dendritic in the central zone. Due to the high amount of interdendritic liquid, the type “A” and “B” cracks were healed completely (Figures 4.78 and 4.79). Therefore, the observed weld metal cracks were mainly type “C” cracks. As the amount of strain is increased, the sizes of the cracks as well as the solidification microstructure size have increased (Figure 4.80 in comparison with Figure 4.78) resulting in greater amount of back-filling of existing cracks. However, at higher strains due to the larger crack openings back filling of cracks could not be completed. At high strain level, the cracks were extended to longer distances. At the same time, the amount of back filling (healing) was also greater as compared to medium strain level. Finally, the resulting open crack lengths can be smaller than the total crack length obtained at medium strain level (Figure 4.81 in comparison with Figure 4.82). For that reason, the total crack length values obtained at medium and high strain levels were very close to each other on the overall weldability range.

In TIG-AC welding BTR sizes were considerably high. In spite of that, experimentally obtained BTR sizes were lower than the theoretically calculated ones (Figure 4.38). The BTR results obtained in TIG-AC welding exhibited a resistance to the hot cracking in wrought state.

In summary, in TIG-AC welding, resistance to hot cracking on 5086 alloy was low. This was mainly connected with the coarse solidification microstructure size obtained. In spite of that, still there is a possibility to build a resistance to hot cracking by the use of a suitable filler material at low line energy levels.

### 5.3 Precipitates Observed During Cooling in 5086 Alloy

In order to find out the supplementary reasons of hot cracking in Modified Vareststraint Test on 5086 alloy, the precipitates formed in the thermal period was inspected. In this frame, metallographic and SEM inspection of quench test specimens and differential thermal analysis (DTA) were performed. In addition, SEM inspection on the crack surfaces gave information about the precipitates.

With quench test the melting range of the alloy was determined. This range was also verified by the DTA analysis as 640 to 585 °C. The liquidus temperature was taken from the result obtained in the heating stage (Figure 4.45) as cooling stage may give error due to the undercooling effect. The solidus temperature was obtained from the cooling stage. The secondary peak observed in the cooling curve was due to a precipitation reaction. This solidification range is in agreement with literature [43] (Table 3.2 in Section 3.2). Figure 4.49 to 4.56 show the as polished and etched quench test samples. Generally, two types of precipitates have formed. However, on the “as received” sample, only one type of precipitate was observed. The precipitates are grey and grey-brown colored (Figure 4.48a, and Figure 4.48b). The dark points seen in these figures are voids resulting from broken precipitates. These precipitates were dissolved at higher temperatures (Figures 4.49 to 4.56).

In Figures 4.51 to 4.56, it can be seen that at above 590°C a second-phase constituent has precipitated on the grain boundaries, preferentially on the junctions. As the temperature in the semi-solid range was increased, this constituent tended to build up a network along the grain boundaries.

Figures 4.57 and 4.59 show the SEM photographs of quench samples. From the sample in Figure 4.58 a X-ray microanalysis of an isolated

precipitate was taken. The precipitate could be seen on polished surface under optical microscope and SEM. This precipitate was identified as an iron and manganese rich precipitate which could be  $(\text{Fe,Mn,Cr})_3\text{SiAl}_{12}$ ,  $(\text{Fe,Mn,Cr})\text{Al}_6$  or  $(\text{Cr,Mn,Fe})\text{Al}_7$  as stated in the literature (Section 3.2). These precipitates were too small to obtain an exact diffraction.

The X-ray microanalysis of the grain boundary precipitate was taken from the sample shown in Figure 4.59. In this sample the amount of grain boundary precipitates was more than that of shown in Figure 4.57. During etching most of the grain boundary precipitates were dissolved out. The analysis taken from the residues of the precipitates had high amount of magnesium. There are two possibilities for this high amount of magnesium. One is the grain boundary second-phase constituent, which could be  $\text{Mg}_2\text{Al}_3$  precipitates. Alternatively, it can come from the last solidified interdendritic liquid, rich in solute segregation (Figure 2.26). To clarify this point an analysis on cracked surfaces has been done.

The X-ray microanalysis on the unetched hot-crack surfaces at the junction point of the grains showed magnesium rich composition with small amounts of silicon (Figure 4.64). Considering the DTA cooling plot shown in Figure 4.46 with aluminum-magnesium-silicon ternary system (Figure 2.27) it may be reasonable to assume that the grain boundary precipitates are  $\text{Mg}_2\text{Si}$  which may have precipitated in the temperature range of 570 to 550 °C. The formation of  $\text{Mg}_2\text{Al}_3$  would be less possible as there was no peak below 450 °C in DTA cooling plot which is the formation range of this precipitate.

From the literature, it is known that the magnesium silicon ( $\text{Mg}_2\text{Si}$ ) precipitates have a great role in the hot cracking tendency of the aluminium magnesium alloys [43]. Similarly, magnesium aluminium precipitates ( $\text{Al}_2\text{Mg}_3$ ) have a tendency to form a continuous network along the grain boundaries. Normally, the magnesium-silicon and aluminium-magnesium

precipitates would be taken into the solution by the thermal treatments in alloy production. For that reason in DTA heating curve, no sign of any thermal process was detected in the melting range of these precipitates (Figure 4.45).

The other type of precipitate that contains mainly iron and manganese was in an inert nature to hot cracking as it has an isolated rod shaped form (Figures 4.65 and 4.66). Since they were found on and beyond the solidification front, it can be said that the formation of this precipitate took place in the solidification interval. The dissolution of these precipitates in the quench test samples heated in the semi-solid temperature range has also proven this argument.

The precipitates, which were seen in this investigation, are in agreement with the study of Balasundaram et.al. [54] who studied the three-dimensional particle cracking damage in wrought 5086 alloy.

The most detrimental precipitate was the one which formed a network along grain boundaries. The amount of these precipitates was directly related with the welding energy. Even if a crack was completely healed, because of its centerline precipitation, this zone was still in a brittle state. The centrelines of healed cracks can be the crack initiation points under the service loads. For that reason, not only prevention of the hot crack formation, the prevention of the formation of the precipitate networks is essential in welding of 5086 alloy. Therefore welding with lower line energies especially with TIG-DC welding gives more hot cracking safety to the 5086 alloy.

## CHAPTER VI

### CONCLUSIONS

From the results obtained in this study, the following conclusions can be drawn:

1. The hot cracking sensitivity of 5086 aluminium alloy can be obtained by Modified Varestraint Test method. Low line energies give more consistent temperature distribution and better fit with the theory.
2. In MVT tests, an increase in line energy and strain increased the hot cracking tendency of 5086 aluminium alloy. In TIG-DC welding, the hot crack safe parameters are obtained at low line energies and at low strains.
3. In TIG-AC welding, low line energies and low strains decrease the hot-cracking tendency. However, the use of filler material is essential to obtain an absolute hot-cracking safety.
4. At low line energies, the main cracking mechanism is solidification cracking. An increase in line energy decreases the tendency of solidification cracking due to increased healing effect. At high line energies liquation cracking dominates the total crack length because of the increased size of the BTR.
5. The line energy and strain dependence of hot cracking trend can be assessed by only measuring the largest crack size.
6. The 5086 alloy in H32 condition has rod shaped precipitates, which are randomly distributed in the grains. Heat of welding at PMZ and weld

metal zones results in  $Mg_2Si$  precipitation, preferentially at grain boundaries, and especially at junction points.

7. At high line energies healing of the cracks through back-filling is possible. However, the centreline precipitates on the back-filled crack, decrease the ductility of the joint.
8. The solidification structure of the weld metal is affected by the applied line energy. Low line energy range causes fine columnar dendritic solidification structures. On the other hand, as the line energy is increased the dendritic structure becomes coarser. Extremely high line energies results in equiaxed dendritic solidification structures.
9. Equiaxed dendritic structures reduce the mechanical properties because of their coarse nature and the presence of networked precipitates.



## REFERENCES

- [1] Pohle, C. (1990). Zerstörende Werkstoffprüfung in der Schweißtechnik. Fachbuchreihe Schweißtechnik. Band 103. Deutscher Verlag für Schweißtechnik, DVS-Verlag GmbH, Düsseldorf.
- [2] Batıgün, C. (1996). Bericht über MVT Untersuchungen an Aluminiumwerkstoffe. Bundesanstalt für Materialforschung und –prüfung (BAM) Berlin.
- [3] Batıgün, C. (1997). Alüminyum malzemelerde kaynaklama işlemine bağlı sıcak çatlama eğilimi. (Bildiri). 9. Uluslararası Metalurji ve Malzeme Kongresi. 11-15 Haziran 1997, İstanbul.
- [4] Caymaz, H.F. (1997). Hot cracking in welding of aluminum and some of its alloys. Master Thesis. METU Metallurgical and Materials Engineering Department, Ankara.
- [5] Olson, D.L. et al. (eds.) (1993). ASM Handbook Volume 6. Welding, Brazing and Soldering. ASM International. USA.
- [6] Kou, S. (2003). Welding Metallurgy (Second Ed.). John Wiley & Sons, Inc., Hoboken, New Jersey.
- [7] Oates, W.R. (eds.) (1996). Welding Handbook. Volume 3 (Eight Ed.). Materials and Applications – Part 1. American Welding Society, Miami.
- [8] Easterling, K. (1992). Introduction to the Physical Metallurgy of Welding. Butterworth-Heinemann Ltd., Oxford.
- [9] Killing, R. (1996). Angewandte Schweißmetallurgie. Anleitung für die Praxis. Fachbuchreihe Schweißtechnik. Band 113. Deutscher Verlag für Schweißtechnik, DVS-Verlag GmbH, Düsseldorf.
- [10] Zacharia, T. (1994). Dynamic stresses in weld metal hot cracking. Welding Journal. 73(7): pp. 164s-172s.

- [11] Borland, J.C. (1979). Fundamentals of solidification in welds; Part 1. *Welding and Metal Fabrication*. 47(1). pp. 19-29.
- [12] Arata, Y., Matsuda, F., Nakata, K. and Sasaki, I. (1976). Solidification crack susceptibility of aluminium alloy weld metals (Report 1): Characteristics of ductility curves during solidification by means of the trans varestRAINT test. *Transactions of JWRI*. 5(2). pp. 53-67.
- [13] Nakata, K. and Matsuda, F. (1995). Evaluations of ductility characteristics and cracking susceptibility of Al alloys during welding. *Transactions of JWRI*. 24(1), pp. 83-94.
- [14] Pellini W.S. (1952). Strain theory of hot tearing. *The Foundry*. 80(11). pp. 125-199.
- [15] Apblett, W.R. and Pellini, W.S. (1954). Factors which influence weld hot cracking. *Welding Journal*. 33(2). pp. 83s-90s.
- [16] Chihoski, R.A. (1972a). The character of stress fields around a weld arc moving on aluminium sheet. *Welding Journal*. 51(1). pp. 9s-18s.
- [17] Chihoski, R.A. (1972b). Understanding weld cracking in aluminum sheet. *Welding Journal*. 51(1). pp. 24-30.
- [18] Johnson, L. (1973). Formation of plastic strains during welding of aluminum alloys. *Welding Journal*. 52(7). pp. 298s-305s.
- [19] Rappaz, M., Drezet, J.M. and Gremaud, M. (1999). A new hot-tearing criterion. *Metallurgical and Materials Transactions A*. 30A(2). pp. 449-455.
- [20] Huang, C. and Kou, S. (2001a). Partially melted zone in Aluminum Welds: Solute segregation and mechanical behavior. *Welding Journal*. 80(1). pp. 9s-17s.
- [21] Huang, C. and Kou, S. (2001b). Partially melted zone in Aluminum Welds: Planar and cellular solidification. *Welding Journal*. 80(2). pp. 46s-53s.

- [22] Huang, C. and Kou, S. (2000). Partially melted zone in Aluminum Welds: Liquation mechanism and directional solidification. *Welding Journal*. 79(5). pp. 113s-120s.
- [23] Huang, C. and Kou, S. (2002). Liquation mechanisms in multicomponent aluminium alloys during welding. *Welding Journal*. 81(10). pp. 211s-222s.
- [24] Huang, C. and Kou, S. (2003). Liquation cracking in partial penetration aluminium welds: Effect of penetration oscillation and backfilling. *Welding Journal*. 82(7). pp. 184s-194s.
- [25] Huang, C. and Kou, S. (2004). Liquation cracking in full penetration Al-Mg-Si welds. *Welding Journal*. 83(4). pp. 111s-122s.
- [26] Klingauf, S. (1980). Theorie zum Entstehen von Heißrisen in hocherwärmten Werkstoffbereich. *Schweißen und Schneiden*. 32(7). pp. 258-263.
- [27] Matsuda, F., Nakata, K., Arai, K. and Tsukamoto, K. (1982). Assesment of solidification cracking test for aluminum alloy welds. *Transactions of JWRI*. 11(1). pp. 67-77.
- [28] Schnadt, H. (1957). Über eine neue Prüfmethode zur Bestimmung der Warmrißanfälligkeit von Schweißraupen. (Fisco-test). *Oerlikon Schweißmitteilungen*. Nr. 27. pp 31-42.
- [29] Wilken, K. (1985). Gebräuchliche Heißrisprüfverfahren im Vergleich. *Schweißen und Schneiden*. 37(4). pp. 170-174.
- [30] Savage, W.F. and Lundin C.D. (1965). The Vareststraint Test. *Welding Journal*. 44(10). pp. 433s-442s.
- [31] Rawlings, G.N. and Wilken, K. (1992). Vergleich der Aussagefähigkeit von neuen Heißrisprüfverfahren. *Schweißen und Schneiden*. 44(4). pp. 210-214.
- [32] Nakagawa, H., Matsuda, F., Nagai, A. and Sakabata, N. (1980). Weldability of Fe-36%Ni alloy (Report I), hot cracking with cross bead test. *Transactions JWRI*. 9(2). pp. 55-62.

- [33] Lundin, C.D., DeLong, W.T. and Spond, D.F. (1976). The fissure bend test. *Welding Journal*. 55(6). pp. 145s-151s.
- [34] Düchting, W. (1978). Einige Betrachtungen zur Heißrissprüfung von Schweißzusatzwerkstoffen. *Schweißen und Schneiden*. 30(12). pp. 498-502.
- [35] Geniş, K. (1993). Determination of hot crack susceptibility of welding fillers with longitudinal bending test. Master Thesis. METU Metallurgical Engineering Department, Ankara.
- [36] Heißrissprüfung. Grundlagen. DVS Merkblatt 1004 Teil 1. Februar 1989. Deutscher Verband für Schweißtechnik.
- [37] Heißrissprüfverfahren mit fremdbeanspruchten Proben. DVS Merkblatt 1004 Teil 2. November 1987. Deutscher Verband für Schweißtechnik.
- [38] Heißrissprüfverfahren mit selbstbeanspruchten Proben. DVS Merkblatt 1004 Teil 3. September 1990. Deutscher Verband für Schweißtechnik.
- [39] Wilken, K. and Kleistner, H. (1990). MVT-Test. Special report. Bundesanstalt für Materialforschung und -prüfung. Berlin.
- [40] Schellhase, M. (1985). Der Schweißlichtbogen; ein technologisches Werkzeug. Fachbuchreihe Schweißtechnik. Band 84. Deutscher Verlag für Schweißtechnik (DVS), Düsseldorf.
- [41] Killing, R. (1999). Handbuch der Schweißverfahren. Teil 1: Lichtbogenschweißverfahren. Fachbuchreihe Schweißtechnik. Band 76-I. Deutscher Verlag für Schweißtechnik, DVS-Verlag GmbH, Düsseldorf.
- [42] Cornu, J. (1988). Advanced welding systems. Vol. 3: TIG and related processes. Springer Verlag, Berlin.
- [43] Davis, J.R. (eds.) (1993). ASM Specialty Handbook: Aluminum and aluminium alloys. ASM International, USA.

- [44] Arata, Y., Matsuda, F., Nakata, K. and Shinozaki, K. (1977). Solidification crack susceptibility of aluminum alloy weld metals (Report 2): Effect of straining rate on cracking threshold in weld metal during solidification. Transactions of JWRI. 6(1). pp. 91-104.
- [45] Nakata, K. and Matsuda, F. (1995). Ductility characteristics of commercial aluminium alloys between liquidus and solidus temperatures during welding and evaluation of weld solidification cracking susceptibility. Welding International. 9(9). pp. 706-717.
- [46] Mondolfo, L.F. (1976). Aluminum alloys: Structure and properties. Butterworths, London.
- [47] Wilken, K. and Schmaleberg, W. (1993). Abnahmeprotokoll MVT Anlage. Special report 07.05.1993. Bundesanstalt für Materialforschung und –prüfung, Laboratorium 6.43 “Fügeeinfluß auf Bauteile; Prüftechnik” (BAM) Berlin.
- [48] Grong, Ø. (1994). Metallurgical Modelling of Welding. The Institute of Materials. London
- [49] EN 26848. (1991). Wolframelektroden für Wolfram-Schutzgasschweißen und für Plasmaschneiden und –schweißen. European Committee for Standardization, Brussels.
- [50] Weck, E. and Leistner, E. (1986). Metallographic instructions for colour etching by immersion. Part III: Non-ferrous metals, cemented carbides and ferrous metals, nickel-base and cobalt-base alloys. Deutscher Verlag für Schweißtechnik (DVS) GmbH. Düsseldorf.
- [51] Petzow, G. (1994). Metallographisches, Keramographisches, Plastographisches Ätzen. Gebrüder Borntraeger. Berlin-Stuttgart.

- [52] EN ISO 13916. (1996). Welding – Guidance on the measurement of preheating temperature, interpass temperature and preheat maintenance temperature. European Committee for Standardization, Brussels.
- [53] Radaj, D. (1988). Wärmewirkungen des Schweißens. Temperaturfeld, Eigenspannungen, Verzug. Springer Verlag. Berlin.
- [54] Balasundaram, A., Gokhale, A.M., Graham, S. and Horstemeyer, M.F. (2003). Three-dimensional particle cracking damage development in an Al-Mg-base wrought alloy. Materials Science and Engineering A355. pp 368-383.

## **APPENDIX A**

### **STANDARD MODIFIED VARESTRAINT TEST PROCEDURE**

#### **1. First stage: Specimen preparation**

- 1.1. Specimen cutting according to the modified varestRAINT test sample dimensions;
- 1.2. Specimen machining in order to have the allowed dimensions: Milling all the side surfaces, grinding the test surface in longitudinal direction;
- 1.3. Specimen test surface degreasing: Surface contaminants, like grease, oil, paint, etc. which can influence the test results, solved with acetone swap;
- 1.4. Additional test surface cleaning using ethyl alcohol to remove the acetone rests;
- 1.5. Test surface drying under hot air blow.

#### **2. Second stage: Adjustment test**

- 2.1. Former set installation: The former set chosen according to the aimed augmented strain;
- 2.2. MVT adjustment specimen placement;
- 2.3. Electrode tip grinding to remove the oxides on the electrode tip;
- 2.4. Arc length and gas shielding range adjustments: Electrode to specimen distance to 3 mm and gas nozzle to specimen distance to 5 mm;
- 2.5. Welding torch positioning at the starting point;
- 2.6. Starting the welding procedure;
- 2.7. Adjustment of the welding parameters like welding current and welding speed to desired values during welding process;

2.8. Specimen removal.

### **3. Third stage: Main test**

- 3.1. Test specimen placement;
- 3.2. Electrode tip grinding to remove the oxides on the electrode tip;
- 3.3. Welding torch positioning at the starting point;
- 3.4. Starting the welding procedure;
- 3.5. Starting to record the welding and bending data;
- 3.6. Automatic stopping of the test procedure;
- 3.7. Stopping the data recording;
- 3.8. Test specimen removal and repeating of the steps 3.1-3.8 until the former radius, *ie* applied strain, has to be changed.

### **4. Fourth stage: Test specimen inspection and evaluation**

- 4.1. Test surface etching to remove the oxides that may shield the formed cracks;
- 4.2. Cleaning of the surface from the etching solution with water and a soft brush;
- 4.3. Cleaning of the test surface in the ethyl alcohol bath with ultrasonic vibration for 5 minutes. With this cleaning, the possible oxides and the rests of the etching solution in the hot cracks were removed;
- 4.4. Hot crack detection on the specimen under microscope with 25X magnification and measuring each individual crack;
- 4.5. Total crack length calculation, *ie* through summation of all the measured individual crack lengths;
- 4.6. Plotting the result into the "total crack length versus amount of strain" diagram,
- 4.7. Repeating of the step 4.1 - 4.6 for each specimen.



## APPENDIX B

### CRACK MEASUREMENT RESULTS

The crack length measurement data of Modified Varestraint Test with TIG-AC welding process is given in Tables B1 to Table B40. The crack measurement results of the TIG-DC welded MVT specimens are given in Tables B41 to Table B112. Crack measurement results for the whole supplementary test series are given in Tables B113 to B144.

**Table B1:** Crack measurement results of specimen TIG-AC-1-1

Line energy kJ/cm	Welding current A	Arc voltage V	Welding speed mm/min	Shielding gas & composition	Shielding gas flow rate lt/min
3.9	140 ~	4.5	80	99.9 % Argon	8.0
Former radius mm	Specimen thickness mm	Nominal Augmented strain %	Real Augmented strain %		
1000	9.3	0.5	0.47		
Length of all cracks (mm)	0.41/0.87/0.41/0.29/0.25/1.61/0.12/0.08/0.17				
	<b>WELD CENTERLINE</b>				
	0.91/1.24/0.29/1.12/1.12/0.62				
Length of HAZ cracks (mm)	0.41/0.41/0.25/0.12/0.08/0.17				
	<b>WELD CENTERLINE</b>				
	0.37/0.29/0.29/0.21				
Length of weld metal cracks (mm)	0.87/0.29/0.25/1.36				
	<b>WELD CENTERLINE</b>				
	0.91/0.87/0.83/0.91/0.62				
Total # of cracks	Total crack length mm	Total # of HAZ cracks	Total HAZ crack length mm	Total # of weld metal cracks	Total weld metal crack length mm
15	9.50	10	2.60	9	6.90

**Table B2:** Crack measurement results of specimen TIG-AC-1-2

Line energy kJ/cm	Welding current A	Arc voltage V	Welding speed mm/min	Shielding gas & composition	Shielding gas flow rate lt/min
3.9	140 ~	4.5	80	99.9 % Argon	8.0
Former radius mm	Specimen thickness mm	Nominal Augmented strain %	Real Augmented strain %		
500	9.3	1.0	0.93		
Length of all cracks (mm)	2.81/1.24/1.49/0.74/0.58				
	WELD CENTERLINE				
	1.03/2.15/2.60/2.44/2.19/0.83				
Length of HAZ cracks (mm)	0.45/0.41/0.33				
	WELD CENTERLINE				
	0.21/0.54				
Length of weld metal cracks (mm)	2.36/0.83/1.16/0.58/0.74				
	WELD CENTERLINE				
	2.15/1.03/2.40/2.44/1.65/0.83				
Total # of cracks	Total crack length mm	Total # of HAZ cracks	Total HAZ crack length mm	Total # of weld metal cracks	Total weld metal crack length mm
11	18.10	5	1.94	11	16.16

**Table B3:** Crack measurement results of specimen TIG-AC-1-3

Line energy kJ/cm	Welding current A	Arc voltage V	Welding speed mm/min	Shielding gas & composition	Shielding gas flow rate lt/min
3.9	140 ~	4.5	80	99.9 % Argon	8.0
Former radius mm	Specimen thickness mm	Nominal Augmented strain %	Real Augmented strain %		
250	9.4	2.0	1.88		
Length of all cracks (mm)	0.62/1.24/0.50/2.98/0.62/2.48/0.66				
	WELD CENTERLINE				
	0.37/0.99/0.95/2.48/0.87/0.54/2.15/0.70/1.28/0.74				
Length of HAZ cracks (mm)	0.62/0.83/0.50/0.50/0.62				
	WELD CENTERLINE				
	0.54/0.70/0.83/0.74				
Length of weld metal cracks (mm)	0.41/2.48/2.48/0.62/0.66				
	WELD CENTERLINE				
	0.37/0.99/0.95/2.48/0.87/1.45/0.70/0.45				
Total # of cracks	Total crack length mm	Total # of HAZ cracks	Total HAZ crack length mm	Total # of weld metal cracks	Total weld metal crack length mm
17	20.79	9	5.87	13	14.92

**Table B4:** Crack measurement results of specimen TIG-AC-1-4

Line energy kJ/cm	Welding current A	Arc voltage V	Welding speed mm/min	Shielding gas & composition	Shielding gas flow rate lt/min
3.9	140 ~	4.5	80	99.9 % Argon	8.0
Former radius mm	Specimen thickness mm	Nominal Augmented strain %	Real Augmented strain %		
125	9.4	4.0	3.76		
Length of all cracks (mm)	0.83/0.74/1.03/0.41/1.40/0.54/3.10/1.12/1.12				
	WELD CENTERLINE				
	2.56/1.74/0.54/2.69/0.54/1.36/0.54/0.54				
Length of HAZ cracks (mm)	0.83/0.74/0.83/0.54/0.83				
	WELD CENTERLINE				
	0.29/0.41/0.54/0.62/0.54/0.54				
Length of weld metal cracks (mm)	0.21/0.41/1.40/2.27/1.12/1.12				
	WELD CENTERLINE				
	2.56/1.45/0.54/2.27/0.74				
Total # of cracks	Total crack length mm	Total # of HAZ cracks	Total HAZ crack length mm	Total # of weld metal cracks	Total weld metal crack length mm
17	20.79	11	6.69	11	14.09

**Table B5:** Crack measurement results of specimen TIG-AC-2-1

Line energy kJ/cm	Welding current A	Arc voltage V	Welding speed mm/min	Shielding gas & composition	Shielding gas flow rate lt/min
4.2	140 ~	4.5	75	99.9 % Argon	8.0
Former radius mm	Specimen thickness mm	Nominal Augmented strain %	Real Augmented strain %		
1000	9.4	0.5	0.47		
Length of all cracks (mm)	0.54/0.95/0.70/0.41/0.37				
	WELD CENTERLINE				
	1.65/0.70/1.61				
Length of HAZ cracks (mm)	0.12				
	WELD CENTERLINE				
	0.25				
Length of weld metal cracks (mm)	0.54/0.95/0.41/0.58/0.37				
	WELD CENTERLINE				
	1.65/0.70/1.36				
Total # of cracks	Total crack length mm	Total # of HAZ cracks	Total HAZ crack length mm	Total # of weld metal cracks	Total weld metal crack length mm
8	6.94	2	0.37	8	6.57

**Table B6:** Crack measurement results of specimen TIG-AC-2-2

Line energy kJ/cm	Welding current A	Arc voltage V	Welding speed mm/min	Shielding gas & composition	Shielding gas flow rate lt/min
4.2	140 ~	4.5	75	99.9 % Argon	8.0
Former radius mm	Specimen thickness mm	Nominal Augmented strain %	Real Augmented strain %		
500	9.3	1.0	0.93		
Length of all cracks (mm)	0.83/0.33/2.27/0.37/0.45/0.74/0.29/1.94/1.45/0.29/0.41/0.95/1.16				
	WELD CENTERLINE				
	0.66/0.21/0.79/2.40/1.78/0.87/3.06/1.65				
Length of HAZ cracks (mm)	0.21/0.33/0.21/0.37/0.45/0.29				
	WELD CENTERLINE				
	0.33/0.33/0.45/0.21				
Length of weld metal cracks (mm)	0.62/2.07/0.74/0.29/1.65/1.45/0.29/0.41/0.95/1.16				
	WELD CENTERLINE				
	0.66/0.21/0.79/2.07/1.78/0.54/1.65/0.95/1.45				
Total # of cracks	Total crack length mm	Total # of HAZ cracks	Total HAZ crack length mm	Total # of weld metal cracks	Total weld metal crack length mm
21	22.89	10	3.18	19	19.71

**Table B7:** Crack measurement results of specimen TIG-AC-2-3

Line energy kJ/cm	Welding current A	Arc voltage V	Welding speed mm/min	Shielding gas & composition	Shielding gas flow rate lt/min
4.2	140 ~	4.5	75	99.9 % Argon	8.0
Former radius mm	Specimen thickness mm	Nominal Augmented strain %	Real Augmented strain %		
250	9.3	2.0	1.86		
Length of all cracks (mm)	0.58/1.36/2.15/1.32/0.33/2.15/1.61/0.99/1.61				
	WELD CENTERLINE				
	1.74/1.03/1.94/3.10/2.02				
Length of HAZ cracks (mm)	0.58/0.70/0.62/0.83/0.33/0.95				
	WELD CENTERLINE				
	1.03/0.79				
Length of weld metal cracks (mm)	0.66/1.53/0.50/2.15/0.66/0.99/1.61				
	WELD CENTERLINE				
	1.74/1.03/1.94/2.07/1.24				
Total # of cracks	Total crack length mm	Total # of HAZ cracks	Total HAZ crack length mm	Total # of weld metal cracks	Total weld metal crack length mm
14	21.94	8	5.83	12	16.12

**Table B8:** Crack measurement results of specimen TIG-AC-2-4

Line energy kJ/cm	Welding current A	Arc voltage V	Welding speed mm/min	Shielding gas & composition	Shielding gas flow rate lt/min
4.2	140 ~	4.5	75	99.9 % Argon	8.0
Former radius mm	Specimen thickness mm	Nominal Augmented strain %	Real Augmented strain %		
125	9.2	4.0	3.68		
Length of all cracks (mm)	0.62/2.81/0.87/3.14/0.50/1.16/0.62/1.53/0.62/0.62				
	WELD CENTERLINE				
	1.03/1.45/1.07/2.40/1.24/3.10/0.41/1.24/0.95				
Length of HAZ cracks (mm)	0.62/1.03/0.87/0.54				
	WELD CENTERLINE				
	0.54/0.21/0.70/0.41/0.62				
Length of weld metal cracks (mm)	1.78/2.60/0.50/1.16/0.62/1.53/0.62/0.62				
	WELD CENTERLINE				
	1.03/1.45/1.07/1.86/0.62/2.40/0.62/0.95				
Total # of cracks	Total crack length mm	Total # of HAZ cracks	Total HAZ crack length mm	Total # of weld metal cracks	Total weld metal crack length mm
19	24.96	9	5.54	16	19.42

**Table B9:** Crack measurement results of specimen TIG-AC-3-1

Line energy kJ/cm	Welding current A	Arc voltage V	Welding speed mm/min	Shielding gas & composition	Shielding gas flow rate lt/min
4.5	140 ~	4.5	70	99.9 % Argon	8.0
Former radius mm	Specimen thickness mm	Nominal Augmented strain %	Real Augmented strain %		
1000	9.4	0.5	0.47		
Length of all cracks (mm)	0.29/1.16/1.03/0.50/0.41/0.83				
	WELD CENTERLINE				
	0.74/0.62/0.29/0.33/0.12/0.21/0.45/0.91/0.58				
Length of HAZ cracks (mm)	0.29/0.41				
	WELD CENTERLINE				
	0.45				
Length of weld metal cracks (mm)	0.74/1.03/0.50/0.41/0.83/0.74				
	WELD CENTERLINE				
	0.62/0.29/0.33/0.12/0.21/0.91/0.58				
Total # of cracks	Total crack length mm	Total # of HAZ cracks	Total HAZ crack length mm	Total # of weld metal cracks	Total weld metal crack length mm
15	8.47	3	1.16	13	7.31

**Table B10:** Crack measurement results of specimen TIG-AC-3-2

Line energy kJ/cm	Welding current A	Arc voltage V	Welding speed mm/min	Shielding gas & composition	Shielding gas flow rate lt/min
4.5	140 ~	4.5	70	99.9 % Argon	8.0
Former radius mm	Specimen thickness mm	Nominal Augmented strain %	Real Augmented strain %		
500	9.4	1.0	0.94		
Length of all cracks (mm)	0.50/2.07/2.48/2.56/1.03/0.74/0.83/1.45				
	WELD CENTERLINE				
	0.74/0.41/1.65/0.74/1.45/1.45/2.19/1.53/0.41/1.03/0.25/0.25				
Length of HAZ cracks (mm)	0.83/1.03/0.83/1.03/1.45				
	WELD CENTERLINE				
	0.12/0.41/0.62/0.50/0.41/0.41/0.25/0.25				
Length of weld metal cracks (mm)	0.50/1.24/1.45/1.74/0.83/0.74				
	WELD CENTERLINE				
	0.62/1.65/0.74/1.45/1.45/1.57/1.03/0.62				
Total # of cracks	Total crack length mm	Total # of HAZ cracks	Total HAZ crack length mm	Total # of weld metal cracks	Total weld metal crack length mm
20	23.76	13	8.14	14	15.62

**Table B11:** Crack measurement results of specimen TIG-AC-3-3

Line energy kJ/cm	Welding current A	Arc voltage V	Welding speed mm/min	Shielding gas & composition	Shielding gas flow rate lt/min
4.5	140 ~	4.5	70	99.9 % Argon	8.0
Former radius mm	Specimen thickness mm	Nominal Augmented strain %	Real Augmented strain %		
250	9.4	2.0	1.88		
Length of all cracks (mm)	1.45/2.07/1.24/0.83/0.41/0.41/0.91/2.07/1.65/0.62				
	WELD CENTERLINE				
	1.53/2.27/3.64/0.74/1.86/1.24/1.86				
Length of HAZ cracks (mm)	0.91/1.24/0.41/0.91/1.03				
	WELD CENTERLINE				
	0.70/1.16/0.74/0.83/1.24/0.62				
Length of weld metal cracks (mm)	0.41/0.83/0.54/0.83/1.24/2.07/0.62/0.62				
	WELD CENTERLINE				
	0.83/2.27/2.48/1.03/1.24				
Total # of cracks	Total crack length mm	Total # of HAZ cracks	Total HAZ crack length mm	Total # of weld metal cracks	Total weld metal crack length mm
17	24.79	11	9.79	13	15.00

**Table B12:** Crack measurement results of specimen TIG-AC-3-4

Line energy kJ/cm	Welding current A	Arc voltage V	Welding speed mm/min	Shielding gas & composition	Shielding gas flow rate lt/min
4.5	140 ~	4.5	70	99.9 % Argon	8.0
Former radius mm	Specimen thickness mm	Nominal Augmented strain %	Real Augmented strain %		
125	9.4	4.0	3.76		
Length of all cracks (mm)	0.62/1.69/2.15/1.57/1.28/0.45/1.12/0.37/0.70/0.29/0.99/0.25/0.62				
	WELD CENTERLINE				
	1.53/0.29/2.36/1.07/3.84/0.74/1.94/0.74/0.74				
Length of HAZ cracks (mm)	0.62/1.03/0.91/0.66/0.41				
	WELD CENTERLINE				
	0.50/1.16/0.74/1.03/0.74/0.74				
Length of weld metal cracks (mm)	0.66/1.24/1.57/0.62/0.45/0.70/0.37/0.70/0.29/0.99/0.25/0.62				
	WELD CENTERLINE				
	1.53/0.29/0.83/1.03/1.07/2.69/0.91				
Total # of cracks	Total crack length mm	Total # of HAZ cracks	Total HAZ crack length mm	Total # of weld metal cracks	Total weld metal crack length mm
22	25.37	11	8.55	19	16.82

**Table B13:** Crack measurement results of specimen TIG-AC-4-1

Line energy kJ/cm	Welding current A	Arc voltage V	Welding speed mm/min	Shielding gas & composition	Shielding gas flow rate lt/min
4.9	140 ~	4.5	65	99.9 % Argon	8.0
Former radius mm	Specimen thickness mm	Nominal Augmented strain %	Real Augmented strain %		
1000	9.4	0.5	0.47		
Length of all cracks (mm)	0.79/0.58/0.12/0.29/0.41/0.21/1.36				
	WELD CENTERLINE				
	0.54/0.79/0.29/1.07/0.87/0.66/0.33/1.16/0.83/0.50/2.56/0.83				
Length of HAZ cracks (mm)	0.21				
	WELD CENTERLINE				
	0.21/0.12/0.21				
Length of weld metal cracks (mm)	0.79/0.58/0.12/0.29/0.41/1.36				
	WELD CENTERLINE				
	0.54/0.79/0.29/0.87/0.87/0.66/0.33/1.03/0.62/0.50/2.56/0.83				
Total # of cracks	Total crack length mm	Total # of HAZ cracks	Total HAZ crack length mm	Total # of weld metal cracks	Total weld metal crack length mm
19	14.17	4	0.74	18	13.43

**Table B14:** Crack measurement results of specimen TIG-AC-4-2

Line energy kJ/cm	Welding current A	Arc voltage V	Welding speed mm/min	Shielding gas & composition	Shielding gas flow rate lt/min
4.9	140 ~	4.5	65	99.9 % Argon	8.0
Former radius mm	Specimen thickness mm	Nominal Augmented strain %	Real Augmented strain %		
500	9.1	1.0	0.91		
Length of all cracks (mm)	0.99/0.21/1.57/0.21/0.83/0.91/0.21/1.45/0.41/0.62/0.54/0.12/0.50/2.48/0.70				
	WELD CENTERLINE				
	0.33/0.45/1.98/0.91/0.37/0.21/1.45/0.83/0.62/2.89/1.94/0.54/1.07				
Length of HAZ cracks (mm)	0.99/0.62/0.62/0.83/0.12/0.50				
	WELD CENTERLINE				
	0.95/0.62/0.83/0.87				
Length of weld metal cracks (mm)	0.21/1.57/0.21/0.21/0.91/0.21/0.83/0.41/0.62/0.54/1.65/0.70				
	WELD CENTERLINE				
	0.33/0.45/1.03/0.91/0.37/0.21/0.83/0.83/0.62/2.07/1.07/0.54/1.07				
Total # of cracks	Total crack length mm	Total # of HAZ cracks	Total HAZ crack length mm	Total # of weld metal cracks	Total weld metal crack length mm
28	25.33	10	6.94	25	18.39

**Table B15:** Crack measurement results of specimen TIG-AC-4-3

Line energy kJ/cm	Welding current A	Arc voltage V	Welding speed mm/min	Shielding gas & composition	Shielding gas flow rate lt/min
4.9	140 ~	4.5	65	99.9 % Argon	8.0
Former radius mm	Specimen thickness mm	Nominal Augmented strain %	Real Augmented strain %		
250	9.4	2.0	1.88		
Length of all cracks (mm)	1.45/1.12/1.98/3.43/0.99/2.40/1.69/2.07				
	WELD CENTERLINE				
	1.45/0.83/0.83/2.98/0.54/1.78/2.73/2.07/0.70/0.70/0.58/0.29/0.29/1.12/0.41				
Length of HAZ cracks (mm)	0.62/1.03/1.24/0.99/0.95/1.24				
	WELD CENTERLINE				
	0.83/0.50/0.62/1.16/1.24/0.58/0.29/0.29/0.70				
Length of weld metal cracks (mm)	0.83/1.12/0.95/2.19/1.45/0.45/2.07				
	WELD CENTERLINE				
	1.45/0.83/1.86/0.54/0.62/1.36/0.99/0.37/0.83/0.70/0.70/0.41/0.41				
Total # of cracks	Total crack length mm	Total # of HAZ cracks	Total HAZ crack length mm	Total # of weld metal cracks	Total weld metal crack length mm
23	32.40	15	12.27	20	20.12



**Table B16:** Crack measurement results of specimen TIG-AC-4-4

Line energy kJ/cm	Welding current A	Arc voltage V	Welding speed mm/min	Shielding gas & composition	Shielding gas flow rate lt/min
4.9	140 ~	4.5	65	99.9 % Argon	8.0
Former radius mm	Specimen thickness mm	Nominal Augmented strain %	Real Augmented strain %		
125	9.4	4.0	3.76		
Length of all cracks (mm)	0.74/0.62/0.41/0.70/1.82/1.03/0.50/3.10/1.03/1.78/0.50/0.50/0.70/0.66/1.12/1.57				
	WELD CENTERLINE				
1.24/1.98/2.69/4.01/1.16/0.83/0.50/0.83/0.45/1.86/0.66					
Length of HAZ cracks (mm)	0.74/0.62/0.41/0.70/1.12/1.03/0.50/0.21/0.62/1.16				
	WELD CENTERLINE				
1.03/1.36/1.16/0.83/0.50/0.83/0.45					
Length of weld metal cracks (mm)	0.70/2.27/1.03/0.62/0.50/0.50/0.70/0.66/1.12/1.57				
	WELD CENTERLINE				
1.24/1.98/1.24/0.41/1.86/0.79/1.86/0.66					
Total # of cracks	Total crack length mm	Total # of HAZ cracks	Total HAZ crack length mm	Total # of weld metal cracks	Total weld metal crack length mm
27	32.98	17	13.26	18	19.71

**Table B17:** Crack measurement results of specimen TIG-AC-5-1

Line energy kJ/cm	Welding current A	Arc voltage V	Welding speed mm/min	Shielding gas & composition	Shielding gas flow rate lt/min
5.3	140 ~	4.5	60	99.9 % Argon	8.0
Former radius mm	Specimen thickness mm	Nominal Augmented strain %	Real Augmented strain %		
1000	9.3	0.5	0.46		
Length of all cracks (mm)	0.99/0.99/0.62/2.11				
	WELD CENTERLINE				
0.91/0.54/0.83/0.79/1.78/0.29					
Length of HAZ cracks (mm)	0.50/0.29/0.62/0.21				
	WELD CENTERLINE				
0.29					
Length of weld metal cracks (mm)	0.50/0.70/1.90				
	WELD CENTERLINE				
0.91/0.54/0.83/0.50/1.78/0.29					
Total # of cracks	Total crack length mm	Total # of HAZ cracks	Total HAZ crack length mm	Total # of weld metal cracks	Total weld metal crack length mm
10	9.83	5	1.90	9	7.93

**Table B18:** Crack measurement results of specimen TIG-AC-5-2

Line energy kJ/cm	Welding current A	Arc voltage V	Welding speed mm/min	Shielding gas & composition	Shielding gas flow rate lt/min
5.3	140 ~	4.5	60	99.9 % Argon	8.0
Former radius mm	Specimen thickness mm	Nominal Augmented strain %	Real Augmented strain %		
500	9.3	1.0	0.93		
Length of all cracks (mm)	0.79/3.10/0.95/0.83/0.37/2.56/0.58/1.20				
	WELD CENTERLINE				
	0.74/0.87/3.14/1.78/1.61/0.21/0.21/0.41/0.58/0.70/0.54/0.62/1.40				
Length of HAZ cracks (mm)	0.79/0.70/0.95/0.83/1.03				
	WELD CENTERLINE				
	0.87/0.79/1.03/0.99/0.54				
Length of weld metal cracks (mm)	1.07/1.32/0.37/1.53/0.58/1.20				
	WELD CENTERLINE				
	0.74/1.45/0.91/0.74/0.62/0.21/0.21/0.41/0.58/0.70/0.62/1.40				
Total # of cracks	Total crack length mm	Total # of HAZ cracks	Total HAZ crack length mm	Total # of weld metal cracks	Total weld metal crack length mm
21	23.18	10	8.51	18	14.67

**Table B19:** Crack measurement results of specimen TIG-AC-5-3

Line energy kJ/cm	Welding current A	Arc voltage V	Welding speed mm/min	Shielding gas & composition	Shielding gas flow rate lt/min
5.3	140 ~	4.5	60	99.9 % Argon	8.0
Former radius mm	Specimen thickness mm	Nominal Augmented strain %	Real Augmented strain %		
250	9.4	2.0	1.88		
Length of all cracks (mm)	0.66/0.25/1.69/4.05/2.60/1.36/0.79/1.90/0.37/0.25/0.25/0.58/3.26/0.45/ 1.49/0.50				
	WELD CENTERLINE				
	0.33/0.70/3.02/2.48/0.33/0.41/4.55/0.62/1.69/1.69/0.50/0.29				
Length of HAZ cracks (mm)	0.66/1.24/1.24/1.45/0.95				
	WELD CENTERLINE				
	1.36/1.65/0.62/1.69/0.50/0.29				
Length of weld metal cracks (mm)	0.25/0.45/1.86/0.95/1.16/0.41/0.79/1.90/0.25/0.58/3.26/0.45/1.49/0.50/ 0.37/0.25/0.12				
	WELD CENTERLINE				
	0.33/0.70/1.65/2.48/0.33/0.41/2.89/1.69/0.83/0.41/0.50				
Total # of cracks	Total crack length mm	Total # of HAZ cracks	Total HAZ crack length mm	Total # of weld metal cracks	Total weld metal crack length mm
29	38.93	11	11.65	28	27.27

**Table B20:** Crack measurement results of specimen TIG-AC-5-4

Line energy kJ/cm	Welding current A	Arc voltage V	Welding speed mm/min	Shielding gas & composition	Shielding gas flow rate lt/min
5.3	140 ~	4.5	60	99.9 % Argon	8.0
Former radius mm	Specimen thickness mm	Nominal Augmented strain %	Real Augmented strain %		
125	9.2	4.0	3.68		
Length of all cracks (mm)	0.33/1.03/1.03/2.77/0.87/2.44/1.78/0.66/0.54				
	WELD CENTERLINE				
	1.24/0.74/1.86/1.12/0.29/1.45/2.36/0.99/0.83				
Length of HAZ cracks (mm)	0.33/1.03/1.65/0.87/0.95/1.03				
	WELD CENTERLINE				
	0.74/0.83/0.62/1.53/0.99/0.83				
Length of weld metal cracks (mm)	1.03/1.12/1.49/0.74/0.66/0.54				
	WELD CENTERLINE				
	1.24/0.41/1.12/0.29/1.45/0.83/0.62/0.45/0.50/0.91				
Total # of cracks	Total crack length mm	Total # of HAZ cracks	Total HAZ crack length mm	Total # of weld metal cracks	Total weld metal crack length mm
18	24.79	12	11.40	16	13.39

**Table B21:** Crack measurement results of specimen TIG-AC-6-1

Line energy kJ/cm	Welding current A	Arc voltage V	Welding speed mm/min	Shielding gas & composition	Shielding gas flow rate lt/min
5.8	140 ~	4.5	55	99.9 % Argon	8.0
Former radius mm	Specimen thickness mm	Nominal Augmented strain %	Real Augmented strain %		
1000	9.35	0.5	0.47		
Length of all cracks (mm)	0.50/1.65/1.12/0.29/0.50/0.58/0.37/0.54/0.83				
	WELD CENTERLINE				
	0.37/1.49/0.91/2.48/0.54/0.70/0.95				
Length of HAZ cracks (mm)	0.41/0.33/0.83				
	WELD CENTERLINE				
	0.37/0.37/0.66/0.54/0.33				
Length of weld metal cracks (mm)	0.50/1.24/0.79/0.50/0.29/0.58/0.37/0.54				
	WELD CENTERLINE				
	1.12/0.25/1.94/0.54/0.70/0.62				
Total # of cracks	Total crack length mm	Total # of HAZ cracks	Total HAZ crack length mm	Total # of weld metal cracks	Total weld metal crack length mm
16	13.8	8	3.84	14	9.96

**Table B22:** Crack measurement results of specimen TIG-AC-6-2

Line energy kJ/cm	Welding current A	Arc voltage V	Welding speed mm/min	Shielding gas & composition	Shielding gas flow rate lt/min
5.8	140 ~	4.5	55	99.9 % Argon	8.0
Former radius mm	Specimen thickness mm	Nominal Augmented strain %	Real Augmented strain %		
500	9.3	1.0	0.93		
Length of all cracks (mm)	0.21/0.74/2.11/1.65/1.12/1.65/0.83/0.91/2.27				
	WELD CENTERLINE				
	0.54/0.45/3.35/0.29/3.02/2.73				
Length of HAZ cracks (mm)	0.21/0.74/0.62/0.83/0.83/1.65				
	WELD CENTERLINE				
	0.54/0.45/1.74/0.29/0.12/1.07				
Length of weld metal cracks (mm)	1.49/0.83/1.12/0.83/0.83/0.91/0.62				
	WELD CENTERLINE				
	1.49/1.74/1.65				
Total # of cracks	Total crack length mm	Total # of HAZ cracks	Total HAZ crack length mm	Total # of weld metal cracks	Total weld metal crack length mm
15	21.86	13	10.37	10	11.49

**Table B23:** Crack measurement results of specimen TIG-AC-6-3

Line energy kJ/cm	Welding current A	Arc voltage V	Welding speed mm/min	Shielding gas & composition	Shielding gas flow rate lt/min
5.8	140 ~	4.5	55	99.9 % Argon	8.0
Former radius mm	Specimen thickness mm	Nominal Augmented strain %	Real Augmented strain %		
250	9.4	2.0	1.88		
Length of all cracks (mm)	2.15/0.91/4.05/1.03/3.35/1.24/0.62/0.70/1.12				
	WELD CENTERLINE				
	0.74/0.66/0.70/0.83/1.24/3.31/0.50/4.01/0.54/3.22/0.29/0.58/2.73/1.74				
Length of HAZ cracks (mm)	1.65/0.91/1.86/1.03/2.27/1.24/0.62/0.70				
	WELD CENTERLINE				
	0.74/0.66/0.70/0.83/1.24/2.27/2.27/2.19/0.58/1.28/1.28				
Length of weld metal cracks (mm)	0.50/2.19/1.07/1.12				
	WELD CENTERLINE				
	1.03/0.50/0.50/1.24/0.54/1.03/0.29/1.45/0.45				
Total # of cracks	Total crack length mm	Total # of HAZ cracks	Total HAZ crack length mm	Total # of weld metal cracks	Total weld metal crack length mm
23	36.24	19	24.34	13	11.90

**Table B24:** Crack measurement results of specimen TIG-AC-6-4

Line energy kJ/cm	Welding current A	Arc voltage V	Welding speed mm/min	Shielding gas & composition	Shielding gas flow rate lt/min
5.8	140 ~	4.5	55	99.9 % Argon	8.0
Former radius mm	Specimen thickness mm	Nominal Augmented strain %	Real Augmented strain %		
125	9.4	4.0	3.76		
Length of all cracks (mm)	1.57/1.74/1.57/2.85/1.07/1.07/1.94/1.65/3.06				
	WELD CENTERLINE				
	1.94/0.62/1.24/1.49/2.19/2.19/2.44/1.98/0.70/1.32				
Length of HAZ cracks (mm)	0.91/1.45/1.57/1.32/0.70/2.07				
	WELD CENTERLINE				
	1.03/0.62/1.24/1.32/1.57/1.03/0.70				
Length of weld metal cracks (mm)	0.66/0.29/1.53/1.07/1.24/1.65/0.99				
	WELD CENTERLINE				
	0.91/1.49/0.87/2.19/0.87/0.95/1.32				
Total # of cracks	Total crack length mm	Total # of HAZ cracks	Total HAZ crack length mm	Total # of weld metal cracks	Total weld metal crack length mm
19	31.57	13	15.54	14	16.03

**Table B25:** Crack measurement results of specimen TIG-AC-7-1

Line energy kJ/cm	Welding current A	Arc voltage V	Welding speed mm/min	Shielding gas & composition	Shielding gas flow rate lt/min
6.4	140 ~	4.5	50	99.9 % Argon	8.0
Former radius mm	Specimen thickness mm	Nominal Augmented strain %	Real Augmented strain %		
1000	9.4	0.5	0.47		
Length of all cracks (mm)	0.62/1.49/0.50/0.41/0.58/0.79/2.73/1.32/1.94				
	WELD CENTERLINE				
	1.12/2.19/3.43/0.62/0.29/2.11/0.33/0.87				
Length of HAZ cracks (mm)	0.62/0.87/0.79/1.03/1.32/0.83				
	WELD CENTERLINE				
	1.36/1.03/0.62/0.29/0.66/0.33/0.87				
Length of weld metal cracks (mm)	0.62/0.50/0.41/0.58/1.69/1.12				
	WELD CENTERLINE				
	1.12/0.83/1.65/0.74/1.45				
Total # of cracks	Total crack length mm	Total # of HAZ cracks	Total HAZ crack length mm	Total # of weld metal cracks	Total weld metal crack length mm
17	21.32	13	10.62	11	10.70

**Table B26:** Crack measurement results of specimen TIG-AC-7-2

Line energy kJ/cm	Welding current A	Arc voltage V	Welding speed mm/min	Shielding gas & composition	Shielding gas flow rate lt/min
6.4	140 ~	4.5	50	99.9 % Argon	8.0
Former radius mm	Specimen thickness mm	Nominal Augmented strain %	Real Augmented strain %		
500	9.45	1.0	0.95		
Length of all cracks (mm)	0.95/1.90/3.55/2.89/1.82/0.25				
	WELD CENTERLINE				
	0.50/0.54/0.66/0.99/0.83/1.65/1.78/2.31/3.10/0.79/0.58/3.55/1.07				
Length of HAZ cracks (mm)	0.95/1.36/2.07/0.83/1.82/0.25				
	WELD CENTERLINE				
	0.50/0.54/0.66/0.99/0.54/1.65/0.12/1.98/0.79/0.58/0.54/1.07				
Length of weld metal cracks (mm)	0.54/1.49/2.07				
	WELD CENTERLINE				
	0.29/1.65/0.33/3.10/1.53/1.49				
Total # of cracks	Total crack length mm	Total # of HAZ cracks	Total HAZ crack length mm	Total # of weld metal cracks	Total weld metal crack length mm
19	29.71	18	17.23	9	12.48

**Table B27:** Crack measurement results of specimen TIG-AC-7-3

Line energy kJ/cm	Welding current A	Arc voltage V	Welding speed mm/min	Shielding gas & composition	Shielding gas flow rate lt/min
6.4	140 ~	4.5	50	99.9 % Argon	8.0
Former radius mm	Specimen thickness mm	Nominal Augmented strain %	Real Augmented strain %		
250	9.4	2.0	1.88		
Length of all cracks (mm)	0.54/2.36/1.86/1.16/3.10/4.46/1.82/0.83				
	WELD CENTERLINE				
	0.74/1.45/4.30/4.17/2.60/1.86/0.50/1.24/0.41/0.70/1.45				
Length of HAZ cracks (mm)	0.54/1.69/1.16/1.90/2.48/1.82				
	WELD CENTERLINE				
	0.74/1.45/2.64/1.61/2.19/1.86/0.50/1.45				
Length of weld metal cracks (mm)	0.66/1.86/0.87/1.20/1.98/0.83				
	WELD CENTERLINE				
	1.65/2.56/0.41/1.24/0.41/1.24/0.41/0.70				
Total # of cracks	Total crack length mm	Total # of HAZ cracks	Total HAZ crack length mm	Total # of weld metal cracks	Total weld metal crack length mm
19	36.40	14	22.02	14	14.38

**Table B28:** Crack measurement results of specimen TIG-AC-7-4

Line energy kJ/cm	Welding current A	Arc voltage V	Welding speed mm/min	Shielding gas & composition	Shielding gas flow rate lt/min
6.4	140 ~	4.5	50	99.9 % Argon	8.0
Former radius mm	Specimen thickness mm	Nominal Augmented strain %	Real Augmented strain %		
125	9.4	4.0	3.76		
Length of all cracks (mm)	0.45/2.19/1.94/1.16/6.20/4.38/1.74/2.31/0.83/1.24				
	WELD CENTERLINE				
	0.45/1.49/2.15/1.53/0.50/0.83/0.54/2.64/1.36/7.89/1.24/0.66/0.74/2.77/ 0.95/1.57/0.95/0.62				
Length of HAZ cracks (mm)	0.45/1.94/1.94/0.83/3.72/0.45/1.45/2.48/1.74/2.31/0.83/1.24				
	WELD CENTERLINE				
	0.45/1.49/2.15/1.53/1.82/0.83/1.36/3.60/1.24/0.66/0.74/2.23/0.95/1.57/ 0.95				
Length of weld metal cracks (mm)	0.25/0.33/2.48				
	WELD CENTERLINE				
	1.20/0.50/0.83/0.54/3.10/0.54/0.62				
Total # of cracks	Total crack length mm	Total # of HAZ cracks	Total HAZ crack length mm	Total # of weld metal cracks	Total weld metal crack length mm
28	51.32	27	40.95	10	10.37

**Table B29:** Crack measurement results of specimen TIG-AC-8-1

Line energy kJ/cm	Welding current A	Arc voltage V	Welding speed mm/min	Shielding gas & composition	Shielding gas flow rate lt/min
7.1	140 ~	4.5	45	99.9 % Argon	8.0
Former radius mm	Specimen thickness mm	Nominal Augmented strain %	Real Augmented strain %		
1000	9.3	0.5	0.47		
Length of all cracks (mm)	0.95/0.56/1.45/0.74/0.21/2.02				
	WELD CENTERLINE				
	0.29/0.62/1.07/0.62/0.91/0.50/0.54/0.79				
Length of HAZ cracks (mm)	0.41/0.54/1.45/0.74/0.21				
	WELD CENTERLINE				
	1.53/0.58/0.54/0.29				
Length of weld metal cracks (mm)	0.54/2.02				
	WELD CENTERLINE				
	0.50/0.29/0.62/0.50/0.62/0.91/0.50/0.50				
Total # of cracks	Total crack length mm	Total # of HAZ cracks	Total HAZ crack length mm	Total # of weld metal cracks	Total weld metal crack length mm
14	13.26	9	6.28	10	6.98

**Table B30:** Crack measurement results of specimen TIG-AC-8-2

Line energy kJ/cm	Welding current A	Arc voltage V	Welding speed mm/min	Shielding gas & composition	Shielding gas flow rate lt/min
7.1	140 ~	4.5	45	99.9 % Argon	8.0
Former radius mm	Specimen thickness mm	Nominal Augmented strain %	Real Augmented strain %		
500	9.4	1.0	0.94		
Length of all cracks (mm)	0.62/0.37/2.07/0.33/0.79/4.67/0.87/1.36/1.90/1.28/0.74/0.50/4.42/0.45/0.70/0.79/0.50/0.66/0.12/0.54/0.79/0.50/0.54/0.83				
	WELD CENTERLINE				
	1.24/2.85/0.58/0.91/0.91/4.21/0.50/0.45/5.21/0.62/4.79/0.45/0.33				
Length of HAZ cracks (mm)	0.62/0.37/2.07/0.33/0.79/1.86/0.87/1.36/1.90/1.28/0.74/0.50/2.27/0.45/0.70/0.79/0.50/0.66/0.12/0.54/0.79/0.50/0.54				
	WELD CENTERLINE				
	2.15/0.58/0.91/0.91/2.77/0.50/0.45/2.52/0.62/2.23/0.45/0.33				
Length of weld metal cracks (mm)	0.66/2.15/0.41/1.74/0.83				
	WELD CENTERLINE				
	1.24/0.70/1.45/1.24/1.45/1.12/1.45				
Total # of cracks	Total crack length mm	Total # of HAZ cracks	Total HAZ crack length mm	Total # of weld metal cracks	Total weld metal crack length mm
37	49.38	35	34.96	12	14.42

**Table B31:** Crack measurement results of specimen TIG-AC-8-3

Line energy kJ/cm	Welding current A	Arc voltage V	Welding speed mm/min	Shielding gas & composition	Shielding gas flow rate lt/min
7.1	140 ~	4.5	45	99.9 % Argon	8.0
Former radius mm	Specimen thickness mm	Nominal Augmented strain %	Real Augmented strain %		
250	9.4	2.0	1.88		
Length of all cracks (mm)	0.99/6.40/0.50/1.28/1.94/5.58/1.03/1.03/0.29/3.39/0.50/0.29/1.65/2.15/1.65/1.40/0.74/1.12/1.07/1.53				
	WELD CENTERLINE				
	1.24/4.13/0.29/0.41/0.41/1.12/0.70/0.91/0.91/3.39/0.83/0.91/0.45/2.48/1.32/4.34/0.87/0.83/4.13/1.86/2.69/0.95/1.86/0.62/0.45/0.54				
Length of HAZ cracks (mm)	0.99/2.69/0.50/1.28/1.94/3.31/1.03/1.03/0.29/2.98/1.62/2.15				
	WELD CENTERLINE				
	1.45/0.29/0.41/0.41/1.12/0.91/1.86/1.53/1.24/3.51/0.87/0.83/2.89/1.86/2.69/0.95/1.86/0.62/0.45/0.54				
Length of weld metal cracks (mm)	1.45/2.27/2.27/0.41/0.50/0.29/1.65/1.40/0.74/1.12/1.07/1.53				
	WELD CENTERLINE				
	0.74/0.50/2.69/0.70/0.91/0.83/0.91/0.45/1.24/1.32/0.83/1.24				
Total # of cracks	Total crack length mm	Total # of HAZ cracks	Total HAZ crack length mm	Total # of weld metal cracks	Total weld metal crack length mm
46	73.18	32	46.12	24	27.07



**Table B32:** Crack measurement results of specimen TIG-AC-8-4

Line energy kJ/cm	Welding current A	Arc voltage V	Welding speed mm/min	Shielding gas & composition	Shielding gas flow rate lt/min
7.1	140 ~	4.5	45	99.9 % Argon	8.0
Former radius mm	Specimen thickness mm	Nominal Augmented strain %	Real Augmented strain %		
125	9.4	4.0	3.76		
Length of all cracks (mm)	0.50/1.74/1.12/5.37/1.86/2.52/1.86/1.40/4.21/1.16/2.64/1.12				
	WELD CENTERLINE				
	1.07/0.99/4.71/1.74/1.40/0.74/7.52/1.69/1.53/0.99/1.69/1.03/1.40/1.24/0.83/1.65/0.83/1.24/1.03				
Length of HAZ cracks (mm)	0.50/1.74/1.12/2.27/1.86/2.52/2.89/1.16/2.07/1.12				
	WELD CENTERLINE				
	1.07/0.99/1.20/2.07/1.74/1.40/3.26/1.69/1.53/0.99/1.69/1.03/1.40				
Length of weld metal cracks (mm)	3.10/1.86/1.40/1.32/0.58				
	WELD CENTERLINE				
	1.45/0.74/2.48/1.78/1.24/0.83/1.65/0.83/1.24/1.03				
Total # of cracks	Total crack length mm	Total # of HAZ cracks	Total HAZ crack length mm	Total # of weld metal cracks	Total weld metal crack length mm
31	58.84	23	37.31	15	21.53

**Table B33:** Crack measurement results of specimen TIG-AC-9-1

Line energy kJ/cm	Welding current A	Arc voltage V	Welding speed mm/min	Shielding gas & composition	Shielding gas flow rate lt/min
7.9	140 ~	4.5	40	99.9 % Argon	8.0
Former radius mm	Specimen thickness mm	Nominal Augmented strain %	Real Augmented strain %		
1000	9.3	0.5	0.47		
Length of all cracks (mm)	1.82/0.70/2.27/1.65/0.91/2.23				
	WELD CENTERLINE				
	3.93/1.03/2.56/0.66/0.21/0.21/0.70				
Length of HAZ cracks (mm)	0.83/0.70/0.70/1.24				
	WELD CENTERLINE				
	1.86/1.12/0.21				
Length of weld metal cracks (mm)	0.99/1.57/0.91/0.41/2.23				
	WELD CENTERLINE				
	2.07/1.03/1.45/0.66/0.21/0.21/0.50				
Total # of cracks	Total crack length mm	Total # of HAZ cracks	Total HAZ crack length mm	Total # of weld metal cracks	Total weld metal crack length mm
13	18.88	7	6.65	12	12.23

**Table B34:** Crack measurement results of specimen TIG-AC-9-2

Line energy kJ/cm	Welding current A	Arc voltage V	Welding speed mm/min	Shielding gas & composition	Shielding gas flow rate lt/min
7.9	140 ~	4.5	40	99.9 % Argon	8.0
Former radius mm	Specimen thickness mm	Nominal Augmented strain %	Real Augmented strain %		
500	9.4	1.0	0.93		
Length of all cracks (mm)	0.54/6.20/0.45/1.03/2.40/2.69/1.86/5.58				
	WELD CENTERLINE				
	4.55/1.45/2.89/1.94/0.50/1.82/4.21/3.90/1.20/ 4.00/8.70/4.70				
Length of HAZ cracks (mm)	0.54/3.72/0.45/0.62/2.69/1.86/0.62				
	WELD CENTERLINE				
	2.89/2.77/3.90/1.20/4.00/8.70				
Length of weld metal cracks (mm)	2.48/1.03/1.78/5.58				
	WELD CENTERLINE				
	4.55/1.45/1.94/0.50/1.82/1.45/4.70				
Total # of cracks	Total crack length mm	Total # of HAZ cracks	Total HAZ crack length mm	Total # of weld metal cracks	Total weld metal crack length mm
21	61.22	13	33.96	11	27.26

**Table B35:** Crack measurement results of specimen TIG-AC-9-3

Line energy kJ/cm	Welding current A	Arc voltage V	Welding speed mm/min	Shielding gas & composition	Shielding gas flow rate lt/min
7.9	140 ~	4.5	40	99.9 % Argon	8.0
Former radius mm	Specimen thickness mm	Nominal Augmented strain %	Real Augmented strain %		
250	9.4	2.0	1.88		
Length of all cracks (mm)	0.29/3.39/0.62/3.10/3.93/1.07/2.48/0.83/1.45/3.64/1.45/2.69/0.50/6.12/1.86/1.65/1.03/0.70				
	WELD CENTERLINE				
	0.83/0.50/3.93/2.07/2.77/6.40/1.36/1.36/2.07/0.83/0.50/2.77/0.50/0.95/1.16/6.40/1.16/1.03				
Length of HAZ cracks (mm)	0.29/2.48/0.62/3.10/1.07/0.83/2.69/1.45/0.50/4.96/1.16/1.65				
	WELD CENTERLINE				
	0.50/1.86/2.07/1.12/1.65/6.40/1.36/1.36/0.83/0.50/0.70/0.50/0.95/1.16/ 2.27/1.16				
Length of weld metal cracks (mm)	0.91/3.93/2.48/1.45/0.95/2.69/1.86/1.03/0.70				
	WELD CENTERLINE				
	0.83/2.07/2.07/2.07/4.13/1.03				
Total # of cracks	Total crack length mm	Total # of HAZ cracks	Total HAZ crack length mm	Total # of weld metal cracks	Total weld metal crack length mm
36	73.34	28	45.16	15	28.18

**Table B36:** Crack measurement results of specimen TIG-AC-9-4

Line energy kJ/cm	Welding current A	Arc voltage V	Welding speed mm/min	Shielding gas & composition	Shielding gas flow rate lt/min
7.9	140 ~	4.5	40	99.9 % Argon	8.0
Former radius mm	Specimen thickness mm	Nominal Augmented strain %	Real Augmented strain %		
125	9.4	4.0	3.76		
Length of all cracks (mm)	1.45/3.06/1.20/3.35/0.33/0.62/1.53/1.16/3.93/1.69/1.65/0.41/1.03/1.28/ 1.36/1.07/2.40/4.13/1.03/1.94/0.62/5.37				
	WELD CENTERLINE				
	2.07/2.85/4.34/2.27/4.96/2.07/0.62/1.65/2.27/4.13/1.65/10.00/1.24/0.50/ 0.62/1.24/2.69				
Length of HAZ cracks (mm)	1.45/3.06/1.20/3.35/0.33/0.62/1.53/1.16/3.93/1.69/1.65/0.41/1.03/1.07/2.40/4.13/0.62/5.37				
	WELD CENTERLINE				
	2.07/2.85/1.03/3.31/2.27/0.83/2.07/0.62/1.65/2.69/1.65/10.00				
Length of weld metal cracks (mm)	1.28/1.36/1.03/1.94				
	WELD CENTERLINE				
	4.13/2.27/1.45/1.24/0.50/0.62/1.24/2.69				
Total # of cracks	Total crack length mm	Total # of HAZ cracks	Total HAZ crack length mm	Total # of weld metal cracks	Total weld metal crack length mm
39	85.79	30	66.03	12	19.75

**Table B37:** Crack measurement results of specimen TIG-AC-10-1

Line energy kJ/cm	Welding current A	Arc voltage V	Welding speed mm/min	Shielding gas & composition	Shielding gas flow rate lt/min
9.1	140 ~	4.5	35	99.9 % Argon	8.0
Former radius mm	Specimen thickness mm	Nominal Augmented strain %	Real Augmented strain %		
1000	9.3	0.5	0.47		
Length of all cracks (mm)	0.41/0.62/0.66/0.25/0.45/0.62/3.51/2.48/0.83/0.83/0.83/0.83/2.48				
	WELD CENTERLINE				
	3.06/1.32/2.27/2.48/0.37/1.65/0.70/1.36/1.57/2.27/2.69/3.51/1.57/1.57/ 1.24				
Length of HAZ cracks (mm)	0.41/0.62/0.66/0.25/0.45/0.62/2.27/2.48/0.83/0.83/0.83/0.83/2.48				
	WELD CENTERLINE				
	0.58/1.24/0.37/0.70/1.57/2.27/2.07				
Length of weld metal cracks (mm)	1.24				
	WELD CENTERLINE				
	2.48/1.32/2.27/1.24/1.65/1.36/2.69/1.45/1.57/1.57/1.24				
Total # of cracks	Total crack length mm	Total # of HAZ cracks	Total HAZ crack length mm	Total # of weld metal cracks	Total weld metal crack length mm
28	42.44	20	22.36	12	20.08

**Table B38:** Crack measurement results of specimen TIG-AC-10-2

Line energy kJ/cm	Welding current A	Arc voltage V	Welding speed mm/min	Shielding gas & composition	Shielding gas flow rate lt/min
9.1	140 ~	4.5	35	99.9 % Argon	8.0
Former radius mm	Specimen thickness mm	Nominal Augmented strain %	Real Augmented strain %		
500	9.4	1.0	0.94		
Length of all cracks (mm)	4.13/4.55/1.65/11.50/2.50/4.80/3.00/3.00/3.00/2.20/3.60/14.00/2.00/				
	WELD CENTERLINE				
	17.50/5.30/17.40/3.00/4.20/1.60/1.80/4.20/3.80/2.00				
Length of HAZ cracks (mm)	4.13/3.51/1.65/11.50/2.50/4.80/3.00/3.00/2.20/3.60/14.00/2.00				
	WELD CENTERLINE				
	17.50/5.30/17.40/3.00				
Length of weld metal cracks (mm)	1.03				
	WELD CENTERLINE				
	4.20/1.60/1.80/4.20/3.80/2.00				
Total # of cracks	Total crack length mm	Total # of HAZ cracks	Total HAZ crack length mm	Total # of weld metal cracks	Total weld metal crack length mm
22	117.73	16	99.10	7	18.63

**Table B39:** Crack measurement results of specimen TIG-AC-10-3

Line energy kJ/cm	Welding current A	Arc voltage V	Welding speed mm/min	Shielding gas & composition	Shielding gas flow rate lt/min
9.1	140 ~	4.5	35	99.9 % Argon	8.0
Former radius mm	Specimen thickness mm	Nominal Augmented strain %	Real Augmented strain %		
250	9.4	2.0	1.88		
Length of all cracks (mm)	14.50/5.50/3.00/8.00/4.00/2.00/4.00/19.80/0.70/3.80/1.10/5.30/5.20/2.00				
	WELD CENTERLINE				
	16.10/5.70/8.90/5.50/4.60/3.70/1.80/10.20/3.20/0.70/3.40/1.90/0.70/2.40				
Length of HAZ cracks (mm)	14.50/5.50/3.00/8.00/4.00/2.00/4.00/19.80/0.70/3.80/1.10/5.30/5.20/				
	WELD CENTERLINE				
	16.10/5.70/8.90/5.50/4.60/3.70/1.80/10.20/3.20/0.70/3.40/1.90/0.70				
Length of weld metal cracks (mm)	2.00				
	WELD CENTERLINE				
	2.40				
Total # of cracks	Total crack length mm	Total # of HAZ cracks	Total HAZ crack length mm	Total # of weld metal cracks	Total weld metal crack length mm
28	147.70	26	143.30	2	4.40

**Table B40:** Crack measurement results of specimen TIG-AC-10-4

Line energy kJ/cm	Welding current A	Arc voltage V	Welding speed mm/min	Shielding gas & composition	Shielding gas flow rate lt/min
9.1	140 ~	4.5	35	99.9 % Argon	8.0
Former radius mm	Specimen thickness mm	Nominal Augmented strain %	Real Augmented strain %		
125	9.3	4.0	3.72		
Length of all cracks (mm)	4.55/2.27/0.70/0.29/0.29/4.96/3.31/1.45/3.31/2.89/2.89/1.86				
	WELD CENTERLINE				
	4.13/4.75/1.86/0.83/0.62/2.89/0.50/3.40/13.30/9.00/5.00				
Length of HAZ cracks (mm)	4.13/2.27/0.70/0.29/0.29/3.10/3.31/1.45/2.89/3.31				
	WELD CENTERLINE				
	1.65/2.89/0.83/0.62/3.40/13.30/9.00/5.00				
Length of weld metal cracks (mm)	0.41/1.86/2.89/1.86				
	WELD CENTERLINE				
	2.48/1.86/1.86/2.89/0.50				
Total # of cracks	Total crack length mm	Total # of HAZ cracks	Total HAZ crack length mm	Total # of weld metal cracks	Total weld metal crack length mm
23	75.04	18	58.43	9	16.61

**Table B41:** Crack measurement results of specimen TIG-DC-1-1

Line energy kJ/cm	Welding current A	Arc voltage V	Welding speed mm/min	Shielding gas & composition	Shielding gas flow rate lt/min
1.8	180 ±	13.0	400	75%He25%Ar	15.0
Former radius mm	Specimen thickness mm	Nominal Augmented strain %	Real Augmented strain %		
1000	9.3	0.5	0.47		
Length of all cracks (mm)	-				
	WELD CENTERLINE				
	-				
Length of HAZ cracks (mm)	-				
	WELD CENTERLINE				
	-				
Length of weld metal cracks (mm)	-				
	WELD CENTERLINE				
	-				
Total # of cracks	Total crack length mm	Total # of HAZ cracks	Total HAZ crack length mm	Total # of weld metal cracks	Total weld metal crack length mm
-	-	-	-	-	-

**Table B42:** Crack measurement results of specimen TIG-DC-1-2

Line energy kJ/cm	Welding current A	Arc voltage V	Welding speed mm/min	Shielding gas & composition	Shielding gas flow rate lt/min
1.8	180 ±	13.0	400	75%He25%Ar	15.0
Former radius mm	Specimen thickness mm	Nominal Augmented strain %	Real Augmented strain %		
500	9.3	1.0	0.93		
Length of all cracks (mm)	-				
	WELD CENTERLINE				
	-				
Length of HAZ cracks (mm)	-				
	WELD CENTERLINE				
	-				
Length of weld metal cracks (mm)	-				
	WELD CENTERLINE				
	-				
Total # of cracks	Total crack length mm	Total # of HAZ cracks	Total HAZ crack length mm	Total # of weld metal cracks	Total weld metal crack length mm
-	-	-	-	-	-

**Table B43:** Crack measurement results of specimen TIG-DC-1-3

Line energy kJ/cm	Welding current A	Arc voltage V	Welding speed mm/min	Shielding gas & composition	Shielding gas flow rate lt/min
1.8	180 ±	13.0	400	75%He25%Ar	15.0
Former radius mm	Specimen thickness mm	Nominal Augmented strain %	Real Augmented strain %		
250	9.5	2.0	1.90		
Length of all cracks (mm)	0.70/0.17/1.12/1.49				
	WELD CENTERLINE				
	2.15/0.66				
Length of HAZ cracks (mm)	0.21				
	WELD CENTERLINE				
	-				
Length of weld metal cracks (mm)	0.50/0.17/1.12/1.49				
	WELD CENTERLINE				
	2.15/0.66				
Total # of cracks	Total crack length mm	Total # of HAZ cracks	Total HAZ crack length mm	Total # of weld metal cracks	Total weld metal crack length mm
6	6.28	1	0.21	6	6.07

**Table B44:** Crack measurement results of specimen TIG-DC-1-4

Line energy kJ/cm	Welding current A	Arc voltage V	Welding speed mm/min	Shielding gas & composition	Shielding gas flow rate lt/min
1.8	180 ±	13.0	400	75%He25%Ar	15.0
Former radius mm	Specimen thickness mm	Nominal Augmented strain %	Real Augmented strain %		
125	9.2	4.0	3.68		
Length of all cracks (mm)	0.25/1.36/0.25/0.29/0.21/1.03/4.30/0.25/0.62/0.54/0.37				
	WELD CENTERLINE				
	1.65/2.07/0.45/0.37/0.74/1.86/0.33/0.66/1.24/0.54				
Length of HAZ cracks (mm)	0.25/0.33/0.29/0.21				
	WELD CENTERLINE				
	0.08/0.12/0.25/0.33/0.33				
Length of weld metal cracks (mm)	0.62/0.25/0.21/0.83/0.29/4.01/0.25/0.62/0.54/0.37				
	WELD CENTERLINE				
	1.65/2.07/0.45/0.37/0.74/1.78/0.21/0.41/0.91/0.21				
Total # of cracks	Total crack length mm	Total # of HAZ cracks	Total HAZ crack length mm	Total # of weld metal cracks	Total weld metal crack length mm
21	18.97	9	2.19	20	16.78

**Table B45:** Crack measurement results of specimen TIG-DC-2-1

Line energy kJ/cm	Welding current A	Arc voltage V	Welding speed mm/min	Shielding gas & composition	Shielding gas flow rate lt/min
1.9	180 ±	13.0	380	75%He25%Ar	15.0
Former radius mm	Specimen thickness mm	Nominal Augmented strain %	Real Augmented strain %		
1000	9.4	0.5	0.47		
Length of all cracks (mm)	-				
	WELD CENTERLINE				
	-				
Length of HAZ cracks (mm)	-				
	WELD CENTERLINE				
	-				
Length of weld metal cracks (mm)	-				
	WELD CENTERLINE				
	-				
Total # of cracks	Total crack length mm	Total # of HAZ cracks	Total HAZ crack length mm	Total # of weld metal cracks	Total weld metal crack length mm
-	-	-	-	-	-

**Table B46:** Crack measurement results of specimen TIG-DC-2-2

Line energy kJ/cm	Welding current A	Arc voltage V	Welding speed mm/min	Shielding gas & composition	Shielding gas flow rate lt/min
1.9	180 ±	13.0	380	75%He25%Ar	15.0
Former radius mm	Specimen thickness mm	Nominal Augmented strain %	Real Augmented strain %		
500	9.3	1.0	0.93		
Length of all cracks (mm)	-				
	WELD CENTERLINE				
	-				
Length of HAZ cracks (mm)	-				
	WELD CENTERLINE				
	-				
Length of weld metal cracks (mm)	-				
	WELD CENTERLINE				
	-				
Total # of cracks	Total crack length mm	Total # of HAZ cracks	Total HAZ crack length mm	Total # of weld metal cracks	Total weld metal crack length mm
-	-	-	-	-	-

**Table B47:** Crack measurement results of specimen TIG-DC-2-3

Line energy kJ/cm	Welding current A	Arc voltage V	Welding speed mm/min	Shielding gas & composition	Shielding gas flow rate lt/min
1.9	180 ±	13.0	380	75%He25%Ar	15.0
Former radius mm	Specimen thickness mm	Nominal Augmented strain %	Real Augmented strain %		
250	9.2	2.0	1.84		
Length of all cracks (mm)	0.54/0.62/2.15				
	WELD CENTERLINE				
	0.41/2.48/0.41/1.03/0.45/1.40/0.66				
Length of HAZ cracks (mm)	0.12				
	WELD CENTERLINE				
	0.12				
Length of weld metal cracks (mm)	0.41/0.62/2.15				
	WELD CENTERLINE				
	0.41/2.48/0.41/1.03/0.45/1.40/0.54				
Total # of cracks	Total crack length mm	Total # of HAZ cracks	Total HAZ crack length mm	Total # of weld metal cracks	Total weld metal crack length mm
10	10.17	2	0.25	10	9.92



**Table B48:** Crack measurement results of specimen TIG-DC-2-4

Line energy kJ/cm	Welding current A	Arc voltage V	Welding speed mm/min	Shielding gas & composition	Shielding gas flow rate lt/min
1.9	180 ±	13.0	380	75%He25%Ar	15.0
Former radius mm	Specimen thickness mm	Nominal Augmented strain %	Real Augmented strain %		
125	9.5	4.0	3.80		
Length of all cracks (mm)	0.62/1.40/0.54/0.95/4.13/1.03/0.74/0.21/0.54/0.62				
	WELD CENTERLINE				
	0.29/1.45/3.10/0.95/0.45/0.74/1.16/0.41/0.25/0.29/0.41				
Length of HAZ cracks (mm)	0.41/0.41/0.33/0.21				
	WELD CENTERLINE				
	0.21/0.12/0.21/0.29/0.41/0.25/0.29/0.41				
Length of weld metal cracks (mm)	0.21/0.99/0.21/0.74/4.13/1.03/0.74/0.21/0.54/0.62				
	WELD CENTERLINE				
	0.29/1.45/3.10/0.74/0.33/0.54/0.87				
Total # of cracks	Total crack length mm	Total # of HAZ cracks	Total HAZ crack length mm	Total # of weld metal cracks	Total weld metal crack length mm
21	20.29	12	3.55	17	16.74

**Table B49:** Crack measurement results of specimen TIG-DC-3-1

Line energy kJ/cm	Welding current A	Arc voltage V	Welding speed mm/min	Shielding gas & composition	Shielding gas flow rate lt/min
2.0	180 ±	13.0	360	75%He25%Ar	15.0
Former radius mm	Specimen thickness mm	Nominal Augmented strain %	Real Augmented strain %		
1000	9.4	0.5	0.47		
Length of all cracks (mm)	-				
	WELD CENTERLINE				
	-				
Length of HAZ cracks (mm)	-				
	WELD CENTERLINE				
	-				
Length of weld metal cracks (mm)	-				
	WELD CENTERLINE				
	-				
Total # of cracks	Total crack length mm	Total # of HAZ cracks	Total HAZ crack length mm	Total # of weld metal cracks	Total weld metal crack length mm
-	-	-	-	-	-

**Table B50:** Crack measurement results of specimen TIG-DC-3-2

Line energy kJ/cm	Welding current A	Arc voltage V	Welding speed mm/min	Shielding gas & composition	Shielding gas flow rate lt/min
2.0	180 ±	13.0	360	75%He25%Ar	15.0
Former radius mm	Specimen thickness mm	Nominal Augmented strain %	Real Augmented strain %		
500	9.4	1.0	0.94		
Length of all cracks (mm)	-				
	WELD CENTERLINE				
	-				
Length of HAZ cracks (mm)	-				
	WELD CENTERLINE				
	-				
Length of weld metal cracks (mm)	-				
	WELD CENTERLINE				
	-				
Total # of cracks	Total crack length mm	Total # of HAZ cracks	Total HAZ crack length mm	Total # of weld metal cracks	Total weld metal crack length mm
-	-	-	-	-	-

**Table B51:** Crack measurement results of specimen TIG-DC-3-3

Line energy kJ/cm	Welding current A	Arc voltage V	Welding speed mm/min	Shielding gas & composition	Shielding gas flow rate lt/min
2.0	180 ±	13.0	360	75%He25%Ar	15.0
Former radius mm	Specimen thickness mm	Nominal Augmented strain %	Real Augmented strain %		
250	9.5	2.0	1.90		
Length of all cracks (mm)	0.70/2.73				
	WELD CENTERLINE				
	1.16/0.21/1.98/0.29				
Length of HAZ cracks (mm)	0.08				
	WELD CENTERLINE				
	-				
Length of weld metal cracks (mm)	0.62/2.73				
	WELD CENTERLINE				
	1.16/0.21/1.98/0.29				
Total # of cracks	Total crack length mm	Total # of HAZ cracks	Total HAZ crack length mm	Total # of weld metal cracks	Total weld metal crack length mm
6	7.07	1	0.08	6	6.98

**Table B52:** Crack measurement results of specimen TIG-DC-3-4

Line energy kJ/cm	Welding current A	Arc voltage V	Welding speed mm/min	Shielding gas & composition	Shielding gas flow rate lt/min
2.0	180 ±	13.0	360	75%He25%Ar	15.0
Former radius mm	Specimen thickness mm	Nominal Augmented strain %	Real Augmented strain %		
125	9.6	4.0	3.84		
Length of all cracks (mm)	0.29/0.70/0.21/0.45/3.39				
	WELD CENTERLINE				
	1.20/0.58/1.65/0.29/1.45/0.66/1.03/0.83/0.54				
Length of HAZ cracks (mm)	0.29/0.41/0.21/0.12				
	WELD CENTERLINE				
	0.25/0.41/0.50/0.54				
Length of weld metal cracks (mm)	0.29/0.33/3.39				
	WELD CENTERLINE				
	1.20/0.58/1.65/0.29/1.45/0.41/0.62/0.33				
Total # of cracks	Total crack length mm	Total # of HAZ cracks	Total HAZ crack length mm	Total # of weld metal cracks	Total weld metal crack length mm
14	13.26	8	2.73	11	10.54

**Table B53:** Crack measurement results of specimen TIG-DC-4-1

Line energy kJ/cm	Welding current A	Arc voltage V	Welding speed mm/min	Shielding gas & composition	Shielding gas flow rate lt/min
2.1	180 ±	13.0	340	75%He25%Ar	15.0
Former radius mm	Specimen thickness mm	Nominal Augmented strain %	Real Augmented strain %		
1000	9.4	0.5	0.47		
Length of all cracks (mm)	-				
	WELD CENTERLINE				
	-				
Length of HAZ cracks (mm)	-				
	WELD CENTERLINE				
	-				
Length of weld metal cracks (mm)	-				
	WELD CENTERLINE				
	-				
Total # of cracks	Total crack length mm	Total # of HAZ cracks	Total HAZ crack length mm	Total # of weld metal cracks	Total weld metal crack length mm
-	-	-	-	-	-

**Table B54:** Crack measurement results of specimen TIG-DC-4-2

Line energy kJ/cm	Welding current A	Arc voltage V	Welding speed mm/min	Shielding gas & composition	Shielding gas flow rate lt/min
2.1	180 ±	13.0	340	75%He25%Ar	15.0
Former radius mm	Specimen thickness mm	Nominal Augmented strain %	Real Augmented strain %		
500	9.1	1.0	0.91		
Length of all cracks (mm)	-				
	WELD CENTERLINE				
	-				
Length of HAZ cracks (mm)	-				
	WELD CENTERLINE				
	-				
Length of weld metal cracks (mm)	-				
	WELD CENTERLINE				
	-				
Total # of cracks	Total crack length mm	Total # of HAZ cracks	Total HAZ crack length mm	Total # of weld metal cracks	Total weld metal crack length mm
-	-	-	-	-	-

**Table B55:** Crack measurement results of specimen TIG-DC-4-3

Line energy kJ/cm	Welding current A	Arc voltage V	Welding speed mm/min	Shielding gas & composition	Shielding gas flow rate lt/min
2.1	180 ±	13.0	340	75%He25%Ar	15.0
Former radius mm	Specimen thickness mm	Nominal Augmented strain %	Real Augmented strain %		
250	9.6	2.0	1.92		
Length of all cracks (mm)	0.41/0.50/2.40				
	WELD CENTERLINE				
	1.12/1.78/0.41/0.62/0.58				
Length of HAZ cracks (mm)	-				
	WELD CENTERLINE				
	0.08				
Length of weld metal cracks (mm)	0.41/0.50/2.40				
	WELD CENTERLINE				
	1.12/1.78/0.41/0.62/0.50				
Total # of cracks	Total crack length mm	Total # of HAZ cracks	Total HAZ crack length mm	Total # of weld metal cracks	Total weld metal crack length mm
8	7.81	1	0.08	8	7.73

**Table B56:** Crack measurement results of specimen TIG-DC-4-4

Line energy kJ/cm	Welding current A	Arc voltage V	Welding speed mm/min	Shielding gas & composition	Shielding gas flow rate lt/min
2.1	180 ±	13.0	340	75%He25%Ar	15.0
Former radius mm	Specimen thickness mm	Nominal Augmented strain %	Real Augmented strain %		
125	9.6	4.0	3.84		
Length of all cracks (mm)	0.25/0.50/1.12/0.62/1.24/0.91/0.50/0.54/2.81/1.49/0.29/0.54				
	WELD CENTERLINE				
	0.45/0.50/0.79/1.74/0.99/1.36/1.16/0.95/2.15/0.70/0.50				
Length of HAZ cracks (mm)	0.25/0.50/0.58/0.37/0.21				
	WELD CENTERLINE				
	0.33/0.50/0.50/0.50				
Length of weld metal cracks (mm)	0.54/0.25/1.03/0.91/0.50/0.54/2.81/1.49/0.29/0.54				
	WELD CENTERLINE				
	0.45/0.50/0.79/1.74/0.99/1.36/1.16/0.62/1.65/0.21				
Total # of cracks	Total crack length mm	Total # of HAZ cracks	Total HAZ crack length mm	Total # of weld metal cracks	Total weld metal crack length mm
23	22.07	9	3.72	20	18.35

**Table B57:** Crack measurement results of specimen TIG-DC-5-1

Line energy kJ/cm	Welding current A	Arc voltage V	Welding speed mm/min	Shielding gas & composition	Shielding gas flow rate lt/min
2.2	180 ±	13.0	320	75%He25%Ar	15.0
Former radius mm	Specimen thickness mm	Nominal Augmented strain %	Real Augmented strain %		
1000	9.3	0.5	0.47		
Length of all cracks (mm)	-				
	WELD CENTERLINE				
	-				
Length of HAZ cracks (mm)	-				
	WELD CENTERLINE				
	-				
Length of weld metal cracks (mm)	-				
	WELD CENTERLINE				
	-				
Total # of cracks	Total crack length mm	Total # of HAZ cracks	Total HAZ crack length mm	Total # of weld metal cracks	Total weld metal crack length mm
-	-	-	-	-	-

**Table B58:** Crack measurement results of specimen TIG-DC-5-2

Line energy kJ/cm	Welding current A	Arc voltage V	Welding speed mm/min	Shielding gas & composition	Shielding gas flow rate lt/min
2.2	180 ±	13.0	320	75%He25%Ar	15.0
Former radius mm	Specimen thickness mm	Nominal Augmented strain %	Real Augmented strain %		
500	9.3	1.0	0.93		
Length of all cracks (mm)	-				
	WELD CENTERLINE				
	-				
Length of HAZ cracks (mm)	-				
	WELD CENTERLINE				
	-				
Length of weld metal cracks (mm)	-				
	WELD CENTERLINE				
	-				
Total # of cracks	Total crack length mm	Total # of HAZ cracks	Total HAZ crack length mm	Total # of weld metal cracks	Total weld metal crack length mm
-	-	-	-	-	-

**Table B59:** Crack measurement results of specimen TIG-DC-5-3

Line energy kJ/cm	Welding current A	Arc voltage V	Welding speed mm/min	Shielding gas & composition	Shielding gas flow rate lt/min
2.2	180 ±	13.0	320	75%He25%Ar	15.0
Former radius mm	Specimen thickness mm	Nominal Augmented strain %	Real Augmented strain %		
250	9.5	2.0	1.90		
Length of all cracks (mm)	0.41/0.41/0.74/1.57/0.12				
	WELD CENTERLINE				
	0.50/2.19/0.33/0.33/0.21/0.54/0.25				
Length of HAZ cracks (mm)	0.08				
	WELD CENTERLINE				
	0.21/0.21/0.33/0.25				
Length of weld metal cracks (mm)	0.33/0.41/0.74/1.57/0.12				
	WELD CENTERLINE				
	0.50/2.19/0.33/0.12/0.21				
Total # of cracks	Total crack length mm	Total # of HAZ cracks	Total HAZ crack length mm	Total # of weld metal cracks	Total weld metal crack length mm
12	7.60	5	1.07	10	6.53

**Table B60:** Crack measurement results of specimen TIG-DC-5-4

Line energy kJ/cm	Welding current A	Arc voltage V	Welding speed mm/min	Shielding gas & composition	Shielding gas flow rate lt/min
2.2	180 ±	13.0	320	75%He25%Ar	15.0
Former radius mm	Specimen thickness mm	Nominal Augmented strain %	Real Augmented strain %		
125	9.2	4.0	3.68		
Length of all cracks (mm)	0.25/0.12/0.21/0.50/0.62/1.45/0.29/2.40/0.62				
	WELD CENTERLINE				
	0.21/0.62/0.58/0.70/1.32/1.20/1.07/1.12/1.98/0.99				
Length of HAZ cracks (mm)	0.25/0.12/0.21/0.25/0.21				
	WELD CENTERLINE				
	0.33/0.50				
Length of weld metal cracks (mm)	0.25/0.41/1.45/0.29/2.40/0.62				
	WELD CENTERLINE				
	0.21/0.62/0.58/0.70/1.32/1.20/1.12/1.07/1.65/0.50				
Total # of cracks	Total crack length mm	Total # of HAZ cracks	Total HAZ crack length mm	Total # of weld metal cracks	Total weld metal crack length mm
19	16.24	7	1.86	16	14.38

**Table B61:** Crack measurement results of specimen TIG-DC-6-1

Line energy kJ/cm	Welding current A	Arc voltage V	Welding speed mm/min	Shielding gas & composition	Shielding gas flow rate lt/min
2.3	180 ±	13.0	300	75%He25%Ar	15.0
Former radius mm	Specimen thickness mm	Nominal Augmented strain %	Real Augmented strain %		
1000	9.4	0.5	0.47		
Length of all cracks (mm)	-				
	WELD CENTERLINE				
	-				
Length of HAZ cracks (mm)	-				
	WELD CENTERLINE				
	-				
Length of weld metal cracks (mm)	-				
	WELD CENTERLINE				
	-				
Total # of cracks	Total crack length mm	Total # of HAZ cracks	Total HAZ crack length mm	Total # of weld metal cracks	Total weld metal crack length mm
-	-	-	-	-	-

**Table B62:** Crack measurement results of specimen TIG-DC-6-2

Line energy kJ/cm	Welding current A	Arc voltage V	Welding speed mm/min	Shielding gas & composition	Shielding gas flow rate lt/min
2.3	180 ±	13.0	300	75%He25%Ar	15.0
Former radius mm	Specimen thickness mm	Nominal Augmented strain %	Real Augmented strain %		
500	9.2	1.0	0.92		
Length of all cracks (mm)	-				
	WELD CENTERLINE				
	0.91				
Length of HAZ cracks (mm)	-				
	WELD CENTERLINE				
	-				
Length of weld metal cracks (mm)	-				
	WELD CENTERLINE				
	0.91				
Total # of cracks	Total crack length mm	Total # of HAZ cracks	Total HAZ crack length mm	Total # of weld metal cracks	Total weld metal crack length mm
1	0.91	-	-	1	0.91

**Table B63:** Crack measurement results of specimen TIG-DC-6-3

Line energy kJ/cm	Welding current A	Arc voltage V	Welding speed mm/min	Shielding gas & composition	Shielding gas flow rate lt/min
2.3	180 ±	13.0	300	75%He25%Ar	15.0
Former radius mm	Specimen thickness mm	Nominal Augmented strain %	Real Augmented strain %		
250	9.2	2.0	1.84		
Length of all cracks (mm)	0.62/2.27/0.50/1.36/0.33				
	WELD CENTERLINE				
	0.62/0.62/1.49/0.87/1.90/0.62				
Length of HAZ cracks (mm)	-				
	WELD CENTERLINE				
	-				
Length of weld metal cracks (mm)	0.62/2.27/0.50/1.36/0.33				
	WELD CENTERLINE				
	0.62/0.62/1.49/0.87/1.90/0.62				
Total # of cracks	Total crack length mm	Total # of HAZ cracks	Total HAZ crack length mm	Total # of weld metal cracks	Total weld metal crack length mm
11	11.20	-	-	11	11.20



**Table B64:** Crack measurement results of specimen TIG-DC-6-4

Line energy kJ/cm	Welding current A	Arc voltage V	Welding speed mm/min	Shielding gas & composition	Shielding gas flow rate lt/min
2.3	180 ±	13.0	300	75%He25%Ar	15.0
Former radius mm	Specimen thickness mm	Nominal Augmented strain %	Real Augmented strain %		
125	9.6	4.0	3.84		
Length of all cracks (mm)	0.21/0.21/0.21/0.29/0.99/1.12/3.72/0.41/0.62/0.62				
	WELD CENTERLINE				
	0.91/0.41/0.17/0.25/3.31/0.50/1.24/0.54/0.91/0.58/0.29/1.24/0.29				
Length of HAZ cracks (mm)	0.21/0.21/0.21/0.29/0.45/0.21				
	WELD CENTERLINE				
	0.25/0.12/0.29/0.37/0.54/0.29				
Length of weld metal cracks (mm)	0.54/0.91/3.72/0.41/0.62/0.62				
	WELD CENTERLINE				
	0.91/0.41/0.17/0.25/3.31/0.50/0.99/0.41/0.62/0.21/0.29/0.70				
Total # of cracks	Total crack length mm	Total # of HAZ cracks	Total HAZ crack length mm	Total # of weld metal cracks	Total weld metal crack length mm
23	15.58	12	3.43	18	15.58

**Table B65:** Crack measurement results of specimen TIG-DC-7-1

Line energy kJ/cm	Welding current A	Arc voltage V	Welding speed mm/min	Shielding gas & composition	Shielding gas flow rate lt/min
2.5	180 ±	13.0	280	75%He25%Ar	15.0
Former radius mm	Specimen thickness mm	Nominal Augmented strain %	Real Augmented strain %		
1000	9.4	0.5	0.47		
Length of all cracks (mm)	-				
	WELD CENTERLINE				
	-				
Length of HAZ cracks (mm)	-				
	WELD CENTERLINE				
	-				
Length of weld metal cracks (mm)	-				
	WELD CENTERLINE				
	-				
Total # of cracks	Total crack length mm	Total # of HAZ cracks	Total HAZ crack length mm	Total # of weld metal cracks	Total weld metal crack length mm
-	-	-	-	-	-

**Table B66:** Crack measurement results of specimen TIG-DC-7-2

Line energy kJ/cm	Welding current A	Arc voltage V	Welding speed mm/min	Shielding gas & composition	Shielding gas flow rate lt/min
2.5	180 ±	13.0	280	75%He25%Ar	15.0
Former radius mm	Specimen thickness mm	Nominal Augmented strain %	Real Augmented strain %		
500	9.6	1.0	0.96		
Length of all cracks (mm)	-				
	WELD CENTERLINE				
	-				
Length of HAZ cracks (mm)	-				
	WELD CENTERLINE				
	-				
Length of weld metal cracks (mm)	-				
	WELD CENTERLINE				
	-				
Total # of cracks	Total crack length mm	Total # of HAZ cracks	Total HAZ crack length mm	Total # of weld metal cracks	Total weld metal crack length mm
-	-	-	-	-	-

**Table B67:** Crack measurement results of specimen TIG-DC-7-3

Line energy kJ/cm	Welding current A	Arc voltage V	Welding speed mm/min	Shielding gas & composition	Shielding gas flow rate lt/min
2.5	180 ±	13.0	280	75%He25%Ar	15.0
Former radius mm	Specimen thickness mm	Nominal Augmented strain %	Real Augmented strain %		
250	9.5	2.0	1.90		
Length of all cracks (mm)	0.74/0.54/2.11/0.29				
	WELD CENTERLINE				
	0.25/0.29/1.86/0.83/1.03				
Length of HAZ cracks (mm)	0.25/0.08				
	WELD CENTERLINE				
	0.29/0.41				
Length of weld metal cracks (mm)	0.50/0.45/2.11/0.29				
	WELD CENTERLINE				
	0.25/0.29/1.86/0.54/0.62				
Total # of cracks	Total crack length mm	Total # of HAZ cracks	Total HAZ crack length mm	Total # of weld metal cracks	Total weld metal crack length mm
9	7.93	4	1.03	9	6.90

**Table B68:** Crack measurement results of specimen TIG-DC-7-4

Line energy kJ/cm	Welding current A	Arc voltage V	Welding speed mm/min	Shielding gas & composition	Shielding gas flow rate lt/min
2.5	180 ±	13.0	280	75%He25%Ar	15.0
Former radius mm	Specimen thickness mm	Nominal Augmented strain %	Real Augmented strain %		
125	9.2	4.0	3.68		
Length of all cracks (mm)	0.25/0.41/0.21/0.37/0.33/0.45/1.20/2.69/0.41/0.25/0.74				
	WELD CENTERLINE				
	0.54/0.21/1.07/0.54/2.52/0.70/2.60/1.28/0.83				
Length of HAZ cracks (mm)	0.25/0.41/0.21/0.37/0.25/0.29				
	WELD CENTERLINE				
	0.33/0.45/0.83				
Length of weld metal cracks (mm)	0.33/0.21/0.91/2.69/0.41/0.25/0.74				
	WELD CENTERLINE				
	0.54/0.21/1.07/0.54/2.52/0.70/2.27/0.83				
Total # of cracks	Total crack length mm	Total # of HAZ cracks	Total HAZ crack length mm	Total # of weld metal cracks	Total weld metal crack length mm
20	17.60	9	3.39	15	14.21

**Table B69:** Crack measurement results of specimen TIG-DC-8-1

Line energy kJ/cm	Welding current A	Arc voltage V	Welding speed mm/min	Shielding gas & composition	Shielding gas flow rate lt/min
2.7	180 ±	13.0	260	75%He25%Ar	15.0
Former radius mm	Specimen thickness mm	Nominal Augmented strain %	Real Augmented strain %		
1000	9.3	0.5	0.47		
Length of all cracks (mm)	-				
	WELD CENTERLINE				
	-				
Length of HAZ cracks (mm)	-				
	WELD CENTERLINE				
	-				
Length of weld metal cracks (mm)	-				
	WELD CENTERLINE				
	-				
Total # of cracks	Total crack length mm	Total # of HAZ cracks	Total HAZ crack length mm	Total # of weld metal cracks	Total weld metal crack length mm
-	-	-	-	-	-

**Table B70:** Crack measurement results of specimen TIG-DC-8-2

Line energy kJ/cm	Welding current A	Arc voltage V	Welding speed mm/min	Shielding gas & composition	Shielding gas flow rate lt/min
2.7	180 ±	13.0	260	75%He25%Ar	15.0
Former radius mm	Specimen thickness mm	Nominal Augmented strain %	Real Augmented strain %		
500	9.6	1.0	0.96		
Length of all cracks (mm)	0.83				
	WELD CENTERLINE				
	1.16				
Length of HAZ cracks (mm)	-				
	WELD CENTERLINE				
	-				
Length of weld metal cracks (mm)	0.83				
	WELD CENTERLINE				
	1.16				
Total # of cracks	Total crack length mm	Total # of HAZ cracks	Total HAZ crack length mm	Total # of weld metal cracks	Total weld metal crack length mm
2	1.98	-	-	2	1.98

**Table B71:** Crack measurement results of specimen TIG-DC-8-3

Line energy kJ/cm	Welding current A	Arc voltage V	Welding speed mm/min	Shielding gas & composition	Shielding gas flow rate lt/min
2.7	180 ±	13.0	260	75%He25%Ar	15.0
Former radius mm	Specimen thickness mm	Nominal Augmented strain %	Real Augmented strain %		
250	9.5	2.0	1.90		
Length of all cracks (mm)	0.25/0.37/0.66/0.58/0.21/1.69/0.17/0.29/0.41				
	WELD CENTERLINE				
	0.33/0.50/0.62/1.74/0.74/0.21				
Length of HAZ cracks (mm)	0.25/0.37/0.33/0.17				
	WELD CENTERLINE				
	0.25/0.21				
Length of weld metal cracks (mm)	0.33/0.41/0.21/1.69/0.17/0.29/0.41				
	WELD CENTERLINE				
	0.33/0.50/0.62/1.74/0.50				
Total # of cracks	Total crack length mm	Total # of HAZ cracks	Total HAZ crack length mm	Total # of weld metal cracks	Total weld metal crack length mm
15	8.76	6	1.57	12	7.19

**Table B72:** Crack measurement results of specimen TIG-DC-8-4

Line energy kJ/cm	Welding current A	Arc voltage V	Welding speed mm/min	Shielding gas & composition	Shielding gas flow rate lt/min
2.7	180 ±	13.0	260	75%He25%Ar	15.0
Former radius mm	Specimen thickness mm	Nominal Augmented strain %	Real Augmented strain %		
125	9.6	4.0	3.84		
Length of all cracks (mm)	0.21/0.21/0.37/0.29/0.66/0.74/2.07/1.49/0.54				
	WELD CENTERLINE				
	0.74/1.32/2.27/1.12/1.20/1.40/0.29/0.41/0.17				
Length of HAZ cracks (mm)	0.21/0.21/0.37/0.29/0.41/0.21				
	WELD CENTERLINE				
	0.37/0.58/0.29/0.41/0.17				
Length of weld metal cracks (mm)	0.25/0.54/1.49/0.27/0.54				
	WELD CENTERLINE				
	0.74/1.32/2.27/1.12/0.83/0.83				
Total # of cracks	Total crack length mm	Total # of HAZ cracks	Total HAZ crack length mm	Total # of weld metal cracks	Total weld metal crack length mm
18	15.50	11	3.51	11	11.98

**Table B73:** Crack measurement results of specimen TIG-DC-9-1

Line energy kJ/cm	Welding current A	Arc voltage V	Welding speed mm/min	Shielding gas & composition	Shielding gas flow rate lt/min
2.9	180 ±	13.0	240	75%He25%Ar	15.0
Former radius mm	Specimen thickness mm	Nominal Augmented strain %	Real Augmented strain %		
1000	9.15	0.5	0.46		
Length of all cracks (mm)	-				
	WELD CENTERLINE				
	0.62				
Length of HAZ cracks (mm)	-				
	WELD CENTERLINE				
	-				
Length of weld metal cracks (mm)	-				
	WELD CENTERLINE				
	0.62				
Total # of cracks	Total crack length mm	Total # of HAZ cracks	Total HAZ crack length mm	Total # of weld metal cracks	Total weld metal crack length mm
1	0.62	-	-	1	0.62

**Table B74:** Crack measurement results of specimen TIG-DC-9-2

Line energy kJ/cm	Welding current A	Arc voltage V	Welding speed mm/min	Shielding gas & composition	Shielding gas flow rate lt/min
2.9	180 ±	13.0	240	75%He25%Ar	15.0
Former radius mm	Specimen thickness mm	Nominal Augmented strain %	Real Augmented strain %		
500	9.6	1.0	0.96		
Length of all cracks (mm)	-				
	WELD CENTERLINE				
	1.86				
Length of HAZ cracks (mm)	-				
	WELD CENTERLINE				
	-				
Length of weld metal cracks (mm)	-				
	WELD CENTERLINE				
	1.86				
Total # of cracks	Total crack length mm	Total # of HAZ cracks	Total HAZ crack length mm	Total # of weld metal cracks	Total weld metal crack length mm
1	1.86	-	-	1	1.86

**Table B75:** Crack measurement results of specimen TIG-DC-9-3

Line energy kJ/cm	Welding current A	Arc voltage V	Welding speed mm/min	Shielding gas & composition	Shielding gas flow rate lt/min
2.9	180 ±	13.0	240	75%He25%Ar	15.0
Former radius mm	Specimen thickness mm	Nominal Augmented strain %	Real Augmented strain %		
250	9.5	2.0	1.90		
Length of all cracks (mm)	1.07/0.58/0.37/1.49/0.50/0.41/0.41				
	WELD CENTERLINE				
	1.03/1.86/0.29/0.29/0.21/0.74/0.29				
Length of HAZ cracks (mm)	0.21				
	WELD CENTERLINE				
	0.33/0.29				
Length of weld metal cracks (mm)	0.87/0.58/0.37/1.49/0.50/0.41/0.41				
	WELD CENTERLINE				
	1.03/1.86/0.29/0.29/0.21/0.41				
Total # of cracks	Total crack length mm	Total # of HAZ cracks	Total HAZ crack length mm	Total # of weld metal cracks	Total weld metal crack length mm
14	9.55	3	0.83	13	8.72

**Table B76:** Crack measurement results of specimen TIG-DC-9-4

Line energy kJ/cm	Welding current A	Arc voltage V	Welding speed mm/min	Shielding gas & composition	Shielding gas flow rate lt/min
2.9	180 ±	13.0	240	75%He25%Ar	15.0
Former radius mm	Specimen thickness mm	Nominal Augmented strain %	Real Augmented strain %		
125	9.2	4.0	3.68		
Length of all cracks (mm)	0.37/0.99/0.29/1.24/0.21/1.16/0.29/0.83/0.74/2.89/0.83				
	WELD CENTERLINE				
	0.41/2.07/0.70/1.86/0.41/0.83/1.24/0.45/0.29/0.41				
Length of HAZ cracks (mm)	0.37/0.50/0.29/0.62/0.21/0.41				
	WELD CENTERLINE				
	0.41/0.45/0.29/0.41				
Length of weld metal cracks (mm)	0.50/0.62/0.74/0.29/0.83/0.74/2.89/0.83				
	WELD CENTERLINE				
	0.41/2.07/0.70/1.86/0.41/0.83/0.83				
Total # of cracks	Total crack length mm	Total # of HAZ cracks	Total HAZ crack length mm	Total # of weld metal cracks	Total weld metal crack length mm
21	18.51	10	3.97	15	14.55

**Table B77:** Crack measurement results of specimen TIG-DC-10-1

Line energy kJ/cm	Welding current A	Arc voltage V	Welding speed mm/min	Shielding gas & composition	Shielding gas flow rate lt/min
3.2	180 ±	13.0	220	75%He25%Ar	15.0
Former radius mm	Specimen thickness mm	Nominal Augmented strain %	Real Augmented strain %		
1000	9.2	0.5	0.46		
Length of all cracks (mm)	0.45/0.83/0.87				
	WELD CENTERLINE				
	1.24				
Length of HAZ cracks (mm)	-				
	WELD CENTERLINE				
	-				
Length of weld metal cracks (mm)	0.45/0.83/0.87				
	WELD CENTERLINE				
	1.24				
Total # of cracks	Total crack length mm	Total # of HAZ cracks	Total HAZ crack length mm	Total # of weld metal cracks	Total weld metal crack length mm
4	3.39	-	-	4	3.39

**Table B78:** Crack measurement results of specimen TIG-DC-10-2

Line energy kJ/cm	Welding current A	Arc voltage V	Welding speed mm/min	Shielding gas & composition	Shielding gas flow rate lt/min
3.2	180 ±	13.0	220	75%He25%Ar	15.0
Former radius mm	Specimen thickness mm	Nominal Augmented strain %	Real Augmented strain %		
500	9.6	1.0	0.96		
Length of all cracks (mm)	0.62/0.50				
	WELD CENTERLINE				
	1.74				
Length of HAZ cracks (mm)	0.21				
	WELD CENTERLINE				
	-				
Length of weld metal cracks (mm)	0.41/0.50				
	WELD CENTERLINE				
	1.74				
Total # of cracks	Total crack length mm	Total # of HAZ cracks	Total HAZ crack length mm	Total # of weld metal cracks	Total weld metal crack length mm
3	2.85	1	0.21	3	2.64

**Table B79:** Crack measurement results of specimen TIG-DC-10-3

Line energy kJ/cm	Welding current A	Arc voltage V	Welding speed mm/min	Shielding gas & composition	Shielding gas flow rate lt/min
3.2	180 ±	13.0	220	75%He25%Ar	15.0
Former radius mm	Specimen thickness mm	Nominal Augmented strain %	Real Augmented strain %		
250	9.6	2.0	1.92		
Length of all cracks (mm)	0.33/0.50/0.74/0.41/0.33/0.33/1.16/1.16/0.54/0.45				
	WELD CENTERLINE				
	0.37/0.41/0.99/1.16/0.41/0.29/0.25/0.33				
Length of HAZ cracks (mm)	0.33/0.50/0.21/0.41/0.33				
	WELD CENTERLINE				
	0.41/0.29/0.25/0.33				
Length of weld metal cracks (mm)	0.54/0.33/1.16/1.16/0.54/0.45				
	WELD CENTERLINE				
	0.37/0.41/0.99/1.16				
Total # of cracks	Total crack length mm	Total # of HAZ cracks	Total HAZ crack length mm	Total # of weld metal cracks	Total weld metal crack length mm
18	10.17	9	3.06	10	7.11



**Table B80:** Crack measurement results of specimen TIG-DC-10-4

Line energy kJ/cm	Welding current A	Arc voltage V	Welding speed mm/min	Shielding gas & composition	Shielding gas flow rate lt/min
3.2	180 ±	13.0	220	75%He25%Ar	15.0
Former radius mm	Specimen thickness mm	Nominal Augmented strain %	Real Augmented strain %		
125	9.6	4.0	3.84		
Length of all cracks (mm)	0.12/0.33/0.45/1.45/1.74/2.31/0.83				
	WELD CENTERLINE				
	1.03/0.79/2.48/1.24/0.33/1.45/0.41/0.41				
Length of HAZ cracks (mm)	0.12/0.33/0.45/0.62/0.41				
	WELD CENTERLINE				
	0.54/0.33/0.74/0.41/0.41				
Length of weld metal cracks (mm)	0.83/1.32/2.31/0.83				
	WELD CENTERLINE				
	1.03/0.79/2.48/0.70/0.70				
Total # of cracks	Total crack length mm	Total # of HAZ cracks	Total HAZ crack length mm	Total # of weld metal cracks	Total weld metal crack length mm
15	15.37	10	4.38	9	10.99

**Table B81:** Crack measurement results of specimen TIG-DC-11-1

Line energy kJ/cm	Welding current A	Arc voltage V	Welding speed mm/min	Shielding gas & composition	Shielding gas flow rate lt/min
3.5	180 ±	13.0	200	75%He25%Ar	15.0
Former radius mm	Specimen thickness mm	Nominal Augmented strain %	Real Augmented strain %		
1000	9.3	0.5	0.47		
Length of all cracks (mm)	-				
	WELD CENTERLINE				
	0.83				
Length of HAZ cracks (mm)	-				
	WELD CENTERLINE				
	-				
Length of weld metal cracks (mm)	-				
	WELD CENTERLINE				
	0.83				
Total # of cracks	Total crack length mm	Total # of HAZ cracks	Total HAZ crack length mm	Total # of weld metal cracks	Total weld metal crack length mm
1	0.83	-	-	1	0.83

**Table B82:** Crack measurement results of specimen TIG-DC-11-2

Line energy kJ/cm	Welding current A	Arc voltage V	Welding speed mm/min	Shielding gas & composition	Shielding gas flow rate lt/min
3.5	180 ±	13.0	200	75%He25%Ar	15.0
Former radius mm	Specimen thickness mm	Nominal Augmented strain %	Real Augmented strain %		
500	9.6	1.0	0.96		
Length of all cracks (mm)	2.07/1.12				
	WELD CENTERLINE				
	0.83/0.70				
Length of HAZ cracks (mm)	0.62				
	WELD CENTERLINE				
	0.29				
Length of weld metal cracks (mm)	1.45/1.12				
	WELD CENTERLINE				
	0.83/0.41				
Total # of cracks	Total crack length mm	Total # of HAZ cracks	Total HAZ crack length mm	Total # of weld metal cracks	Total weld metal crack length mm
4	4.71	2	0.91	4	3.80

**Table B83:** Crack measurement results of specimen TIG-DC-11-3

Line energy kJ/cm	Welding current A	Arc voltage V	Welding speed mm/min	Shielding gas & composition	Shielding gas flow rate lt/min
3.5	180 ±	13.0	200	75%He25%Ar	15.0
Former radius mm	Specimen thickness mm	Nominal Augmented strain %	Real Augmented strain %		
250	9.2	2.0	1.84		
Length of all cracks (mm)	1.12/0.83/1.57/0.50				
	WELD CENTERLINE				
	0.33/1.24/2.48/0.45/0.21/0.17/0.25/0.21/0.21				
Length of HAZ cracks (mm)	0.83				
	WELD CENTERLINE				
	0.21/0.17/0.21/0.21				
Length of weld metal cracks (mm)	0.29/0.83/1.57/0.50				
	WELD CENTERLINE				
	0.33/1.24/2.48/0.45/0.25				
Total # of cracks	Total crack length mm	Total # of HAZ cracks	Total HAZ crack length mm	Total # of weld metal cracks	Total weld metal crack length mm
13	9.55	5	1.61	9	7.93

**Table B84:** Crack measurement results of specimen TIG-DC-11-4

Line energy kJ/cm	Welding current A	Arc voltage V	Welding speed mm/min	Shielding gas & composition	Shielding gas flow rate lt/min
3.5	180 ±	13.0	200	75%He25%Ar	15.0
Former radius mm	Specimen thickness mm	Nominal Augmented strain %	Real Augmented strain %		
125	9.6	4.0	3.84		
Length of all cracks (mm)	0.25/0.21/0.25/0.62/1.57/0.74/0.87/1.61/0.25/0.62/0.41				
	WELD CENTERLINE				
	0.83/2.07/0.41/0.74/1.03/0.33/0.91/0.41/0.62/0.21				
Length of HAZ cracks (mm)	0.25/0.21/0.25/0.62/0.91/0.62				
	WELD CENTERLINE				
	0.74/0.41/0.33/0.91/0.41/0.62/0.21				
Length of weld metal cracks (mm)	0.66/0.12/0.87/1.61/0.25/0.62/0.41				
	WELD CENTERLINE				
	0.83/2.07/0.41/0.62				
Total # of cracks	Total crack length mm	Total # of HAZ cracks	Total HAZ crack length mm	Total # of weld metal cracks	Total weld metal crack length mm
21	14.96	13	6.49	11	8.47

**Table B85:** Crack measurement results of specimen TIG-DC-12-1

Line energy kJ/cm	Welding current A	Arc voltage V	Welding speed mm/min	Shielding gas & composition	Shielding gas flow rate lt/min
3.9	180 ±	13.0	180	75%He25%Ar	15.0
Former radius mm	Specimen thickness mm	Nominal Augmented strain %	Real Augmented strain %		
1000	9.6	0.5	0.48		
Length of all cracks (mm)	0.33				
	WELD CENTERLINE				
	1.07				
Length of HAZ cracks (mm)	-				
	WELD CENTERLINE				
	-				
Length of weld metal cracks (mm)	0.33				
	WELD CENTERLINE				
	1.07				
Total # of cracks	Total crack length mm	Total # of HAZ cracks	Total HAZ crack length mm	Total # of weld metal cracks	Total weld metal crack length mm
2	1.40	-	-	2	1.40

**Table B86:** Crack measurement results of specimen TIG-DC-12-2

Line energy kJ/cm	Welding current A	Arc voltage V	Welding speed mm/min	Shielding gas & composition	Shielding gas flow rate lt/min
3.9	180 ±	13.0	180	75%He25%Ar	15.0
Former radius mm	Specimen thickness mm	Nominal Augmented strain %	Real Augmented strain %		
500	9.2	1.0	0.92		
Length of all cracks (mm)	1.32/1.45/0.83				
	WELD CENTERLINE				
	0.83/1.40/0.91/1.16/0.33				
Length of HAZ cracks (mm)	0.41				
	WELD CENTERLINE				
	0.70/0.33				
Length of weld metal cracks (mm)	0.91/1.45/0.83				
	WELD CENTERLINE				
	0.83/1.40				
Total # of cracks	Total crack length mm	Total # of HAZ cracks	Total HAZ crack length mm	Total # of weld metal cracks	Total weld metal crack length mm
8	6.86	3	1.45	5	5.42

**Table B87:** Crack measurement results of specimen TIG-DC-12-3

Line energy kJ/cm	Welding current A	Arc voltage V	Welding speed mm/min	Shielding gas & composition	Shielding gas flow rate lt/min
3.9	180 ±	13.0	180	75%He25%Ar	15.0
Former radius mm	Specimen thickness mm	Nominal Augmented strain %	Real Augmented strain %		
250	9.5	2.0	1.90		
Length of all cracks (mm)	0.41/0.62/0.79/0.12/0.37/1.65				
	WELD CENTERLINE				
	0.29/1.65/1.82/0.91/0.50				
Length of HAZ cracks (mm)	0.41/0.62/0.25/0.12/0.37				
	WELD CENTERLINE				
	1.03/0.91/0.50				
Length of weld metal cracks (mm)	0.54/1.65/0.91/0.45				
	WELD CENTERLINE				
	0.29/1.65/0.79				
Total # of cracks	Total crack length mm	Total # of HAZ cracks	Total HAZ crack length mm	Total # of weld metal cracks	Total weld metal crack length mm
11	10.49	8	4.21	7	6.28

**Table B88:** Crack measurement results of specimen TIG-DC-12-4

Line energy kJ/cm	Welding current A	Arc voltage V	Welding speed mm/min	Shielding gas & composition	Shielding gas flow rate lt/min
3.9	180 ±	13.0	180	75%He25%Ar	15.0
Former radius mm	Specimen thickness mm	Nominal Augmented strain %	Real Augmented strain %		
125	9.6	4.0	3.84		
Length of all cracks (mm)	0.50/0.62/0.25/0.83/2.23/0.83/1.45/0.41				
	WELD CENTERLINE				
	0.91/0.74/0.41/0.91/2.48/1.03/0.62/0.62				
Length of HAZ cracks (mm)	0.50/0.62/0.25/0.83/0.83/0.62				
	WELD CENTERLINE				
	1.03/1.03/0.62/0.62				
Length of weld metal cracks (mm)	1.40/0.21/1.45/0.41				
	WELD CENTERLINE				
	0.91/0.74/0.41/0.91/1.45				
Total # of cracks	Total crack length mm	Total # of HAZ cracks	Total HAZ crack length mm	Total # of weld metal cracks	Total weld metal crack length mm
16	14.83	10	6.94	9	7.89

**Table B89:** Crack measurement results of specimen TIG-DC-13-1

Line energy kJ/cm	Welding current A	Arc voltage V	Welding speed mm/min	Shielding gas & composition	Shielding gas flow rate lt/min
4.1	180 ±	13.0	170	75%He25%Ar	15.0
Former radius mm	Specimen thickness mm	Nominal Augmented strain %	Real Augmented strain %		
1000	9.2	0.5	0.46		
Length of all cracks (mm)	0.70/0.83/0.58				
	WELD CENTERLINE				
	1.65				
Length of HAZ cracks (mm)	-				
	WELD CENTERLINE				
	-				
Length of weld metal cracks (mm)	0.70/0.83/0.58				
	WELD CENTERLINE				
	1.65				
Total # of cracks	Total crack length mm	Total # of HAZ cracks	Total HAZ crack length mm	Total # of weld metal cracks	Total weld metal crack length mm
4	3.76	-	-	4	3.76

**Table B90:** Crack measurement results of specimen TIG-DC-13-2

Line energy kJ/cm	Welding current A	Arc voltage V	Welding speed mm/min	Shielding gas & composition	Shielding gas flow rate lt/min
4.1	180 ±	13.0	170	75%He25%Ar	15.0
Former radius mm	Specimen thickness mm	Nominal Augmented strain %	Real Augmented strain %		
500	9.6	1.0	0.96		
Length of all cracks (mm)	0.54/0.66/0.83/2.40/0.95				
	WELD CENTERLINE				
	1.49/0.25/1.94/0.41/0.62				
Length of HAZ cracks (mm)	0.54/0.66/0.83/1.03				
	WELD CENTERLINE				
	0.95/0.41/0.62				
Length of weld metal cracks (mm)	1.36/0.95				
	WELD CENTERLINE				
	1.49/0.25/0.99				
Total # of cracks	Total crack length mm	Total # of HAZ cracks	Total HAZ crack length mm	Total # of weld metal cracks	Total weld metal crack length mm
10	10.08	7	5.04	5	5.04

**Table B91:** Crack measurement results of specimen TIG-DC-13-3

Line energy kJ/cm	Welding current A	Arc voltage V	Welding speed mm/min	Shielding gas & composition	Shielding gas flow rate lt/min
4.1	180 ±	13.0	170	75%He25%Ar	15.0
Former radius mm	Specimen thickness mm	Nominal Augmented strain %	Real Augmented strain %		
250	9.1	2.0	1.82		
Length of all cracks (mm)	0.12/0.29/0.74/0.50/2.07/1.65/0.91				
	WELD CENTERLINE				
	1.07/1.49/1.28/0.83				
Length of HAZ cracks (mm)	0.74				
	WELD CENTERLINE				
	0.66/0.83				
Length of weld metal cracks (mm)	0.12/0.29/0.50/2.07/1.65/0.91				
	WELD CENTERLINE				
	1.07/1.49/0.62				
Total # of cracks	Total crack length mm	Total # of HAZ cracks	Total HAZ crack length mm	Total # of weld metal cracks	Total weld metal crack length mm
11	10.95	3	2.23	9	8.72

**Table B92:** Crack measurement results of specimen TIG-DC-13-4

Line energy kJ/cm	Welding current A	Arc voltage V	Welding speed mm/min	Shielding gas & composition	Shielding gas flow rate lt/min
4.1	180 ±	13.0	170	75%He25%Ar	15.0
Former radius mm	Specimen thickness mm	Nominal Augmented strain %	Real Augmented strain %		
125	9.2	4.0	3.68		
Length of all cracks (mm)	0.37/0.70/0.66/1.28/2.98/1.65/0.62/1.65				
	WELD CENTERLINE				
	2.07/2.48/2.07/1.78/0.50/0.74				
Length of HAZ cracks (mm)	0.37/0.70/0.66/0.66/1.24				
	WELD CENTERLINE				
	1.24/1.16/0.50/0.74				
Length of weld metal cracks (mm)	0.62/1.74/1.65/0.62/1.65				
	WELD CENTERLINE				
	2.07/2.48/0.83/0.62				
Total # of cracks	Total crack length mm	Total # of HAZ cracks	Total HAZ crack length mm	Total # of weld metal cracks	Total weld metal crack length mm
14	19.55	9	7.27	9	12.27

**Table B93:** Crack measurement results of specimen TIG-DC-14-1

Line energy kJ/cm	Welding current A	Arc voltage V	Welding speed mm/min	Shielding gas & composition	Shielding gas flow rate lt/min
4.4	180 ±	13.0	160	75%He25%Ar	15.0
Former radius mm	Specimen thickness mm	Nominal Augmented strain %	Real Augmented strain %		
1000	9.15	0.5	0.46		
Length of all cracks (mm)	0.66/1.86				
	WELD CENTERLINE				
	2.27				
Length of HAZ cracks (mm)	0.45				
	WELD CENTERLINE				
	-				
Length of weld metal cracks (mm)	0.21/1.86				
	WELD CENTERLINE				
	2.27				
Total # of cracks	Total crack length mm	Total # of HAZ cracks	Total HAZ crack length mm	Total # of weld metal cracks	Total weld metal crack length mm
3	4.79	1	0.45	3	4.34

**Table B94:** Crack measurement results of specimen TIG-DC-14-2

Line energy kJ/cm	Welding current A	Arc voltage V	Welding speed mm/min	Shielding gas & composition	Shielding gas flow rate lt/min
4.4	180 ±	13.0	160	75%He25%Ar	15.0
Former radius mm	Specimen thickness mm	Nominal Augmented strain %	Real Augmented strain %		
500	9.5	1.0	0.95		
Length of all cracks (mm)	0.33/0.62/1.07				
	WELD CENTERLINE				
	0.83/0.83/0.83/0.41/0.62				
Length of HAZ cracks (mm)	0.33/0.62				
	WELD CENTERLINE				
	0.41/0.41/0.62				
Length of weld metal cracks (mm)	0.95/1.07/1.01				
	WELD CENTERLINE				
	0.83/0.83/0.41				
Total # of cracks	Total crack length mm	Total # of HAZ cracks	Total HAZ crack length mm	Total # of weld metal cracks	Total weld metal crack length mm
10	7.50	5	2.40	5	5.10

**Table B95:** Crack measurement results of specimen TIG-DC-14-3

Line energy kJ/cm	Welding current A	Arc voltage V	Welding speed mm/min	Shielding gas & composition	Shielding gas flow rate lt/min
4.4	180 ±	13.0	160	75%He25%Ar	15.0
Former radius mm	Specimen thickness mm	Nominal Augmented strain %	Real Augmented strain %		
250	9.5	2.0	1.90		
Length of all cracks (mm)	0.29/0.66/0.50/0.41/1.03/2.40/1.24/0.50				
	WELD CENTERLINE				
	1.16/1.40/0.91/0.41/0.33/1.03/0.87/0.54				
Length of HAZ cracks (mm)	0.29/0.66/0.50/0.41/1.03				
	WELD CENTERLINE				
	0.91/1.03/0.87/0.54				
Length of weld metal cracks (mm)	2.40/1.24/0.50				
	WELD CENTERLINE				
	1.16/1.40/0.41/0.33				
Total # of cracks	Total crack length mm	Total # of HAZ cracks	Total HAZ crack length mm	Total # of weld metal cracks	Total weld metal crack length mm
16	13.68	9	6.24	7	7.44



**Table B96:** Crack measurement results of specimen TIG-DC-14-4

Line energy kJ/cm	Welding current A	Arc voltage V	Welding speed mm/min	Shielding gas & composition	Shielding gas flow rate lt/min
4.4	180 ±	13.0	160	75%He25%Ar	15.0
Former radius mm	Specimen thickness mm	Nominal Augmented strain %	Real Augmented strain %		
125	9.2	4.0	3.68		
Length of all cracks (mm)	0.50/0.70/1.24/2.27/1.45/0.95/0.91/1.03				
	WELD CENTERLINE				
	2.89/1.03/3.31/0.83/0.70/0.62/0.54/0.41				
Length of HAZ cracks (mm)	0.50/0.70/1.03/1.03				
	WELD CENTERLINE				
	0.21/1.65/0.83/0.70/0.62/0.54/0.41				
Length of weld metal cracks (mm)	0.21/1.24/1.45/0.95/0.91/1.03				
	WELD CENTERLINE				
	2.89/0.83/1.65				
Total # of cracks	Total crack length mm	Total # of HAZ cracks	Total HAZ crack length mm	Total # of weld metal cracks	Total weld metal crack length mm
16	19.38	11	8.22	9	11.16

**Table B97:** Crack measurement results of specimen TIG-DC-15-1

Line energy kJ/cm	Welding current A	Arc voltage V	Welding speed mm/min	Shielding gas & composition	Shielding gas flow rate lt/min
4.7	180 ±	13.0	150	75%He25%Ar	15.0
Former radius mm	Specimen thickness mm	Nominal Augmented strain %	Real Augmented strain %		
1000	9.2	0.5	0.46		
Length of all cracks (mm)	0.91/0.50/0.58/1.78/0.41				
	WELD CENTERLINE				
	1.86				
Length of HAZ cracks (mm)	-				
	WELD CENTERLINE				
	-				
Length of weld metal cracks (mm)	0.91/0.50/0.58/1.78/0.41				
	WELD CENTERLINE				
	1.86				
Total # of cracks	Total crack length mm	Total # of HAZ cracks	Total HAZ crack length mm	Total # of weld metal cracks	Total weld metal crack length mm
6	6.03	-	-	6	6.03

**Table B98:** Crack measurement results of specimen TIG-DC-15-2

Line energy kJ/cm	Welding current A	Arc voltage V	Welding speed mm/min	Shielding gas & composition	Shielding gas flow rate lt/min
4.7	180 ±	13.0	150	75%He25%Ar	15.0
Former radius mm	Specimen thickness mm	Nominal Augmented strain %	Real Augmented strain %		
500	9.6	1.0	0.96		
Length of all cracks (mm)	0.58/0.25/0.54/1.45/1.12/1.57/0.83				
	WELD CENTERLINE				
	1.82/1.24/0.41/1.03/0.50				
Length of HAZ cracks (mm)	0.58/0.25/0.54/1.45				
	WELD CENTERLINE				
	0.41/0.41/1.03/0.50				
Length of weld metal cracks (mm)	1.12/1.57/0.83				
	WELD CENTERLINE				
	1.82/0.83				
Total # of cracks	Total crack length mm	Total # of HAZ cracks	Total HAZ crack length mm	Total # of weld metal cracks	Total weld metal crack length mm
12	11.32	8	5.17	5	6.16

**Table B99:** Crack measurement results of specimen TIG-DC-15-3

Line energy kJ/cm	Welding current A	Arc voltage V	Welding speed mm/min	Shielding gas & composition	Shielding gas flow rate lt/min
4.7	180 ±	13.0	150	75%He25%Ar	15.0
Former radius mm	Specimen thickness mm	Nominal Augmented strain %	Real Augmented strain %		
250	9.2	2.0	1.84		
Length of all cracks (mm)	0.41/1.03/1.24/1.20/1.03				
	WELD CENTERLINE				
	0.87/1.65/1.49/1.32/1.65/0.66/0.66				
Length of HAZ cracks (mm)	0.41/1.03				
	WELD CENTERLINE				
	1.32/0.66/0.66				
Length of weld metal cracks (mm)	1.24/1.20/1.03				
	WELD CENTERLINE				
	0.87/1.65/1.49/1.65				
Total # of cracks	Total crack length mm	Total # of HAZ cracks	Total HAZ crack length mm	Total # of weld metal cracks	Total weld metal crack length mm
12	13.22	5	4.09	7	9.13

**Table B100:** Crack measurement results of specimen TIG-DC-15-4

Line energy kJ/cm	Welding current A	Arc voltage V	Welding speed mm/min	Shielding gas & composition	Shielding gas flow rate lt/min
4.7	180 ±	13.0	150	75%He25%Ar	15.0
Former radius mm	Specimen thickness mm	Nominal Augmented strain %	Real Augmented strain %		
125	9.5	4.0	3.80		
Length of all cracks (mm)	0.50/0.54/0.91/0.91/2.81/1.94/0.54				
	WELD CENTERLINE				
	2.11/3.47/1.16/1.03/0.41/0.62/0.83/0.41				
Length of HAZ cracks (mm)	0.50/0.54/0.91/0.91/1.32				
	WELD CENTERLINE				
	1.82/1.16/1.03/0.41/0.62/0.83/0.41				
Length of weld metal cracks (mm)	1.49/1.94/0.54				
	WELD CENTERLINE				
	2.11/1.65				
Total # of cracks	Total crack length mm	Total # of HAZ cracks	Total HAZ crack length mm	Total # of weld metal cracks	Total weld metal crack length mm
15	18.18	12	10.45	5	7.73

**Table B101:** Crack measurement results of specimen TIG-DC-16-1

Line energy kJ/cm	Welding current A	Arc voltage V	Welding speed mm/min	Shielding gas & composition	Shielding gas flow rate lt/min
5.0	180 ±	13.0	140	75%He25%Ar	15.0
Former radius mm	Specimen thickness mm	Nominal Augmented strain %	Real Augmented strain %		
1000	9.5	0.5	0.48		
Length of all cracks (mm)	1.69/0.70				
	WELD CENTERLINE				
	1.86/0.50				
Length of HAZ cracks (mm)	-				
	WELD CENTERLINE				
	-				
Length of weld metal cracks (mm)	1.69/0.70				
	WELD CENTERLINE				
	1.86/0.50				
Total # of cracks	Total crack length mm	Total # of HAZ cracks	Total HAZ crack length mm	Total # of weld metal cracks	Total weld metal crack length mm
4	4.75	-	-	4	4.75

**Table B102:** Crack measurement results of specimen TIG-DC-16-2

Line energy kJ/cm	Welding current A	Arc voltage V	Welding speed mm/min	Shielding gas & composition	Shielding gas flow rate lt/min
5.0	180 ±	13.0	140	75%He25%Ar	15.0
Former radius mm	Specimen thickness mm	Nominal Augmented strain %	Real Augmented strain %		
500	9.6	1.0	0.96		
Length of all cracks (mm)	0.91/1.53/0.83/1.07/0.62/0.62/1.86				
	WELD CENTERLINE				
	1.74/1.32/1.12/0.54				
Length of HAZ cracks (mm)	0.91/1.03/0.83/0.62/0.62				
	WELD CENTERLINE				
	1.12/0.54				
Length of weld metal cracks (mm)	0.50/1.07/1.86				
	WELD CENTERLINE				
	1.74/1.32				
Total # of cracks	Total crack length mm	Total # of HAZ cracks	Total HAZ crack length mm	Total # of weld metal cracks	Total weld metal crack length mm
11	12.15	7	5.66	5	6.49

**Table B103:** Crack measurement results of specimen TIG-DC-16-3

Line energy kJ/cm	Welding current A	Arc voltage V	Welding speed mm/min	Shielding gas & composition	Shielding gas flow rate lt/min
5.0	180 ±	13.0	140	75%He25%Ar	15.0
Former radius mm	Specimen thickness mm	Nominal Augmented strain %	Real Augmented strain %		
250	9.2	2.0	1.84		
Length of all cracks (mm)	0.62/0.74/0.91/0.66/1.24/0.45/0.41/0.50/0.83/0.83/1.32/1.36/1.32				
	WELD CENTERLINE				
	2.89/0.83/1.45/0.50/1.65/1.03				
Length of HAZ cracks (mm)	0.62/0.74/0.91/1.24/0.83				
	WELD CENTERLINE				
	1.45/1.03				
Length of weld metal cracks (mm)	0.66/0.45/0.41/0.50/0.83/1.32/1.36/1.32				
	WELD CENTERLINE				
	2.89/0.83/0.50/1.65				
Total # of cracks	Total crack length mm	Total # of HAZ cracks	Total HAZ crack length mm	Total # of weld metal cracks	Total weld metal crack length mm
19	19.55	7	6.82	12	12.73

**Table B104:** Crack measurement results of specimen TIG-DC-16-4

Line energy kJ/cm	Welding current A	Arc voltage V	Welding speed mm/min	Shielding gas & composition	Shielding gas flow rate lt/min
5.0	180 ±	13.0	140	75%He25%Ar	15.0
Former radius mm	Specimen thickness mm	Nominal Augmented strain %	Real Augmented strain %		
125	9.6	4.0	3.84		
Length of all cracks (mm)	0.37/0.62/0.83/1.12/1.32/0.87/2.07/0.54/3.51				
	WELD CENTERLINE				
	1.65/1.65/1.65/2.15/0.50/1.07/0.74/0.70/0.62/0.41				
Length of HAZ cracks (mm)	0.37/0.62/0.83/1.12/1.32/1.36/0.62				
	WELD CENTERLINE				
	1.65/0.91/0.50/1.07/0.74/0.70/0.62/0.41				
Length of weld metal cracks (mm)	0.87/0.70/0.54/2.89				
	WELD CENTERLINE				
	1.65/1.65/1.24				
Total # of cracks	Total crack length mm	Total # of HAZ cracks	Total HAZ crack length mm	Total # of weld metal cracks	Total weld metal crack length mm
19	22.40	15	12.85	7	9.55

**Table B105:** Crack measurement results of specimen TIG-DC-17-1

Line energy kJ/cm	Welding current A	Arc voltage V	Welding speed mm/min	Shielding gas & composition	Shielding gas flow rate lt/min
5.4	180 ±	13.0	130	75%He25%Ar	15.0
Former radius mm	Specimen thickness mm	Nominal Augmented strain %	Real Augmented strain %		
1000	9.5	0.5	0.48		
Length of all cracks (mm)	2.61/2.07/2.07				
	WELD CENTERLINE				
	1.24				
Length of HAZ cracks (mm)	1.45				
	WELD CENTERLINE				
	-				
Length of weld metal cracks (mm)	1.16/2.07/2.07				
	WELD CENTERLINE				
	1.24				
Total # of cracks	Total crack length mm	Total # of HAZ cracks	Total HAZ crack length mm	Total # of weld metal cracks	Total weld metal crack length mm
4	7.98	1	1.45	4	6.53

**Table B106:** Crack measurement results of specimen TIG-DC-17-2

Line energy kJ/cm	Welding current A	Arc voltage V	Welding speed mm/min	Shielding gas & composition	Shielding gas flow rate lt/min
5.4	180 ±	13.0	130	75%He25%Ar	15.0
Former radius mm	Specimen thickness mm	Nominal Augmented strain %	Real Augmented strain %		
500	9.2	1.0	0.92		
Length of all cracks (mm)	0.29/0.70/1.45/1.98				
	WELD CENTERLINE				
	2.89/1.03/1.12/0.54/1.24				
Length of HAZ cracks (mm)	0.58/0.70				
	WELD CENTERLINE				
	0.69/0.67				
Length of weld metal cracks (mm)	0.29/1.45/1.98				
	WELD CENTERLINE				
	2.89/1.03/1.12/0.54/1.24				
Total # of cracks	Total crack length mm	Total # of HAZ cracks	Total HAZ crack length mm	Total # of weld metal cracks	Total weld metal crack length mm
12	13.18	4	2.64	8	10.54

**Table B107:** Crack measurement results of specimen TIG-DC-17-3

Line energy kJ/cm	Welding current A	Arc voltage V	Welding speed mm/min	Shielding gas & composition	Shielding gas flow rate lt/min
5.4	180 ±	13.0	130	75%He25%Ar	15.0
Former radius mm	Specimen thickness mm	Nominal Augmented strain %	Real Augmented strain %		
250	9.2	2.0	1.84		
Length of all cracks (mm)	0.83/0.91/1.24/3.10/0.70/0.74/3.31/1.03				
	WELD CENTERLINE				
	2.27/0.70/0.21/0.62/1.16/1.45/0.83/0.91				
Length of HAZ cracks (mm)	0.83/0.91/1.24/0.70/0.74				
	WELD CENTERLINE				
	0.70/0.21/0.62/1.16/0.91				
Length of weld metal cracks (mm)	0.62/1.86/3.31/1.03				
	WELD CENTERLINE				
	2.27/1.45/0.83				
Total # of cracks	Total crack length mm	Total # of HAZ cracks	Total HAZ crack length mm	Total # of weld metal cracks	Total weld metal crack length mm
16	19.38	10	8.02	7	11.36

**Table B108:** Crack measurement results of specimen TIG-DC-17-4

Line energy kJ/cm	Welding current A	Arc voltage V	Welding speed mm/min	Shielding gas & composition	Shielding gas flow rate lt/min
5.4	180 ±	13.0	130	75%He25%Ar	15.0
Former radius mm	Specimen thickness mm	Nominal Augmented strain %	Real Augmented strain %		
125	9.6	4.0	3.84		
Length of all cracks (mm)	0.91/0.95/1.45/3.10/0.41/1.57/1.69				
	WELD CENTERLINE				
	1.45/3.31/1.24/1.86/1.65/1.03/1.03/1.03/0.83				
Length of HAZ cracks (mm)	0.91/0.95/1.45/1.65/0.41				
	WELD CENTERLINE				
	1.86/1.24/1.65/1.03/1.03/1.03/0.83				
Length of weld metal cracks (mm)	1.45/1.57/1.69				
	WELD CENTERLINE				
	1.45/1.45/1.86				
Total # of cracks	Total crack length mm	Total # of HAZ cracks	Total HAZ crack length mm	Total # of weld metal cracks	Total weld metal crack length mm
16	23.51	12	14.05	6	9.46

**Table B109:** Crack measurement results of specimen TIG-DC-18-1

Line energy kJ/cm	Welding current A	Arc voltage V	Welding speed mm/min	Shielding gas & composition	Shielding gas flow rate lt/min
5.9	180 ±	13.0	120	75%He25%Ar	15.0
Former radius mm	Specimen thickness mm	Nominal Augmented strain %	Real Augmented strain %		
1000	9.5	0.5	0.48		
Length of all cracks (mm)	2.07				
	WELD CENTERLINE				
	1.24				
Length of HAZ cracks (mm)	-				
	WELD CENTERLINE				
	-				
Length of weld metal cracks (mm)	2.07				
	WELD CENTERLINE				
	1.24				
Total # of cracks	Total crack length mm	Total # of HAZ cracks	Total HAZ crack length mm	Total # of weld metal cracks	Total weld metal crack length mm
2	3.31	-	-	2	3.31

**Table B110:** Crack measurement results of specimen TIG-DC-18-2

Line energy kJ/cm	Welding current A	Arc voltage V	Welding speed mm/min	Shielding gas & composition	Shielding gas flow rate lt/min
5.9	180 ±	13.0	120	75%He25%Ar	15.0
Former radius mm	Specimen thickness mm	Nominal Augmented strain %	Real Augmented strain %		
500	9.2	1.0	0.92		
Length of all cracks (mm)	3.39/0.33/0.54/1.45/0.62/1.32/0.62				
	WELD CENTERLINE				
	0.83/2.19/1.32/1.82/0.95/0.87/0.29/0.25				
Length of HAZ cracks (mm)	1.24/1.45/0.62				
	WELD CENTERLINE				
	-				
Length of weld metal cracks (mm)	2.15/0.33/0.54/1.32/0.62				
	WELD CENTERLINE				
	0.83/2.19/1.32/1.82/0.95/0.87/0.29/0.25				
Total # of cracks	Total crack length mm	Total # of HAZ cracks	Total HAZ crack length mm	Total # of weld metal cracks	Total weld metal crack length mm
15	16.78	3	3.31	13	13.47

**Table B111:** Crack measurement results of specimen TIG-DC-18-3

Line energy kJ/cm	Welding current A	Arc voltage V	Welding speed mm/min	Shielding gas & composition	Shielding gas flow rate lt/min
5.9	180 ±	13.0	120	75%He25%Ar	15.0
Former radius mm	Specimen thickness mm	Nominal Augmented strain %	Real Augmented strain %		
250	9.5	2.0	1.9		
Length of all cracks (mm)	0.91/0.83/1.45/1.78/0.62/2.27/1.78/1.03/3.93				
	WELD CENTERLINE				
	1.86/2.89/0.62/3.93/1.36/1.03/0.74/1.03				
Length of HAZ cracks (mm)	0.91/0.83/0.41/1.78/0.62/1.24/1.78/1.03/1.03				
	WELD CENTERLINE				
	1.86/1.45/2.48/1.36/1.03/0.74/1.03				
Length of weld metal cracks (mm)	1.03/1.03/2.89				
	WELD CENTERLINE				
	1.45/0.62/1.45				
Total # of cracks	Total crack length mm	Total # of HAZ cracks	Total HAZ crack length mm	Total # of weld metal cracks	Total weld metal crack length mm
17	28.06	16	19.59	6	8.47



**Table B112:** Crack measurement results of specimen TIG-DC-18-4

Line energy kJ/cm	Welding current A	Arc voltage V	Welding speed mm/min	Shielding gas & composition	Shielding gas flow rate lt/min
5.9	180 ±	13.0	120	75%He25%Ar	15.0
Former radius mm	Specimen thickness mm	Nominal Augmented strain %	Real Augmented strain %		
125	9.6	4.0	3.84		
Length of all cracks (mm)	0.70/0.95/1.78/2.27/0.62/1.24/1.03/0.83/4.55				
	WELD CENTERLINE				
	1.12/1.57/1.86/1.03/0.58/5.16/1.40/1.03/1.53/1.12				
Length of HAZ cracks (mm)	0.70/0.95/1.78/2.27/0.62/1.24/0.83/1.45				
	WELD CENTERLINE				
	1.57/1.03/0.58/2.27/1.40/1.03/1.53/1.12				
Length of weld metal cracks (mm)	1.03/3.10				
	WELD CENTERLINE				
	1.12/1.86/2.89				
Total # of cracks	Total crack length mm	Total # of HAZ cracks	Total HAZ crack length mm	Total # of weld metal cracks	Total weld metal crack length mm
19	30.37	16	20.37	5	10.00

**Table B113:** Crack measurement results of specimen TIG-AC-SUP-1-1

Line energy kJ/cm	Welding current A	Arc voltage V	Welding speed mm/min	Shielding gas & composition	Shielding gas flow rate lt/min
3.9	140 ~	4.5	80	99.9 % Argon	8.0
Former radius mm	Specimen thickness mm	Nominal Augmented strain %	Real Augmented strain %		
1000	9.3	0.5	0.47		
Length of all cracks (mm)	1.03/1.45/0.21/1.65				
	WELD CENTERLINE				
	1.91/0.41/0.62/0.83/1.24/1.03				
Length of HAZ cracks (mm)	1.03				
	WELD CENTERLINE				
	0.41/0.62/0.83				
Length of weld metal cracks (mm)	1.45/0.21/1.65				
	WELD CENTERLINE				
	1.94/1.24/1.03				
Total # of cracks	Total crack length mm	Total # of HAZ cracks	Total HAZ crack length mm	Total # of weld metal cracks	Total weld metal crack length mm
10	10.41	4	2.89	6	7.52

**Table B114:** Crack measurement results of specimen TIG-AC-SUP-1-2

Line energy kJ/cm	Welding current A	Arc voltage V	Welding speed mm/min	Shielding gas & composition	Shielding gas flow rate lt/min
3.9	140 ~	4.5	80	99.9 % Argon	8.0
Former radius mm	Specimen thickness mm	Nominal Augmented strain %	Real Augmented strain %		
500	9.3	1.0	0.93		
Length of all cracks (mm)	1.86/0.83/1.03/2.69/0.83/1.24				
	WELD CENTERLINE				
	0.83/1.65/2.28/0.83/0.83/1.65/1.03				
Length of HAZ cracks (mm)	0.83/1.03/0.83				
	WELD CENTERLINE				
	0.83/0.83/0.83/1.65/1.03				
Length of weld metal cracks (mm)	1.86/1.86/0.83/1.24				
	WELD CENTERLINE				
	0.83/1.65/1.45				
Total # of cracks	Total crack length mm	Total # of HAZ cracks	Total HAZ crack length mm	Total # of weld metal cracks	Total weld metal crack length mm
13	17.56	8	7.85	7	9.71

**Table B115:** Crack measurement results of specimen TIG-AC-SUP-1-3

Line energy kJ/cm	Welding current A	Arc voltage V	Welding speed mm/min	Shielding gas & composition	Shielding gas flow rate lt/min
3.9	140 ~	4.5	80	99.9 % Argon	8.0
Former radius mm	Specimen thickness mm	Nominal Augmented strain %	Real Augmented strain %		
250	9.4	2.0	1.88		
Length of all cracks (mm)	1.45/1.45/1.66/1.24/2.27/1.32				
	WELD CENTERLINE				
	1.24/1.86/1.12/1.65/0.83/0.83/1.65/0.83				
Length of HAZ cracks (mm)	0.83/0.83/0.83/0.83/0.62				
	WELD CENTERLINE				
	0.83/1.12/1.03/0.83/0.83/1.65/0.83				
Length of weld metal cracks (mm)	0.62/0.62/0.83/0.41/1.65/1.32				
	WELD CENTERLINE				
	1.24/1.03/0.62				
Total # of cracks	Total crack length mm	Total # of HAZ cracks	Total HAZ crack length mm	Total # of weld metal cracks	Total weld metal crack length mm
14	19.38	12	11.03	9	8.35

**Table B116:** Crack measurement results of specimen TIG-AC-SUP-1-4

Line energy kJ/cm	Welding current A	Arc voltage V	Welding speed mm/min	Shielding gas & composition	Shielding gas flow rate lt/min
3.9	140 ~	4.5	80	99.9 % Argon	8.0
Former radius mm	Specimen thickness mm	Nominal Augmented strain %	Real Augmented strain %		
125	9.4	4.0	3.76		
Length of all cracks (mm)	0.62/0.62/1.24/0.87/1.86/0.87/0.87/2.90/1.24				
	WELD CENTERLINE				
	2.69/3.31/0.91/1.57/1.12/1.03				
Length of HAZ cracks (mm)	0.62/0.62/0.83/0.87/1.03/0.87/0.87/0.83				
	WELD CENTERLINE				
	0.83/0.91/1.16/1.12/1.03				
Length of weld metal cracks (mm)	0.41/0.83/2.07/1.24				
	WELD CENTERLINE				
	2.69/2.48/0.41				
Total # of cracks	Total crack length mm	Total # of HAZ cracks	Total HAZ crack length mm	Total # of weld metal cracks	Total weld metal crack length mm
15	21.69	13	11.57	7	10.12

**Table B117:** Crack measurement results of specimen TIG-AC-SUP-2-1

Line energy kJ/cm	Welding current A	Arc voltage V	Welding speed mm/min	Shielding gas & composition	Shielding gas flow rate lt/min
4.9	140 ~	4.5	65	99.9 % Argon	8.0
Former radius mm	Specimen thickness mm	Nominal Augmented strain %	Real Augmented strain %		
1000	9.4	0.5	0.47		
Length of all cracks (mm)	1.65				
	WELD CENTERLINE				
	0.82/0.70				
Length of HAZ cracks (mm)	-				
	WELD CENTERLINE				
	0.41/0.70				
Length of weld metal cracks (mm)	1.65				
	WELD CENTERLINE				
	0.41				
Total # of cracks	Total crack length mm	Total # of HAZ cracks	Total HAZ crack length mm	Total # of weld metal cracks	Total weld metal crack length mm
3	3.18	2	1.12	2	2.07

**Table B118:** Crack measurement results of specimen TIG-AC-SUP-2-2

Line energy kJ/cm	Welding current A	Arc voltage V	Welding speed mm/min	Shielding gas & composition	Shielding gas flow rate lt/min
4.9	140 ~	4.5	65	99.9 % Argon	8.0
Former radius mm	Specimen thickness mm	Nominal Augmented strain %	Real Augmented strain %		
500	9.1	1.0	0.91		
Length of all cracks (mm)	0.62/1.86/1.03/1.99/1.24/1.03				
	WELD CENTERLINE				
	1.32/0.50/1.03/0.87				
Length of HAZ cracks (mm)	0.62/0.62/0.62/0.83/0.62				
	WELD CENTERLINE				
	1.32/0.50/1.03/0.87				
Length of weld metal cracks (mm)	1.24/0.41/1.16/0.62/1.03				
	WELD CENTERLINE				
	-				
Total # of cracks	Total crack length mm	Total # of HAZ cracks	Total HAZ crack length mm	Total # of weld metal cracks	Total weld metal crack length mm
10	11.49	9	7.02	5	4.46

**Table B119:** Crack measurement results of specimen TIG-AC-SUP-2-3

Line energy kJ/cm	Welding current A	Arc voltage V	Welding speed mm/min	Shielding gas & composition	Shielding gas flow rate lt/min
4.9	140 ~	4.5	65	99.9 % Argon	8.0
Former radius mm	Specimen thickness mm	Nominal Augmented strain %	Real Augmented strain %		
250	9.4	2.0	1.88		
Length of all cracks (mm)	1.24/1.45/0.41/0.29/1.86/2.90/4.14				
	WELD CENTERLINE				
	5.25/0.91/1.36/0.66/1.69/0.70				
Length of HAZ cracks (mm)	0.62/0.83/0.41/0.29/0.83/0.83/0.83				
	WELD CENTERLINE				
	1.94/0.91/1.36/0.66/1.69/0.70				
Length of weld metal cracks (mm)	0.62/0.62/1.03/2.07/3.31				
	WELD CENTERLINE				
	3.31				
Total # of cracks	Total crack length mm	Total # of HAZ cracks	Total HAZ crack length mm	Total # of weld metal cracks	Total weld metal crack length mm
13	22.85	13	11.90	6	10.95

**Table B120:** Crack measurement results of specimen TIG-AC-SUP-2-4

Line energy kJ/cm	Welding current A	Arc voltage V	Welding speed mm/min	Shielding gas & composition	Shielding gas flow rate lt/min
4.9	140 ~	4.5	65	99.9 % Argon	8.0
Former radius mm	Specimen thickness mm	Nominal Augmented strain %	Real Augmented strain %		
125	9.4	4.0	3.76		
Length of all cracks (mm)	0.83/1.32/0.83/2.60/0.62/1.66/3.02				
	WELD CENTERLINE				
	3.43/2.48/2.27/0.91/1.03/1.44				
Length of HAZ cracks (mm)	0.83/1.32/0.83/1.32/0.62/1.45				
	WELD CENTERLINE				
	1.24/1.24/0.91/1.03/1.03				
Length of weld metal cracks (mm)	1.28/0.21/3.02				
	WELD CENTERLINE				
	3.43/1.24/1.03/0.41				
Total # of cracks	Total crack length mm	Total # of HAZ cracks	Total HAZ crack length mm	Total # of weld metal cracks	Total weld metal crack length mm
13	22.44	11	11.82	7	10.62

**Table B121:** Crack measurement results of specimen TIG-AC-SUP-3-1

Line energy kJ/cm	Welding current A	Arc voltage V	Welding speed mm/min	Shielding gas & composition	Shielding gas flow rate lt/min
6.4	140 ~	4.5	50	99.9 % Argon	8.0
Former radius mm	Specimen thickness mm	Nominal Augmented strain %	Real Augmented strain %		
1000	9.4	0.5	0.47		
Length of all cracks (mm)	1.24				
	WELD CENTERLINE				
	-				
Length of HAZ cracks (mm)	-				
	WELD CENTERLINE				
	-				
Length of weld metal cracks (mm)	1.24				
	WELD CENTERLINE				
	-				
Total # of cracks	Total crack length mm	Total # of HAZ cracks	Total HAZ crack length mm	Total # of weld metal cracks	Total weld metal crack length mm
1	1.24	-	-	1	1.24

**Table B122:** Crack measurement results of specimen TIG-AC-SUP-3-2

Line energy kJ/cm	Welding current A	Arc voltage V	Welding speed mm/min	Shielding gas & composition	Shielding gas flow rate lt/min
6.4	140 ~	4.5	50	99.9 % Argon	8.0
Former radius mm	Specimen thickness mm	Nominal Augmented strain %	Real Augmented strain %		
500	9.45	1.0	0.945		
Length of all cracks (mm)	1.45/3.39/3.48/1.45/3.51				
	WELD CENTERLINE				
	1.32/2.07/0.62/1.24/1.03/1.53				
Length of HAZ cracks (mm)	1.45/1.65/1.12/0.83/1.45				
	WELD CENTERLINE				
	1.32/2.07/0.62/1.24/1.03/1.53				
Length of weld metal cracks (mm)	1.74/1.53/3.51				
	WELD CENTERLINE				
	-				
Total # of cracks	Total crack length mm	Total # of HAZ cracks	Total HAZ crack length mm	Total # of weld metal cracks	Total weld metal crack length mm
11	21.07	11	14.30	3	6.78

**Table B123:** Crack measurement results of specimen TIG-AC-SUP-3-3

Line energy kJ/cm	Welding current A	Arc voltage V	Welding speed mm/min	Shielding gas & composition	Shielding gas flow rate lt/min
6.4	140 ~	4.5	50	99.9 % Argon	8.0
Former radius mm	Specimen thickness mm	Nominal Augmented strain %	Real Augmented strain %		
250	9.4	2.0	1.88		
Length of all cracks (mm)	1.65/2.69/1.65/2.57/2.48/1.03/0.62/2.48				
	WELD CENTERLINE				
	4.13/1.45/2.69/1.03/0.83/0.83				
Length of HAZ cracks (mm)	1.65/2.07/1.65/2.07/2.48/1.03/0.62				
	WELD CENTERLINE				
	2.89/1.45/1.86/1.03/0.83/0.83				
Length of weld metal cracks (mm)	0.62/0.50/2.48				
	WELD CENTERLINE				
	1.24/0.83				
Total # of cracks	Total crack length mm	Total # of HAZ cracks	Total HAZ crack length mm	Total # of weld metal cracks	Total weld metal crack length mm
14	26.12	13	20.45	5	5.66

**Table B124:** Crack measurement results of specimen TIG-AC-SUP-3-4

Line energy kJ/cm	Welding current A	Arc voltage V	Welding speed mm/min	Shielding gas & composition	Shielding gas flow rate lt/min
6.4	140 ~	4.5	50	99.9 % Argon	8.0
Former radius mm	Specimen thickness mm	Nominal Augmented strain %	Real Augmented strain %		
125	9.4	4.0	3.76		
Length of all cracks (mm)	1.24/0.95/1.24/2.61/1.65/3.31/1.65/1.65/0.50/3.92/2.07/4.13/1.65/3.63				
	WELD CENTERLINE				
	1.24/2.90/6.41/2.07/1.86/4.05/1.65/4.14/1.03/1.45				
Length of HAZ cracks (mm)	1.24/0.95/1.24/2.07/1.65/2.07/1.65/1.65/0.50/2.27/2.07/2.48/1.65/2.27				
	WELD CENTERLINE				
	2.07/4.55/2.07/1.86/3.02/1.65/2.69/1.03/1.45				
Length of weld metal cracks (mm)	0.54/1.24/1.65/1.65/1.36				
	WELD CENTERLINE				
	1.24/0.83/1.86/1.03/1.45				
Total # of cracks	Total crack length mm	Total # of HAZ cracks	Total HAZ crack length mm	Total # of weld metal cracks	Total weld metal crack length mm
24	56.98	23	44.13	10	12.85

**Table B125:** Crack measurement results of specimen TIG-AC-SUP-4-1

Line energy kJ/cm	Welding current A	Arc voltage V	Welding speed mm/min	Shielding gas & composition	Shielding gas flow rate lt/min
7.9	140 ~	4.5	40	99.9 % Argon	8.0
Former radius mm	Specimen thickness mm	Nominal Augmented strain %	Real Augmented strain %		
1000	9.3	0.5	0.465		
Length of all cracks (mm)	-				
	WELD CENTERLINE				
	0.91/1.32/2.48/10.30				
Length of HAZ cracks (mm)	0.91/1.32/2.48/10.30				
	WELD CENTERLINE				
	-				
Length of weld metal cracks (mm)	-				
	WELD CENTERLINE				
	-				
Total # of cracks	Total crack length mm	Total # of HAZ cracks	Total HAZ crack length mm	Total # of weld metal cracks	Total weld metal crack length mm
4	15.01	4	15.01	-	-

**Table B126:** Crack measurement results of specimen TIG-AC-SUP-4-2

Line energy kJ/cm	Welding current A	Arc voltage V	Welding speed mm/min	Shielding gas & composition	Shielding gas flow rate lt/min
7.9	140 ~	4.5	40	99.9 % Argon	8.0
Former radius mm	Specimen thickness mm	Nominal Augmented strain %	Real Augmented strain %		
500	9.4	1.0	0.94		
Length of all cracks (mm)	2.69/10.60/5.99/9.60				
	WELD CENTERLINE				
	12.60/8.50/3.72/2.07				
Length of HAZ cracks (mm)	2.69/10.60/4.13/9.60				
	WELD CENTERLINE				
	12.60/8.50/3.72/2.07				
Length of weld metal cracks (mm)	1.86				
	WELD CENTERLINE				
	-				
Total # of cracks	Total crack length mm	Total # of HAZ cracks	Total HAZ crack length mm	Total # of weld metal cracks	Total weld metal crack length mm
8	55.76	8	53.90	1	1.86

**Table B127:** Crack measurement results of specimen TIG-AC-SUP-4-3

Line energy kJ/cm	Welding current A	Arc voltage V	Welding speed mm/min	Shielding gas & composition	Shielding gas flow rate lt/min
7.9	140 ~	4.5	40	99.9 % Argon	8.0
Former radius mm	Specimen thickness mm	Nominal Augmented strain %	Real Augmented strain %		
250	9.4	2.0	1.88		
Length of all cracks (mm)	0.91/2.07/1.03/2.48/5.78/1.03/1.65/4.55/5.38/4.34/1.65/0.33/5.37				
	WELD CENTERLINE				
	5.37/2.07/2.89/1.24/2.69/2.48/1.03/4.75/0.41				
Length of HAZ cracks (mm)	0.91/2.07/1.03/2.48/2.27/1.03/1.65/2.07/3.31/2.69/1.65/0.33/1.24				
	WELD CENTERLINE				
	2.89/2.07/2.48/0.41/1.45/2.48/1.86/0.41				
Length of weld metal cracks (mm)	3.51/0.41/2.48/2.07/1.65/1.86/4.13				
	WELD CENTERLINE				
	2.48/0.41/0.83/1.24/2.07/1.03/2.89				
Total # of cracks	Total crack length mm	Total # of HAZ cracks	Total HAZ crack length mm	Total # of weld metal cracks	Total weld metal crack length mm
22	63.84	21	36.78	14	27.07



**Table B128:** Crack measurement results of specimen TIG-AC-SUP-4-4

Line energy kJ/cm	Welding current A	Arc voltage V	Welding speed mm/min	Shielding gas & composition	Shielding gas flow rate lt/min
7.9	140 ~	4.5	40	99.9 % Argon	8.0
Former radius mm	Specimen thickness mm	Nominal Augmented strain %	Real Augmented strain %		
125	9.4	4.0	3.76		
Length of all cracks (mm)	1.24/0.91/1.12/1.24/1.24/1.65/6.61/1.24/1.65/1.03/1.24/1.45/1.65/8.26/ 2.48/6.62/7.02/4.55				
	WELD CENTERLINE				
	1.65/1.45/2.07/2.48/2.89/7.44/4.96/7.44/2.69/3.72/2.89/9.70/10.00				
Length of HAZ cracks (mm)	1.24/0.91/1.12/1.24/1.24/1.65/4.13/1.24/1.65/1.03/1.24/1.45/1.65/8.26/2.48/4.55/4. 13/4.55				
	WELD CENTERLINE				
	2.48/2.89/4.13/4.96/7.44/2.69/3.72/2.89/9.70/10				
Length of weld metal cracks (mm)	2.48/2.07/2.89				
	WELD CENTERLINE				
	1.65/1.45/2.07/3.31				
Total # of cracks	Total crack length mm	Total # of HAZ cracks	Total HAZ crack length mm	Total # of weld metal cracks	Total weld metal crack length mm
31	110.57	28	94.66	7	15.91

**Table B129:** Crack measurement results of specimen TIG-DC-SUP-1-1

Line energy kJ/cm	Welding current A	Arc voltage V	Welding speed mm/min	Shielding gas & composition	Shielding gas flow rate lt/min
2.3	180 ±	13.0	300	75%He25%Ar	15.0
Former radius mm	Specimen thickness mm	Nominal Augmented strain %	Real Augmented strain %		
1000	9.4	0.5	0.47		
Length of all cracks (mm)	-				
	WELD CENTERLINE				
	0.91				
Length of HAZ cracks (mm)	-				
	WELD CENTERLINE				
	-				
Length of weld metal cracks (mm)	-				
	WELD CENTERLINE				
	0.91				
Total # of cracks	Total crack length mm	Total # of HAZ cracks	Total HAZ crack length mm	Total # of weld metal cracks	Total weld metal crack length mm
1	0.91	-	-	1	0.91

**Table B130:** Crack measurement results of specimen TIG-DC-SUP-1-2

Line energy kJ/cm	Welding current A	Arc voltage V	Welding speed mm/min	Shielding gas & composition	Shielding gas flow rate lt/min
2.3	180 ±	13.0	300	75%He25%Ar	15.0
Former radius mm	Specimen thickness mm	Nominal Augmented strain %	Real Augmented strain %		
500	9.2	1.0	0.92		
Length of all cracks (mm)	0.87/0.33/0.33/0.41/0.62/0.21/0.83/0.50				
	WELD CENTERLINE				
	0.29/0.62/0.83/0.62/0.62/0.33				
Length of HAZ cracks (mm)	-				
	WELD CENTERLINE				
	-				
Length of weld metal cracks (mm)	0.87/0.33/0.33/0.41/0.62/0.21/0.83/0.50				
	WELD CENTERLINE				
	0.29/0.62/0.83/0.62/0.62/0.33				
Total # of cracks	Total crack length mm	Total # of HAZ cracks	Total HAZ crack length mm	Total # of weld metal cracks	Total weld metal crack length mm
14	7.40	-	-	14	7.40

**Table B131:** Crack measurement results of specimen TIG-DC-SUP-1-3

Line energy kJ/cm	Welding current A	Arc voltage V	Welding speed mm/min	Shielding gas & composition	Shielding gas flow rate lt/min
2.3	180 ±	13.0	300	75%He25%Ar	15.0
Former radius mm	Specimen thickness mm	Nominal Augmented strain %	Real Augmented strain %		
250	9.2	2.0	1.84		
Length of all cracks (mm)	0.41/0.21/0.62/1.24/1.03				
	WELD CENTERLINE				
	0.25/0.91/1.03/1.12/0.50/0.45/0.33				
Length of HAZ cracks (mm)	0.41/0.21				
	WELD CENTERLINE				
	0.33				
Length of weld metal cracks (mm)	0.62/1.24/1.03				
	WELD CENTERLINE				
	0.25/0.91/1.03/1.12/0.50/0.45				
Total # of cracks	Total crack length mm	Total # of HAZ cracks	Total HAZ crack length mm	Total # of weld metal cracks	Total weld metal crack length mm
12	8.10	3	0.95	9	7.15

**Table B132:** Crack measurement results of specimen TIG-DC-SUP-1-4

Line energy kJ/cm	Welding current A	Arc voltage V	Welding speed mm/min	Shielding gas & composition	Shielding gas flow rate lt/min
2.3	180 ±	13.0	300	75%He25%Ar	15.0
Former radius mm	Specimen thickness mm	Nominal Augmented strain %	Real Augmented strain %		
125	9.6	4.0	3.84		
Length of all cracks (mm)	0.17/0.25/0.29/0.45/0.45/0.95				
	WELD CENTERLINE				
	1.24/0.79/0.29/0.25/0.25/0.25				
Length of HAZ cracks (mm)	0.17/0.25/0.29/0.45/0.50				
	WELD CENTERLINE				
	0.25/0.25/0.25				
Length of weld metal cracks (mm)	0.45/0.95				
	WELD CENTERLINE				
	1.24/0.79/0.29				
Total # of cracks	Total crack length mm	Total # of HAZ cracks	Total HAZ crack length mm	Total # of weld metal cracks	Total weld metal crack length mm
12	6.12	8	2.40	5	3.72

**Table B133:** Crack measurement results of specimen TIG-DC-SUP-2-1

Line energy kJ/cm	Welding current A	Arc voltage V	Welding speed mm/min	Shielding gas & composition	Shielding gas flow rate lt/min
3.9	180 ±	13.0	180	75%He25%Ar	15.0
Former radius mm	Specimen thickness mm	Nominal Augmented strain %	Real Augmented strain %		
1000	9.6	0.5	0.48		
Length of all cracks (mm)	0.62				
	WELD CENTERLINE				
	-				
Length of HAZ cracks (mm)	-				
	WELD CENTERLINE				
	-				
Length of weld metal cracks (mm)	0.62				
	WELD CENTERLINE				
	-				
Total # of cracks	Total crack length mm	Total # of HAZ cracks	Total HAZ crack length mm	Total # of weld metal cracks	Total weld metal crack length mm
1	0.62	-	-	1	0.62

**Table B134:** Crack measurement results of specimen TIG-DC-SUP-2-2

Line energy kJ/cm	Welding current A	Arc voltage V	Welding speed mm/min	Shielding gas & composition	Shielding gas flow rate lt/min
3.9	180 ±	13.0	180	75%He25%Ar	15.0
Former radius mm	Specimen thickness mm	Nominal Augmented strain %	Real Augmented strain %		
500	9.2	1.0	0.92		
Length of all cracks (mm)	0.79/0.87/0.62/0.41/0.41				
	WELD CENTERLINE				
	0.91/0.12/0.37/0.45/0.87/0.08/0.33				
Length of HAZ cracks (mm)	-				
	WELD CENTERLINE				
	-				
Length of weld metal cracks (mm)	0.79/0.87/0.62/0.41/0.41				
	WELD CENTERLINE				
	0.91/0.12/0.37/0.45/0.87/0.08/0.33				
Total # of cracks	Total crack length mm	Total # of HAZ cracks	Total HAZ crack length mm	Total # of weld metal cracks	Total weld metal crack length mm
12	6.24	-	-	12	6.24

**Table B135:** Crack measurement results of specimen TIG-DC-SUP-2-3

Line energy kJ/cm	Welding current A	Arc voltage V	Welding speed mm/min	Shielding gas & composition	Shielding gas flow rate lt/min
3.9	180 ±	13.0	180	75%He25%Ar	15.0
Former radius mm	Specimen thickness mm	Nominal Augmented strain %	Real Augmented strain %		
250	9.5	2.0	1.90		
Length of all cracks (mm)	0.62/0.45/0.95/2.61				
	WELD CENTERLINE				
	3.18/0.66				
Length of HAZ cracks (mm)	0.21/0.25				
	WELD CENTERLINE				
	0.50				
Length of weld metal cracks (mm)	0.41/0.45/0.95/2.36				
	WELD CENTERLINE				
	2.69/0.66				
Total # of cracks	Total crack length mm	Total # of HAZ cracks	Total HAZ crack length mm	Total # of weld metal cracks	Total weld metal crack length mm
6	8.47	3	0.95	6	7.52

**Table B136:** Crack measurement results of specimen TIG-DC-SUP-2-4

Line energy kJ/cm	Welding current A	Arc voltage V	Welding speed mm/min	Shielding gas & composition	Shielding gas flow rate lt/min
3.9	180 ±	13.0	180	75%He25%Ar	15.0
Former radius mm	Specimen thickness mm	Nominal Augmented strain %	Real Augmented strain %		
125	9.6	4.0	3.84		
Length of all cracks (mm)	0.50/0.41/1.03/1.24/0.83/0.21/1.03				
	WELD CENTERLINE				
	3.10/0.62/0.21/1.24/1.03/0.62/0.66/0.66/0.41				
Length of HAZ cracks (mm)	0.50/0.41/1.03/1.24/0.83				
	WELD CENTERLINE				
	0.21/1.24/1.03/0.62/0.66/0.66/0.41				
Length of weld metal cracks (mm)	0.21/1.03				
	WELD CENTERLINE				
	3.10/0.62				
Total # of cracks	Total crack length mm	Total # of HAZ cracks	Total HAZ crack length mm	Total # of weld metal cracks	Total weld metal crack length mm
16	13.80	12	8.84	4	4.96

**Table B137:** Crack measurement results of specimen TIG-DC-SUP-3-1

Line energy kJ/cm	Welding current A	Arc voltage V	Welding speed mm/min	Shielding gas & composition	Shielding gas flow rate lt/min
4.7	180 ±	13.0	150	75%He25%Ar	15.0
Former radius mm	Specimen thickness mm	Nominal Augmented strain %	Real Augmented strain %		
1000	9.2	0.5	0.46		
Length of all cracks (mm)	-				
	WELD CENTERLINE				
	-				
Length of HAZ cracks (mm)	-				
	WELD CENTERLINE				
	-				
Length of weld metal cracks (mm)	-				
	WELD CENTERLINE				
	-				
Total # of cracks	Total crack length mm	Total # of HAZ cracks	Total HAZ crack length mm	Total # of weld metal cracks	Total weld metal crack length mm
-	-	-	-	-	-

**Table B138:** Crack measurement results of specimen TIG-DC-SUP-3-2

Line energy kJ/cm	Welding current A	Arc voltage V	Welding speed mm/min	Shielding gas & composition	Shielding gas flow rate lt/min
4.7	180 ±	13.0	150	75%He25%Ar	15.0
Former radius mm	Specimen thickness mm	Nominal Augmented strain %	Real Augmented strain %		
500	9.6	1.0	0.96		
Length of all cracks (mm)	0.45/0.54/1.24/1.86				
	WELD CENTERLINE				
	1.98/0.62/0.41				
Length of HAZ cracks (mm)	0.45/0.54/1.24				
	WELD CENTERLINE				
	0.62/0.41				
Length of weld metal cracks (mm)	1.86				
	WELD CENTERLINE				
	1.98				
Total # of cracks	Total crack length mm	Total # of HAZ cracks	Total HAZ crack length mm	Total # of weld metal cracks	Total weld metal crack length mm
7	7.11	5	3.26	2	3.84

**Table B139:** Crack measurement results of specimen TIG-DC-SUP-3-3

Line energy kJ/cm	Welding current A	Arc voltage V	Welding speed mm/min	Shielding gas & composition	Shielding gas flow rate lt/min
4.7	180 ±	13.0	150	75%He25%Ar	15.0
Former radius mm	Specimen thickness mm	Nominal Augmented strain %	Real Augmented strain %		
250	9.2	2.0	1.84		
Length of all cracks (mm)	0.50/0.58/0.29/2.60				
	WELD CENTERLINE				
	1.45				
Length of HAZ cracks (mm)	0.50/0.58/0.29/0.29/0.74				
	WELD CENTERLINE				
	-				
Length of weld metal cracks (mm)	1.86				
	WELD CENTERLINE				
	1.45				
Total # of cracks	Total crack length mm	Total # of HAZ cracks	Total HAZ crack length mm	Total # of weld metal cracks	Total weld metal crack length mm
6	5.70	5	2.40	2	3.31

**Table B140:** Crack measurement results of specimen TIG-DC-SUP-3-4

Line energy kJ/cm	Welding current A	Arc voltage V	Welding speed mm/min	Shielding gas & composition	Shielding gas flow rate lt/min
4.7	180 ±	13.0	150	75%He25%Ar	15.0
Former radius mm	Specimen thickness mm	Nominal Augmented strain %	Real Augmented strain %		
125	9.5	4.0	3.80		
Length of all cracks (mm)	0.50/0.62/0.50/0.91/0.70				
	WELD CENTERLINE				
	3.31/0.41/0.91/1.03/1.07/0.79/0.66/0.54				
Length of HAZ cracks (mm)	0.50/0.62/0.50/0.91/0.70				
	WELD CENTERLINE				
	0.41/0.91/1.03/1.07/0.79/0.66/0.54				
Length of weld metal cracks (mm)	-				
	WELD CENTERLINE				
	3.31				
Total # of cracks	Total crack length mm	Total # of HAZ cracks	Total HAZ crack length mm	Total # of weld metal cracks	Total weld metal crack length mm
13	11.94	12	8.64	1	3.31

**Table B141:** Crack measurement results of specimen TIG-DC-SUP-4-1

Line energy kJ/cm	Welding current A	Arc voltage V	Welding speed mm/min	Shielding gas & composition	Shielding gas flow rate lt/min
5.9	180 ±	13.0	120	75%He25%Ar	15.0
Former radius mm	Specimen thickness mm	Nominal Augmented strain %	Real Augmented strain %		
1000	9.5	0.5	0.48		
Length of all cracks (mm)	1.65/2.07				
	WELD CENTERLINE				
	1.24/0.83				
Length of HAZ cracks (mm)	-				
	WELD CENTERLINE				
	-				
Length of weld metal cracks (mm)	1.65/2.07				
	WELD CENTERLINE				
	1.24/0.83				
Total # of cracks	Total crack length mm	Total # of HAZ cracks	Total HAZ crack length mm	Total # of weld metal cracks	Total weld metal crack length mm
4	5.79	-	-	4	5.79

**Table B142:** Crack measurement results of specimen TIG-DC-SUP-4-2

Line energy kJ/cm	Welding current A	Arc voltage V	Welding speed mm/min	Shielding gas & composition	Shielding gas flow rate lt/min
5.9	180 ±	13.0	120	75%He25%Ar	15.0
Former radius mm	Specimen thickness mm	Nominal Augmented strain %	Real Augmented strain %		
500	9.2	1.0	0.92		
Length of all cracks (mm)	0.62/1.03/0.21/0.25/1.32/2.48				
	WELD CENTERLINE				
	0.91/0.62/0.50				
Length of HAZ cracks (mm)	0.62/1.03/0.21/0.25/1.32				
	WELD CENTERLINE				
	0.91/0.62/0.50				
Length of weld metal cracks (mm)	2.48				
	WELD CENTERLINE				
	-				
Total # of cracks	Total crack length mm	Total # of HAZ cracks	Total HAZ crack length mm	Total # of weld metal cracks	Total weld metal crack length mm
9	7.93	8	5.45	1	2.48

**Table B143:** Crack measurement results of specimen TIG-DC-SUP-4-3

Line energy kJ/cm	Welding current A	Arc voltage V	Welding speed mm/min	Shielding gas & composition	Shielding gas flow rate lt/min
5.9	180 ±	13.0	120	75%He25%Ar	15.0
Former radius mm	Specimen thickness mm	Nominal Augmented strain %	Real Augmented strain %		
250	9.5	2.0	1.9		
Length of all cracks (mm)	2.48/2.56				
	WELD CENTERLINE				
	0.62/1.32/0.41				
Length of HAZ cracks (mm)	-				
	WELD CENTERLINE				
	-				
Length of weld metal cracks (mm)	2.48/2.56				
	WELD CENTERLINE				
	0.62/1.32/0.41				
Total # of cracks	Total crack length mm	Total # of HAZ cracks	Total HAZ crack length mm	Total # of weld metal cracks	Total weld metal crack length mm
5	7.40	-	-	5	7.40



**Table B144:** Crack measurement results of specimen TIG-DC-SUP-4-4

Line energy kJ/cm	Welding current A	Arc voltage V	Welding speed mm/min	Shielding gas & composition	Shielding gas flow rate lt/min
5.9	180 ±	13.0	120	75%He25%Ar	15.0
Former radius mm	Specimen thickness mm	Nominal Augmented strain %	Real Augmented strain %		
125	9.6	4.0	3.84		
Length of all cracks (mm)	0.17/0.83/0.62/1.45/0.70/1.20/1.57/1.86				
	WELD CENTERLINE				
	2.48/1.74/1.24/1.16/1.24/0.99/0.91				
Length of HAZ cracks (mm)	0.17/0.83/0.62/1.45/0.70/1.20/1.57/1.86				
	WELD CENTERLINE				
	2.48/1.74/1.24/1.16/1.24/0.99/0.91				
Length of weld metal cracks (mm)	-				
	WELD CENTERLINE				
	-				
Total # of cracks	Total crack length mm	Total # of HAZ cracks	Total HAZ crack length mm	Total # of weld metal cracks	Total weld metal crack length mm
15	18.14	15	18.14	-	-

## CURRICULUM VITAE

### PERSONAL INFORMATION

Surname, Name : Batigün, Caner

Nationality: Turkish (TC)

Date and Place of Birth: 17 May 1967, Sakarya

Marital Status: Married

Phone: +90 312 210 36 94

Fax: +90 312 210 11 68

E-mail: bgun@metu.edu.tr

### EDUCATION

Degree	Institution	Year of Graduation
MS	METU Metallurgical Eng.	1994
BS	METU Metallurgical Eng.	1989
High School	Keçiören High School, Ankara	1984

### DIPLOMAS

Degree	Institution	Year of Graduation
International Welding Eng.	IIW & SLV-München	2001
European Welding Eng.	SLV-München	1991
Schweißfachingenieur	SLV-München	1991

### WORK EXPERIENCE

Year	Place	Enrolment
1993-Present	METU Welding Tech. Center	Expert, Trainer
1991 December	BAM-Berlin	Researcher
1989 October	METU Metallurgical Eng. Dept.	Research Assistant

## **FOREIGN LANGUAGES**

German, English.

## **PUBLICATIONS**

1. Ankara, A., Filiz, Z., Batıgün, C. (1998). Training and Certification of Welding Personnel. (proc. conf.) Pipeline Welding'98. Istanbul Technical University 11-13 May 1998 Istanbul, Turkey.
2. Batıgün, C. (1997). Alüminyum malzemelerde kaynaklama işlemine bağlı sıcak çatlama eğilimi. (Bildiri). 9. Uluslararası Metalurji ve Malzeme Kongresi. 11-15 Haziran 1997, İstanbul.
3. Batıgün, C. Akçam, Ö. (1995). Kaynaklı birleştirmelerin ısı işlemleri. Metalurji. 95. pp. 27-30.

## **MEMBERSHIPS**

American Welding Society, Florida. Since 1993.

UCTEA Chamber of Metallurgical Engineers, Ankara. Since 1995.

## **HOBBIES**

Nature and Plants, Photography, Listening Music.